
Taphonomy of the fossils of the Herefordshire
(Silurian) Konservat-Lagerstätte

Thesis submitted for the degree of
Doctor of Philosophy
At the University of Leicester

By

David Anthony Riley MGeol. (Leicester) FGS

Department of Geology
University of Leicester



January 2012

Preservation and taphonomy of the fossils of the Herefordshire (Silurian) Konservat-Lagerstätte

David Anthony Riley

The Herefordshire Lagerstätte represents a fully marine Silurian ecosystem, three dimensionally soft-bodied fossils, preserved by sparry calcite, which are recovered from carbonate concretions. Although, a taphonomic model exists it does not determine the pathways that led to their preservation, nor has it been tested on the other taxa recovered from the Lagerstätte. X-ray fluorescence (XRF) analysis indicates the sediment originated from an andesitic volcano from a destructive plate margin. Field relationships suggest that the bed was deposited from either a turbidity current or debris flow. Given the highly reactive nature of the volcanic ash, the cation exchanges that occur provide a mechanism for supersaturating the pore-fluid with carbonates. Examination of the four common taxa; *Offacolus kingi* (arthropod), *Tanazios dokeron* (arthropod), *Kenostrychus clementsii* (polychaete worm) and *Acaenoplax hayae* (mollusc), indicates a similar pathway of preservation. Energy-dispersive X-ray spectroscopy (EDX) identifies the only impurity within the fossil calcite is manganese; in comparison the concretion carbonates contain a variety of different cations. Therefore, the fossils and the concretions are the result of different processes, which were not coeval.

Comparing the preservation *Kenostrychus clementsii* (polychaete) against experimental work indicates that preservation occurred within 6 days and rules out the occurrence of a void stage as previously thought. In addition, it also suggests that preservation was either instantaneous or there must have been an intermediate “medusa” stage that preserved the tissue prior to templating. Electron microprobe analysis (EMPA) data indicate that the clay minerals that precipitated around the decaying animal were templating the organic matter. To precipitate the sparry calcite without the void stage, an hypothesis is proposed in which the sparry calcite nucleates and grows through the soft tissues. Isotopic data indicates that the concretions are not produced by organic matter decay. This is supported by the lack of correlation between the concretion and the fossil and the occurrence of barren concretions. Radial variation in the mineralogy, chemistry and isotopic ratios support the hypothesis that these concretions grew concentrically around a non-organic nucleus. These exceptional conditions may account for a preservation style that is so far unique to this single exposure.

ACKNOWLEDGMENTS

I would like to thank my supervisors for their help and guidance, but particularly Sarah Gabbott and David Siveter, who persevered and helped me improve my writing style, but also to Mike Norry for the many discussions we had (geologically related or not), and to Derek Siveter for letting me use the Oxford University Museum of Natural History collections and providing me with the valuable samples I needed to complete this work. Thank you to Derek Briggs and Mark Sutton for their advice and comments, but also for seeing how fast I could catch concretions during fieldwork. Many thanks to the support and encouragement I had from my family: Mr Robert Riley, Mrs Maggie Riley, Mr Ian Phillips, and also to my late grandparents Mrs Catherine Phillips and Mr Anthony Phillips to whom this work is dedicated.

Steve Grebby, Chris Willcox, Irfan Jan, Jawad Afzal, Dinah Smith, Mohibullah Kakar thank you for your help, advice and friendship, but also for electing me president when we made F32 an independent country. A big thank you to Sarah Lee and Alison Tasker who offered to read through my work and helped me improve my grammar. Thanks to Jan Zalasiewicz, Mark Williams, Andrea Snelling, Vince Williams and Carys Bennett. I would also like to acknowledge the Daniel Pidgeon Fund from The Geological Society of London for support with thin section preparation and the Timothy Jefferson Field Research Fund for supporting my field work at the exposure of the Lagerstätte.

Rob Wilson, Nick Marsh, Rob Kelly, Colin Cunningham, Lyn Marvin, Kay Hawkins and all the administrative staff at the Geology Department at the University of Leicester, and the support staff and the Oxford University Museum of Natural History

are thanked for their help and support. I'd also like to thank Prof. Warren Huff (Cincinnati) for extra data on the Welsh Borderland Bentonites, Phil Wilby (BGS) for advice and help with the CL imaging, Melanie Leng and Ian Millar (NIGL) for the isotope analysis.

A further thank you to my colleagues and friends at Argos Fosse Park who made my part time job fun and interesting, and gave me the moral support and encouragement I sometimes needed, in particular I'd like to thank Henry Bonner, Martin Perchard, Wendy Brown, Chris Payne, Shaun Tunaley, Sarah Nutt, Abby Fenn, Michelle Cook, Sam Clarkson, James Lockton, Andy Brewin, Mel Key and Chris Medhurst. The list is endless so we'll leave it there, but thank you to those I have not personally mentioned.

TABLE OF CONTENTS

ABSTRACT.....	I
ACKNOWLEDGMENTS	II
TABLE OF CONTENTS.....	IV
LIST OF FIGURES	IX
LIST OF TABLES.....	XII
DEDICATION.....	XV
INTRODUCTION	1
AIMS AND OBJECTIVES OF THIS THESIS.....	2
MATERIAL.....	4
CURRENT TAPHONOMIC MODEL FOR THE HEREFORDSHIRE LAGERSTÄTTE	4
VOLCANISM AND THE FOSSIL RECORD.....	6
FOSSILS AND CONCRETIONS	8
STRUCTURE OF THE THESIS.....	9
NATURE, PROVENANCE, AND EMPLACEMENT OF THE HOST DEPOSIT OF THE HEREFORDSHIRE LAGERSTÄTTE (SILURIAN), UK.....	11
GEOLOGICAL SETTING.....	12
MATERIALS AND ANALYTICAL METHODS.....	16
COMPOSITION OF THE HOST BENTONITE	17
<i>Petrology of the host bentonite</i>	<i>17</i>
<i>XRF and geochemistry of the host bentonite</i>	<i>21</i>

DISCUSSION	25
<i>Composition of the sedimentary deposit</i>	25
<i>Provenance and emplacement of the volcanic ash</i>	27
<i>Significance of the host geochemistry to the taphonomy of the Herefordshire Lagerstätte</i>	34
THE TAPHONOMY OF THE SILURIAN HEREFORDSHIRE KONSERVAT LAGERSTÄTTE (SILURIAN): THE EVOLUTION OF A PRESERVATIONAL PATHWAY AS CONTROLLED BY EH-PH	
GEOLOGICAL CONTEXT	38
MATERIALS AND METHODS.....	40
RESULTS	43
<i>Clay Mineralisation</i>	43
<i>Calcite Mineralisation</i>	45
<i>Sparry Calcite Stable Isotope Analysis</i>	48
<i>Concretion Matrix</i>	49
DISCUSSION	50
<i>Decay</i>	50
<i>Clay Mineralisation</i>	51
<i>Calcite Precipitation</i>	57
<i>Discussion of the Stable Isotope Analysis</i>	59
<i>Discussion of the Carbonate Concretions</i>	62
<i>Discussion of the Eh-pH</i>	63
TAPHONOMIC MODEL.....	65
<i>Entombment</i>	65
<i>Hydrolysis of the volcanic ash</i>	65

<i>Initial Decay of the Organism and Clay Mineral Accumulation</i>	67	
<i>Calcite precipitation</i>	69	
CONCLUSION.....	73	
ISOTOPE ANALYSIS AND THE MECHANISM OF CONCRETION FORMATION WITHIN THE HEREFORDSHIRE KONSERVAT LAGERSTÄTTE (SILURIAN)... 74		
GEOLOGICAL SETTING	76	
METHODS	77	
ANALYTICAL RESULTS	81	
<i>Distribution and shape of the concretions</i>	81	
<i>Mineralogy of the concretions</i>	83	
<i>Geochemistry of the concretions</i>	90	
<i>Isotope analysis of the concretions</i>	93	
DISCUSSION	96	
<i>Textures, mineralogy and geochemistry</i>	96	
<i>Isotope discussion</i>	104	
<i>Mechanism of concretion formation</i>	108	
<i>Relationship to the fossils</i>	113	
CONCLUSIONS	114	
CONCLUSIONS AND FURTHER WORK		115
GEOCHEMISTRY OF THE VOLCANIC ASH.....	115	
PRESERVATION AND TAPHONOMIC PATHWAY	116	
CONCRETION FORMATION	117	
OUTCOMES	118	
EVALUATION OF THE TAPHONOMIC MODEL.....	119	

FUTURE WORK.....	122
APPENDIX A: POWDER PELLET	124
APPENDIX B: FUSION BEAD.....	124
APPENDIX C: XRD ANALYSES OF HOST BENTONITE.....	126
APPENDIX D: EDX POINT-AND-ID DATA OF THE BENTONITE HOST.	127
APPENDIX E: XRF DATA OF HOST BENTONITE	134
APPENDIX F: AVERAGE ANDESITE.....	136
APPENDIX G: COMPOSITION OF LOCALLY COLLECTED COALBROOKDALE FORMATION.....	136
APPENDIX H: CLAY MINERAL EMPA ANALYSES.....	137
<i>Kenostrychus clementsi</i>	137
<i>Tanazios dokeron</i>	140
<i>Acaenopax hayae</i>	142
<i>Offacolus kingi</i>	145
Barren Concretion.....	146
APPENDIX I: EDX MAPS OF <i>A. HAYAE</i>	148
APPENDIX J: EDX MAPS OF <i>K. CLEMENTSI</i>	149
APPENDIX K: EDX MAPS OF <i>O. KINGI</i>	150
APPENDIX L: EDX MAPS OF <i>T. DOKERON</i>	151
APPENDIX M: EDX POINT-AND-ID DATA OF CONCRETION MATRIX.....	152
APPENDIX N: XRD OF CARBONATE CONCRETION	163
APPENDIX O: XRF OF CARBONATE CONCRETION.....	165

APPENDIX P: ISOTOPIC DATA 170

APPENDIX Q: CALCULATIONS BASED ON STOICHIOMETRY 172

REFERENCES 176

LIST OF FIGURES

FIGURE 1.1: LOCATION OF HEREFORDSHIRE AND THE STRATIGRAPHY OF THE SILURIAN WITH THE AGE OF THE HEREFORDSHIRE LAGERSTÄTTE MARKED.....	1
FIGURE 1.1: PREVAILING TAPHONOMIC MODEL OF THE HEREFORDSHIRE LAGERSTÄTTE BASED ON THE ARTHROPOD <i>O. KINGI</i>	5
FIGURE 2.1: PALAEOGEOGRAPHY FOR SOUTHERN BRITAIN IN THE LATE WENLOCK.	13
FIGURE 2.2: SEDIMENTARY LOG OF THE HOST BENTONITE OF THE HEREFORDSHIRE LAGERSTÄTTE AND ITS POSITION WITHIN THE LOCAL LITHOSTRATIGRAPHY.	14
FIGURE 2.3: IMAGE OF THE HEREFORDSHIRE BENTONITE WITH CONCRETIONS.....	15
FIGURE 2.4: EXAMPLE OF THE CONCRETIONS AND FOSSILS RECOVERED FROM THE HEREFORDSHIRE LAGERSTÄTTE.	16
FIGURE 2.5: TRIANGULAR DISCRIMINATION DIAGRAMS (A) Si-CA-AL PLOT. (B) MG+FE- CA-P. (C) VELDE AND MEUNIER	19
FIGURE 2.6: SEM BACKSCATTER IMAGE OF BENTONITE MATRIX	20
FIGURE 2.7: QUARTZ AND TITANIUM RICH MINERAL.....	21
FIGURE 2.8: (A) Zr/TiO ₂ - Nb/Y DISCRIMINATION DIAGRAM. (B) Th-Nb/16-Zr/117	22
FIGURE 2.9: DOUBLE NORMALISED XRF DATA.....	23
FIGURE 2.10: COALBROOKDALE FORMATION-NORMALISED PLOTS	24
FIGURE 2.11: Zr/TiO ₂ - Nb/Y DISCRIMINATION DIAGRAM WITH HEREFORD DATA AND OTHER STUDIES	28
FIGURE 2.12: POSSIBLE EMPLACEMENT METHOD OF THE HEREFORDSHIRE LAGERSTÄTTE BENTONITE.....	33
FIGURE 3.1: LOG THROUGH HOST BENTONITE CONTAINING EXCEPTIONALLY PRESERVED FOSSILS	39
FIGURE 3.2: EXAMPLE OF CONCRETIONS RECOVERED FROM THE BENTONITE.....	40

FIGURE 3.3: K/AL VS. SI/AL PLOT	44
FIGURE 3.4: REPRESENTATIVE SEM BACKSCATTER IMAGES AND EDX OF FAUNAL ELEMENTS	46
FIGURE 3.5: REPRESENTATIVE CATHODOLUMINESCENCE (CL) AND PLAIN-POLARISED LIGHT IMAGES OF FAUNAL ELEMENTS	48
FIGURE 3.6: TRANSVERSE SECTION OF <i>K. CLEMENTSI</i>	51
FIGURE 3.7: DISTANCE FROM THE FOSSIL PLOTTED AGAINST THE K/AL RATIO	54
FIGURE 3.8: EH-PH DIAGRAMS GENERATED AT STANDARD LABORATORY CONDITIONS A. IRON SPECIES. B. MAGNESIUM SPECIES.....	57
FIGURE 3.9: SCHEMATIC PRESERVATION PATHWAY THROUGH EH-PH SPACE.	63
FIGURE 3.10: REVISED TAPHONOMIC MODEL FOR THE HEREFORDSHIRE LAGERSTÄTTE. .	72
FIGURE 4.1: THREE CONCRETION SHAPES RECOVERED FROM THE HOST BENTONITE. A. SPHERICAL.....	77
FIGURE 4.2: A. SAMPLING AXIS OF CONCRETIONS. B. EXAMPLE OF SAMPLING TECHNIQUE.	79
FIGURE 4.3: IMAGE OF THE HOST BENTONITE WITH CONCRETIONS.....	81
FIGURE 4.4: RANDOM DISCRIMINATION GRAPH.....	83
FIGURE 4.5: A: ANALYSIS TOTAL AGAINST WEIGHT PERCENT SiO ₂ . B: POINT-AND-ID ANALYSIS OF CaO wt% AGAINST FeO wt%	84
FIGURE 4.6: HABITS OF CLAY MINERALS WITHIN THE CONCRETIONS.	85
FIGURE 4.7: BACKSCATTER SEM IMAGE OF A PART OF THE CONCRETION MATRIX WITH VOLCANIC TITANIUM MINERAL	86
FIGURE 4.8: SEM BACKSCATTER IMAGES OF THE MATRIX OF A SINGLE CONCRETION. A. EXSOLUTION FEATURES ON THE ANKERITE CRYSTAL, B. IRON OXIDE COATING GRAINS WITHIN THE MATRIX.	87

FIGURE 4.9: COMPARISON OF THE XRD TRACES FROM THE BLUE UNWEATHERED CENTRE WITH THE BROWN WEATHERED RIM OF A CONCRETION.	89
FIGURE 4.10: VARIATION IN PERCENTAGE OF MINERALS ACROSS THE WIDTH OF THE CONCRETION.	90
FIGURE 4.11: VOLCANIC CLASSIFICATION PLOT WITH THE CONCRETION ANALYSIS AND BENTONITE ANALYSIS.	91
FIGURE 4.12: A. REPRESENTATIVE XRF DATA FROM THE CARBONATE CONCRETIONS WHICH HAVE BEEN DOUBLE NORMALISED. B. REPRESENTATIVE XRD DATA FROM THE HOST BENTONITE WHICH HAVE BEEN DOUBLE NORMALISED.	92
FIGURE 4.13: MOLECULAR PROPORTIONS OF CATIONS ACROSS THE WIDTH OF THE CONCRETION	93
FIGURE 4.14: ISOTOPIC TRENDS A. CONCRETION 1. B. CONCRETION 2.	95
FIGURE 4.15: PLOT OF ALUMINIUM AND SILICON DATA AFTER THE STOICHIOMETRY REMOVAL OF CLAY MINERALS.....	99
FIGURE 4.16: PLOT OF THE MOLECULAR PROPORTIONS OF CALCIUM, MAGNESIUM, MANGANESE, AND IRON WITH THE PLOTS OF MINERAL PERCENTAGE	100
FIGURE 4.17: MG:CA RATIO ACROSS THE CONCRETION AND THE PERCENTAGE OF DOLOMITE AND CALCITE.	102
FIGURE 4.18: SCHEMATIC CONCRETION FORMATION.	113
FIGURE I.2: EDX MAPS OF <i>A. HAYAE</i>	148
FIGURE J.1: EDX MAPS OF <i>K. CLEMENTSI</i>	149
FIGURE K.1: EDX MAPS OF <i>O. KINGI</i>	150
FIGURE L.1: EDX MAPS OF <i>T. DOKERON</i>	151

LIST OF TABLES

TABLE 1.1: VOLCANIC ACTIVITY AND ASSOCIATED FOSSIL FINDS	6
TABLE 2.1: COMPARISON OF THE HEREFORDSHIRE BENTONITE TO THE BENTONITES OF THE WELSH BORDERLANDS	29
TABLE 3.1— SUMMARY OF FOSSIL PRESERVATION FROM THE HEREFORDSHIRE LAGERSTÄTTE. OUM = OXFORD UNIVERSITY MUSEUM OF NATURAL HISTORY CATALOGUE NUMBERS OF SPECIMENS USED IN THIS STUDY.....	41
TABLE 3.2— SUMMARY OF FOSSIL PRESERVATION	43
TABLE 3.3— PRELIMINARY ISOTOPE STUDY OF FOSSIL CALCITE	49
TABLE 3.4— TWO WAY T-TEST TO STATISTICAL TEST FOR A DIFFERENCE BETWEEN THE K/AL RATIO OF THE CLAY MINERALS IN <i>T. DOKERON</i> AND <i>A. HAYAE</i>	52
TABLE 4.1: NUMBER OF CONCRETIONS RECORDED WITHIN EACH SQUARE OF THE GRID...	82
TABLE C.2: MINERALOGY OF BENTONITE	126
TABLE D.1: EDX DATA OF MINERAL CHEMICAL COMPOSITION FROM BENTONITE THIN SECTIONS	127
TABLE E.1: XRF ANALYSES OF HOST BENTONITE	134
TABLE F.1: MAJOR ELEMENT DATA USED FOR THE NORMALISATION OF THE DATA FROM FITTON <i>ET AL.</i> 1982	136
TABLE G.1: MAJOR ELEMENTAL DATA	136
TABLE G.2: TRACE ELEMENTAL DATA	137
TABLE H.1: EMPA DATA OF CLAY ACCUMULATIONS IMMEDIATELY ADJACENT TO <i>K.</i> <i>CLEMENTSI</i>	137
TABLE H.2: EMPA DATA OF CLAY ACCUMULATIONS IN THE MATRIX OF THE CONCRETION THAT CONTAINED <i>K. CLEMENTSI</i>	139

TABLE H.3: EMPA DATA OF CLAY ACCUMULATIONS IMMEDIATELY ADJACENT TO <i>T</i> .	
<i>DOKERON</i>	140
TABLE H.4: EMPA DATA OF CLAY ACCUMULATIONS IN THE MATRIX OF THE CONCRETION	
THAT CONTAINED <i>T. DOKERON</i>	142
TABLE H.5: EMPA DATA OF CLAY ACCUMULATIONS IMMEDIATELY ADJACENT TO <i>A</i> .	
<i>HAYAE</i>	142
TABLE H.6: EMPA DATA OF CLAY ACCUMULATIONS IN THE MATRIX OF THE CONCRETION	
THAT CONTAINED <i>A. HAYAE</i>	145
TABLE H.7: EMPA DATA OF CLAY ACCUMULATIONS IMMEDIATELY ADJACENT TO <i>O</i> .	
<i>KINGI</i>	145
TABLE H.8: EMPA DATA OF CLAY ACCUMULATIONS WITHIN A BARREN CONCRETION..	146
TABLE M.1: EDX CHEMICAL ANALYSES OF MINERALS WITHIN THE CARBONATE	
CONCRETIONS.	152
TABLE N.1: WHOLE ROCK XRD DATA OF CONCRETION 1	163
TABLE N.2: WHOLE ROCK XRD DATA OF CONCRETION 2.....	164
TABLE O.1: XRF MAJOR ELEMENTS OF CONCRETION 1	165
TABLE O.2: TRACE ELEMENT DATA FOR CONCRETION 1; MEASURED AS PPM.....	166
TABLE O.3: XRF MAJOR ELEMENTS OF CONCRETION 2.....	167
TABLE O.4: TRACE ELEMENT DATA FOR CONCRETION 2; MEASURED AS PPM.	168
TABLE P.1: CARBON AND OXYGEN ISOTOPE DATA (A) CONCRETION 1, (B) CONCRETION	
2.	170
TABLE P.2: CARBON AND OXYGEN ISOTOPE DATA PRESENTED IN CHAPTER 3 OF 4	
ENIGMATIC FOSSILS AND, IN ADDITION, A SAMPLE OF LOCALLY COLLECTED	
DOLYHIR-NASH SCAR LIMESTONE FORMATION.	171

TABLE P.3: SR ISOTOPE DATA MEASURED FROM A SELECTION OF CONCRETION SAMPLES.	171
TABLE Q.1: STOICHIOMETRY.....	172
TABLE Q.2: STOICHIOMETRY CALCULATIONS	174
TABLE Q.3: DATA AND ABBREVIATIONS USED IN TABLE Q.2	175

DEDICATION

This work is dedicated to the memory of Catherine Phillips and Anthony Phillips.
You both taught me the value of education, to do my best at whatever I do, and to put
my pride in my work. I will never forget either of you.

INTRODUCTION

The science of taphonomy examines the physical, chemical and biological processes that affect an organism after death until the point of fossilisation. The word taphonomy comes from the Greek *taphos*, ‘burial’ and *nomos* ‘law’ and literally means ‘study of the grave’. On death all organisms begin to decay by autolysis, in which the cells go through a ‘self-destruct’ process making the cell structures more amenable to decomposition by microorganisms. The decomposition of an organism is usually a rapid event; the fossilisation process is paramount in retarding the full process of decay. Soft tissues such as guts and muscle are most susceptible to decay, but are in some cases replaced rapidly by authigenic mineral formation as in the case of the fossils of the Cretaceous Santana Formation Konservat Lagerstätte, Brazil (Martill, 1988).

The Herefordshire (Silurian) Konservat Lagerstätte (Briggs *et al.*, 1996; 2008) occurs in the late Wenlock Series of the Welsh Borderlands and it is found at a single locality in the county of Herefordshire, England (Fig. 1.1).

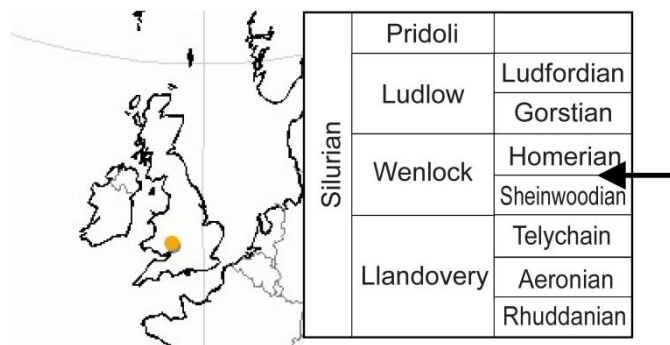


Figure 1.1: Location of Herefordshire and the stratigraphy of the Silurian with the age of the Herefordshire Lagerstätte marked

The Lagerstätte contains three-dimensionally (3-D) preserved soft-bodied organisms within calcareous concretions in a volcanic ash, but there is very little distinguishable soft tissue or cuticle seen within the fossils. The base of the exposed

succession comprises the Dolyhir-Nash Scar Limestone Formation that is dominated by algal colonies (Bassett, 1974). Overlying the Dolyhir-Nash Scar Limestone Formation is the Coalbrookdale Formation, which comprises a sequence of thinly-bedded nodular dark shales, approximately 300m in thickness. The Herefordshire Lagerstätte occurs as a lens and is entirely within the Coalbrookdale Formation. Microfossil and graptolitic evidence indicates a late Sheinwoodian stage to early Homeric stage stratigraphic range (Fig. 1.1), giving an approximate age of 425 million years (Siveter *et al.*, 2007d).

AIMS AND OBJECTIVES OF THIS THESIS

The Herefordshire deposit represents a rare Silurian Lagerstätte (Briggs *et al.*, 1996). There have been many papers detailing the three-dimensionally preserved invertebrate fossils including a polychaete worm (Sutton *et al.*, 2001c), a chelicerate (Orr *et al.*, 2000b), ostracods (Siveter *et al.* 2003, 2007c, 2010), a pycnogonid (Siveter *et al.*, 2004), a barnacle (Briggs *et al.*, 2005), a crustacean (Siveter *et al.*, 2007a), a marrellomorph (Siveter *et al.*, 2007b), a lophophorate (Sutton *et al.*, 2011), a mollusc (Sutton *et al.*, 2001a, 2001b), a gastropod (Sutton *et al.* 2006), and a brachiopod (Sutton *et al.*, 2005). However, little has been done to elucidate the taphonomy and the geochemical pathways of preservation of the fossils of the Lagerstätte. A pilot study that addressed the taphonomy of a single arthropod species, *Offacolus kingi*, was undertaken by Orr *et al.* (2000a) and is the current published taphonomic model for the biota.

Elucidation of the taphonomy of the other animals in the biota and chemical analysis of the host sediment and carbonate concretions remains to be undertaken. Such analyses are critical in order to assess the paragenetic sequence of authigenic minerals and the potential source of the ion(s) responsible for the preservation of the fossils.

Geochemical fingerprinting of the bentonite itself by the use of immobile elements should indicate the type of volcanism responsible for the deposit, a possible provenance and may help to determine why this style of exceptional preservation is only recovered from a single locality. Assessing the possible species specific modes of fossilization will inform on any preservational bias within the deposit and aid morphological reconstruction of the animals themselves and help understand the completeness, or otherwise of a Silurian ecosystem.

The aim of this research is to study the modes of preservation and the pathways of fossilisation of the Herefordshire biota. The key objectives of this project are to:

1. document the elemental and mineralogical distributions, mineral textures and fabrics of the different minerals across a range of taxa and determine the paragenetic sequence of authigenic mineral formation;
2. determine the potential source of the ion(s) responsible for the preservation of the fossils;
3. ascertain any species specific preservation and establish any preservational bias within the deposit;
4. document the size, shape and stratigraphic distribution of the nodules within the host deposit;
5. determine the chemistry of the minerals within the host bentonite in order to evaluate its source and the extent to which the nature of the volcanic ash contributed to the exceptional preservation;
6. undertake stable isotope, mineralogical and other chemical analyses of the carbonate concretions and the host sediment in order to determine the processes of concretion formation;

7. reconstruct the local environment of deposition pertaining to the preservation of the Herefordshire Lagerstätte.

MATERIAL

This study has used samples of fossil material, carbonate concretions and host sediment have been analysed. Some concretions and fossils were collected by the author from the field site. However, the majority of the fossils and concretions that were subject to destructive and non-destructive analysis were provided by Professor Derek J. Siveter, Oxford University Museum of Natural History, where the entire collection of fossils and concretions of the Herefordshire Lagerstätte is housed. The bulk of this material was collected by Professors David Siveter, Derek Siveter, Derek Briggs and Dr Mark Sutton during their initial field studies at the site.

Material that was collected by the author from the field site in Herefordshire is identified by the prefix “DAR”. The material provided by Oxford University Museum of Natural History is identified with the prefix “OUM C.”. Some data tables also contain references to “LF” numbers; these are University of Leicester Department of Geology fusion bead numbers. Material from Oxford University Museum of Natural History forms the basis of polished thin sections for analysis.

CURRENT TAPHONOMIC MODEL FOR THE HEREFORDSHIRE

LAGERSTÄTTE

The current published taphonomic model for the Herefordshire Lagerstätte focuses on studies of the arthropod *Offacolus kingi*. (Orr *et al.*, 2000a). The taphonomic pathway begins with the entombment of the biota within a fine grained ash (Fig. 1.1a). Decay products then leak into the surrounding matrix and through the newly established

chemical gradients clay minerals accumulate in the pore space adjacent to the carcass and calcium phosphate precipitates authigenically in the gut traces (Fig. 1.1b). Complete decay of the organic matter results in an external mould (Fig. 1.1c). Precipitation of the sparry calcite within the void generates a cast of the animal and at this point it is also suggested, tentatively, that the fossils were incorporated into the carbonate concretion (Fig. 1.1d). The final stage is the formation of dolomite rhombs adjacent to the clays and calcite crystals (Fig. 1.1e).

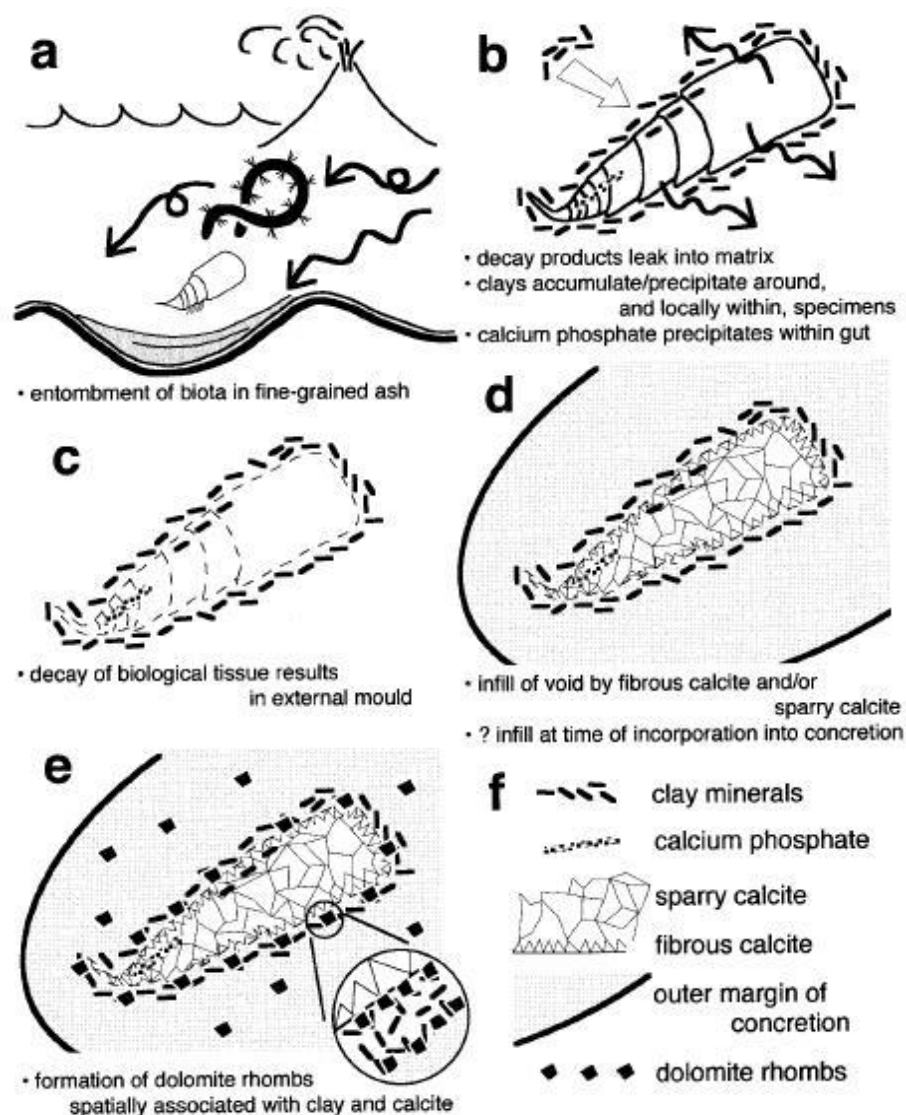


Figure 1.1: Prevailing taphonomic model of the Herefordshire Lagerstätte based on the arthropod *O. kingi* (after Orr *et al.*, 2000a)

VOLCANISM AND THE FOSSIL RECORD

There is an established link between the occurrence of volcanic activity and the preservation of fossils (Table 1.1), including some recognised Lagerstätten. Volcanic deposits have several characteristics that help enable fossilisation, fine grained volcanoclastic deposits provide a kill mechanism for the fauna, limits the effect of scavengers, and offer fine grained sediment to encase the carcasses and preserve the details in high fidelity of the animal. Such deposits are also very chemically reactive and through fall deposits or associated hydrothermal activity are able to alter the geochemistry of the environment to preserve the biota (Park, 1995; Mustoe, 2008). The majority of known fossil-associated volcanic deposits occur throughout the Cenozoic, although there are examples within the Cretaceous, Jurassic, Devonian and the Silurian. Such deposits occur in a range of sedimentary environments including terrestrial, lacustrine and marine. They also exhibit different styles of fossil preservation: for example trace fossils in the Laetoli site of Tanzania (Hay & Leakey, 1982), skeletal remains in the Ashfall Fossil Beds of Nebraska (Rose *et al.*, 2003), and 3-D soft bodied fossils in the Herefordshire Lagerstätte.

Table 1.1: Volcanic activity and associated fossil finds

Name	Fossils	Nature of Volcanism	Age	Country	Reference
Pompeii	<i>Homo sapiens</i>	Pyroclastic flows	Recent 79AD	Italy	Guarino <i>et al.</i> (2006)
Bouri Formation	Australopithecines, <i>Homo</i> fossils, bones of large mammals	Bentonitic tuffs	Pleistocene	Ethiopia	Clark <i>et al.</i> (2003); de Heinzelin <i>et al.</i> (1999)

Laetoli	<i>Homo</i> footprints	Volcanic ash	Plio-Pleistocene	Tanzania	Hay & Leakey (1982)
James Ross Island Volcanic Group	Echinoderms, trace fossils	Tuff	Late Miocene	James Ross Island Antarctic	Williams <i>et al.</i> (2006)
Rusinga Island	Mammals	Volcanic ash	Miocene	Kenya	Harrison (1981)
Barstow Formation	Insects, arachnids	Volcanic springs	Miocene	USA Barstow California	Park (1995)
Ashfall Fossil Beds	Mammals	Volcanic ash fall	Miocene	USA Nebraska	Rose <i>et al.</i> (2003)
Tinguiririca fauna	Mammals	Volcanic mudflows and ash layers	Oligocene	Chile	Flynn <i>et al.</i> (2007)
The Princeton Cherts	Plants	Volcanic ash	Eocene	British Columbia	Stockey (2001)
Florissant Fossil Beds	Petrified redwoods, insects, plants	Volcanic ash	Eocene	USA Teller County Colorado	Mustoe (2008)
Clarno Formation	Mammals, flowering plants	Volcanic ash	Eocene	USA John Day River Basin Oregon	Retallack (2004); Manchester (1994)
Fur Formation	Insects, fish, birds, reptiles, plants	Volcanic ash	Palaeocene - Eocene boundary	Denmark	Dyke <i>et al.</i> (2004)
Santa Marta Formation	Microfossils, invertebrates, fish	Tuff derived deposits	Late Cretaceous	Antarctica	Olivero (2007)
Jehol Biota	Bivalves, ostracods, insects, mammals,	Volcanic ash	Late Jurassic - early	China	Zhonghe <i>et al.</i> (2003)

fish		Cretaceous			
Curio Bay	Ancient conifers	Volcanic mudflows	Jurassic	New Zealand Southland	Pole (2001)
Old Red Sandstone	Trace fossils	Tuffs	Lower Devonian	UK, SW Wales	Marriott <i>et al.</i> (2009)
Herefordshire	Range of invertebrates,	Volcanic ash	Mid Silurian	UK Herefordshire	This study; Orr <i>et al.</i> (2000a)
Lagerstätte	especially arthropods			England	

FOSSILS AND CONCRETIONS

The fossils of the Herefordshire Lagerstätte are recovered from spherical carbonate concretions. A check of the literature will illustrate the ambiguity between the use of the terms concretion and nodule. Concretion is a term given to spherical bodies that are primary and precipitate within the pore space. Nodules however are replacement bodies and therefore the term concretion will be used consistently throughout this study. The timing of formation of the concretions is uncertain. The preservation of 3-D soft bodied fossils (Orr *et al.*, 2000a) and deformation of lamination in and around the concretions (Raiswell, 1971) implies rapid formation. However, a study carried out by Al-Agha *et al.* (1995), indicates that concretion development can be much slower.

Concretions usually form at the sediment-water interface during early diagenesis (Raiswell & Fisher, 2000). Apart from potentially aiding fossilisation their formation also dramatically increases the long-term preservation potential of a fossil by, for example, reducing the effects of diagenesis, weathering and compaction. There is a documented association between the occurrence of carbonate concretions and

Lagerstätten. The Lagerstätte associated with carbonate concretions however, demonstrate significant variation in the composition of the carbonate and the shape of the concretions. For example, the late Palaeozoic Mazon Creek Lagerstätte contains a diverse flora and fauna recovered from sideritic concretions formed within a estuarine environment that experienced fresh water influxes (Baird *et al.*, 1985). This variation in the carbonate mineral reflects the environment of formation; the fresh water influxes contain no dissolved sulphates. The lack of dissolved sulphates leaves the available Fe^{2+} to react with carbonate forming siderite instead of pyrite (Mozley, 1989).

The shape of the concretions can be influenced by the organism that is being preserved. For example, in the Cretaceous Santana Formation Lagerstätte of Brazil fish fossils are preserved within calcium carbonate concretions, which have taken on the shape of the entombed fish (Martill, 1988).

STRUCTURE OF THE THESIS

This thesis consists of 5 chapters of which 3 are in the form of manuscripts for publication.

Chapter 2 Nature, provenance and emplacement of the host deposits of the Herefordshire Lagerstätte.

This chapter details the geochemical characteristics of the host volcanic deposit. Trace element geochemistry is used to identify the original source composition, the geotectonic setting and possible source region(s) for the deposit, comment on the method of emplacement and suggest the effect of the volcanic deposit on the taphonomic pathway of the fossils.

Chapter 3 Taphonomy of the Herefordshire (Silurian) Lagerstätte. This chapter evaluates differences in preservational style between some common faunal elements and presents a new detailed taphonomic model of the Herefordshire Lagerstätte. This chapter is formatted in the style of Palaios.

Chapter 4 Isotope analysis and the mechanism of concretion formation within the Herefordshire Lagerstätte. This chapter elucidates the mechanism of concretion formation, based in part on newly acquired isotopic data.

Chapter 5 Summary and conclusions of the taphonomic model and suggestions for further work.

NATURE, PROVENANCE, AND EMPLACEMENT OF THE HOST DEPOSIT
OF THE HEREFORDSHIRE LAGERSTÄTTE (SILURIAN), UK

Chapter Abstract: *The Herefordshire Konservat Lagerstätte (late Wenlock Epoch, Silurian) represents one of the most important Lagerstätte in the world, providing a rare glimpse into a Silurian marine ecosystem. X-ray fluorescence (XRF) geochemistry demonstrates the volcanic origin of the Lagerstätte host sediment, a bentonite, identifying the source as an andesitic eruption on a destructive plate margin. Depletion within the bentonite of calcium, magnesium, iron and manganese, and their enrichment within the exceptional fossil-bearing carbonate concretions support the hypothesis that these elements were principally supplied by the volcanic ash. The bentonite host is geochemically similar to the approximately coeval volcanic rocks of the late Wenlock Mendip Hills, Somerset, and the Dingle Peninsula, South West Ireland, suggesting two possible source areas.*

The Herefordshire Konservat Lagerstätte provides a rare ‘window’ into a Silurian marine ecosystem by preserving a range of soft bodied invertebrate fossils including a polychaete worm (Sutton *et al.*, 2001c), a chelicerate (Orr *et al.*, 2000b), ostracods (Siveter *et al.*, 2003, 2007c, 2010), a pycnogonid (Siveter *et al.*, 2004), a barnacle (Briggs *et al.*, 2005), a crustacean (Siveter *et al.* 2007a), a marrellomorph (Siveter *et al.*, 2007b), a lophophorate (Sutton *et al.*, 2011), a mollusc (Sutton *et al.*, 2001a, 2001b), a gastropod (Sutton *et al.* 2006), and a brachiopod (Sutton *et al.*, 2005). The fossils are three-dimensional and are composed of a calcite infill within carbonate

concretions, hosted within a fine-grained bentonite (Briggs *et al.*, 1996; Orr *et al.*, 2000a).

Orr *et al.* (2000a) established a taphonomic model describing the preservational pathway for a single taxon, the arthropod *Offacolus kingi*, from the Herefordshire Lagerstätte. In the Orr *et al.* (2000a) model the biota was entombed within a volcanic ash fall. Decay products were released from the carcasses into the surrounding pore fluid, establishing chemical gradients, which promoted the diffusion of cations. Clay minerals accumulated, either as new precipitates or as existing particulates in the pore spaces immediately adjacent to the fossil, and were at least in part thought to be possibly responsible for retention of the three dimensional void left by the decayed carcass prior to the precipitation of the calcite in the external mould. At the same time, carbonate concretions grew around the fossils.

Whilst this model considered aspects of fossil preservation and concretion formation, it did not include analysis of the host sediment. This is vital to understanding the conditions that resulted in the exceptional preservation within the Herefordshire Lagerstätte. Here, for the first time, this study will characterise the host sediment geochemically, try to determine its original composition and suggest a possible provenance for the ash. Furthermore, this study will demonstrate that the composition and emplacement mechanism of the ash may have been crucial to the unique preservational mode of this Lagerstätte.

GEOLOGICAL SETTING

The host bentonite was deposited on an outer shelf environment (Briggs *et al.*, 1996). The sediments, which typically furnished the sedimentary basin, comprised turbiditic sands and shelly, graptolitic, muds/silts (Fig 2.1). The turbiditic sands were

periodically sourced from the landmasses to the south. Two volcanic centres were present in the area; these were the Mendip Hills to the South and the Dingle Peninsula to the West (Fig 2.1).

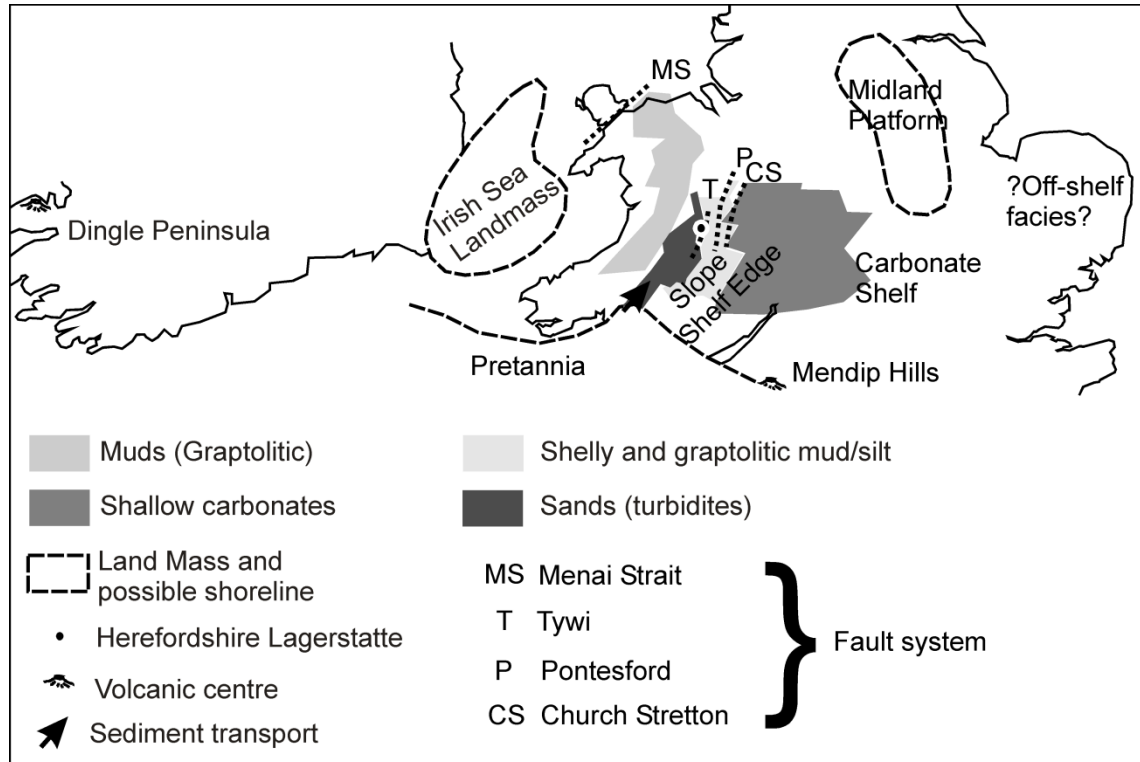


Figure 2.1: Palaeogeography for southern Britain in the late Wenlock. (modified after Siveter *et al.* 1989).

The bentonite hosting the Lagerstätte is exposed in a quarry in the county of Herefordshire in the central Welsh Borderlands. The base of the exposed succession of the Herefordshire Lagerstätte comprises the Dolyhir-Nash Scar Limestone Formation, a deposit dominated by algal colonies (Bassett, 1974). The overlying Coalbrookdale Formation, comprises a sequence of thinly bedded nodular dark shales, which regionally are approximately 300 m thick. The bentonite occurs entirely within the Coalbrookdale Formation with which it has sharp lower and upper contacts (Fig. 2.2). Based on the radiolarian fauna, the Coalbrookdale Formation here is of late Sheinwoodian to early Homeric age (see Siveter *et al.*, 2007d)

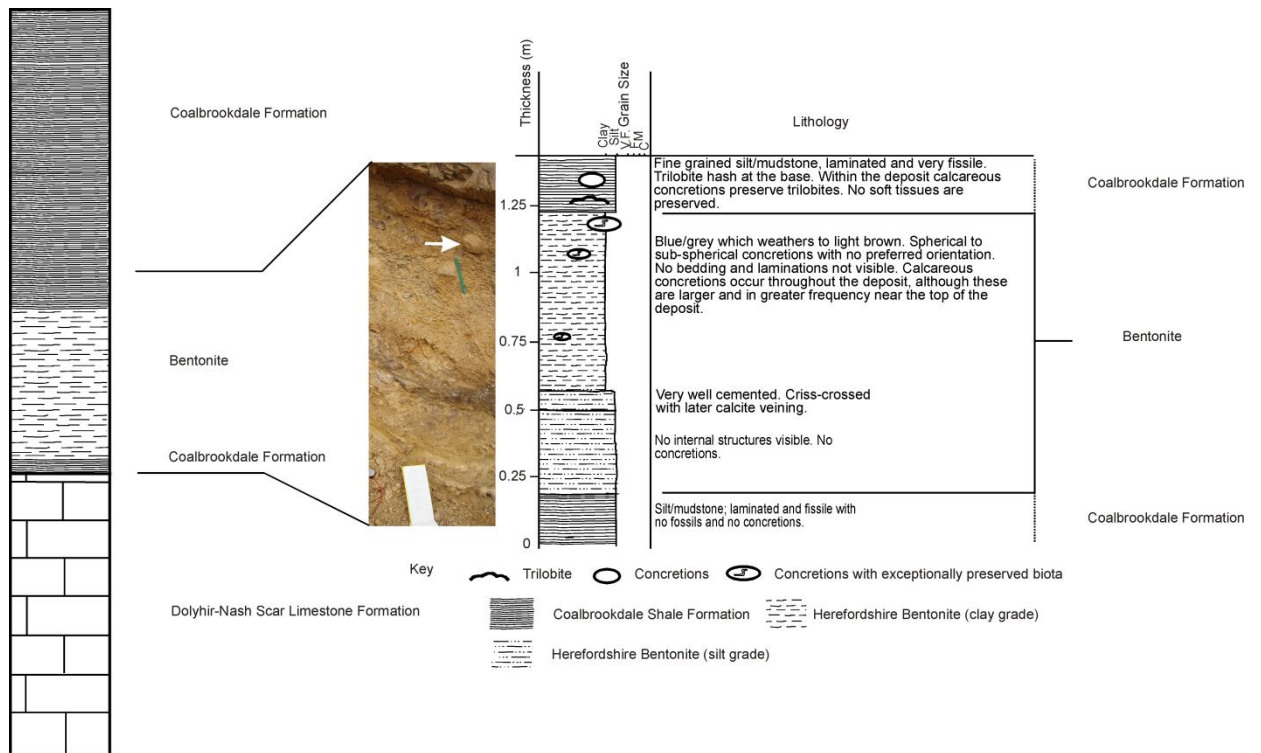


Figure 2.2: Sedimentary log of the host bentonite of the Herefordshire Lagerstätte and its position within the local lithostratigraphy. Arrow indicates concretions.

The base of the bentonite lies about 10 cm above the boundary between the Dolyhir-Nash Scar Limestone Formation and the Coalbrookdale Formation. A series of minor extensional faults (throw approximately 0.5 m) cut the upper contact of the bentonite.

The bentonite extends approximately 40 metres laterally with a maximum thickness of one metre. Its singular occurrence and limited lateral extent has been attributed to being deposited on an undulating sea floor in an outer shelf environment (Briggs *et al.*, 1996). However, the west contact of the host bentonite is a normal fault which has down thrown the host bentonite and the Coalbrookdale Formation against the Dolyhir-Nash Scar Limestone Formation, and the east contact has yet to be established. Therefore, it is worth considering that there has been a tectonic control on the distribution, and possibly on its thickness. The bentonite has been heavily weathered to a light brown colour. Concretions occur throughout the bentonite. Although, they appear to be slightly larger and more abundant in the thickest and central part of the

outcrop, within the top 30 cm (Fig. 2.3), a statistical test carried out on the spatial distribution of the concretions within the host bentonite (Chapter 4) indicates that the concretions are distributed randomly within the host deposit.



Figure 2.3: Image of the Herefordshire bentonite with concretions (painted blue), geological hammer is 28cm in length. (Photo David Siveter, August 1997).

The concretions are rounded to sub-rounded and are 5 mm to 200 mm in diameter. Only about 1 in 3 concretions contain fossils within them, but where they do occur the fossils are rarely found at the centre of the concretions. The concretions recovered are either completely weathered throughout and are a dull brown colour; some larger concretions (usually > 80 mm in diameter) are weathered on the outside but preserve a blue-grey unweathered heart (Fig. 2.4), and other concretions are completely unweathered.

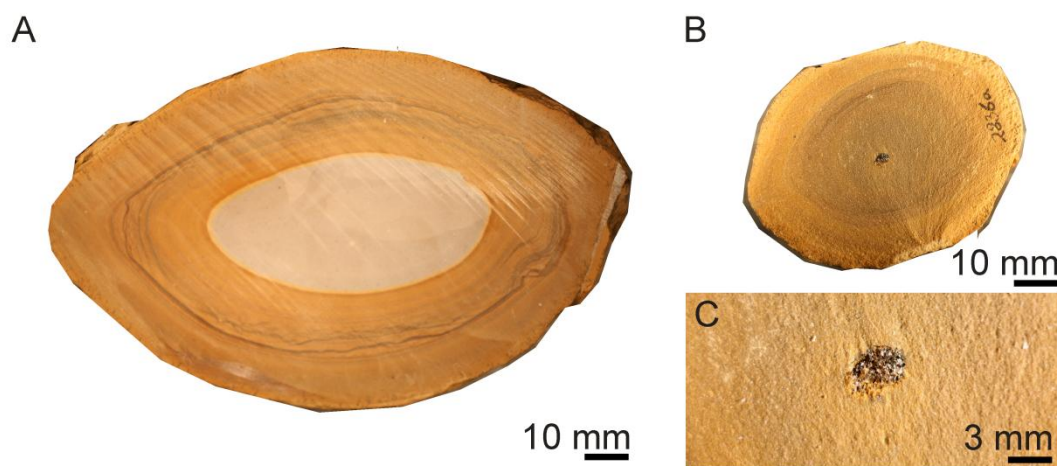


Figure 2.4: Example of the concretions and fossils recovered from the Herefordshire Lagerstätte. (A) Larger, partly weathered concretion with blue heart preserved; scale bar: 1 cm. (B) Smaller concretion, weathered through with a fossil at the centre; scale bar: 1 cm. (C) Fossil *Offacolus kingi* from B (OUM C.31314); scale bar: 3 mm.

MATERIALS AND ANALYTICAL METHODS

Thirteen samples of the bentonite and one concretion (11.5 cm in diameter 75 cm from the base of the bentonite) were collected from the exposure. The unweathered blue heart of the concretion was separated from the outer, buff-coloured, weathered material and both prepared for analyses. All the samples were dried and milled in a Retsch PM 400 Planetary Ball mill for 20 minutes at 260 rpm.

X-Ray Diffraction (XRD) analysis was conducted on a Phillips model PW1732 X-ray generator, with a PW1716 diffractometer and PW 1050/25 detector controlled by a PW1710 linked to a PC (Department of Geology, University of Leicester). A copper anode was used, with current conditions of 40 kV and 30 mA. Samples were scanned from 4° to 64° 2θ and at a step size of 0.02° 2θ at a speed of 1° /min. Angle calibration was by a synthetic silicon sintered standard. The scans were processed using GBC Scientific's Trace V6.7.13 software. XRD analysis was conducted on both whole rock and $< 2\mu\text{m}$ fractions.

X-Ray Fluorescence (XRF) analysis was conducted on a PANalytical PW 4400 Axios Advanced X-Ray Fluorescence spectrometer (Department of Geology, University of Leicester), with a 4Kw Rhodium (Rh) anode and a PC running PANalytical SuperQ software. Major elements were measured from fusion beads, while the trace elements were measured from 32 mm diameter pressed powder pellets (see Appendix A & B).

For petrographic analysis, samples were stabilised with epoxy resin before being prepared as standard, polished, uncovered thin sections. Thin sections were then carbon-coated prior to examination on a Hitachi S-3600N Environmental Scanning Electron Microscope (SEM), with an Oxford INCA 350 Energy-dispersive X-ray spectroscopy (EDX) system (Department of Geology, University of Leicester). The SEM was operated with a voltage of 15kV. Elemental mapping, point-and-ID chemical analyses were standardised against cobalt (99.99% pure sample). SEM Point-and-ID analysis is only semi-quantitative, but the extremely fine-grained nature of the sediment prevents meaningful analysis by electron microprobe. The EDX point-and-ID is able to resolve the compositions of silicates and carbonates in very fine-grained sediments.

COMPOSITION OF THE HOST BENTONITE

Petrology of the host bentonite

Whole rock XRD analysis of the host sediment samples indicated that quartz and clay minerals predominate, with two samples containing a minor trace of calcite. Analysis of the <2 μ m fraction showed the dominant clay species to be illite; there are also minor occurrences of smectite, kaolinite and chlorite. Mixed layer Illite-smectite inter-layering is only present within three of the samples analysed.

A quantitative list of minerals present (Appendix C) has been normalised from the XRF and XRD data. Normalisation of the data is a method which assigns a

particular element to a mineral that has been identified by XRD; from this, the percentage of the mineral is then calculated. Within all samples, clay minerals and quartz are the dominant phases.

Polished thin sections from the thirteen sediment samples were examined using the SEM and EDX analysis (see Appendix D for data). As evident from the Si-Ca-Al plot (Fig. 2.5A), the matrix of the bentonite is dominated by clay minerals and quartz, which concurs with the XRD data. There are also a few occurrences of calcium-rich minerals, which represent either calcium phosphate or calcium carbonate. Plotting the analyses rich in calcium on an Mg+Fe-Ca-P plot indicates a varying range of carbonate minerals present within the bentonite and also confirms the presence of apatite within the samples (Fig. 2.5B). Analyses with calcium percentages of 40 to 60 and iron/magnesium content of 40 to 60 represent ankerites ($\text{CaFe}^{2+}_{0.6}\text{Mg}_{0.3}\text{Mn}^{2+}_{0.1}(\text{CO}_3)_2$) or dolomites ($\text{CaMg}(\text{CO}_3)_2$), while minerals with a higher proportion of calcium represent calcites (CaCO_3). There is also a significant proportion of iron hydroxide within the samples as evident from the point-and-ID analyses (Fig. 2.5B). Iron hydroxide would account for the deposit's weathered brown buff colour, and commonly occurs as a coating around other grains. Minerals with a phosphorus content of between 40 and 50 percent represent analyses of calcium phosphates. Data were also plotted on the Velde and Meunier (1987) clay diagram (Fig. 2.5C) and this confirms the XRD analysis that the clay minerals present include kaolinite, illite, and chlorite.

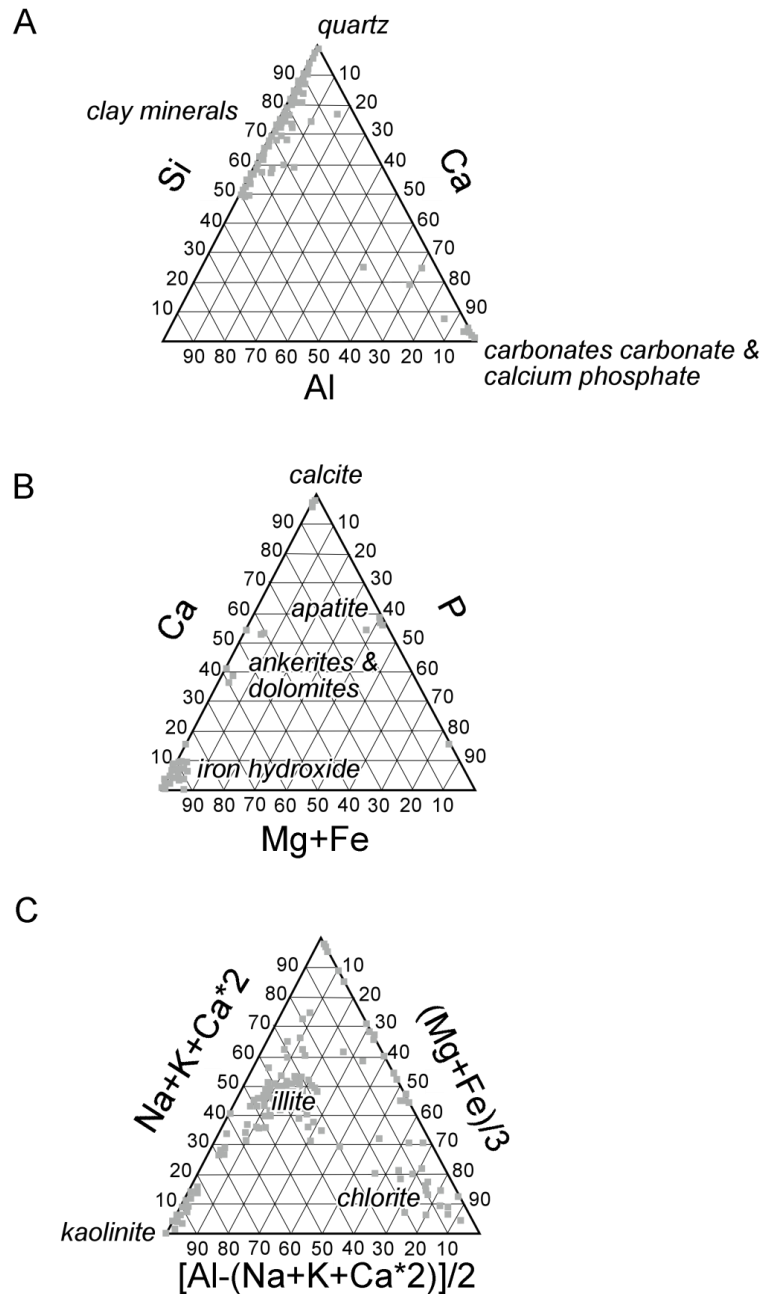


Figure 2.5: Triangular discrimination diagrams (A) Si-Ca-Al plot with fields for quartz, clay minerals, and carbonates. (B) Mg+Fe-Ca-P plot with fields for calcite, dolomite and calcium phosphate. (C) Velde and Meunier (1987) diagram for clay minerals with fields for kaolinite, illite and chlorite.

SEM backscatter analysis of the bentonite reveals a fine-grained matrix of interlocking quartz and clay minerals (Fig. 2.6A). In addition, there is also a minor occurrence of pyrite crystals; these may occur either as clusters of crystals, framboids or as isolated crystals. Coatings of iron hydroxide are also present along the grain

boundaries of some of the minerals (ih in Fig. 2.6A). Pyrite occurs in a variety of sizes (from 3 μm to $>50 \mu\text{m}$) as cubes (Fig. 2.6B), octahedra and, more rarely, spherulites. All the pyrite crystals examined also show iron and sulphur enriched cores (A in Fig 2.6B) relative to rims depleted in sulphur; Gabbott *et al.* (2004) observed similar features in the fossils of the Chengjiang (Cambrian) Lagerstätte from China and inferred the loss of sulphur to be a result of the alteration of pyrite crystals to iron oxides. This conclusion is also supported by the work of Rimstidt and Vaughan (2003), who demonstrated that during the weathering of pyrite, sulphur is oxidised, and as a result sulphur and iron(II) are released from the mineral lattice into solution. Ankerite crystals and the pyrite crystals (B in Fig. 2.6B) show ragged edges. This morphology can be accounted for either by pore fluid undersaturation during precipitation causing the mineral to redissolve into solution (Hall & Cullen, 1996; Geeslin & Chafetz, 1982), or by later weathering.

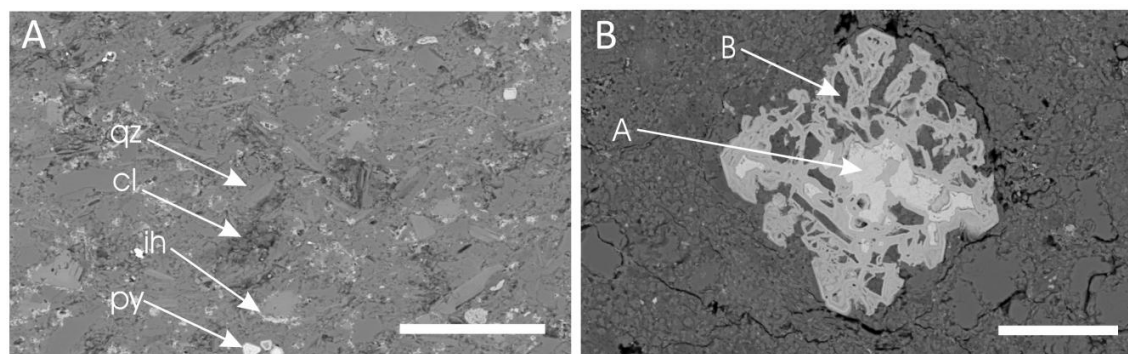


Figure 2.6: SEM backscatter image of bentonite matrix and pyrite crystals. (A) Fine grained matrix of interlocking clay minerals (cl) and quartz (qz); minor occurrences of pyrite crystals (py) and iron hydroxide (ih); scale: 50 μm . (B) Isolated cubic pyrite showing extremely ragged edges and variable iron content from centre (lighter grey) to the margin (darker grey); scale: 50 μm .

Some of the quartz within the bentonite is in the form of euhedral hexagonal crystals with straight edges (Fig. 2.7A), while other crystals demonstrate anhedral crystal habits with rounded edges (Fig. 2.7B). These different habits exhibited by the

quartz crystals represent their having different origins; the first originates from a volcanic source, whilst the latter has a detrital source (Dai *et al.*, 2008). In addition, euhedral, titanium rich minerals have also been found within the bentonite (Fig. 2.7C), as confirmed by EDX analysis (Fig. 2.7D) these are thought to be either rutile or anatase.

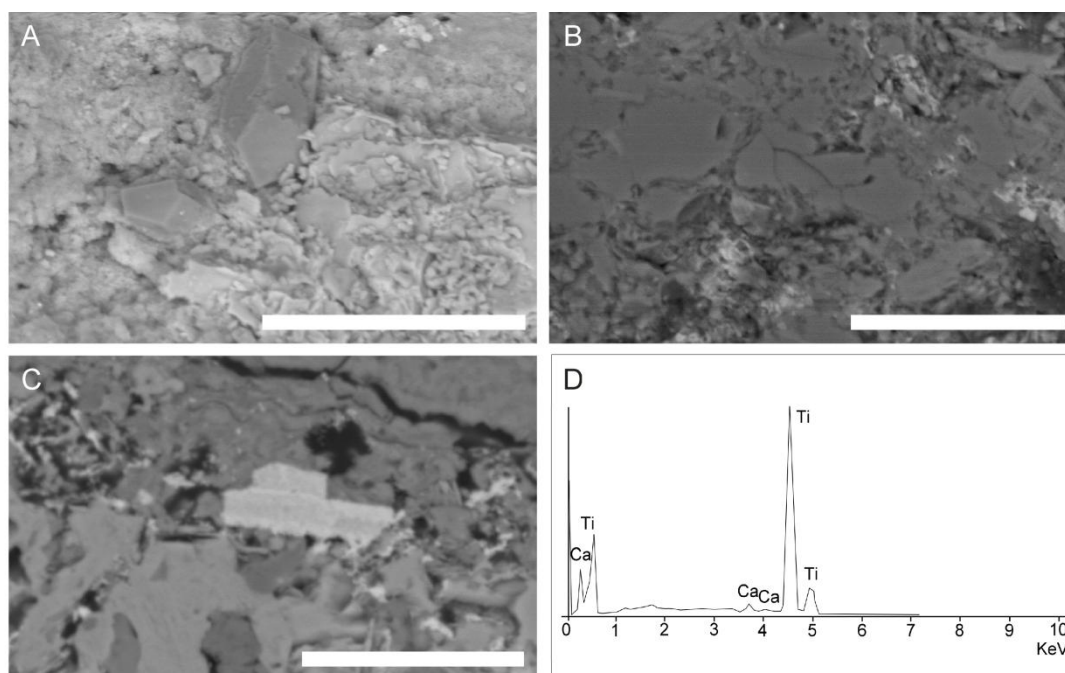


Figure 2.7: (A) Hexagonal quartz recovered from the bentonite; scale bar: 40 μ m. (B) Anhedral style quartz; scale bar: 20 μ m. (C): Euhedral titanium rich mineral; scale bar: 20 μ m. (D) EDX analysis of euhedral mineral shown in (C); note the prominent titanium peaks.

XRF and geochemistry of the host bentonite

Major and trace elemental analyses were conducted on all samples (Appendix E). Elements that remain immobile during the alteration process were utilised to determine the original volcanic composition of the deposit.

XRF data were plotted on geochemical classification and geotectonic discrimination diagrams. The Zr/TiO₂ versus Nb/Y plot (after Winchester & Floyd, 1977), using the GCDkit (Janoušek *et al.*, 2006), uses the immobile elements to

determine the original source of the rock. The majority of the samples from the bentonite cluster within the upper portion of the andesite field. Two samples plot in the rhyodacite field (Fig. 2.8A).

The triangular diagram (Wood *et al.*, 1979) uses the immobile elements of Th, Zr, and Nb to determine the tectonic setting of the source volcanism. It discriminates between destructive plate margins, constructive plate margins and within-plate volcanic rocks. The chemistry of the host bentonite of the Herefordshire Lagerstätte is characteristic of a destructive plate margin (Fig. 2.8B).

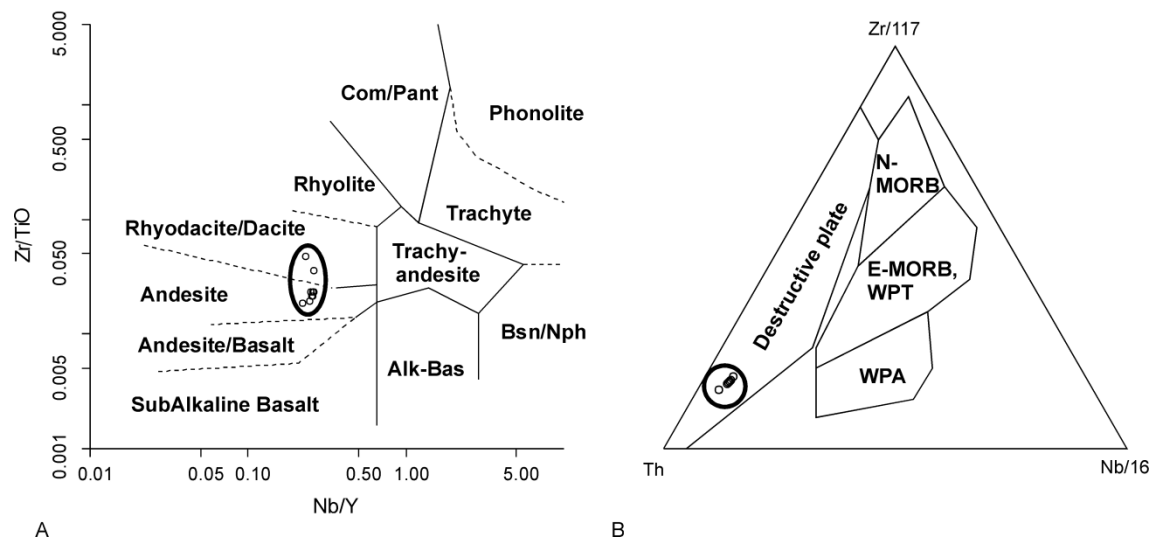


Figure 2.8: (A) Zr/TiO - Nb/Y discrimination diagram (Winchester & Floyd, 1977) showing that most samples from the host bentonite plot in the andesite field, with two in the rhyodacite/dacite field. (B) Th-Nb/16-Zr/117 ternary diagram (Wood, 1979) showing that the host bentonite originated on a destructive plate margin. In (A) the axes are Nb/Y ppm ratio and $(\text{Zr}/\text{TiO}_2) \cdot 0.0001$ ppm ratio. In (B) N-MORB = Mid-Ocean Ridge Basalt; E-MORB, WPT = E-type Mid-Ocean Ridge Basalts and Within Plate Tholeiites; WPA = Alkaline Within-Plate Basalts.

Major element data were normalised to average andesite (Fitton *et al.*, 1982) (see Appendix F for the average andesite composition) and then normalised again to aluminium (Fig. 2.9). Double normalising the data, to an average andesite and to aluminium, shows which elements are enriched and which are depleted relative to the average used. Normalisation is carried out to aluminium, because experimental work

has shown that aluminium only reaches a point of highest solubility at low pH (Spokes & Jickells, 1996). Therefore, aluminium can be considered relatively immobile under marine conditions.

The host bentonite and concretions display a distinct geochemistry: the concretions are highly enriched in calcium and manganese, whilst the host bentonite is slightly depleted in these elements, relative to average andesite. Both the concretions and the host bentonite are enriched in phosphorus although this may be due to the normalisation of the data. Magnesium is depleted in the host bentonite and the weathered concretion compared with average andesite. The weathered and unweathered concretion samples show enrichment in iron, due to the presence of iron-bearing carbonates such as ankerite and ferroan dolomite. Both the concretions and the host bentonite show heavy depletion in sodium (Fig. 2.9).

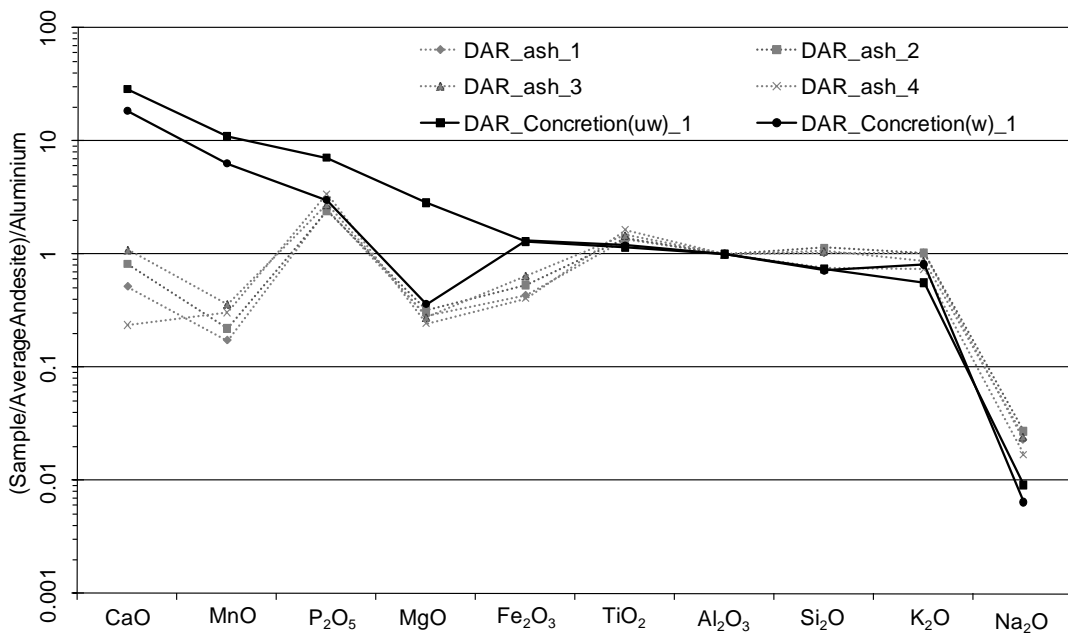


Figure 2.9: XRF data normalised to average andesite and then to aluminium. Note the calcium and magnesium enrichment in the unweathered concretion, compared with depletion in the host bentonite. Sodium depletion is also apparent within all samples.

Additionally, trace elemental data has also been normalised to the Coalbrookdale Shale Formation (Appendix F) sampled from the exposure, to establish how the bentonite differs from the surrounding strata. The results demonstrate that the bentonite samples are enriched in thorium, niobium, yttrium, and zirconium when compared to the Coalbrookdale Formation (Fig. 2.10).

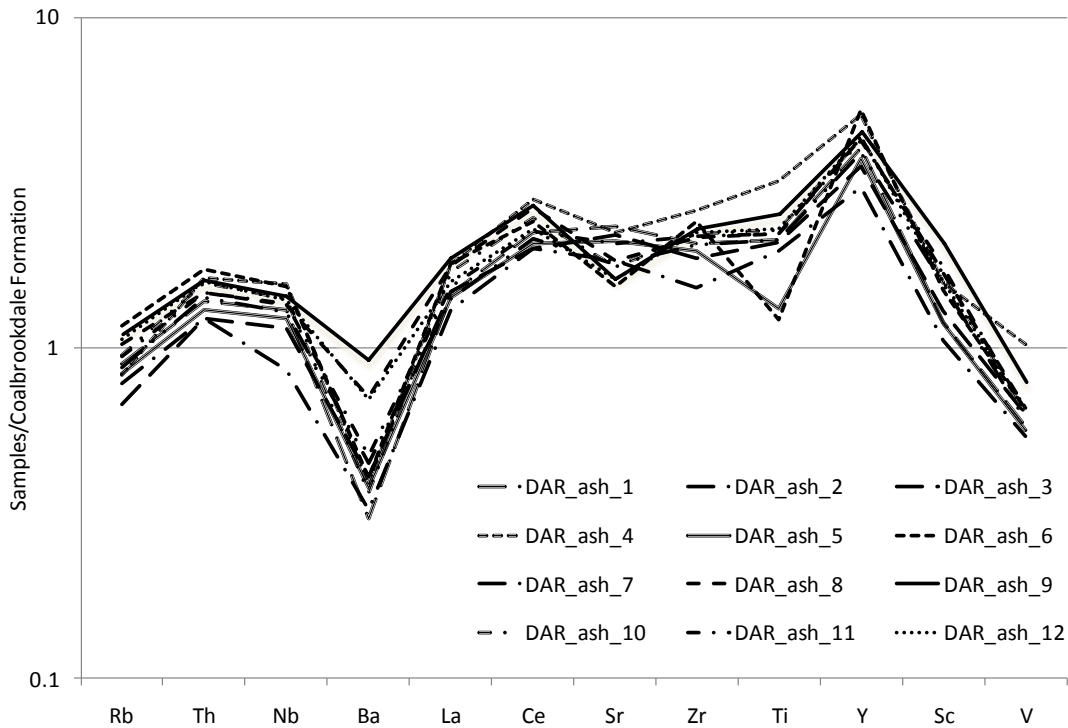


Figure 2.10: Shale of the Coalbrookdale Formation-normalised plots for selected elements. Note the enrichment of Nb, Y, Zr and Ti.

Analysis of conodonts recovered from the Dolyhir-Nash Scar Limestone Formation adjacent to the bentonite helps to infer the thermal history of the bentonite. Specimens of *Wurmiella excavata* were extracted by acetic acid processing (Richard Aldridge, pers. comm. 2010). Because of their composition and mode of growth, conodonts undergo systematic alteration during exposure to heat, which is characterised by recognisable changes in colour: these colour changes have been tabulated into a colour alteration index (CAI) (Königshof, 2003). The conodonts from the Herefordshire

Lagerstätte site are CAI 1, which infers that the deposit has not been subjected to temperatures over 80°C. This temperature range is also supported by the occurrence of smectite, which is usually altered to illite at higher temperatures. This palaeotemperature is also consistent with the palaeogeographic reconstruction (Fig 2.1), which indicates the site of the Herefordshire Lagerstätte is on the edge of the sedimentary basin and which therefore would not be subjected to the high temperatures experienced by the sediment in the centre of the basin.

DISCUSSION

Composition of the sedimentary deposit

The Herefordshire Lagerstätte was originally identified as being hosted by a volcanic ash by Briggs *et al.* (1996), and later Sutton *et al.* (2001a) revised this identification to a bentonite. This study has demonstrated that the host deposit has some characteristics consistent with other Welsh Borderland Silurian bentonites (Teale & Spears 1986). For example, when seen at the exposure, it has the sharp upper and lower contacts, a soapy-like texture, is blue/grey in fresh exposure and weathers to a light, brown buff colour. Mineralogical evidence such as the presence of smectite, which is a key component of bentonites, and identifiable illite/smectite mixed layer clays (Batchelor & Jeppsson, 1999) also confirms the volcanic origin of this sediment.

However, two habits of quartz crystals have been recorded within the deposit, which may indicate two possible sources. The euhedral habit of some of the quartz precludes a detrital source for these crystals and indicates a possible volcanic source whereas the rounded quartz component was most likely sourced from transported detrital grains and represents the weathering of quartz-bearing rock (see Dai *et al.*, 2008). The chlorite, and illite recorded by XRD analyses can also be attributed to input from a detrital clastic source (Kiipli *et al.*, 2008). The formation of illite by diagenetic

illitization is unlikely as the conodont CAI indicates that the Herefordshire Lagerstätte bentonite never reached above a temperature of 80°C, and illitization through diagenesis requires temperatures of about 100 and 140°C (Bjørkym *et al.*, 1993; Cuadros & Linares, 1996; Cuadros, 2006).

The clay mineralogical analyses conducted here demonstrate that the host sedimentary deposit is not a typical bentonite; the high illite:smectite ratio indicates that this deposit should strictly be classed as a metabentonite (Batchelor & Jeppsson, 1999). The occurrence of kaolinite within the bentonite along with the illite/smectite allows an estimate of the depositional depth to be made: Kiipli *et al.* (2008) noted that bentonites with an associated kaolinite and illite/smectite interlayering are typically formed in deep shelf environments. This is consistent with the outer shelf environment proposed by Briggs *et al.* (1996).

Geochemical evidence also supports the hypothesis that this deposit has a volcanic origin because of its enrichment in niobium, yttrium, zirconium, and titanium (Fig. 10) relative to the local Coalbrookdale Shale Formation. These elements are immobile during weathering and, as a result, the proportions recorded within the sediment represent the primary signature of the source of the deposit. Other minerals, which are typically enriched in immobile elements, and are characteristic evidence of a volcanic source, such as apatite, biotite, feldspar and zircons (Batchelor & Jeppsson, 1999) have yet to be found within the deposit and their absence may reflect the environment and processes of deposition. One of the possible methods of emplacement is as a pyroclastic flow (see Provenance and emplacement of the volcanic ash, below). Pyroclastic flows deposit their finest sediment distally from the source volcano (Yamada, 1984). If deposition occurred by pyroclastic flow, then the most dense minerals could have been winnowed out, leaving only the fine ash.

Provenance and emplacement of the volcanic ash

It would appear that the source for the Herefordshire Lagerstätte bentonite is different to other Welsh Borderland Silurian bentonites, as it has an andesitic derivation, whereas other bentonites in the region are more silicic (Fig. 2.11). For example, geochemical studies of the immobile elements, have demonstrated that the other Welsh Borderland Silurian bentonites originated from a rhyodacite to a rhyolitic volcanic source, which indicates that the magma source was not evolving in composition during the eruptions (Teale & Spears, 1986; Huff *et al.*, 1996). Huff *et al.* (1996) recorded 23 rhyodacite to rhyolitic bentonite horizons spanning the entire Wenlock Series and occurring stratigraphically above and below the position of the Herefordshire Lagerstätte. This demonstrates that the source volcano(es) of the Herefordshire Lagerstätte metabentonite did not usually furnish ash to the Welsh Basin.

There are two possible sources for the metabentonite material within reasonably close proximity of the Welsh Borderlands. During the Wenlock the Mendip Hills (Somerset) and the Dingle Peninsula (SW Ireland) were volcanic centres producing lavas and pyroclastic rocks with andesitic to rhyodacitic (van de Kamp, 1969) and basaltic to rhyolitic compositions (Sloan & Bennett, 1990), respectively. Both of these volcanic sources are geochemically consistent with the Herefordshire Lagerstätte and either of them could represent a possible source. However, it is questionable that these volcanic centres are too remote to produce a pyroclastic flow as described previously. In addition, a volcanic centre of Wenlock age also occurred in the Prague Basin of the Czech Republic. However, the 'diabasic' compositions of the lavas produced from this volcanic centre (Patočka *et al.*, 1993) are inconsistent as a possible source for the Herefordshire host sediment.

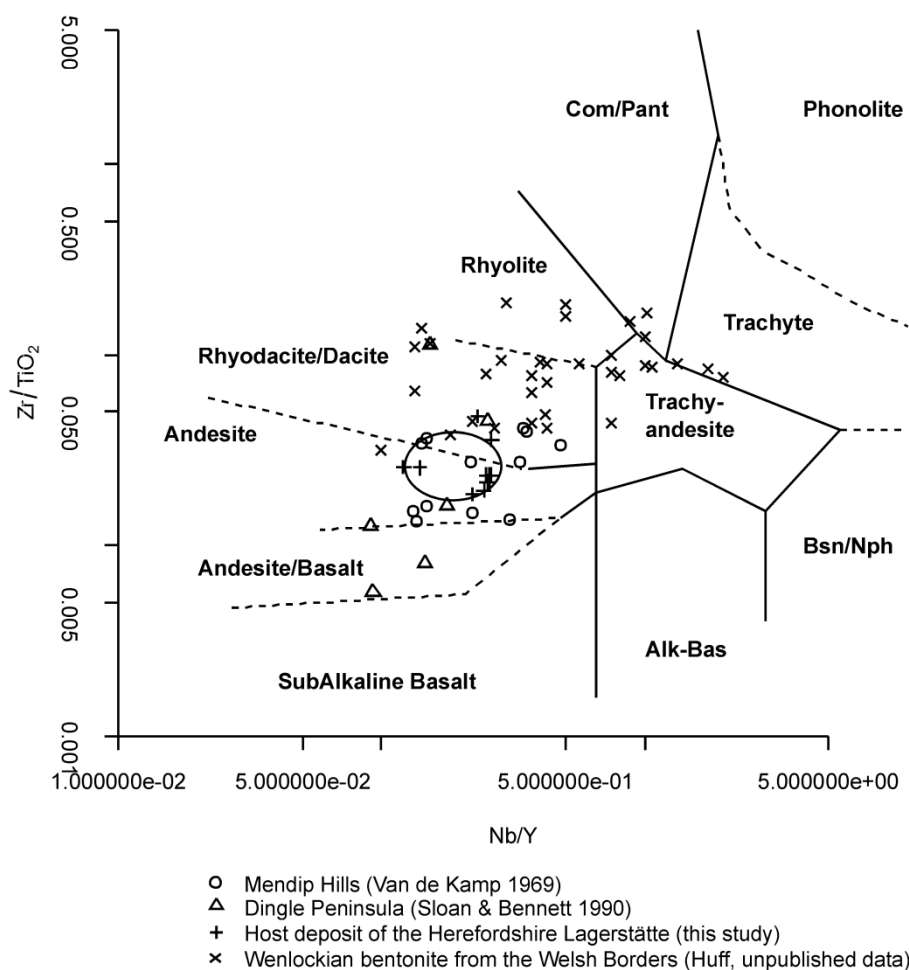


Figure 2.11: Winchester and Floyd (1977) diagram with Hereford data (circled) and other studies plotted on the GCDkit (Janoušek *et al.*, 2006). The host bentonite, data points circled, is chemically distinct from the other bentonites from the Welsh Borderlands of the same age, but is similar to those in the Mendip Hills and the Dingle Peninsula.

Bentonites are typically the products of gravitational deposition of volcanic ash (Slaughter & Hamail, 1970). The bentonites that occur throughout the Welsh Borderlands are consistent with this emplacement style, being thinly-bedded and laterally extensive over 3 km. Teale and Spears (1986) suggested that they represent the distal fallout deposits of a volcanic source northeast of the Welsh Borderlands.

However, the metabentonite host of the Herefordshire Lagerstätte is quite distinctive compared with other bentonites from the area (Table 2.1); it is massive and thick, limited in lateral extent, is currently only known from a single locality and is less silicic in composition.

Table 2.1: Comparison of the Herefordshire bentonite to the bentonites of the Welsh Borderlands

Other Welsh Borderlands bentonites	Herefordshire Lagerstätte host deposit
Rhyolitic †	Andesitic
Traced over 2-3 km*	Localised to 40m
concretions absent	Concretions
Thin (0.01 – 0.015 m*)	Thick (1 m)
Frequent occurrence†	Only occurrence

*Data from Teale and Spears (1986), † data from Huff *et al.* (1996).

There are five possible hypotheses for the emplacement of the host metabentonite: 1) deposition by an ash fall, from a single eruption phase; 2) deposition by an ash fall, from a succession of small fallout deposits; 3) deposition by a subaqueous pyroclastic flow; 4) re-deposition of the ash by a debris flow; or 5) a tectonic control on the sediment, post deposition.

Deposition of the ash through the water column by a single eruption event is unlikely as the Herefordshire metabentonite is unusually thick, which would require an as-yet unidentified nearby volcanic source. This is because there is a correlation between the thickness of an ash deposit and its distance from the source volcano (Fisher & Schmincke, 1984; Pyle, 1989). In addition, fallout deposits of the thickness of the Herefordshire metabentonite are usually associated with caldera collapse during the eruption of a super volcano (Martin & Bindeman, 2009); this is unlikely, as such an event would be evident globally, not just in Herefordshire.

Emplacement through a series of volcanic eruptions producing a succession of thin fallout deposits is equally unlikely. In this scenario, the gravitational settling of a fallout deposit through the water column (Fig. 2.12A2) would bury the biota on the

seafloor (Fig. 2.12A2) and subsequent lithification of this layer would allow it to be re-colonised by benthos (Fig. 2.12A3). Repetition of ash fall, burial of fauna (Fig. 2.12A4) and re-colonisation of the seafloor would be expected to produce a bedded deposit with concretions occurring throughout each bed (Fig. 2.12A5). The strongest argument against this method of emplacement, though, is that a deposit produced through a succession of volcanic eruptions would be traceable across a greater distance. This is especially so given that a typical bentonite in the Welsh Borderlands is 1.5 cm thick (cf. Teale & Spears 1986) whereas the Herefordshire Lagerstätte metabentonite is one metre thick. Additionally, work by Manville and Wilson (2004) indicates that the settling of volcanic ash through the water column has little impact on nektobenthic fauna because the high drag to low density ratio of ash particles results in low settling velocities. Moreover, Manville and Wilson (2004) also demonstrated that volcanic ash fallout rarely reaches the sea floor directly because the ash becomes entrained in a polydispersive suspension and is ultimately delivered to the sea floor as a dilute turbidity current, which spreads out in every direction.

This suggests that the unusually thick and localized nature of the host metabentonite is more consistent with emplacement through a sedimentary mass movement, such as a pyroclastic flow which developed into turbidity current on entering the water, or a debris flow from the reworking of sediment deposited upslope. In order to form a bed one metre thick, deposition possibly filled a pre-existing topographic low. Deposits from pyroclastic flows are typically thin on topographic highs, but thick within topographic lows (Scarpati *et al.*, 1993; Bryan *et al.*, 1998). Furthermore, in sedimentary mass movement, involving both turbidity currents and debris flows, the resulting deposits are thicker in topographic lows than on topographic highs.

A pyroclastic flow may be generated by the collapse of an eruption column, the collapse of a lava dome, or the interaction of an ash cloud with topography (Doyle *et al.*, 2008). Experimental work has demonstrated that when pyroclastic flows make the transition from land to water they divide into two portions: a fine ash cloud that travels on the surface of the water and a portion that travels through the water (Freundt, 2003). When a pyroclastic flow enters the water most of the pumice floats to the surface, the coarse ash and lithics settle out onto the sea floor, and the ash in suspension moves along the sea floor in a turbidity current (Freundt, 2003). Emplacement by a submarine pyroclastic flow would account for the fine-grained nature of the Herefordshire bentonite, as all the heavier clasts would have already settled out. Typically, a debris is characterized by a lack of internal structure, a sharp upper contact and a lack of inverse or normal grading at the base of the unit (Amy *et al.*, 2005), all of which occur in the host metabentonite.

The scenario of mass movement, either turbidity current or debris flow, requires transportation of the sediment and the fauna into the topographic low (Fig. 2.12B1) which would account for the apparent lack of fossils at the base of the bentonite. Transportation of fauna into the depositional environment would also potentially explain why nektonic fauna and the concretions occur towards the top of the deposit (Fig. 2.12B2). Transportation of the animals is unlikely to have caused any damage or distortion: experimental work by Alison (1988) has demonstrated that freshly killed soft-bodied animals can be buried within sediment and show no evidence of compaction or distortion, being unaffected by the weight of the sediment. It could be suggested that the fossils were preserved elsewhere and the Herefordshire bentonite represents a reworked deposit. However, this seems unlikely, as any transportation of the concretions would result in deposition with a preferred orientation. The lack of

orientation of the concretions therefore suggests that they formed post-depositionally (Fig. 2.12B3).

The fifth hypothesis, which might explain the unusual thickness and localisation, is one of a tectonic control. Situated to the East of the field site is the Welsh Borderland fault system (Fig. 2.1) and as already noted previously normal faulting is associated with the field site indicating previous periods of extension. During extension boudins can form through the process of boudinage, which can result in lens shaped bodies. However, it is more likely that tectonic activity has only played a minor role in developing the localised and limited outcrop of the host bentonite, by faulting out sequences of strata that have been subsequently eroded. Boudinage is not a suitable explanation for the extent and thickness of the deposit because boudins typically form from a ridged unit that is surrounded by a weak unit; on examination the host bentonite appears weaker than the surrounding Coalbrookdale Formation. In addition, had boudinage occurred then the trilobite hash preserved within the Coalbrookdale Formation (Fig. 2.2) would show evidence of distortion, and the concretions within the Herefordshire bentonite and Coalbrookdale Formation (Fig. 2.2) would be expected to show evidence of cracking or distortion.

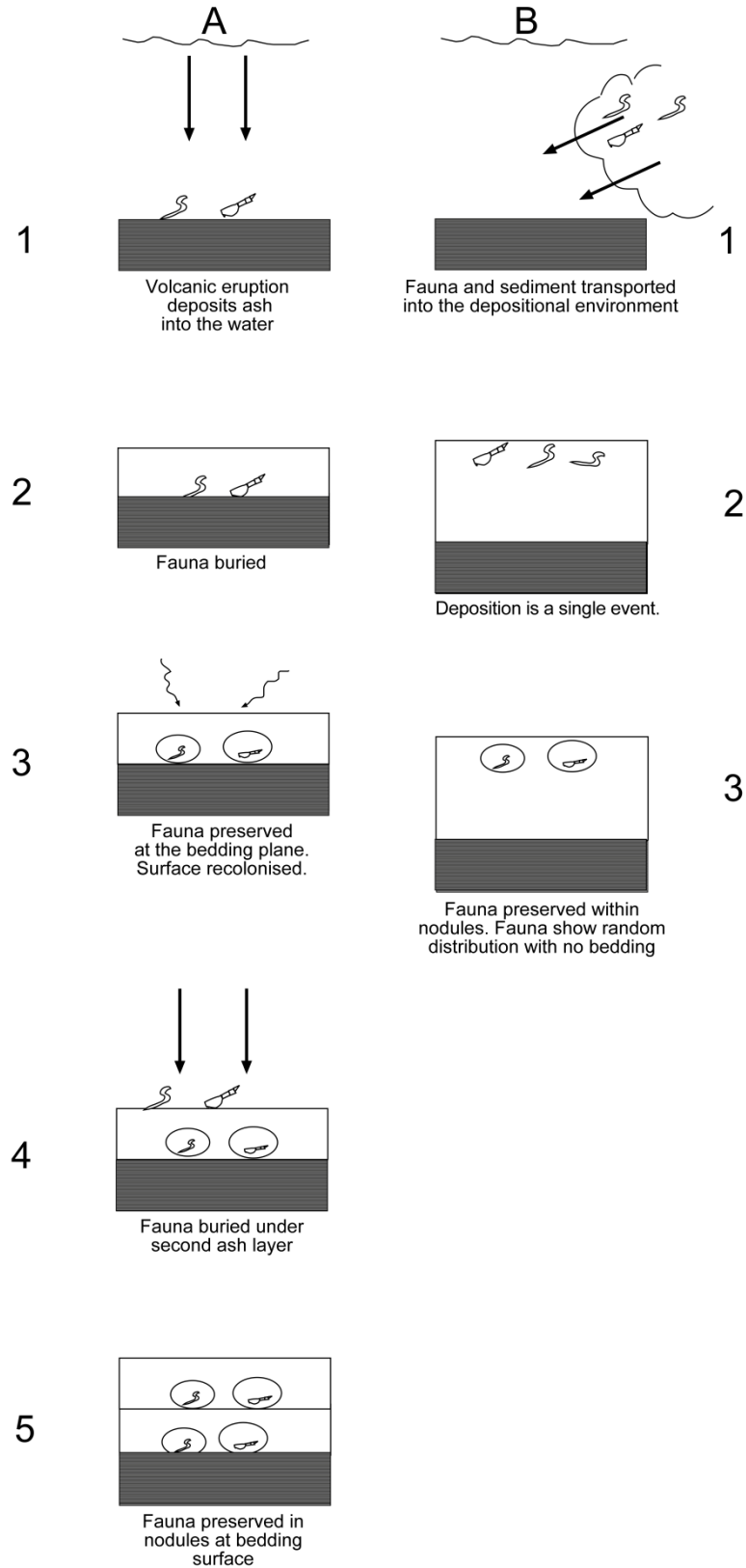


Figure 2.12: Possible emplacement method of the Herefordshire Lagerstätte bentonite. (A) a series of volcanic eruptions. (B) a debris flow or a turbidity current.

Significance of the host geochemistry to the taphonomy of the Herefordshire Lagerstätte

The style of preservation of the Herefordshire Lagerstätte appears to be unique. However, the preservation of carcasses by calcite infills of three-dimensional casts and their inclusion within the carbonate concretions may be in part explained by the chemical nature and enhanced reactivity of the ash.

Microscopic shards of volcanic glass, which form by the rapid crystallisation of magma during eruptions, are a key component of volcanic ash (Nakagawa & Ohba, 2002). Volcanic glass is very chemically reactive and as a result undergoes alteration, through a variety of cation exchanges, during early diagenesis within the upper layers of ash deposits (Kiipli *et al.*, 2008). Under experimental conditions volcanic material, when reacted with seawater, was seen to take up iron, magnesium and potassium, while sodium, calcium, and manganese were released from the suspended material into the pore fluid (Stefánsdóttir & Gíslason, 2006). The rate of this alteration is exceptionally rapid; the volcanic glass reached total dissolution within several hours (Oelkers & Gíslason, 2001).

The Herefordshire Lagerstätte host ash is andesitic in composition and as such contains the cations required to precipitate both the pure sparry calcite preserving the fossil and the carbonates, such as ankerite, dolomite and high magnesium calcites, which form the concretions. A rhyolitic ash, comprising of silica, aluminium, sodium and potassium, would have insufficient quantities of calcium, magnesium, iron and manganese required to produce the quantities of carbonate minerals required for this particular style of preservation. Furthermore, sparry calcite does not typically precipitate within marine settings because magnesium within the seawater poisons the nucleating crystal faces, resulting instead in the precipitation of fibrous calcite (Folk, 1974). Rapid absorption of seawater magnesium by volcanic glass would thus

encourage the formation of sparry calcite, which is an essential component of the exceptional preservation of the fossils of the Herefordshire Lagerstätte.

A further critical taphonomic pathway in the Herefordshire Lagerstätte is the formation of carbonate concretions enclosing the fossils. The lack of sodium in the host ash, as shown in the normalized plots (Fig 2.9), provides a possible means of increasing the pH of the pore water sufficiently to form carbonates rapidly. During early diagenetic alteration, the sodium may have been leached from the volcanic glass into solution: sodium ions would then have formed sodium hydroxide, which as a strong base would have increased the pH of the solution within the pore water. Carbonates may have existed within aqueous solutions and would have been present in one or more of the forms, CO_3^{2-} , HCO_3^- or H_2CO_3 . Of these three forms, CO_3^{2-} is the dominant form in aqueous environments that have an alkaline pH ($\text{pH} > 8$), such as may have occurred by rapid leaching of alkali metal ions into the pore fluid from volcanic ash. With the readily available CO_3^{2-} and the calcium leached from the volcanic ash, the pore fluid would have been supersaturated with calcium carbonate, resulting in the rapid precipitation of calcium carbonate.

This volcanic sediment appears to have played a very important role in the preservation of this Lagerstätte. Its emplacement has provided a suitable kill mechanism for the fauna, rapidly buried them, acted as a source of cations, and most importantly created a pore fluid with a pH that not only favoured the rapid formation of carbonates, but also removed inhibitors to the formation of sparry calcite.

THE TAPHONOMY OF THE SILURIAN HEREFORDSHIRE KONSERVAT
LAGERSTÄTTE (SILURIAN): THE EVOLUTION OF A
PRESERVATIONAL PATHWAY AS CONTROLLED BY EH-PH

Chapter abstract: *The Herefordshire Lagerstätte preserves three-dimensional fossils from a Silurian, fully marine, ecosystem. The entombment of the animals of the Herefordshire Lagerstätte within an andesitic ash appears to be key to the unique style of preservation exhibited here: andesitic ash being enriched in cations such as calcium, magnesium, manganese, and iron, all of which are essential to the preservation mechanism. The newly presented electron microprobe analysis demonstrates that the clay minerals observed, precipitated authigenically and that the composition of decaying organic matter can have an influence on their composition. A comparison of the preservation of *Kenostrychus clementsi* (polychaete) with decay experiments demonstrates the incompatibility of a void stage with this preservation mechanism. Instead, a direct replacement method is suggested, mitigating the need for a void stage. Newly acquired isotopic data indicates that the carbon originated from organic matter. The lack of iron within the calcite and the presence of manganese allows an estimation of the pore fluids Eh-pH, and the stepwise cation exchange during the alteration of volcanic ash with seawater provides a mechanism to keep magnesium out of the calcite crystals, which promotes the formation of sparry calcite. The absence of pyrite within these fossils further demonstrates the positioning on the Eh-pH diagram, suggesting that conditions were reducing enough for the substitution of manganese within the sparry calcite of the fossils but not enough to supersaturate the pore fluid with pyrite.*

The exceptionally preserved, three-dimensional fossils of the Herefordshire Konservat Lagerstätte record a fully marine, Silurian, ecosystem. Since its discovery in 1996 the deposit has yielded a diversity of taxa including a polychaete worm (Sutton *et al.* 2001c), a chelicerate (Orr *et al.* 2000b), ostracods (Siveter *et al.* 2003, 2007c, 2010), a pycnogonid (Siveter *et al.* 2004), a barnacle (Briggs *et al.* 2005), a crustacean (Siveter *et al.* 2007a), a marrellomorph (Siveter *et al.* 2007b), a lophophorate (Sutton 2011), a mollusc (Sutton *et al.* 2001a, 2001b), a gastropod (Sutton *et al.* 2006), and a brachiopod (Sutton *et al.* 2005). The fossils are three-dimensional and are composed of a sparry calcite infill within carbonate concretions, hosted within a fine-grained bentonite (Briggs *et al.*, 1996; Orr *et al.*, 2000a). The only study of the taphonomy and preservation of this Lagerstätte was conducted by Orr *et al.* (2000a); this study focused on the taphonomy of a single arthropod species, *Offacolus kingi*. Orr *et al.* (2000a) suggested that the biota were entombed within a fine grained volcanic ash, and that the decay of the soft tissues resulted in the formation of external moulds which were later filled with sparry calcite producing an accurate cast of the carcass. Subsequently fossils were incorporated into carbonate concretions (Orr *et al.*, 2000a).

This investigation aims to establish what role the volcanic ash had on the preservation pathway(s), to test the prevailing taphonomic model against other taxa, and to map the evolution of the preservation pathway(s) through Eh-pH space. Here I demonstrate that the complex and unique taphonomy in this Lagerstätte is principally controlled by the interaction of the carcass with the host ash. Linking the evolution of the Eh-pH environment through the process of decay and preservation is a novel approach in considering complex taphonomic pathways.

GEOLOGICAL CONTEXT

The host unit of the Herefordshire Lagerstätte is found well exposed within a single locality in a quarry in the county of Herefordshire, England. At the base of the exposure in the quarry is an algal limestone, the Dolyhir-Nash Scar Limestone Formation, and this is overlain by the Coalbrookdale Formation, which has a regional thickness of approximately 300 metres. Based on micropalaeontological evidence the Coalbrookdale Formation is of late Sheinwoodian to early Homerian age (Siveter *et al.*, 2007d), approximately 425 million years old. For a full description of the local stratigraphy, the reader is referred to Bassett (1974).

The host bentonite of the Herefordshire Lagerstätte occurs as a bed with limited lateral extent, entirely within the base of the Coalbrookdale Formation with which it has sharp lower and upper contacts (Fig. 3.1). The bed has a maximum thickness of one metre and has a visible lateral extent of 40 metres. The deposit has no noticeable bedding or sedimentary structures and its limited lateral extent, which has been attributed to deposition on an undulating sea floor in an outer shelf environment (Briggs *et al.*, 1996); though there are other possible controls responsible for its limited lateral extent and thickness (Chapter 2). The deposit is heavily weathered to a light brown colour, but appears a blue/grey colour when seen fresh. Use of immobile elements, in the methods described by Winchester and Floyd (1977), indicate that this bentonite originated from an andesitic source. Chemical analysis of the ash demonstrates it to be depleted in calcium, manganese, magnesium, iron and sodium (Chapter 2).

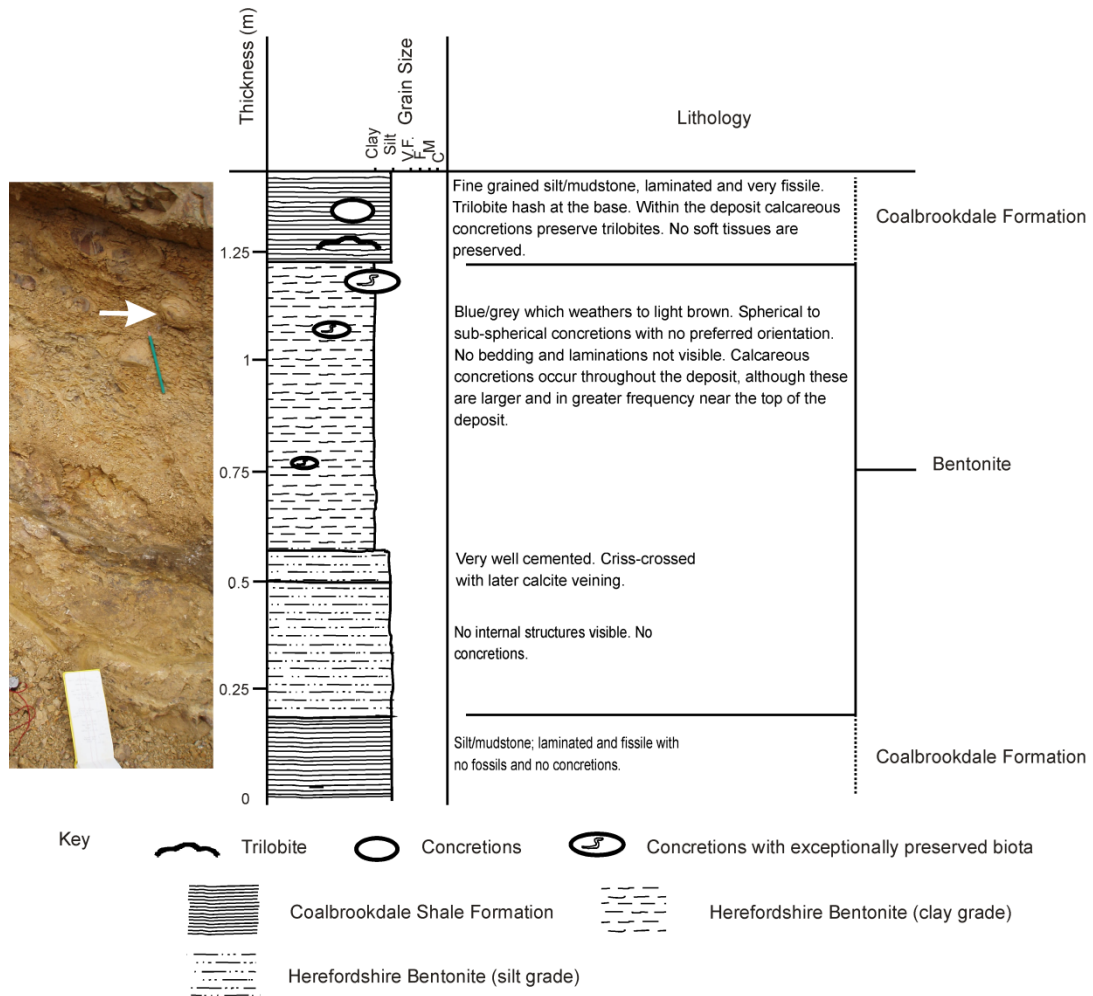


FIGURE 3.1— Log through host bentonite containing exceptionally preserved fossils

The concretions occur throughout the bed, but appear slightly larger and are more abundant towards the thickest part of the deposit, and within the top 30 cm. Concretion diameter varies from 5 mm to 200 mm; they are rounded to sub-rounded in shape. Not all the concretions contain fossils, but where they do occur, the fossils are rarely found at the centre of the concretion. Most concretions are completely weathered and are a dull brown colour; larger concretions (usually >80 mm) are also weathered but preserve a blue grey heart (Orr *et al.*, 2000a) (Fig. 3.2).

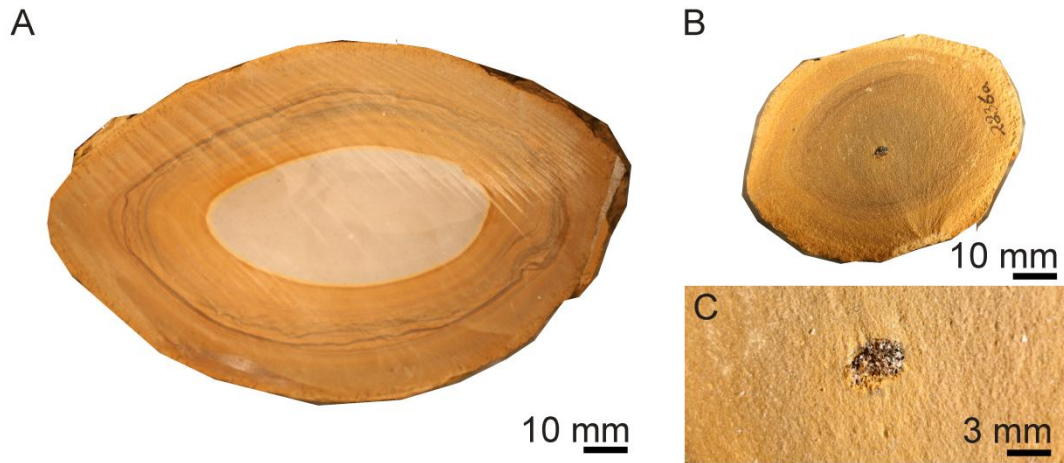


FIGURE 3.2— Example of concretions recovered from the bentonite. A) a partly weathered concretion with a blue heart. B) smaller weathered concretion; note the fossil at the centre of the concretion. C) an example of a fossil within a concretion, this specimen is *O. kingi* (OUM C.31314).

MATERIALS AND METHODS

Fossil-bearing concretions were cut and prepared as standard, uncovered polished thin sections, which contained the fossil and the adjacent concretion matrix. The four specimens selected for this study represent the most common faunal elements in the Lagerstätte. The specimens are all three-dimensional, but there is slight variation in the degree of compaction exhibited between the specimens within each taxon. The arthropods selected for this study were *Tanazios dokeron* ($n = 3$), and *Offacolus kingi* ($n = 4$). Both have been previously identified as non bio-mineralized arthropods (Siveter *et al.*, 2007a; Orr *et al.*, 2000b) and were most likely comprised of a chitinous exoskeleton; a polysaccharide carbohydrate within a proteinaceous matrix which is resistant to decay (Gabbott, 1998). *Acaenoplax hayae* ($n = 2$), a worm-shaped mollusc (Sutton *et al.*, 2001a), was originally covered by valves that were thought to be aragonitic in composition although the rest of the body was thought to be cuticular (Sutton *et al.*, 2001a). These specimens represent those most resilient to collapse of the four taxa being studied and as a result show very little evidence of distortion.

Kenostrychus clementsi (n = 3), an annelid (Sutton *et al.*, 2001c), was not biomineralized, and in life comprised a flexible collagenous cuticle. These specimens show varying degrees of collapse, which indicates that the specimens were in various stages of decay— while some specimens only show slight collapse, other specimens terminate abruptly with no evidence of the end body segment. Table 3.1 summarises these details.

TABLE 3.1— Summary of fossil preservation from the Herefordshire Lagerstätte. OUM = Oxford University Museum of Natural History catalogue numbers of specimens used in this study.

Fossils	OUM Number	Original Composition	Fossil Composition	Mode of Preservation
<i>O. kingi</i> (Arthropoda)	C.31314, C.29508, C.29506, C.29507	Chitinous	Sparry Calcite	Mouldic, Replacement
<i>T. dokeron</i> (Arthropoda)	C.31304, C.31306 & C.31307	Chitinous	Sparry Calcite	Mouldic, Replacement
<i>K. clementsi</i> (Polychaeta)	C.31302, C.31303 & C.31305	Collagen	Sparry Calcite	Mouldic, Replacement
<i>A. hayae</i> (Mollusca)	C.31300 & C.31313	Cuticle/aragonite valves	Sparry Calcite	Mouldic, Replacement

Analysis of the clay minerals associated with the fossils and within the concretion matrix were carried out on a Jeol JXA8600 Superprobe (Department of Geology, University of Leicester), using an operating voltage of 15 kV, and a beam current of 30 nA. A beam diameter of 30 µm was used to limit the amount of potassium vaporisation during the analysis. The clay accumulations adjacent to the fossil were analysed and clay within the concretion matrix was similarly analysed and its distance

from the fossil was recorded. The size of the clay accumulations analysed had to be sufficiently large to accommodate a microprobe beam diameter of 30 μm .

Cathodoluminescence was carried out on a Technosyn cold cathodoluminescence stage (model 8200 Mk II) attached to a Nikon microscope. Images were recorded on a Nikon Coolpix™ 4100 digital camera. Cathodoluminescence (CL) is a technique used to examine minor compositional variations within carbonate rocks. Manganese is the most important activator of luminescence while iron is the principle quencher of luminescence. However, caution must be used when interpreting CL images, as manganese ions have the ability to self-quench luminescence and calcite weathering may affect the luminescence pattern (Boggs & Krinsley, 2006). Cathodoluminescence can demonstrate zonation within crystals that precipitate from an evolving pore fluid. It is a useful technique to examine re-crystallised material, as carbonates precipitated from seawater rarely show any luminescence due to the lack of manganese substitution within the calcite structure (Boggs and Krinsley, 2006).

Analysis of the fossil and concretion matrix carbonate was carried out on a Hitachi S-3600N Environmental Scanning Electron Microscope (Department of Geology, University of Leicester). Chemical analysis was undertaken using an Oxford INCA 350 EDX system, providing elemental mapping and point-and-ID spectrum. The system operated with a voltage of 15kV; the semi-quantitative chemical analysis from the SEM was calibrated against a 99.99% pure cobalt standard.

Stable isotope analysis was carried out on four unidentified fossil specimens. 10 mg of calcite was drilled out and reacted with anhydrous phosphoric acid under a vacuum for 72 hours at a constant 25°C (this is sufficient to react all of the calcium and magnesium carbonates including dolomite). The carbon dioxide liberated was separated

from water vapour under vacuum and collected for analysis. The carbon dioxide was measured on a VG Optima mass spectrometer at the NIGL laboratory, Keyworth. Isotope values ($\delta^{13}\text{C}$, $\delta^{18}\text{O}$) are reported as parts per mil (‰), with deviations of the isotopic ratios ($^{13}\text{C}/^{12}\text{C}$, $^{18}\text{O}/^{16}\text{O}$) calculated to the VPDB scale using a within-run laboratory standard calibrated against NBS standards.

RESULTS

The results of chemical analyses, summarised in Table 3.2, are arranged below to reflect the sequence of events, from early through too late, which resulted in exceptional preservation.

TABLE 3.2— Summary of fossil preservation

Species	Animal group	Fossil composition	Clay localisation	Clay composition	Calcite impurities	Iron species
<i>O. kingi</i>	arthropod	sparry calcite	tergites	illite:kaolinite	+Mn, - Fe, - Mg	pyrite & iron hydroxide
<i>K. clementsi</i>	polychaete	sparry calcite	parapodial	illite:kaolinite	+Mn, - Fe, - Mg	pyrite & iron hydroxide
<i>T. dokeron</i>	arthropod	sparry calcite	appendages	illite:kaolinite	+Mn, - Fe, - Mg	pyrite & iron hydroxide
<i>A. hayae</i>	mollusc	sparry calcite	body	kaolinite:illite	+Mn, - Fe, - Mg	pyrite & iron hydroxide

Clay Mineralisation

Clay mineralisation is found associated with all of the specimens examined and typically surrounds the fossils as a thin layer (approximately <1 μm thick). However,

clay mineralization is thickest and more extensively developed when associated with anatomical features that extend beyond the main body margin, such as spines or appendages. For example, clay mineralization is most extensive: between the appendages of *T. dokeron*, associated with the spines that project from the aragonitic valves in *A. hayae* (Sutton et al., 2004a), and between the laterally-positioned parapodial structures in *K. clementsii*. However, in *O. kingi* clay minerals are most extensive between the tergites.

Clay minerals associated closely with the fossils, and those within the concretion matrix, but unassociated with the fossil, were analysed using EMPA (Appendix H). In order to distinguish different clay phases, data were plotted on a graph of K/Al versus Si/Al (Fig 3.3). Figure 3.3 demonstrates clearly that the clay minerals associated with fossils are intergrowths of kaolinite and illite.

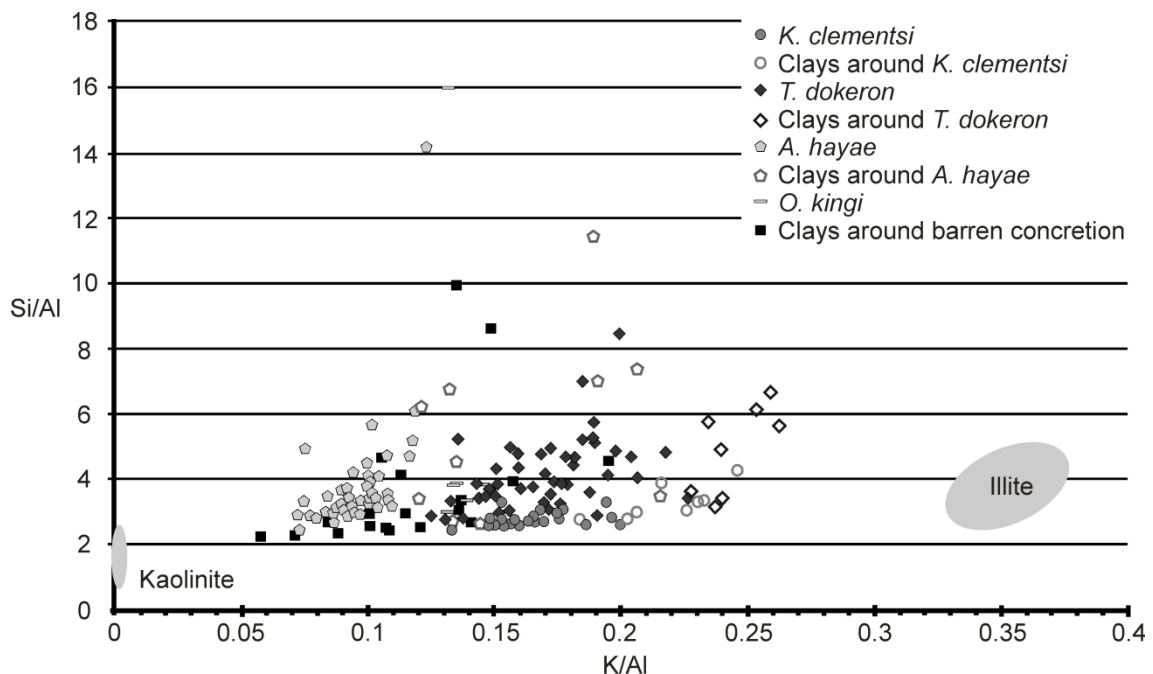


FIGURE 3.3— K/Al vs. Si/Al plot with the idealised kaolinite and illite compositions shown as grey fields. Note there are some abnormally high values on the Si/Al axis indicating that there are possible intergrowths of chalcedony or quartz.

Clay composition appears to vary between the specimens; from the clay analyses two groups can be identified (Fig. 3.3). *A. hayae* is associated with clays that are more kaolinitic than those associated with *K. clementsi*, *T. dokeron*, and *O. kingi*, which are chemically more illitic in composition. Clays analysed from the barren concretion demonstrate the greatest range along the K/Al axis, suggesting that they are more varied in the composition of their clay minerals.

Calcite Mineralisation

All specimens have their anatomy principally preserved as calcite, the euhedral habit of which is identical across all the taxa studied; larger (approximately 2 mm in length) coarse crystals occur within the centre of the fossil and smaller (approximate 0.18 mm in length) micro-granular calcite occurs towards the margins. Chemical analyses, via EDX, of all the calcite within the taxa examined demonstrate that crystals contain no significant concentrations of iron and magnesium (Fig. 3.4A, B, C), but that they do contain a significant quantity of manganese (Appendices I-L). In addition, some specimens of *O. kingi* have been shown, by EDX, to have an elevated content of manganese within the micro-granular calcite at the edge of the fossils (Fig. 3.4E, F). In addition, *O. kingi* and *K. clementsi* specimens have calcium phosphate locally precipitated within the centre of the fossils. These local occurrences of calcium phosphate are likely to be biologically mediated by native microbial activity in the gut (Fig. 3.4G, H, I) (Orr *et al.*, 2000a; c.f., Wilby and Briggs, 1997). SEM backscatter imaging and EDX has also identified the occurrence of pyrite as isolated crystals in all of the specimens analysed, which are located near the margin of the fossils. However, the majority of the iron is present either as iron hydroxide, which has coated grains

within the matrix, or as ankerite ($\text{CaFe}(\text{CO}_3)_2$) or dolomite ($\text{CaMg}(\text{CO}_3)_2$) within the matrix.

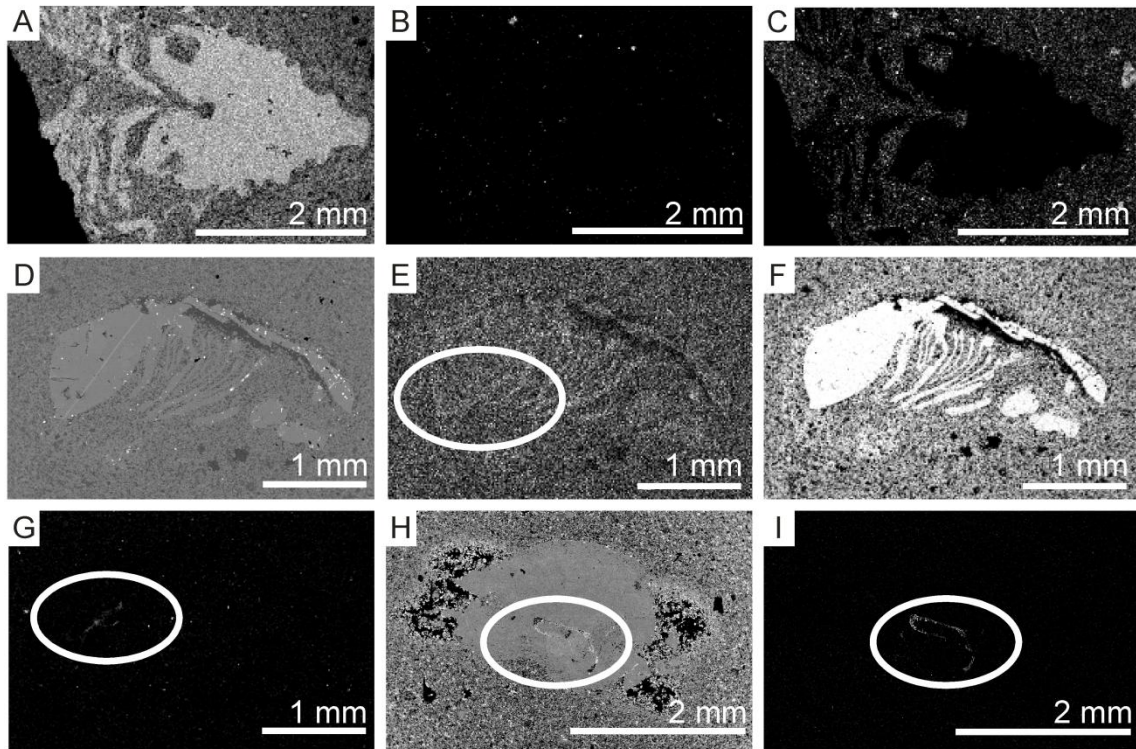


FIGURE 3.4— Representative SEM backscatter images and EDX maps of *T. dokeron* (A-C), *O kingi* (D-G) and *K clementsii* (H,I). A. Calcium distribution. B. Iron distribution of *T. dokeron*. C. Magnesium distribution of *T. dokeron*. D. Backscatter image, note that its almost indistinguishable from the surrounding matrix. E. Manganese distribution of *O. kingi*, note that the circled area shows the crystals at the edge of the fossil enriched with manganese. F. Calcium distribution of *O. kingi*. G. Phosphorus map of *O. kingi*, note the circled area enriched in phosphorus. H. Phosphorous map of *K. clementsii*, note the circled area rich in phosphorous. I. Backscatter image of *K. clementsii*, note the circled area which is enriched in phosphorus.

Taxa are characterized by two distinct styles of luminescence. One style of luminescence, only apparent in the specimens of *O. kingi*, is patchy and this suggests that the precipitation of the calcite within the carcass did not occur in a uniform manner (Fig. 3.5A, B). The patchy luminescence includes a dull luminescing calcite at the margin of the specimens (Fig. 3.5C, D); this was also identified by Orr *et al.* (2000a). As Orr *et al.* (2000a) noted, these crystals correspond to the areas enriched with manganese (see Figure 3.4E), and they suggested that a corresponding enrichment of

iron may have been the cause of the dull luminescence. Another possible explanation for the dull luminescence may be that manganese self-quenches because it occurs with sufficient concentration to inhibit its own luminescence (Boggs and Krinsley, 2006).

The second style of luminescence is shown by the specimens of *K. clementsi*, *T. dokeron* and *A. hayae*. All three show a distinct banding pattern that mimics the shape of the perimeter of the fossils (Fig. 3.5E-G). In each fossil the calcite at the centre is coarse sparry calcite (SC in Fig. 3.5H), which has the same luminescence as the microgranular calcite at the fossil margin (MC in Fig. 3.5H). This infers that both these calcites precipitated from a pore fluid with the same chemical composition. However, between the sparry calcite and the microgranular calcite there are two bands with distinct luminescence. The band juxtaposed to the sparry calcite is characterized by euhedral calcite with dull luminescence (Y in Fig. 3.5H); peripheral to this is a band which is very dull, almost black under luminescence, comprising anhedral crystals (Z in Fig. 3.5H).

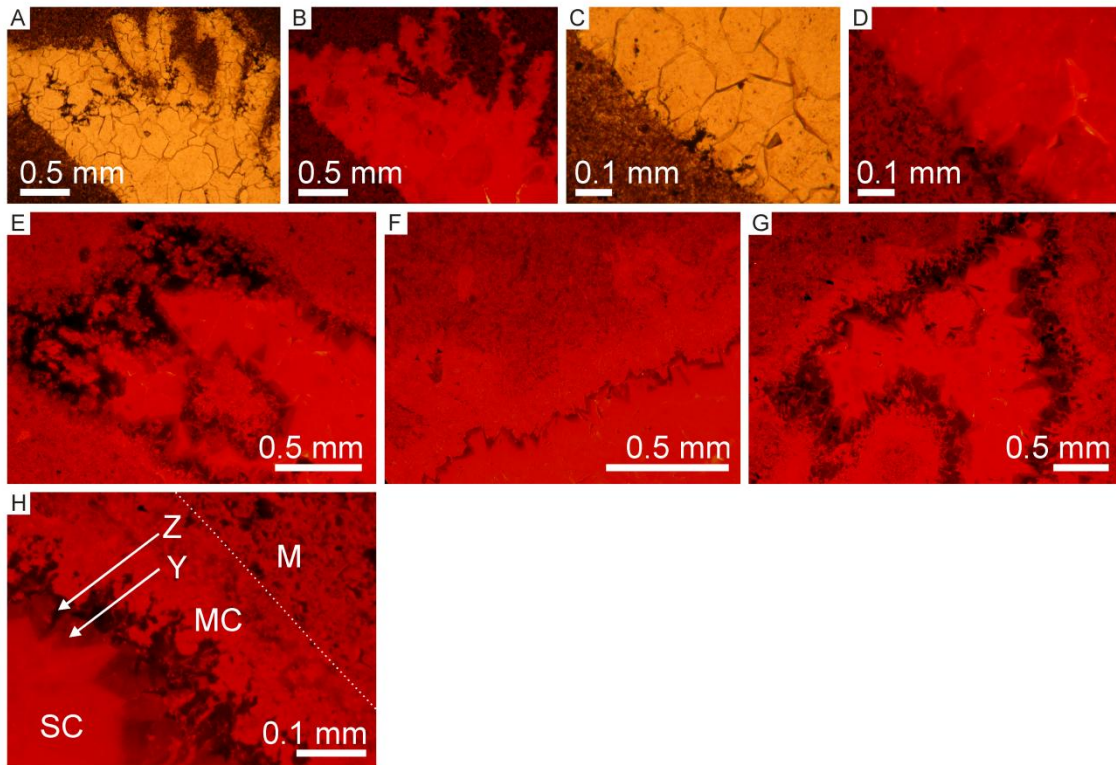


FIGURE 3.5— Representative cathodoluminescence (CL) and plain-polarised light images of the fossil fauna. A. Plain-polarised light image of *O. kingi*. B. CL image of *O. kingi*, note the patchy appearance. C. Plain-polarised light image of the margin of *O. kingi*. D. CL image of the margin of *O. kingi*, note the dull luminescence at the margin of the fossil. E. CL image of *A. hayae*, note the relative uniform luminescence within the centre of the fossil. F. CL image of the margin of *A. hayae*, note the dark band that runs along the edge of the fossil. G. CL image of *T. dokeron*, note the dark band associated with the margin of the fossil. H. CL image of margin of *K. clementsii*. Note the sparry calcite (SC) and the microgranular calcite (MC), the two different types of calcite in between (Y and Z) and the matrix (M).

Sparry Calcite Stable Isotope Analysis

A preliminary carbon and oxygen isotope analysis was carried out on the sparry calcite from four unidentified fossils of the Herefordshire Lagerstätte (Table 3.3).

TABLE 3.3— Preliminary isotope study of fossil calcite

Specimen	$\delta^{13}\text{C}$	$\delta^{18}\text{O}$
HF1	-11.83	-6.97
HF2	-2.25	-8.03
HF3	-13.10	-7.67
HF4	-17.31	-7.43
Average	-11.12	-7.53
Standard Dev	6.361	0.446

All data relative to PDB standard.

The oxygen isotopes obtained from the calcite specimens were all found to be enriched in oxygen-16 (i.e., they were all isotopically light). Azym *et al.* (1998) examined brachiopods from the entire Silurian Period, and from the specimens that were the best preserved, most likely to preserve a primary isotopic signature, recorded a $\delta^{18}\text{O}$ range of -2‰ to -6.5‰ (PDB). The calcite analysed within this study are therefore considerably lighter than brachiopods from the Silurian. In terms of their relationship to seawater, estimates for the oxygen isotopic values for the Silurian are about -3.5‰ standard mean ocean water (SMOW) (Azmy *et al.*, 1998), so, the $\delta^{18}\text{O}$ values recorded within calcite fossils are lighter than estimates of Wenlockian seawater. Carbon isotope data were more varied between the specimens, but with the exception of HF2 the carbon isotopes indicated that the calcites were significantly enriched in light carbon from organic matter. The heavier carbon within sample HF2 infers that organic matter was not the primary provider of the carbon and it may have originated from another carbon reservoir such as Wenlockian seawater.

Concretion Matrix

The matrix of the concretions is revealed by SEM backscatter to be an interlocking mosaic of minerals. EDX analysis has confirmed the presence of quartz

(and chalcedony) and carbonate minerals (including ankerite, ferroan dolomite and magnesium calcite) and clay minerals. The ankerite crystals are euhedral and are often associated with poorly crystalline dolomite. Crystal boundaries between dolomite and calcite are ambiguous and poorly defined. EMPA analyses of clay minerals shows them to have a composition representing a mix of interlocking kaolinite and illite (see Figure 3.3). Pyrite crystals were found to occur only rarely.

DISCUSSION

Decay

An assessment of the degree of decay, and thus anatomical loss, prior to the preservation of these fossils may be estimated via comparison of *K. clementsii* with decay experiments on polychaetes (Briggs & Kear 1993). Briggs and Kear (1993) recorded six stages of decay in polychaetes: freshly killed, whole/shrivelled, flaccid, loss of the supported gut, retention of just the cuticle sac/jaws and finally the retention of only the jaws/setae. *K. clementsii* is three-dimensional and has begun to show the early signs of trunk collapse; on comparison with decay experiments this is consistent with exceptional preservation occurring within 2 to 4 days post mortem. However, this time period does not take into account any retardation of the decay process that may have occurred (see below). In addition, *K. clementsii* preserves the gut dorsally in life position (Fig. 3.6). Gut collapse occurs after day 4 in decay experiments, again suggesting a narrow window post mortem prior to fossilization. The exact point of mortality cannot be pinpointed; escape tracts preserved within the concretions indicates that some of the animals were alive shortly after burial, but the variable state of collapse

identified within the specimens of *K. clementsii*, (see previous) infers that some of the animals may have been dead prior to deposition of the bentonite.

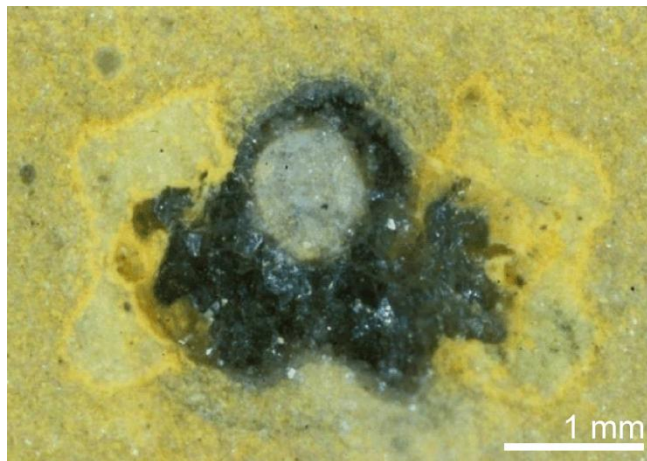


FIGURE 3.6— Transverse section of *K. clementsii*. Note the circular feature in the centre.

(Photo David Siveter, Derek Siveter, Mark Sutton and Derek Briggs)

However, more crucially, the presence of the gut in life position is incompatible with a void occurring at any stage in the taphonomic pathway(s) (see Orr *et al.*, 2000a). This is because the gut, even if preferentially preserved, would have collapsed within a void, leaving it coincident with the body margin.

Clay Mineralisation

Interestingly, three of the taxa examined (*T. dokeron*, *K. clementsii* and *O. kingi*) are characterised by more illitic clay mineral accumulations, whereas *A. hayae* is characterised by more kaolinitic clay (see Table 3.2). To identify if this difference is significant, the K/Al component of the clay mineral analyses associated with *T. dokeron* and *A. hayae* was subjected to a two way T-test (Table 3.4). The analysis of *K. clementsii* and *O. kingi* were not subjected to the statistical test, because of the limited

availability of clay patches within the samples analysed meant the number of analyses collected were not equal and would consequently not make a fair and meaningful test.

TABLE 3.4— Two way T-test to statistical test for a difference between the K/Al ratio of the clay minerals in *T. dokeron* and *A. hayae*

	<i>Tanazios dokeron</i> K/AL	<i>Acaenoplax hayae</i> K/AL
Mean	0.169277189	0.09284702
Variance	0.000568164	0.000117671
Observations	47	47
Pooled Variance	0.000342918	
Hypothesized Mean Difference	0	
Df	92	
t Stat	20.00800221	
P(T<=t) one-tail	1.42086E-35	
t Critical one-tail	2.367565735	
P(T<=t) two-tail	2.84171E-35	
t Critical two-tail	2.630329602	

The T-test calculated is greater than the critical t value for the degrees of freedom. Therefore, these clays represent two statistically different populations and the two samples have less than a 99 per cent probability of being from the same population.

As the variation between these two groups is a function of the K/Al ratio, it denotes the presence of a control on the chemical pathways leading to their formation. A possible explanation is that the chemistry of organic matter decay products differed across taxa and thus may have controlled the authigenic clay mineral formation. Gabbott *et al.* (2001) highlighted the relationship of kaolinite to illite as primarily being governed by the ratio $H^+ : K^+$ ions in the pore fluid (Equation 3.1).



Illite

Kaolinite

Arthropods such as *T. dokeron* and *O. kingi* are rich in protein. For example, some arthropod cuticle, alone, is 70 per cent protein (Richards, 1951). Proteins break down to amino acids, which subsequently go through the processes of deamination and decarboxylation to produce basic products such as ammonia and amines (Berner, 1968). This would result in a pore fluid with a low H^+ to K^+ ion ratio concentration. As evident from Equation 3.1, in a pore fluid with a low hydrogen ion concentration the reaction proceeds to the left and the formation of illite would be promoted over kaolinite. However, the greater proportion of kaolinite associated with the specimens of *A. hayae* would indicate that the chemistry of the pore fluid adjacent to the carcass favoured the formation of kaolinite with respect to illite (i.e. a higher H^+ to K^+ ratio). Analyses of modern molluscs show them to have a greater proportion of fats relative to protein (Karakoltsidis *et al.*, 1995). Upon decay, fatty acids released into solution (Martin *et al.*, 2004) would increase the H^+ : K^+ ratio and as a result kaolinite would have been preferentially precipitated around *A. hayae*. If the clay mineral composition is controlled by different decay products, it supports the hypothesis that clays were authigenic and precipitated rapidly after the death of the animal.

In *K. clementsi*, *T. dokeron* and *A. hayae*, kaolinite occurs surrounding the fossil, but moving outwards away from the fossil, illite becomes the prevalent clay mineral species. Plotting the distance from the fossil against the K/Al ratio demonstrates that the clays around these specimens become increasingly illitic with distance from the fossil, before returning to a more kaolinitic composition. This change is gradual (see Fig 3.7) and requires an explanation. A low K/Al ratio signifies a deficiency of potassium ions in

solution and as a result the formation of kaolinite is favoured over the precipitation of illite. Therefore, the K/Al ratio can be used as a proxy for H^+/K^+ , and may reflect the pH of the local environment. An increase in the proportion of illite with respect to kaolinite with increasing distance from the fossil may suggest the limit of the decay halo (Fig. 3.7). This trend appears to be related to the volume of the animal. *T. dokeron* has the greatest volume of the specimens analysed and has the largest apparent decay halo (8 mm from the fossil). In comparison, *K. clementsii*, with the smallest volume has the smallest decay halo (4 mm from the fossil).

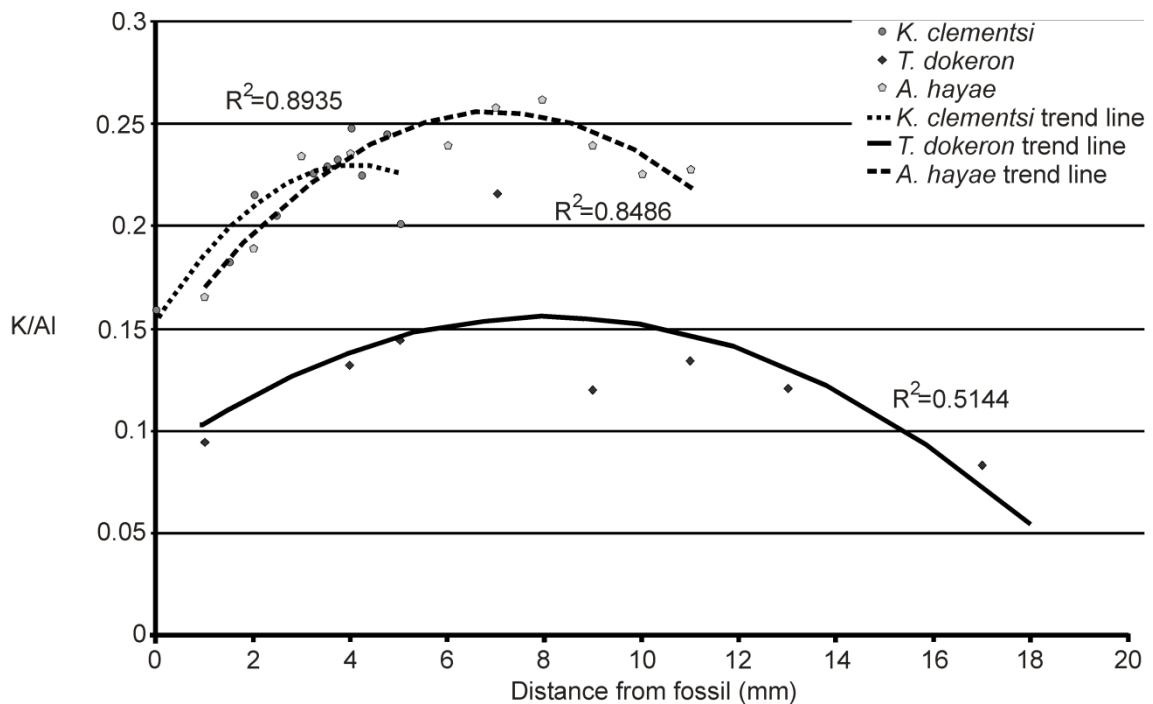


FIGURE 3.7— Distance from the fossil plotted against the K/Al ratio with lines of best fit and their R^2 values. Note that all the specimens analysed demonstrate an increase in the K/Al ratio, indicating that the clay minerals become increasingly illitic in composition before resuming a more kaolinitic composition. *O. kingi* was omitted from the results because there was insufficient clay accumulation within the matrix to collect data. Data has been fitted with a polynomial trend line.

The clay minerals associated with fossils do not appear to be templating the organic matter in a similar manner to that described by Gabbott (1998) to explain the preservation in the Ordovician Soom Shale, South Africa. Nevertheless, they may still

play an important role in the retardation of the decay process and so extend the preservation window. Orr *et al.* (2000a) suggested that the clay minerals prevented the collapse of the void after the decay of the organic matter by physically strengthening the sediment around the carcass. However, it may be that these clay minerals, which formed during the initial stages of decay, have acted to chemically retard the decay process and so extended the preservation window.

There are several mechanisms through which the clay minerals may have retarded the decay process. The fundamental principle behind these mechanisms involves limiting the diffusion of microbes and oxygen to the site of decay. Fontes *et al.* (1991) suggested that precipitating clay minerals within the pore space would reduce the permeability around the carcass and thus limit the transport of microbes to the site of decay and as a result the rate of decay would be limited. Gaines *et al.* (2005) suggested a similar mechanism for the preservation of the Cambrian Wheeler Formation, Utah, which exhibits Burgess Shale type preservation. Gaines *et al.* (2005) suggested that reduced permeability, owing to the prevalence of clay minerals, limited the supply of available oxidants (including SO_4^{2-}) to microbes and in effect reduced their capacity to recycle organic carbon. The reduction of permeability may also have led to the rapid transition of aerobic to anaerobic decay as oxygenated pore waters would be prevented from circulating. Anaerobic decay is a multi step process and occurs at a much slower rate than aerobic decay rates (Henrichs, 1995). Reducing the rates of microbe and oxidant diffusion and aerobic decay in and around the vicinity of the carcass may well have acted to extend the preservation window. Furthermore, clay minerals that interact with decaying organic matter have the effect of stabilising it and reducing its putrefaction. Keil *et al.* (1994) noted that when clay minerals interacted with decaying organic matter they reduced its decay rate by five times order of magnitude, which

would significantly extend the preservation window. Therefore, the early precipitation of clays was likely vital to the preservation of Herefordshire Lagerstätte fossils. Clays may have played a role in the retention of a void stage as in the taphonomic model proposed by Orr *et al.* (2000a) (but see above), but they also acted to limit the decay rate.

Authigenic clay mineral formation associated with decaying organic matter is a well documented phenomenon (Odom, 1984; Orr *et al.*, 1998). These acidic decay products would result in the formation of a micro-environment within the pore space adjacent to the carcass (Briggs & Kear, 1993; 1994). As demonstrated in Equation 3.1, an acidic micro-environment would favour the formation of kaolinite, which has superior stability at acidic pH to illite, which in comparison is more stable at alkaline pH (Gabbott *et al.*, 2001). The affinity of clay minerals for organic substrates is enhanced at a low pH and in the presence of cations (Gabbott *et al.*, 2001).

These fossils are recovered from an andesitic volcanic ash. Volcanic ash goes through rapid alteration, during early diagenesis, in aqueous environments (Oelkers & Gíslason, 2001). During this alteration high concentrations of cations, such as Ca^{2+} , Na^+ , and H^+ , are released into the water (Shiraki *et al.*, 1987; Stefánsdóttir & Gíslason, 2006). Combined with the acidity of the organic matter, this would promote the clay/organic interactions. Gabbott (1998) describes how dissolved cations can enable clay minerals to interact with organic matter, allowing the negatively charged organics and clay minerals to overcome their repelling forces and reposition to allow forces, which attract, to establish.

Calcite Precipitation

The chemistry of the calcite, as defined by the cathodoluminescence and SEM EDX analyses, demonstrate that it contains no iron or magnesium. For magnesium and iron ions to substitute into the structure of the calcite crystal they must be in a 2+ state. In addition, iron requires slightly acidic and reducing conditions to become stable as Fe^{2+} (Fig. 3.8.A), but magnesium can exist as Mg^{2+} across a range of pH and Eh (Fig. 3.8.B).

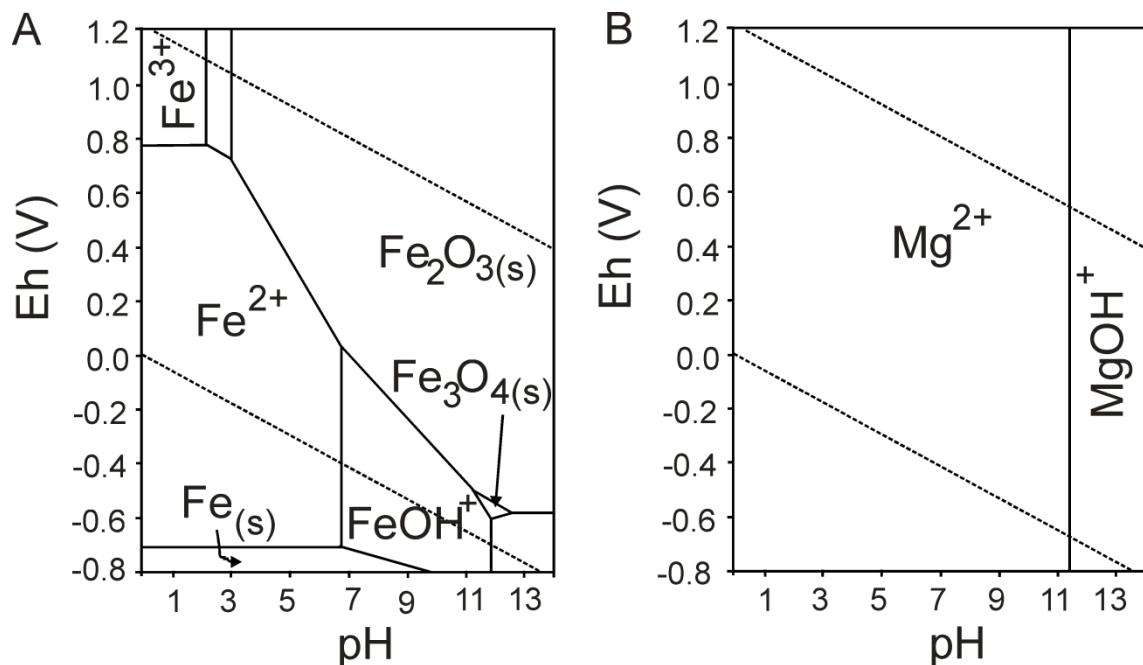


FIGURE 3.8— Eh-pH diagrams generated at standard laboratory conditions (298.15K, 105 Pa) (Takeno, 2005). A. Iron species. B. Magnesium species. Unless stated all species are in an aqueous solution state.

Magnesium is a common ion within seawater (Krauskopf, 1989) and as result calcite crystals formed in a marine setting typically contain a significant amount of magnesium (Astilleros *et al.*, 2010). It is therefore unusual that the calcite crystals contained in these fossils have precipitated without the substitution of magnesium into

their crystal structure. This study argues here that cation exchanges which occur between the volcanic ash and the seawater provide a possible explanation. During early diagenesis of volcanic ash within the seawater, Mg^{2+} ions are typically absorbed into the volcanic ash (Shiraki *et al.*, 1987; Stefánsdóttir & Gíslason, 2006). Magnesium ions have been demonstrated to have an effect on the precipitation of calcite crystals by poisoning their nucleating crystal faces. This causes elongation of the calcite crystal c-axis, resulting in the precipitation of fibrous calcite (Folk, 1974; Davis *et al.*, 2000). The removal of magnesium ions early in the diagenetic process explains the formation of low-magnesium sparry calcite in marine settings.

EDX analysis has also demonstrated the occurrence of manganese within the sparry calcite crystal structure. Manganese, unlike magnesium, is not a major component of seawater, because the Eh-pH of normal marine settings are typically too oxidising. Under these conditions manganese is oxidised to either Mn^{3+} or Mn^{4+} ions; both these forms are insoluble in seawater and precipitate out. Therefore, for the manganese to have substituted into the sparry calcite, conditions would need to have been slightly reducing so that the oxidation of manganese to an insoluble form was prevented. In addition, an available source of manganese would need to have been present within the environment at the time of calcite precipitation, and the likely candidate is the andesitic volcanic ash.

This Lagerstätte lacks significant quantities of pyrite, with the exception of a few crystals associated with fossils. This noticeable lack of pyrite would suggest a deficiency of Fe^{2+} ions and/or sulphide ions within the pore fluid. There are two possible causes of this: the lack of organic matter as a reducing agent and the absorption of sulphate, and iron, ions by the cation exchanges between the seawater and the

volcanic glass. Both processes would have prevented the supersaturation of the pore-fluid with respect to pyrite.

Decay experiments have already demonstrated the link between decaying organic matter, the activity of carbonate ions and the precipitation of calcite crystals within animal carcasses (Berner 1968; Hof & Briggs 1997). Berner (1968) used experimental decay of butterfish to demonstrate that carbonate ion activity increased during decay, but recorded no actual carbonate precipitation. This may have been owing to an excess of fatty acids produced during the decay of the fish inhibiting calcite precipitation (Berner 1968). However, other decay experiments have demonstrated the precipitation of calcite crystals as a direct result of the decay of organic matter. Experiments carried out by Hof and Briggs (1997) identified the precipitation of calcite on mantis shrimps. Calcite showed three different morphologies— crystal bundles, an outer crust of crystals on the cuticle and an amorphous crystalline mass within the cuticle. Furthermore, chitinous cuticle of arthropods has been identified as the perfect medium to accommodate and initiate the precipitation of the calcite (Manoli *et al.* 1997). The experimental work by Manoli *et al.* (1997) suggested that the formation of calcite overgrowths on chitin was the result of a surface diffusion controlled mechanism and that the crystallization of the calcite initiated through the interaction of Ca^{2+} ions with the C=O bond in the chitin molecule.

Discussion of the Stable Isotope Analysis

The preliminary isotopic analyses demonstrate that the calcite within these fossils is enriched in light carbon (carbon-12) and enriched in light oxygen (oxygen-16). The sparry calcite of the fossils' enrichment in carbon-12 demonstrates that the carbon was primarily sourced from the decay of organic matter. Mozley and Burns (1993) state

that positive values are the result of methanogenesis, while negative values are indicative of iron, manganese and sulphate reduction and large negative values are the result of methane oxidation. However, Fisher *et al.* (1998) concluded that methanogenesis can generate both low and high $\delta^{13}\text{C}$ values. Therefore, it is likely that the decay pathway was either sulphate-reduction and/or methanogenesis, but it is impossible to distinguish between them.

The oxygen isotopic signature of these fossils is significantly lighter than values recorded for brachiopods of Wenlock age, and are lighter than the estimates for Wenlockian seawater (c.f., Azmy *et al.*, 1998). There are four possible causes for these negative values: resetting with meteoric water during diagenesis, decay of organic matter, initial incorporation of meteoric water, or precipitation of authigenic minerals.

Diagenetic alteration of the isotopic ratios through later interaction with meteoric water is a possible explanation for the unusual enrichment in oxygen-16. It is arguable that isotopic resetting should have happened, as the sedimentary deposit has had 425 million years to go through diagenesis and interact with meteoric water. Although, the bentonite has not been subjected to temperatures in excess of 80°C, as inferred from conodont CAI, low temperature would have an affect on the oxygen isotopic ratios. Oxygen isotopes in sedimentary rocks, and marine organisms, are utilised to infer palaeotemperatures, because minerals which precipitate from low temperature fluids are preferentially enriched with ^{18}O , and in comparison minerals precipitated from warmer fluid are enriched in ^{16}O (Kasting *et al.*, 2006). Estimates for the temperature of formation of the calcite crystals within these fossils based on the temperature equation (Equation 3.2) of O'Neil *et al.* (1969) produce temperature estimates of ~40°C, which infers low temperature diagenesis.

$$T = 16.9 - 4.38(\delta^{18}\text{O}_C - \delta^{18}\text{O}_{\text{SW}}) + 0.10(\delta^{18}\text{O}_C - \delta^{18}\text{O}_{\text{SW}})^2 \quad (\text{Eq. 3.2})$$

Decay of organic matter is a likely explanation for the light oxygen values. Coleman and Raiswell (1981) suggested that light oxygen isotopic signatures could be derived from the bacterial oxidation of organic matter by sulphate reduction. This was later supported by the work of Sass *et al* (1991); who devised a mechanism for the enrichment of pore fluid in oxygen-16 by sulphate reduction.

Initial incorporation of meteoric water in the preservation is unlikely and can be ruled out as the environment of deposition has already been identified by Briggs *et al.* (1996) to be an outer marine shelf environment.

Precipitation of authigenic clay minerals is another possible explanation. This pathway requires the precipitation of $\delta^{18}\text{O}$ rich authigenic minerals before precipitation of the sparry calcite. Mozley and Burns (1993) suggested that as a result of precipitating minerals enriched in oxygen-18, the pore fluid from which the calcite eventually precipitated from would have been enriched in ^{16}O .

However, the isotopic data are inconclusive. While the negative carbon values are indicative of organic carbon it is impossible to determine if the organic matter decayed by sulphate reduction or methanogenesis. Both methanogenesis and sulphate reduction could result in a negative value but there is no way to discriminate between the two on the basis of this evidence. The oxygen isotopic data is unable to distinguish between a primary signature and a latter resetting event, since all the mechanisms described above may all account for the enrichment in light oxygen. If these isotopic values represent a primary signature then they are unusually enriched in light oxygen. These signatures are thought to be primary, because the cathodoluminescence was consistent between the samples analysed; three of the samples demonstrated a similar

concentric pattern that followed the margin of the fossil. In addition, the sparry calcite is low magnesium calcite; low Mg-calcite is more stable and resilient to diagenetic alteration, thus minimising, but not mitigating, the potential for oxygen resetting (Korte *et al.*, 2009). However, the temperatures of formation calculated (see previous) are not compatible with an outer shelf setting and are more likely to indicate low temperature diagenesis.

Discussion of the Carbonate Concretions

As the fossil calcite is characterised by sparry calcite, which lacks any magnesium and iron substituted into its crystal structure, and the concretion matrix is characterised by carbonates rich in iron and magnesium, it is unlikely that the fossil calcite and the concretion matrix precipitated simultaneously. This is because a process that would have prevented the magnesium ions being substituted into the fossils' calcite structure during the coeval precipitation of the magnesium rich carbonate concretion has not been identified.

A more likely scenario is that the formation of the carbonate concretions occurred after the precipitation of the sparry calcite within the fossils. The lack of magnesium within the sparry calcite can be explained by the initial, and early, diagenetic reactions which occur when volcanic ash enters the seawater. Shiraki *et al.* (1987) and Stefánsdóttir and Gíslason (2006) have identified a series of cation exchanges that occur between the volcanic glass and seawater. One of these exchanges involves the absorption of magnesium ions into the volcanic glass, but is released at a later point in time. This consequently means that the magnesium would initially be unavailable to form the matrix of the concretions until it was released back into solution by the volcanic glass, after the preservation of the fossils.

Discussion of the Eh-pH

The cations available for mineral formation within this Lagerstätte are controlled by the Eh and pH of the pore-water. Using the chemical compositions of the sparry calcite, in the fossil, and the minerals in the concretion matrix this study has identified a possible pathway of the preservation through Eh-pH space (Fig. 3.9).

Here this study assumes that the Eh-pH of Silurian seawater is similar to that of modern seawater. Eh-pH diagrams were taken from the FACT Eh-pH database and generated from a concentration of 10^{-10} mole/kg at standard laboratory conditions (temperature of 298.15K, 105 Pa of pressure) (Takeno, 2005).

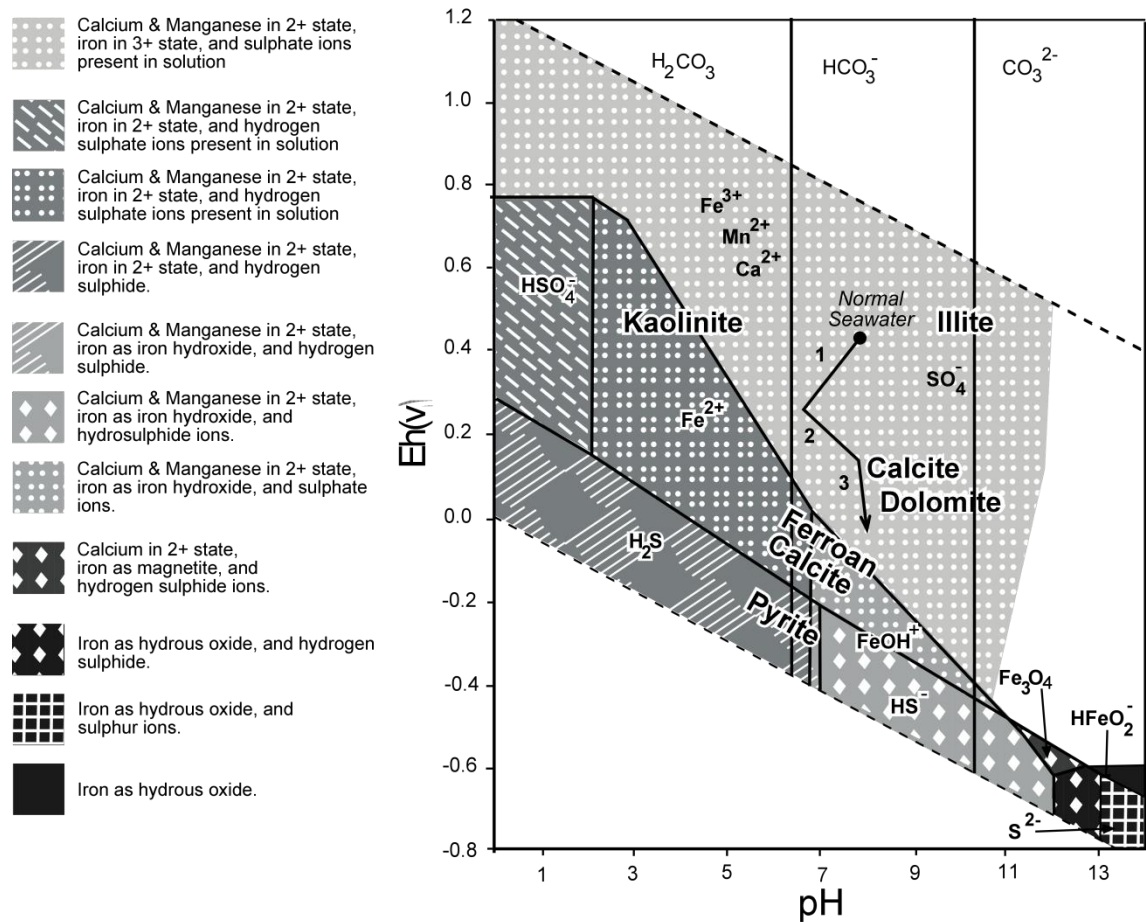


FIGURE 3.9— Schematic preservation pathway through Eh-pH space. These boundaries represent gradients which move as the concentration of the ion changes, but this diagram does not take into account the concentration of the ions involved.

Starting at normal seawater the initial decay of the organic matter would have caused an acidic excursion through the release of acidic products into the pore-fluid; acidity was also promoted by hydrolysis of the volcanic glass (1 in Fig. 3.9). The increase in the hydrogen ion activity, which results in increased acidity, promoted the formation of authigenic kaolinite around the fossil (see Eq. 3.1). The cations released from the volcanic ash during the cation exchanges promoted the clay organic interactions. The increased acidity also resulted in the precipitation of apatite within the gut traces.

An excursion towards alkaline pH was then caused by the combined effect of the decay of proteinaceous material, sulphate reduction/methanogenesis and/or the leaching of sodium from the host volcanic ash (2 in Fig. 3.9). This alkalinity supersaturated the pore fluid with carbonate ions and promoted the precipitation of sparry calcite in the fossils. There is no magnesium to substitute into the calcite as the Mg^{2+} ions would have been removed from solution by the absorption in to the volcanic glass. Conditions were not sufficiently reducing to promote the formation of iron(II) ions which prohibited iron from substituting into the calcite mineral structure. The lack of reducing conditions also prevented the formation of sulphide ions, and as a result pyrite formation was inhibited.

The concretions contain ankerites, carbonates that are rich in iron and magnesium, which implies an alkaline and reducing excursion (3 in Fig. 3.9). The formation of the ankerite and dolomite suggests that Mg^{2+} and Fe^{2+} ions were available in solution; their increased activity and the pore-fluid supersaturated with carbonate ions promoted carbonate formation. The pH drivers in this system are easily identified as the decaying organic matter and the hydrolysis of the volcanic ash creating initial acidic conditions. Alkaline pH was generated by the interaction of sodium from the volcanic ash and the sulphate reduction of the organic matter. However, the reducing agents are

harder to identify, but they would include the organic matter and the leaching of alkali metals from the volcanic ash; the oxidation of iron(II) to iron(III) may also have driven the reduction excursion.

TAPHONOMIC MODEL

Entombment

The fauna of the Herefordshire Lagerstätte were emplaced and entombed within a volcanic ash; geochemical analysis of immobile elements as described by Winchester and Floyd (1977) has demonstrated it to be of andesitic origin. The entombment process buried the fauna rapidly without disarticulation. This assumption is made because some of the ostracod fauna appear to be preserved with complete appendages that are protruding from the carapace and so were probably in the process of locomotion (c.f., Siveter *et al.*, 2007c). In addition, evidence such as escape tracks support the hypothesis that some of the animals were alive shortly after burial (Orr *et al.*, 2000a). It also implies that the volcanic ash provided an intermediate stage. Fine grained sediment usually displays a thixotropic behaviour so it could have infiltrated around the animals to “freeze” them in locomotion and prevent damage.

Hydrolysis of the volcanic ash

Volcanic ash is mainly composed of volcanic glass which is very reactive and unstable, and in an aqueous environment would undergo early, and rapid, diagenetic alteration through a series of pore water-volcanic glass cation exchanges (Fig. 3.10. A) (Stefánsdóttir & Gíslason, 2006). Other authors (Shiraki *et al.*, 1987; Stefánsdóttir & Gíslason, 2006) through experimental work have demonstrated that as the ash begins to be hydrolysed the volcanic glass absorbs OH^- , SO_4^{2-} , Mg^{2+} , K^+ and Fe^{2+} from the

surrounding pore fluid, but releases Ca^{2+} and Na^+ . These exchanges results in an initial decrease of the pore fluids pH because the absorption of OH^- results in an excess of H^+ left in solution. The rate of alteration makes it possible for the volcanic glass to reach total dissolution within several hours of entering the aqueous environment (Oelkers & Gíslason, 2001). However, it is important to note that the experiments carried out on the dissolution of volcanic ash were carried out under laboratory conditions and at high temperature, which would speed up the kinetics of the reactions. Consequently, in an outer shelf environment where the temperatures are lower it is conceivable to expect these reactions to take longer to accomplish, and possibly putting them on par with the decay of the organic matter. To summarise, after these cation exchanges have occurred the remaining pore fluid is acidic and has a high concentration of dissolved cations. This pore fluid is ideal to facilitate the clay organic interactions as described by Gabbott (1998).

However, the fall in pH may be countered by the release of sodium ions into solution. Sodium ions will react with water to produce sodium hydroxide, which has an alkaline pH, and this would cause the pH of the solution to return to a more alkaline pH and favour the formation of carbonates.

An andesitic ash would be enriched in cations such as calcium, magnesium, manganese and iron, which are important for the formation of carbonates. Interestingly, when compared to a fresh andesite the bentonite is depleted in all these ions but the concretions are highly enriched in these ions. The unique preservation model described in this Lagerstätte may be attributed to the somewhat unusual occurrence of an andesitic ash composition. In comparison, other Welsh Borderland bentonites of similar age, are acidic in composition (Teal & Spears, 1986) and are enriched in silica, aluminium,

sodium and potassium, but are depleted in the cations essential for carbonate precipitation.

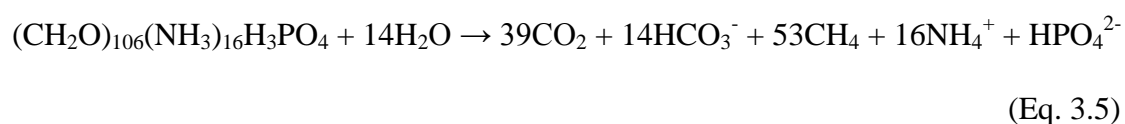
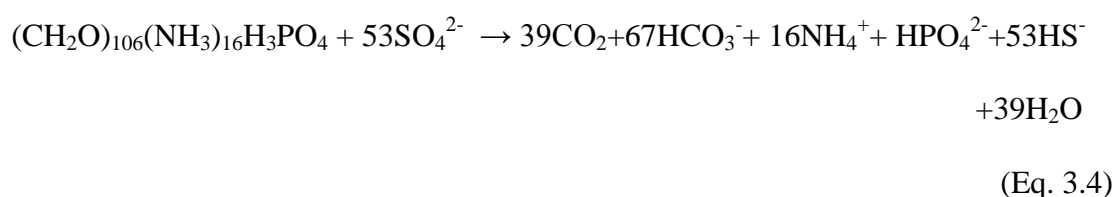
Initial Decay of the Organism and Clay Mineral Accumulation

Immediately post mortem the animal carcass begins to undergo aerobic decay (Equation 3.3), which causes a number of products to be released into the surrounding pore fluid (Allison & Briggs, 1991).



The decay products dissolved into the pore fluid surrounding the carcass causes a localised reduction in pH (Briggs & Kear, 1993; 1994); combined with the increased concentration of dissolved cations there would be increased interaction between the clay minerals and the organic matter (Fig. 3.10. B) (Gabbott, 1998; Orr *et al.*, 1998). As demonstrated above, the composition of the clay minerals formed would be a function of the ratio of H^+ : K^+ (Gabbott *et al.*, 2001) which in turn is related to the chemical composition of the decaying organic matter. In addition, as discussed previously the clay mineralisation around the decaying carcass may extend the preservation window and retard the decay process. It is hypothesised that at this time calcium phosphate precipitated locally within the guts of the carcass, because the decay experiments of Hof and Briggs (1997) have demonstrated an initial drop in pH at the site of decay, but also the phosphatization of the decaying soft tissues. It can be assumed that as the guts of *K. clementsii* are preserved in the dorsal, life, position, some of the soft tissue would therefore still need to be retained at this stage to support the original shape of the animal and maintain the position of the gut.

At some point post mortem the dissolved oxygen in the pore fluid would become exhausted; with all the available oxygen used up the decay would proceed by either sulphate reduction (Equation 3.4) and/or methanogenesis (Equation 3.5) (Allison & Briggs, 1991) as inferred from the isotopic data (Fig. 3.10. C). However, as the sulphate ions may have been already absorbed by the volcanic glass (see above), methanogenesis is perhaps a more likely decay pathway, but sulphate reduction cannot be ruled out.



Both sulphate reduction and methanogenesis have been shown to elevate the alkalinity of the pore fluid (Mazzullo, 2000; Sivan *et al.*, 2007), which favours the precipitation of calcite. In addition, sulphate ions were demonstrated by Walter (1986) to have reduced the rate of calcium carbonate precipitation. Furthermore, sulphate reducing bacteria, apart from promoting pore fluid alkalinity and removing any kinetic inhibitors, may further aid calcium carbonate precipitation by acting as a point of calcite nucleation (Braissant *et al.* 2007).

The level of exceptional preservation seen in the Herefordshire fossils necessitates rapid precipitation of calcium carbonate. Elevated alkalinity and removal of kinetic inhibitors, either through sulphate reduction or by absorption into altering volcanic glass, would facilitate this taphonomic pathway.

Calcite precipitation

The high alkalinity and the removal of a kinetic inhibitor would promote the precipitation of calcium carbonate (Fig. 3.10. D). Elemental mapping and cathodoluminescence of the sparry calcite indicates that there was an available source of manganese, but also an active process that removed the magnesium from the seawater. Two calcite textures have been identified within all the specimens examined in this study, micro-granular calcite and sparry calcite. The cathodoluminescence of the micro-granular and sparry calcite suggests that their precipitation was coeval. However, this study concurs with the findings of Orr *et al.* (2000a), that preservation is of an external mould. So the problem arises of how to precipitate the external mould (i.e. after removal of the cuticle), and maintain an 'in life' gut position? Decay experiments carried out by Hof and Briggs (1997) may provide one possible answer; as calcite precipitation was documented to have initiated as an amorphous calcite crystal mass within the cuticle structure. Alternatively, the pH fluctuations previously described, as a result of the altering volcanic ash, might facilitate the dissolution of the cuticle structure. As the cuticle structure is dominantly protein, chitin, it would be at risk of hydrolysis within an acidic solution (Rinaudo 2006). Furthermore, alkalis are also known to degrade chitin and produce water-soluble alkali chitin (WSC) (Pillai *et al.*, (2009). Pillai *et al.* (2009) noted that WSC is produced when chitin is reacted with sodium hydroxide, and a number of the products are water soluble. Sodium hydroxide was suggested to elevate the pH prior to calcium carbonate precipitation and it could provide a mechanism to remove the cuticle prior to the precipitation of calcite. Calcite could then precipitate within the centre of the animal and in the space occupied by the cuticle, this mechanism would account for the formation of an external mould and for the coeval precipitation of the two calcite phases seen within *K. clementsii*, *T. dokeron* and *A. hayae*.

The sparry calcite within the fossils is not typically precipitated within a normal marine setting because magnesium ions in the seawater poison the nucleating crystal faces leading to the precipitation of fibrous calcite. Therefore, the precipitation of the sparry calcite is thought to have occurred after the volcanic glass absorbed the magnesium ions during its early diagenetic alteration.

Additionally, the positioning of the gut in *K. clementsii* towards the dorsal position has ruled out the possibility of a void stage; based on the results from decay experiments carried out by Briggs and Kear (1993). However, the calcite crystals, which were enriched in manganese (see above), at the edge of *O. kingi* were argued by Orr *et al.* (2000a) to infer that a void stage had occurred. Examination of the calcite crystals along the margin of the specimens of *O. kingi* confirmed that they lacked any significant trace of magnesium and they had a height-to-width ratio of 1.3:1, undulose extinction and pyramid terminations. These calcite crystals should not be classified as fibrous calcite because fibrous calcite crystals are typically magnesium rich, since it is the magnesium ion that is responsible for inducing the growth of the fibrous crystal habit (Folk, 1974; Davis *et al.*, 2000), and they are also characterised by a height-to-width ratio of >6:1. Based on the criteria identified by Flügel (2009) the calcite crystals on the edge of *O. kingi* are considered to be more characteristic of micro-granular to bladed calcite and not fibrous calcite.

It is important to note that there is little soft tissue preserved within these fossils; the textures exhibited by the calcite crystals within the fossils do not show any distinct features, such as bilateral symmetry, which would indicate the position of different tissues, or organs, which could be argued is evidence of a void stage. However, apart from the gut preserved within some of the specimens there is soft tissue preservation, for example, within the brachiopod examined by Sutton *et al.* (2005) the lophophore is

preserved, and ostracod eggs have been recorded, preserved, within the ostracod specimens (Siveter *et al.*, 2007c). As already noted previously the size of the calcite crystals decrease from the centre of the animal to the edge of the fossil, consequently, it can be suggested that the calcite crystals within the central body mass of the animal are too coarse to preserve the fine detail of the soft tissues compared to the smaller crystals at the edge of the fossils, or alternatively, the lophophore and the ostracod eggs may represent more resilient tissues than those found within the body chamber.

The author therefore suggests a mechanism in which the calcite crystals nucleated and precipitated within the body cavity, replacing the tissues that were either more resilient or were large enough to be replicated by this style of preservation. Upon death, cell membranes would have become permeable to calcite ions (Gabbott, 1998); allowing the free diffusion of calcium ions throughout the carcass and obtaining the carbonate ions generated from the recycled organic carbon, which means there would be no limit on the precipitation of calcite. In addition, animal cells are relatively weak structures and would not provide any resistance to a calcite crystal growth.

The concretion matrix (Fig. 3.10E) is composed of an interlocking mosaic of clay minerals, fine calcite crystals and larger, euhedral, rhomb shaped crystals of ankerite. The ankerite crystals illustrate exsolution features and are typically associated with anhedral dolomite. The formation of the anhedral dolomite was attributed to the alteration of the smectite clays, which had been illitized (Orr *et al.*, 2000a). However, they are unlikely to be related as the process of illitization typically occurs between 100 and 140°C, but it has been suggested to initiate at temperatures as low as 70°C (Bjørkym *et al.*, 1993; Cuadros & Linares, 1996; Cuadros, 2006) and, as previously stated, the conodont colour alteration index indicates the Herefordshire deposit was not heated above 80°C. An increase in the solutions pH (i.e., alkaline solutions), a greater

Mg^{2+} and Fe^{2+} ion activity and the supersaturation of the pore fluid with carbonate ions would favour the precipitation of ankerite and dolomite (Hardie, 1986). A defined relationship between the concretions and the fossils, if there is one, has yet to be identified, although it does appear that the inclusion of the fossils into the concretions is a random event.

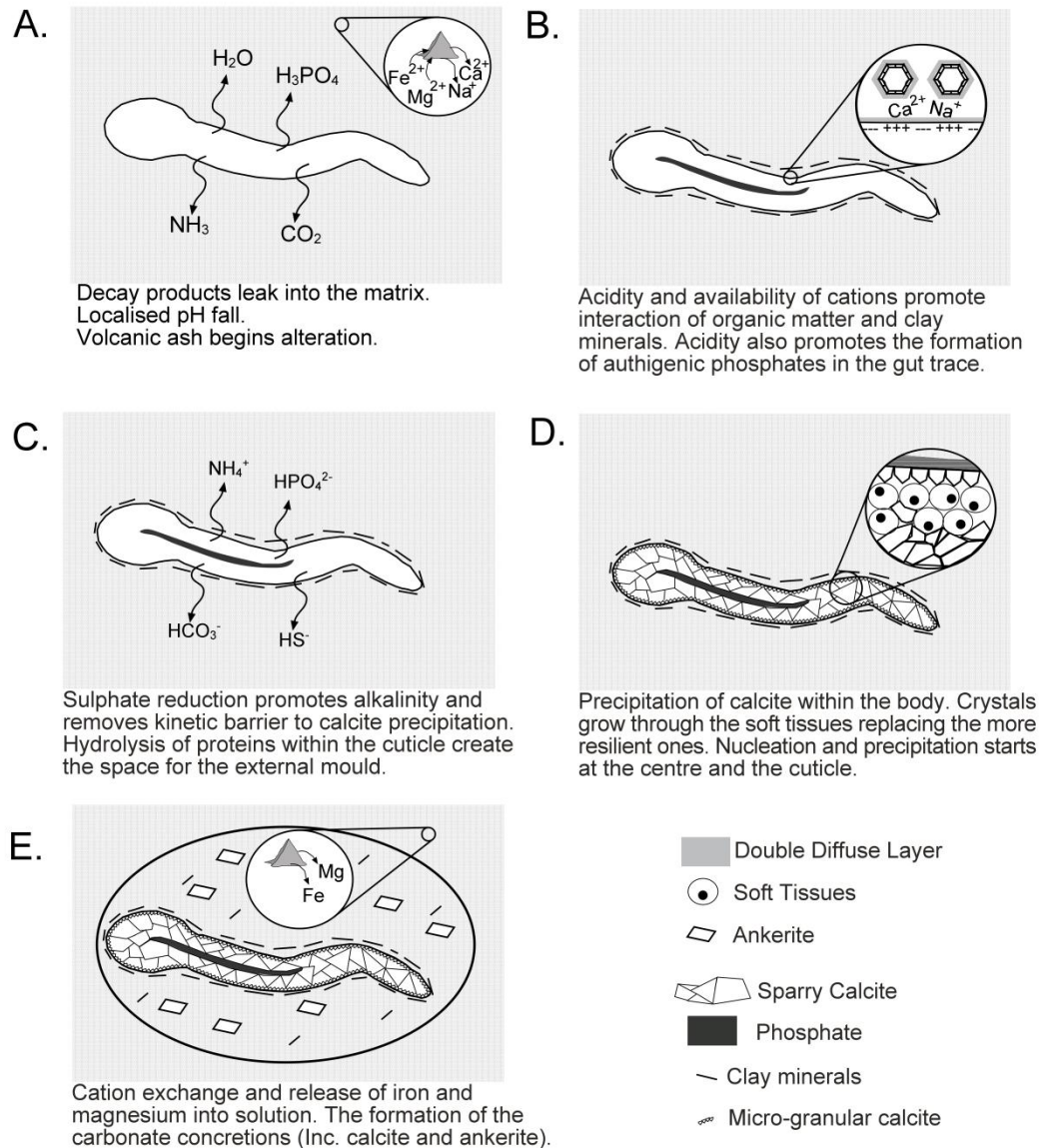


FIGURE 3.10— Revised taphonomic model for the Herefordshire Lagerstätte.

CONCLUSION

For the first time EMPA data has suggested a link between the composition of the organic matter and the composition of the clay minerals that authigenically precipitated with the organic matter, and which this study suggests may have retarded the decay process. Having identified the variations between the compositions of the sparry calcite, in the fossil, and the minerals in the concretion matrix, this study has mapped the taphonomic pathway through Eh-pH space. In addition, new evidence presented herein suggests a void stage never occurred within the preservation pathway; instead it proposes a direct and rapid replacement of the organic matter by sparry calcite.

The original composition of the volcanic ash has played an important role not only in providing the cations for mineralization, but also in mediating the stepwise cation exchanges that occur during early diagenesis and which played an equally important role in removing inhibitors and contaminants to calcite precipitation from the pore fluid. The volcanic ash removed the magnesium, which promoted the formation of the sparry calcite within the fossils, this being unusual for a marine setting. After an unknown time period, magnesium and iron ions again became available in solution, which promoted the formation of ankerite and dolomite in the carbonate concretion matrix.

ISOTOPE ANALYSIS AND THE MECHANISM OF CONCRETION
FORMATION WITHIN THE HEREFORDSHIRE KONSERVAT
LAGERSTÄTTE (SILURIAN)

Chapter Abstract: *A review of the literature concerning concretion formation suggests that a mechanism for the formation of carbonate concretions in a marine setting has not been fully identified: the evidence is inconclusive and contradictory. Extensive XRD, XRF and SEM analysis of the host carbonate concretions of the Herefordshire Konservat Lagerstätte (Silurian) has demonstrated a uniform fabric, which has preserved some volcanic minerals, across the concretions and also a radial variation in chemical composition and mineral percentage. In addition, carbon isotopic analysis has indicated that these concretions are not the result of organic matter decay as previously thought within other studies: instead, it is likely that they formed close to the sediment water interface and were gradually buried. Oxygen isotopic analysis shows that the concretions are enriched in oxygen-16, which is unusual for a marine carbonate, indicating the oxygen isotope ratio may have been reset by the interaction with meteoric water, and/or different fractionation processes may have occurred during formation. The uniform fabric and the lack of concentric structures support a pervasive mechanism of concretion formation. However, the radial chemical variations favour a concentric nucleation mechanism (although this may reflect a difference between early and late cement phases). A pervasive mechanism of formation would explain why some fossils can be found off centre and why some concretions lack fossils. As existing models were defined on concretions formed in mudrocks it is unknown how they can be applied to concretions formed in volcanic ash. An andesitic volcanic ash may account for the*

rapid precipitation of the concretions, by facilitating a suitable pH and by supplying the cations required.

The Herefordshire Konservat-Lagerstätte (Silurian) contains three-dimensional soft bodied fossils which represent a fully marine ecosystem (Briggs, 1996). The fossils represent a range of soft bodied invertebrate animals including a polychaete worm (Sutton *et al.*, 2001c), a chelicerate (Orr *et al.*, 2000b), ostracods (Siveter *et al.*, 2003, 2007c, 2010), a pycnogonid (Siveter *et al.*, 2004), a barnacle (Briggs *et al.*, 2005), a crustacean (Siveter *et al.*, 2007a), a marrellomorph (Siveter *et al.*, 2007b), a lophophorate (Sutton *et al.*, 2011), a mollusc (Sutton *et al.*, 2001a, 2001b), a gastropod (Sutton *et al.*, 2006), and a brachiopod (Sutton *et al.*, 2005). The fossils are recovered from carbonate concretions which randomly distributed within a host bentonite.

The majority of studies which have focused on the formation of carbonate concretions were undertaken on those formed in mudrocks and limestones and their precise mechanism of formation has yet to be fully elucidated (e.g. Raiswell, 1987; Irwin *et al.*, 1977; Mozley & Burns, 1993; Al-Agha *et al.*, 1995; Raiswell & Fisher, 2000). However, the occurrence of concretions within volcanic ash is even rarer and their mechanism of formation has periodically lacked detailed scientific study. Although there have been several attempts to constrain the timing of concretion formation this is also poorly understood. The occurrences of three-dimensional unflattened fossils and distorted laminations within the concretions have been suggested to be evidence of early formation in uncompacted sediment (Raiswell & Fisher, 2000). However, other studies that have focused on the formation of concretions, on the east coast of England, have demonstrated that the rate of formation may be as slow as 100 μm per year (Al-Agha *et al.*, 1995). Host carbonate concretions are fundamental to the Herefordshire Lagerstätte,

as they greatly increase the long term preservation potential of the fossils entombed within them.

Since the 1960s there has been a documented association, supported by isotopic studies, between the formation of calcium carbonate and the decay of organic matter. These studies have confirmed that the formation of carbonate concretions is associated with the microbial decay of organic matter (Raiswell, 1987; Irwin *et al.*, 1977; Mozley & Burns, 1993; Morese *et al.*, 2007). Orr *et al.* (2000a) hypothesised that the formation of the carbonate concretions within the Herefordshire Lagerstätte was the result of the decay of more labile organic tissues, which were not preserved. This study will test that hypothesis with new isotopic data and suggest an alternate possible mechanism of formation of the concretions.

New mineralogical, geochemical and isotopic analyses are used to identify radial variations across the concretions, to elucidate the mechanism of concretion formation and also suggest a mechanism for the incorporation of the fossils into the concretions.

GEOLOGICAL SETTING

The host bentonite deposit of the Herefordshire Lagerstätte occurs at a single locality, a well exposed face in a quarry in the county of Herefordshire, England. The deposit has a maximum thickness of one metre and a 40 metre long single exposure; its limited lateral extent has been attributed to deposition on an undulating sea floor (Briggs *et al.*, 1996). At the base of the regional succession are algal limestones of the Dolyhir-Nash Scar Limestone Formation and stratigraphically above this is the Coalbrookdale Shale Formation, which locally is approximately 300 metres thick (Bassett, 1974). The host bentonite of the Herefordshire Lagerstätte occurs within the

Coalbrookdale Formation, 10 cm above the top of the Dolyhir-Nash Scar - Coalbrookdale Formation boundary.

The concretions appear to be slightly more abundant within the thickest portion of the bentonite and are more concentrated within its top 30 cm. The concretions are rounded and show variation in their shape, from, e.g. spherical to lens to plano-convex shaped (Fig. 4.1). The sizes of the concretions also vary between 5 and 200 millimetres in diameter. Smaller concretions are typically spherical, whilst the larger concretions in many cases are lens-shaped. Some concretions lack fossils. If a concretion contains a fossil it rarely occurs in the centre. Typically, the concretions are weathered to a brown buff colour, but the larger concretions, usually those over 80 millimetres in diameter, may preserve an unweathered blue/grey centre.



Figure 4.1: Three concretion shapes recovered from the host bentonite. A. Spherical, B. Lens, C. Plano-convex. All scale bars: 10 mm.

METHODS

Samples for SEM and petrographic analysis were prepared as standard, uncovered polished thin sections, which were carbon coated. Analysis of the carbonate within the concretion matrix was carried out on a Hitachi S-3600N Environmental Scanning Electron Microscope (SEM) at the Department of Geology, University of Leicester. In addition, 100 concretions, from the Herefordshire Konservat Lagerstätte

collection housed at the University of Oxford Museum of Natural History, were examined to assess any relationship between the fossil and host concretion. Particular attention was paid to the eccentricity of the fossil, the size of the concretion, and the size and taxonomic affinity of the fossil.

Chemical analysis was carried out using an Oxford INCA 350 Energy-Dispersive X-ray spectroscope (EDX) system attached to the SEM, providing elemental mapping and semi-quantitative chemical data by the point-and-ID spectrum. The system was operated at an acceleration voltage of 15kV. Chemical analysis was normalised against a standard, which is 99.99% pure cobalt. The fine-grained nature of the rock makes meaningful analysis by electron microprobe analysis unobtainable.

Two larger concretions were selected for geochemical transects. These were first cleaned to remove any loose material and then cut into sections on a 14" phosphor-bronze rock saw. The sections were then divided into one-centimetre square cubes and the three main growth axes were sampled (Fig. 4.2). The cubes were then milled on a Retsch PM 400 Planetary Ball Mill at 260 rpm for 20 minutes and the fine powders from these were processed as standard fusion beads. Each sample subsequently derived from the large concretion was catalogued according to the sample's LF number (University of Leicester fusion bead number).

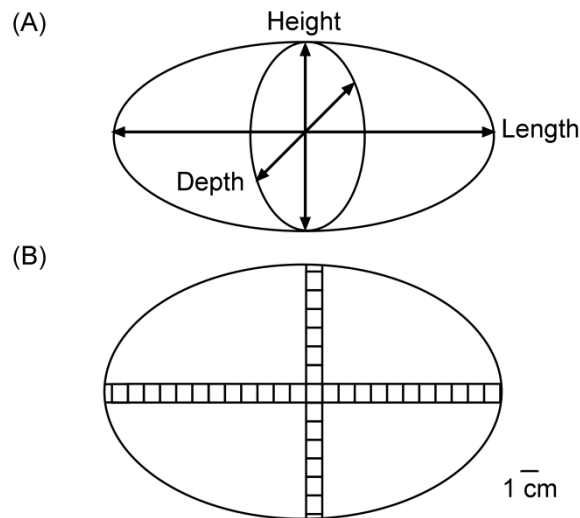


Figure 4.2: A. Sampling axis of concretions. B. Example of sampling technique each black square represents an individual sample. Scale bar: 10 mm.

X-Ray Diffraction (XRD) analysis was conducted on a Bruker D8 Advance with DaVinci at the Department of Geology, University of Leicester. A copper anode was used, with current conditions of 40 kV and 40 mA. Samples were scanning from 4° to $64^\circ 2\theta$ and at a step size of $0.0195^\circ 2\theta$; each scan was completed in 24 minutes. The scans were processed using Bruker DIFFRAC^{plus} Software Suite (release 2009). The ICDD PDF-4+ Scholar crystallographic database (release 2009) from the International Centre for Diffraction Data was used to identify the mineral phases present, while TOPAS software was used for quantitative analysis. In addition, some samples were analysed on a Phillips model PW1732 X-ray generator, with a PW1716 diffractometer and PW 1050/25 detector controlled by a PW1710 at the Department of Geology, University of Leicester. A Copper (Cu) anode, was used, with current conditions of 40 kV and 30 mA. Samples were scanned from 4° to $64^\circ 2\theta$ at a step size of $0.02^\circ 2\theta$ and a speed of $1^\circ /\text{min}$. Angle calibration was by a synthetic silicon sintered standard. The scans were processed using GBC Scientific's Trace V6.7.13 software. Results from this instrument were consistent to those analysed by the Bruker XRD. Analyses were carried out on both the whole rock and the clay fraction.

X-Ray Fluorescence (XRF) analysis was conducted on a PANalytical PW 4400 Axios Advanced X-Ray Fluorescence spectrometer in the Department of Geology, University of Leicester, with a 4Kw Rhodium (Rh) anode, and a PC running PANalytical SuperQ software system with IQ+, WROXI and ProTrace extensions. Major and trace elements were measured from fusion beads; the determination of trace elements in fused beads is obtained through mass absorption corrections, which are made from values calculated from the major element composition and the tables of Thinh and Leroux (1979). It is important to note that the method of analysing trace elements from the fusion beads is not as accurate as those analysed from standard powdered pellets.

Carbon and sulphur content of the samples was measured on a LECO™ CS230 carbon and sulphur analyser at the Department of Geology, University of Leicester. The analyses were carried out on 0.2 grams of sample, with iron and tungsten/tin chips added to act as accelerants. The samples were loaded into the instrument and heated to 850°C in the presence of oxygen.

Samples were analysed for carbon and oxygen isotopes at the NERC Isotope Geosciences Laboratories (NIGL) at Keyworth, Nottingham. To measure for carbon and oxygen isotopes across the concretion axis, 10 mg of carbonate from each sample was reacted with anhydrous phosphoric acid under a vacuum for 72 hours at a constant 25°C (this is sufficient to react all calcium and magnesium carbonates including dolomite). The carbon dioxide liberated was separated from water vapour under vacuum and collected for analysis. The carbon dioxide was measured on a VG Optima mass spectrometer at NIGL. Isotope values ($\delta^{13}\text{C}$, $\delta^{18}\text{O}$) are reported as parts per mil (‰), deviations of the isotopic ratios ($^{13}\text{C}/^{12}\text{C}$, $^{18}\text{O}/^{16}\text{O}$) calculated to the VPDB scale using a within-run laboratory standard calibrated against NBS standards.

ANALYTICAL RESULTS

Distribution and shape of the concretions

The concretions appear to be more frequent within the top 30 centimetres of the host bentonite (Fig. 4.3).



Figure 4.3: Image of the host bentonite with concretions (painted blue). The geological hammer is 28cm in length. (Photo: David Siveter, August 1997).

Objects, such as concretions, can be dispersed in three ways: randomly, regularly, or clumped together (Fowler *et al.*, 1998). It was possible to quantitatively assess the distribution of the concretions within the bentonite and to calculate an index of dispersion, by recording the concretions set against a 30x30cm grid placed at the exposure (Table 4.1).

Table 4.1: Number of concretions recorded within each square of the grid.

0	2	0	4	2	1	0	0	1	0
0	0	1	0	0	1	1	1	0	1
Not exposed						1	0	1	0

The mean and standard deviation of the data were calculated. These were 0.708333 and 0.954585, respectively. The standard deviation is then squared to obtain the variance (0.911232) and the dispersion index is then calculated (1.286445) by dividing the variance by the mean. A factor, which is denoted by the symbol X^2 (29.58824), is calculated by multiplying the dispersion index by the degrees of freedom (n-1) (23). The factor (X^2) and the degrees of freedom are then read off a reference graph (Fig. 4.4) to identify the dispersal pattern. The reader is referred to Fowler *et al.* (1998) for a full description of the methodology.

This statistical test indicates that the concretions are distributed through the bentonite randomly. However, a point to note when considering the implications of this test is that it was done on a two-dimensional surface; it tests the visible 2-D surface of the exposure, and does not consider any possible 3-D variation of the concretion distribution within the rocks. The test was done on a relatively small sample, but this particular statistical test is in any event most suited to small sample areas (Fowler *et al.*, 1998).

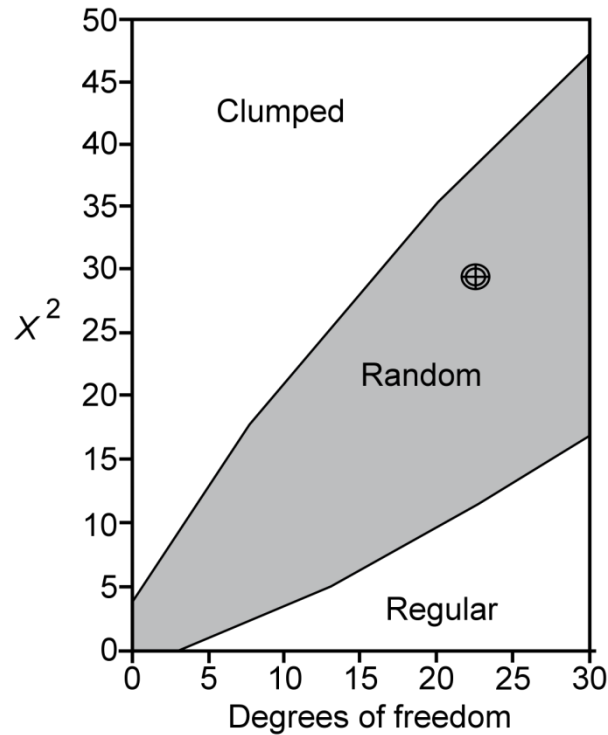


Figure 4.4: Random discrimination graph (after Fowler *et al.* 1998). The shaded area is the area of 95% confidence zone of random dispersal. The marked point is the test results for the concretions of the Herefordshire Lagerstätte.

Mineralogy of the concretions

The fine crystal size of the concretion matrix precluded it from being examined using a standard petrographic microscope. EDX analysis was therefore utilised for semi-quantitative chemical analyses to identify the composition of the minerals present within the concretion matrix (Appendix M).

Examination by SEM backscatter revealed a matrix of interlocking carbonate and clay minerals. EDX data was plotted on discrimination diagrams to identify the minerals present. From each analysis the analytical total of elements (TOT) was plotted against weight percent SiO_2 (Fig. 4.5A). Three distinct clusters were apparent. Those with an analysis total of 50 - 60 % with no silicon were carbonates; those with an analysis total of 80 - 100 % and a silicon content of 40 - 60 % were clays; and those with an analysis total of 90 - 100 % and a silicon content of 100 % were quartz.

Adjacent to the quartz group, a distinct cluster could be identified with an analysis total of between 75 - 80 % and silicon total of between 75 - 80 %; these analyses identify chalcedony, which is a cryptocrystalline variety of quartz.

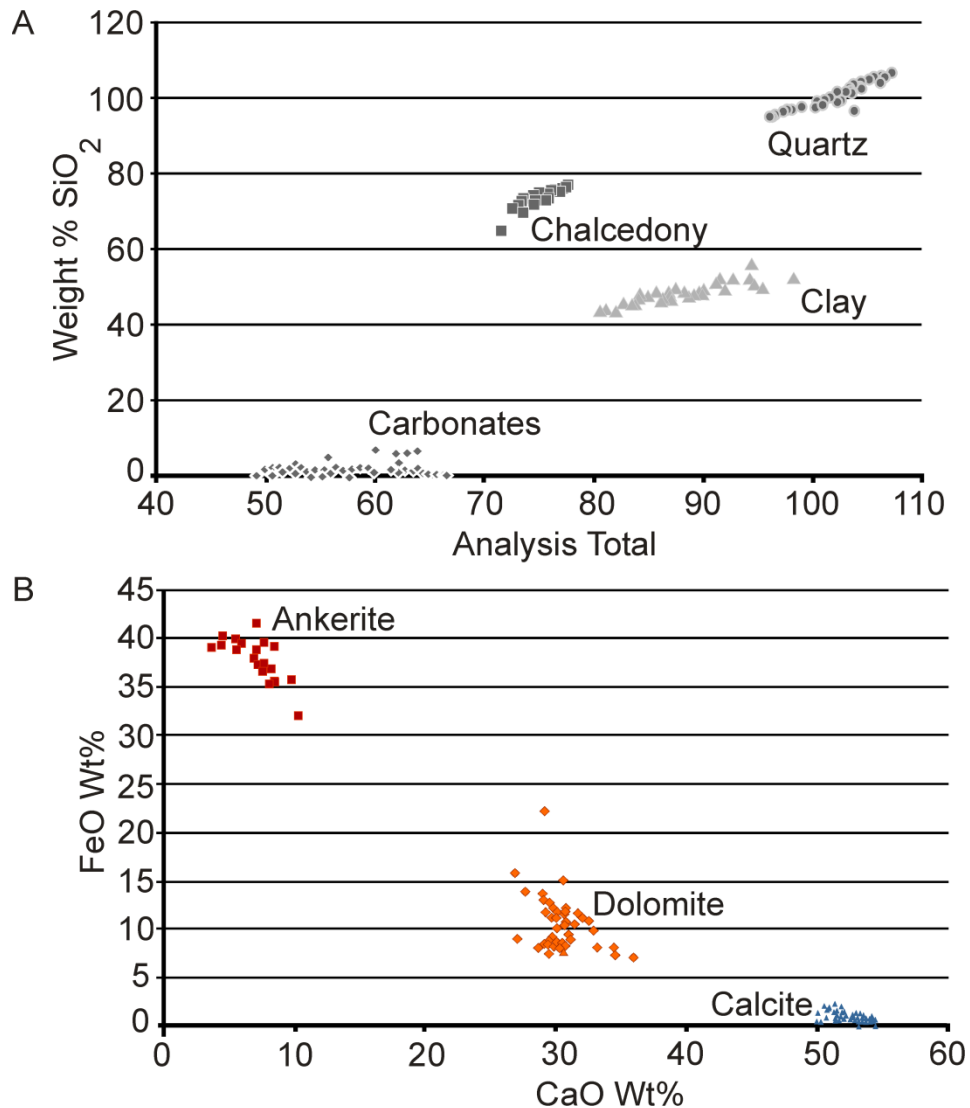


Figure 4.5: A: Analysis total against weight percent SiO₂. Plots discriminate mineral phases as indicated. B: Point-and-ID analysis of CaO wt% against FeO wt% demonstrating the three separate carbonate mineral phases within the host sediment.

Analyses of the carbonate minerals within the concretion matrix revealed the presence of three carbonate minerals: ankerite, dolomite and calcite (including magnesium calcite) (Fig. 4.5B). Clay minerals are also visible in acid-etched blocks of

concretion matrix: Kaolinite with a foliated habit (Fig. 4.6A), and illite crystals with a fibrous habit (Fig. 4.6B).

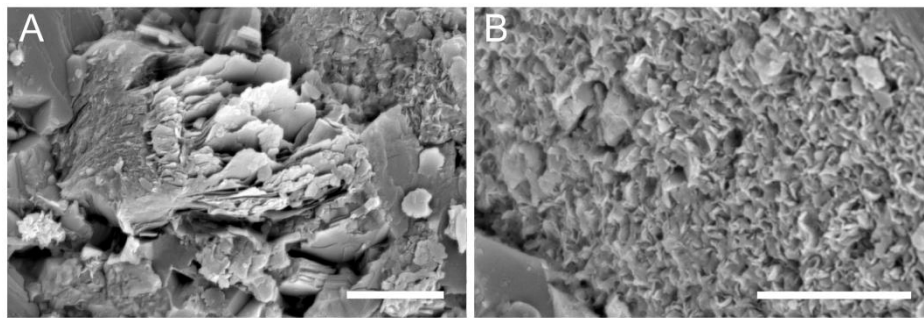


Figure 4.6: Habits of clay minerals within the concretions. A. Kaolinite. B. Illite. Scale bars are 5 μm .

Analysis by SEM and EDX identified minerals in the concretions that may be volcanic in origin. The mineral rich in titanium (Fig. 4.7A), which is either rutile, an accessory mineral commonly associated with igneous rocks, or anatase, which is derived from the alteration of other titanium minerals. This titanium mineral is surrounded by kaolinitic clays, which themselves are then sequentially surrounded by carbonates. The clay minerals surrounding the titanium mineral are interpreted as the remains of the volcanic ash that originally encapsulated it. The composition of the carbonates varies with distance from the titanium mineral as demonstrated by EDX elemental mapping; ferroan dolomite (iron and magnesium rich carbonates) immediately surrounds the clays (Fig. 4.7), and this is then in turn surrounded by calcites depleted of magnesium and iron. There are no distinct euhedral crystal faces between the calcite and the ferroan dolomite.

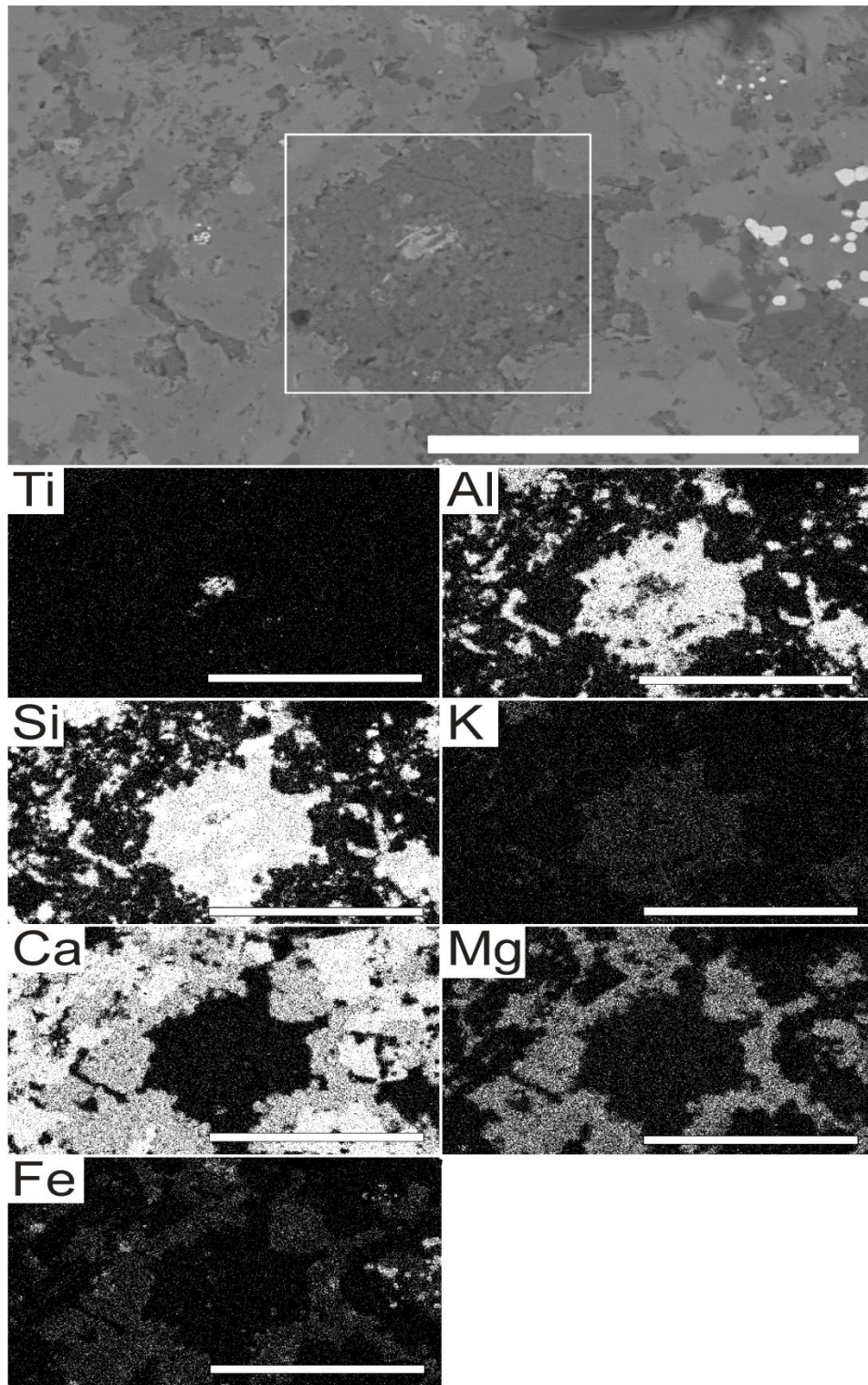


Figure 4.7: Backscatter SEM image of a part of the concretion matrix (A). Note the area within the white box, and below its corresponding elemental maps, individually labelled, which indicate the mineral to be a titanium mineral surrounded by clays, Mg and Fe carbonates, and calcites. All scale bars: 80 μm

At least three different carbonate minerals were identified within the concretion matrix: ankerite ($\text{Ca}(\text{Fe, Mg, Mn})(\text{CO}_3)_2$), dolomite ($\text{CaMg}(\text{CO}_3)_2$) and calcite (CaCO_3). Crystals of ankerite (Fig. 4.8A) show ragged edges which are interpreted as exsolution features. These occur if the pore fluid becomes undersaturated during the precipitation of the crystals and the mineral dissolves back into solution (Hall & Cullen, 1996; Geeslin & Chafetz, 1982), although they may also represent later weathering and alteration. These ankerite crystals are surrounded by dolomite (Fig. 4.8A), which lacks any euhedral crystal shape. The dolomite is itself surrounded by calcite.

Iron hydroxide is also commonly found during SEM backscatter imaging of the thin sections as a coating around other minerals (Fig. 4.8B). This may have been derived from either the weathering of minor amounts of pyrite, from iron(II) present in solution from the final stages of volcanic ash alteration, or it could have been transported into the concretion during weathering.

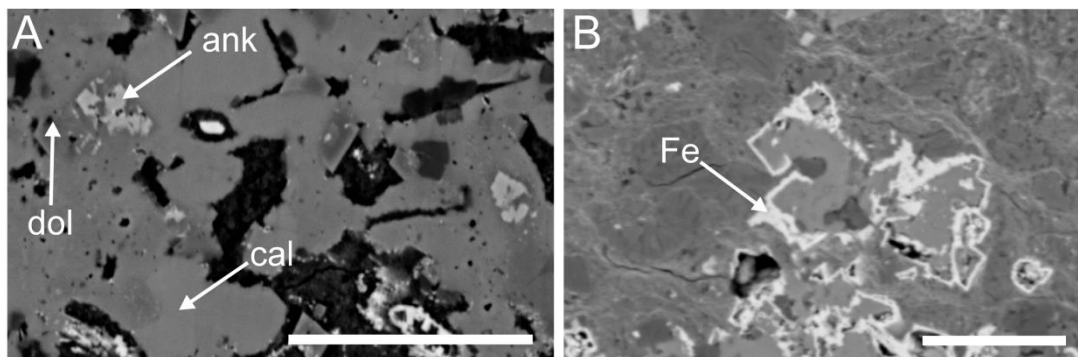


Figure 4.8: SEM backscatter images of the matrix of a single concretion. A. Exsolution features on the ankerite crystal (ank) surrounded by an anhedral dolomite (dol) surrounded by calcite (cal). B. Iron oxide (Fe) coating grains within the matrix. Scale bars A: $30\mu\text{m}$, B: $20\mu\text{m}$.

Whole rock XRD analyses demonstrated that calcite is the dominant carbonate phase present within the concretions (Appendix N). In addition, samples that correspond to the blue-heart central regions of the concretion had elevated percentages of dolomite (Fig. 4.9). Ankerite was not recorded within the XRD analysis of the samples, because

ankerite and dolomite belong to the Trigonal – Rhombohedra crystal system and are part of a solid solution series, which is dependent on the substitution of iron and magnesium (Reeder & Dollase, 1989). So the XRD peaks of the end members of dolomite ($\text{CaMg}(\text{CO}_3)_2$) and ankerite ($\text{CaFe}(\text{CO}_3)_2$) are very close together and indistinguishable from each other. Within the whole rock analysis the dominate clay phases were demonstrated to be kaolinite and illite. This is in contrast to the host bentonite which has greater proportions of illite and smectite and lacks significant percentages of kaolinite (Chapter 2). In addition, whole rock XRD identified the minor occurrence of quartz within all of the samples.

XRD analyses of the clay fraction have demonstrated that the concretions contain a small proportion (3 %) of smectite, which is identical to the proportions recorded in the host bentonite (Chapter 2). Illite is the dominant clay recorded from the clay fraction analysis, but kaolinite only makes up 1 % of the clays present, and is found in both the weathered and unweathered parts of the concretion. In addition, chlorite has also been recorded within the concretions and makes up 19% of the clay fraction in both the weathered and unweathered parts of the concretion. Chlorite is an indication of terrestrial clastic input (Kipli *et al.*, 2008).

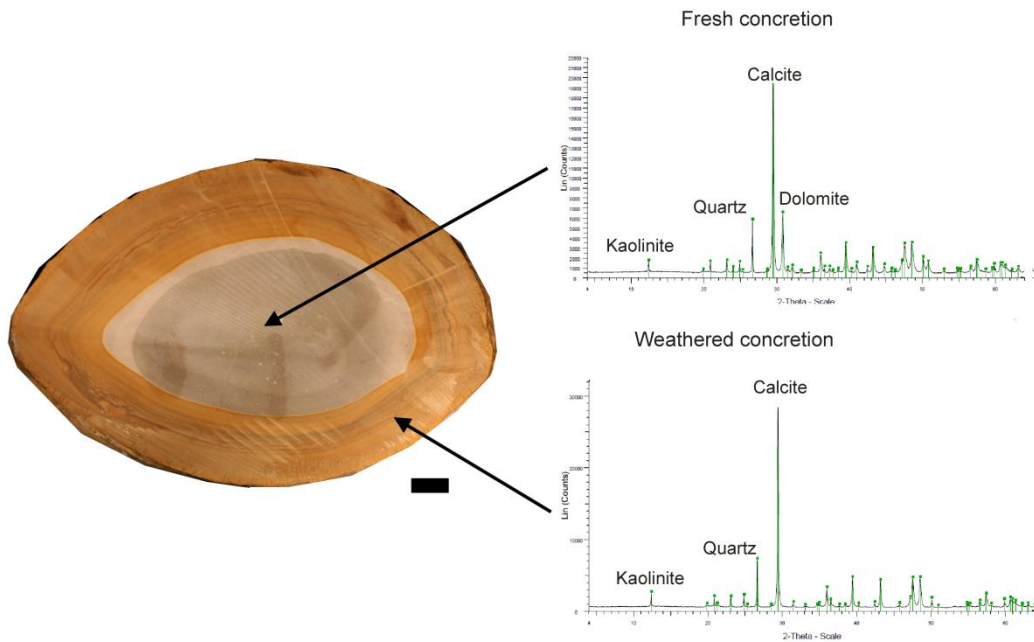


Figure 4.9: Comparison of the XRD traces from the blue unweathered centre with the brown weathered rim of a concretion. Note the absence of dolomite within the weathered rim. The unlabelled peaks are secondary peaks of the minerals identified. Scale bar: 10 mm.

Plotting the percentage of minerals across the diameter of the concretion demonstrates an increase in the percentage of calcite from the centre outwards. This is in contrast to the trend of the dolomite percentages, which demonstrate a decrease from the centre to the edge. Although minor anomalies are present within the data, the overall trending is symmetrical about the centre of the concretion (Fig. 4.10). In addition, the XRD analyses have also identified the presence of siderite in the concretion matrix, which decreases from the centre of the concretion outwards (Fig. 4.10). The percentage of quartz shows a decrease from the centre of the concretion to the transition from the blue/grey centre into the brown edges. Interestingly, at the edge of the concretion, which corresponds to the brown weathering, there is a rapid increase in the percentage of quartz by approximately 10 %. Kaolinite shows a general increase from the centre of the concretion outwards (Fig. 4.10).

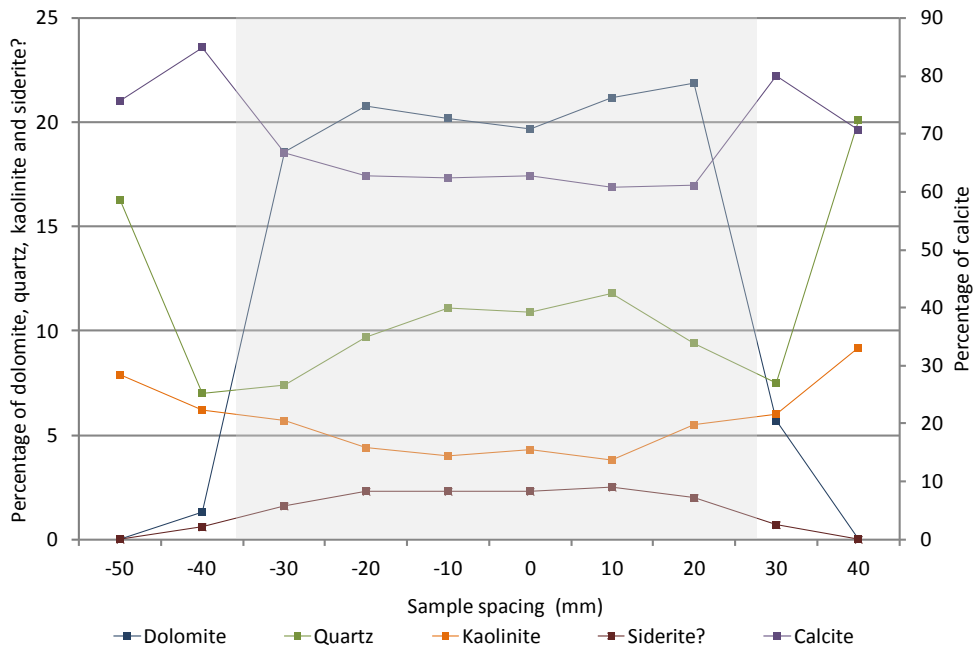


Figure 4.10: Variation in percentage of minerals across the width of the concretion. Point 0 represents the centre of the concretion. The grey shading represents the position of the unweathered heart

Geochemistry of the concretions

XRF analyses were carried out on the 46 samples from the two largest concretions available (Appendix O). The trace elements that are considered immobile were used to identify the original source of the sediment within the concretions, through the use of the Nb/Y versus Zr/TiO₂ plot as in the methods described by Winchester and Floyd (1977). Data from the analyses are plotted on Figure 4.11 along with the analyses of the host bentonite samples.

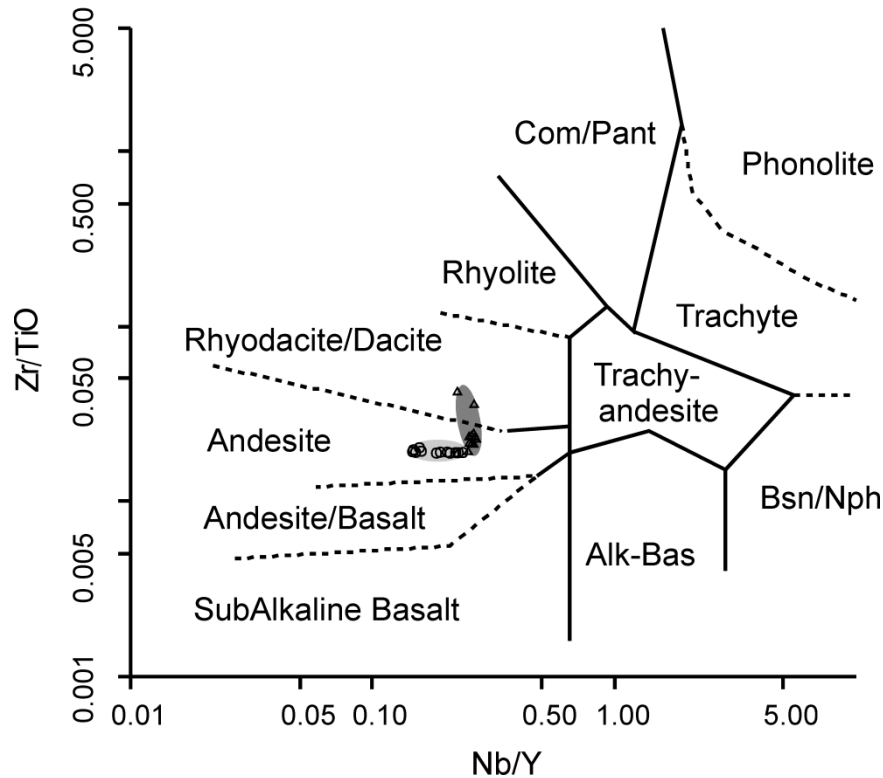


Figure 4.11: Volcanic classification plot (after Winchester and Floyd 1977). The circled markers in the light grey ellipse denote the concretion analysis, and the triangles in the dark grey ellipse denote the bentonite analysis (Chapter 2).

These analyses confirm the findings that the sediment within these carbonate concretions originated from an andesitic volcanic eruption (Chapter 2). As the protolith has been established, the major elemental data was normalised to an average andesite (Fitton *et al.*, 1982) and then to aluminium, because experimental work carried out by Spokes and Jickells (1996) has demonstrated that aluminium is only soluble under low pH conditions, and can therefore be considered immobile under normal marine conditions. This allowed the elemental enrichments and depletions in the concretions to be identified. The double normalised data of the concretions, shown in Figure 4.12.A, demonstrate that they are highly enriched in calcium, manganese, phosphorus, and iron, and depleted in silicon, potassium and sodium. Some samples also demonstrated depletion in magnesium, but this can be attributed to leaching out during weathering. For comparison, the double normalised XRF analysis of the host bentonite, shown in

Figure 4.12.B, has demonstrated that the bentonite is depleted in calcium, manganese, magnesium and iron. Interestingly, both the concretions and the host bentonite are heavily depleted in sodium.

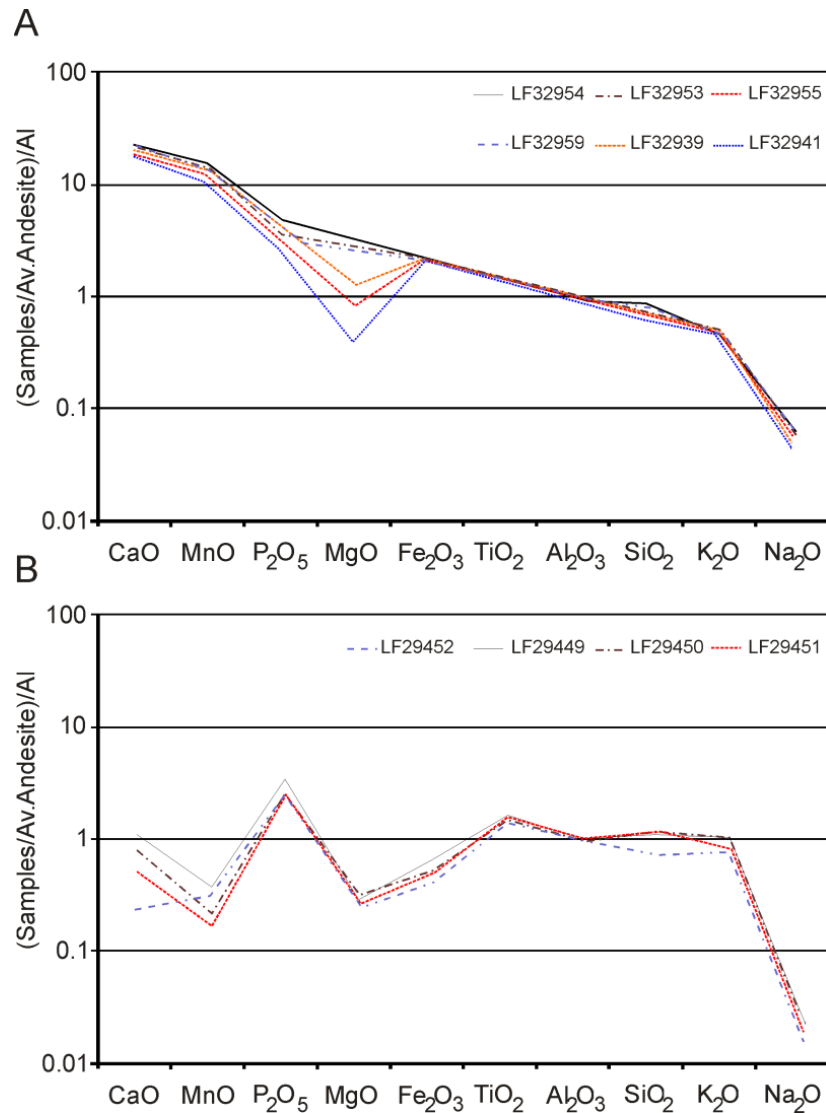


Figure 4.12: A. Representative XRF data from the carbonate concretions which have been double normalised. Note the enrichment in calcium and manganese, the variation in magnesium content, and the enrichment in iron. B. Representative XRD data from the host bentonite which have been double normalised. Note the depletion in calcium, manganese, magnesium, and iron. In addition, note that both the concretions and the bentonite are heavily depleted in sodium.

Transects were taken across the major growth axes of the concretions to examine the chemical variation which occurred during the growth of the concretion. Examination of the cations showed that those able to substitute into the calcite structure

(iron, magnesium, and manganese) showed a degree of symmetry about the centre of the concretion. The centre of the concretion is enriched in magnesium in comparison to the weathered rim (Fig. 4.13). This high proportion of magnesium is complemented by a decrease in the molecular proportion of calcium. Although the molecular proportion of iron appears relatively consistent across the concretion, it does increase within the brown weathered rim, while the molecular proportion of manganese has a uniform distribution across the width of the concretions.

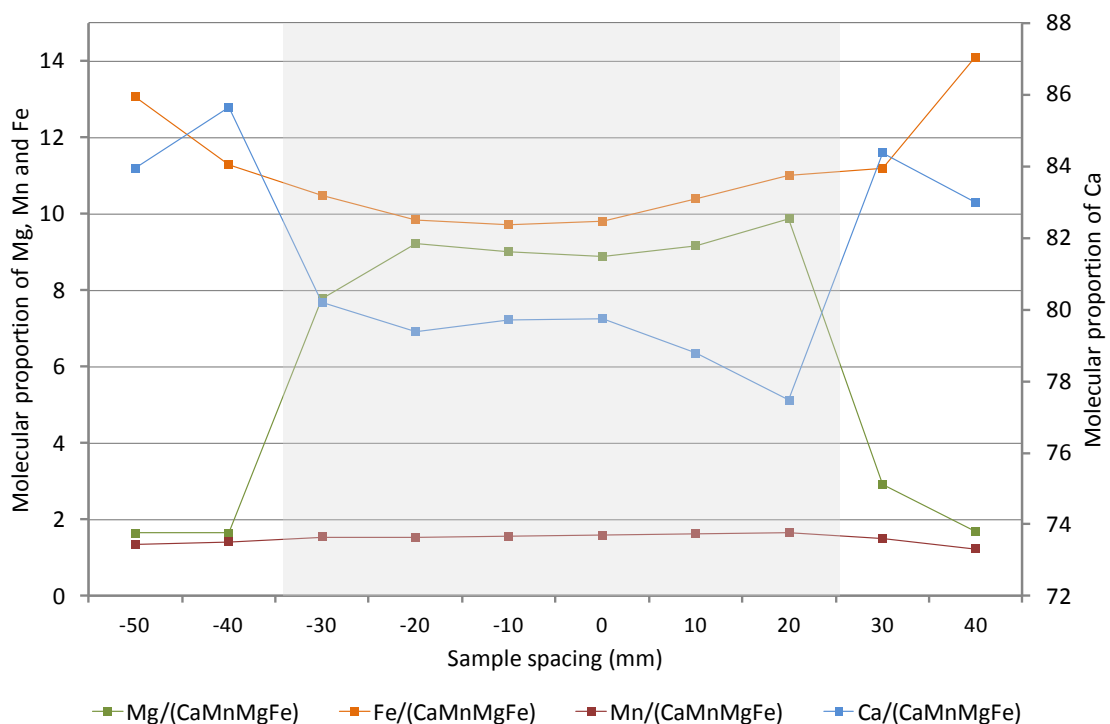


Figure 4.13: Molecular proportions of cations across the width of the concretion (HC2). Point 0 represents the centre of the concretion. Calcium molecular proportion has been plotted on the secondary axis. The grey shading represents the position of the unweathered blue heart.

Isotope analysis of the concretions

Transects of $\delta^{18}\text{O}$ and $\delta^{13}\text{C}$ were measured from bulk rock across the major axis of the concretions (Appendix P). The oxygen isotopic analyses are of whole rock carbonate ($\delta^{18}\text{O}^{\text{WRC}}$). However, the whole rock carbonate oxygen isotopes are affected by the ratio of dolomite to calcite, since the measured oxygen isotope value for dolomite

is higher by 3.8‰ relative to calcite (Ehrenberg *et al.* 2002). Therefore, they need to be corrected to equivalent calcite values by the following formula:

$$\delta^{18}\text{O}_c^{\text{WRC}} = \delta^{18}\text{O}_{\text{MEASURED}}^{\text{WRC}} - 3.8(\text{DOL}/(\text{DOL}+\text{CAL})) \quad (\text{Eq. 4.1})$$

Whilst $\delta^{18}\text{O}_c^{\text{WRC}}$ is the calculated calcite equivalent, $\delta^{18}\text{O}_{\text{MEASURED}}^{\text{WRC}}$ is the oxygen isotope value measured from the sample. DOL and CAL are the percentages of dolomite and calcite respectively derived from XRD whole rock analysis. Figure 4.14 A and B demonstrate the typical trends observed in the isotopic ratios. The carbon in the centre of the concretions is characteristically heavier and becomes lighter towards the concretion edges. The oxygen isotopic trends (an example of which is depicted in Figure 4.14 A and B) are the reverse; the oxygen isotopic ratios are lighter in the centre and become increasingly heavier with distance from the centre. The oxygen isotope ratio becomes lighter again at the transition between the brown weathered and blue fresh concretion (Fig. 4.14 A and B).

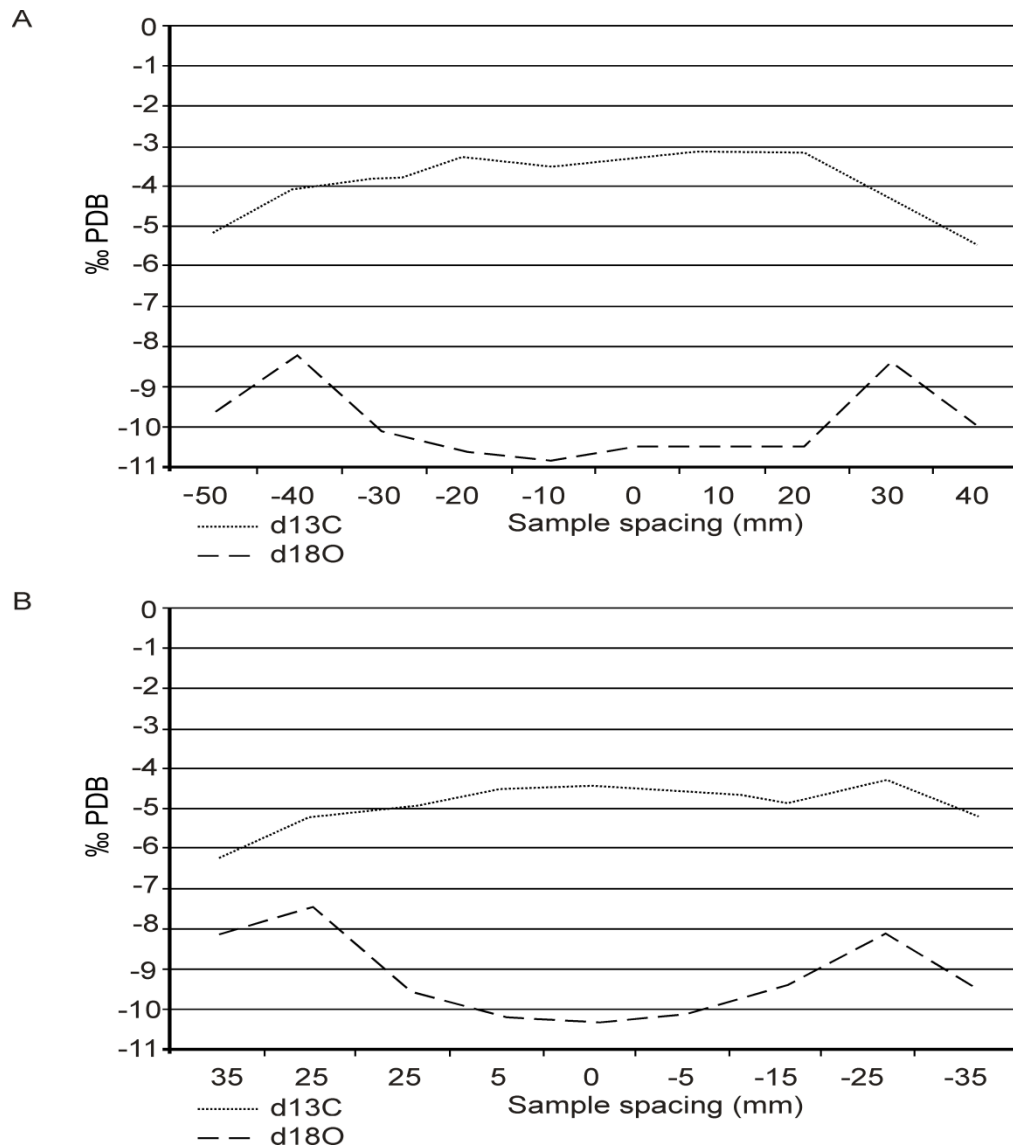


Figure 4.14: A. Concretion 1. B. Concretion 2. These are the typical observed carbon and oxygen isotopic transects across the diameter of the concretion. Point 0 represents the centre of the concretion. Note the slight variation between the left and right hand side of B, indicating that diffusion may have not been equal in all directions.

These isotopic trends are consistent throughout between the concretions, suggesting an identical mechanism of formation.

DISCUSSION

Textures, mineralogy and geochemistry

The concretions are characterised by an extremely fine-grained, interlocking matrix of carbonates, clays and quartz (both detrital and authigenic), which show no textural variation across the concretion axis of growth (see Figure 4.2). The fine grain size (<2 μm) must be the result of rapid crystal nucleation and slow growth. Work by Lin *et al.* (2002) demonstrated that during the formation of carbonates the ratio of nucleation to growth determines the size of the crystals formed; high nucleation and low growth rate results in the formation of smaller carbonate crystals, while larger crystals are the result of low nucleation and rapid growth.

At the time of concretion formation the volcanic ash may have been contributing ions to the pore fluid that inhibit carbonate precipitation. For example, the occurrence of Mg-calcite, dolomite and ankerite all infer that Mg^{2+} ions were present in solution, along with iron and calcium. Folk (1974) and Davis *et al.* (2000) have both demonstrated the effect magnesium ions have on precipitating calcite crystals; the magnesium ions poison specific crystal faces, which causes the crystal to elongate through its c-axis and grow fibrously. Essentially, the magnesium ions act as an inhibitor to the precipitation of large calcite crystals.

Immobile trace element data has confirmed that the protolith of this bentonite was originally an andesitic ash. Andesites are typically enriched in elements such as calcium, manganese, magnesium and iron. Interestingly, these are the elements that the host bentonite is depleted in, but the unweathered concretions are enriched in (Fig. 4.12 A&B). This study has presented strong evidence that the andesitic ash supplied the cations which are essential for carbonate precipitation. In addition, as carbonates are unable to accommodate ions such as zirconium, yttrium, titanium or zirconium it

suggests that the carbonate precipitated rapidly within the pore space entombing the volcanic ash.

An interesting comparison can be made between the fossils, which are composed of sparry calcite, and enriched in manganese, and the concretions, which are composed of high-magnesium calcite, ankerite and dolomite. This suggests a significant change in the chemistry of the carbonate precipitating fluid during the early diagenetic processes. During the precipitation of the sparry calcite in the fossil, the Eh conditions of the pore fluid need to be reducing enough to allow the formation of Mn^{2+} ions, which are soluble in seawater in comparison with the insoluble Mn^{3+} , but not so reducing that they promote the formation of Fe^{2+} ions, which can substitute into the calcite mineral structure. Subsequently, during the precipitation of the carbonate matrix, which does contain iron, the Eh of the pore fluid must have been further reduced in order to promote the formation of the Fe^{2+} ions. However, the noticeable lack of pyrite within this Lagerstätte indicates that the reducing conditions were never such that the formation of sulphide ions was promoted, and as a result the formation of pyrite was inhibited. Sufficient Fe^{2+} for pyritization is evident because the carbonates contain iron.

As well as Eh, the pH of the pore fluid must also be considered. Carbonate is the principal mode of preservation in the Herefordshire Lagerstätte and this indicates that the pH was alkaline, because carbonate dissolution is inhibited at $pH > 8$ (Pokrovsky & Scott, 2001). As evident from the double normalised plots the concretions and the bentonite are all depleted in sodium. Sodium ions that enter solution would react with the water to produce sodium hydroxide, which has a high pH and can drive the system to conditions favourable for the rapid precipitation of carbonate minerals.

It is important also to consider the difference between an andesitic ash, which hosts the Lagerstätte, and a rhyolitic ash, the composition of most non-fossiliferous

ashes found in the Welsh Borderlands (Teal & Spears, 1986). Rhyolitic bentonites are compositionally evolved (Teal & Spears, 1986), meaning that they are enriched in silica, aluminium and sodium, but are depleted in calcium, magnesium, manganese, and iron. Therefore, they are unable to supply the cations necessary for carbonate formation and are unlikely to be associated with exceptional preservation involving replacement of non-biomineralized tissues with carbonate phases.

As well as the occurrence of carbonates, the EDX analyses have also identified the presence of chalcedony within the matrix of the concretions. Chalcedony is an amorphous phase of silica, which contains 1-2 weight percent water, and consequently does not appear on XRD traces (Heaney, 1993). It is a common product of volcanic ash alteration (Morad *et al.*, 2010). Volcanic ash is composed of microscopic fragments of siliceous volcanic glass and, during weathering, this silica typically becomes liberated during alteration and enters solution (Murata, 1940), where it is available for the formation of chalcedony. Chalcedony is typically formed under near surface conditions, at temperatures no higher than 150°C in a solution with a high availability of silica and an alkaline pH (White & Corwin, 1962). This supports my hypothesis that the pH of the pore fluid was alkaline, in addition the cryptocrystalline form of chalcedony is indicative of relatively fast precipitation.

The XRD and XRF data demonstrate a radial variation in the minerals present within the matrix of the concretions. Using stoichiometry it is possible to determine the amount of silicon present as kaolinite and infer the amount of silicon present as quartz (and chalcedony). It must be noted that this method makes the assumption that all the aluminium detected is present as kaolinite since it was the only clay mineral detected on the whole rock XRD. Plotting the XRD mineral percentages and the calculated concentrations together (Fig. 4.15) demonstrates that the weight percent aluminium is

consistent with the kaolinite trend, increasing from the centre outwards. In addition, the silicon (minus the silicon in the clay percentage), is consistent with the XRD whole rock percentage of quartz (Fig. 4.15).

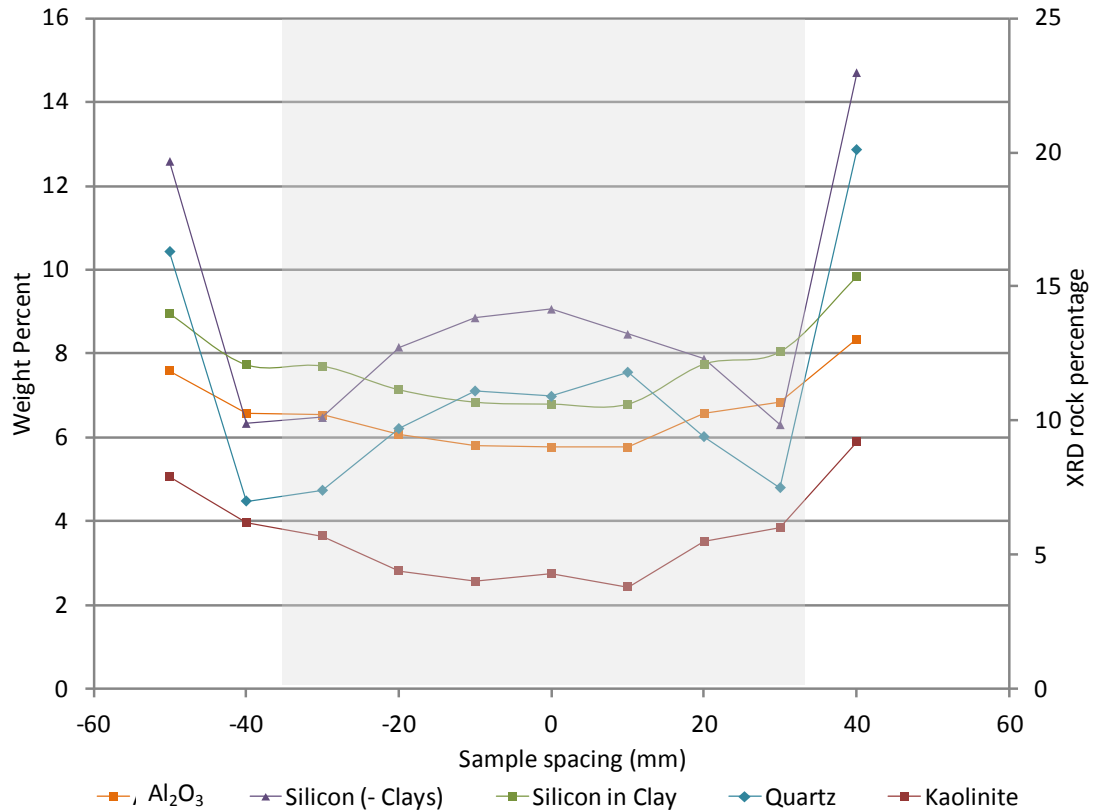


Figure 4.15: Plot of aluminium and silicon data after the stoichiometric removal of clay minerals with the plots of mineral percentage from the XRD. Note the consistency between the two analytical techniques. Point 0 represents the centre of the concretion and the grey shading represents the position of the unweathered concretion.

The increase in the formation of clays at the edges of the concretions may reflect a point during their formation when carbonate precipitation slowed, giving way to the precipitation of clay minerals. This may be the result of a pH shift towards more acidic conditions, which result in quartz precipitation, or the pore fluid becoming exhausted of the cations necessary for carbonate precipitation.

A similar relationship can be identified within the different carbonate minerals, by plotting the percentage of dolomite, calcite, and siderite with the molecular proportions of calcium, magnesium, manganese and iron (Fig. 4.16). Figure 4.16

provides further ground truth of the XRD data and demonstrates that the decrease in the percentage of dolomite is consistent with the decrease in the proportion of magnesium.

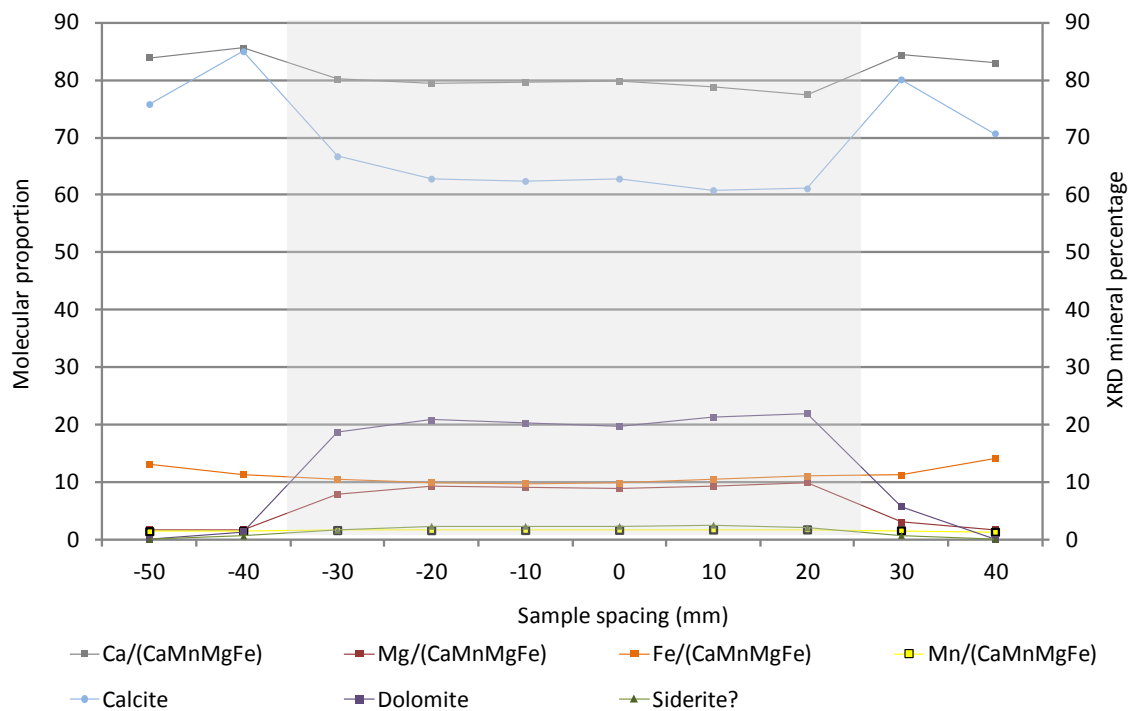


Figure 4.16: Plot of the molecular proportions of calcium, magnesium, manganese, and iron with the plots of mineral percentage from the XRD. Note the consistency between the two analytical techniques. Point 0 represents the centre of the concretion.

Figure 4.16 also demonstrates that the increase in molecular proportion of calcium from the centre of the concretion is consistent with the increase in percentage of calcite within the concretion. However, there is a contrast between the molecular percentage of iron and the XRD percentage of siderite (Fig. 4.16), as the percentage of siderite decreases from the centre outwards, but the proportion of iron increases towards the margins. However, XRF is an analysis of total iron whilst siderite is a specific iron mineral, thus the iron is present as a form that the XRD cannot identify, such as an amorphous phase, possibly iron hydroxide. So, to ascertain the amount, if any, of iron which had been transported into the concretions during weathering this study used a series of calculations based on stoichiometry, using the elements Ca, Mn, Mg, and Fe

obtained from XRF, the total carbon data obtained from LECO™ analysis and the molecular formula of the minerals involved (see Appendix Q). This was carried out in the following steps:

- The %C, obtained from the LECO™, is converted into weight percent CO₂ and the Fe₂O₃, obtained from the XRF, is converted into FeO.
- The weight % CO₂ is then converted into CaCO₃. At this point it can be inferred that there is not enough calcite within the samples to account for the levels of carbon analysed (see DCO₂ in Appendix Q).
- Then with each successive stage the cations Mg, Mn and Fe are assigned to the remaining CO₂, eliminating their carbonate phase.
- After the removal of the iron the remaining carbon is converted back into %C.

These stoichiometric calculations suggest that no further iron has been added to the concretions, even during weathering. Interestingly, the excess component is not iron, but carbon. There is excess carbon present within the samples which is not in the form of carbonates. It is highly likely that this excess carbon is organic carbon, which cannot be detected by the XRD and it is possible that the carbon is bound to the surface of clay minerals (Hedges & Keil, 1995). Therefore, based on these calculations it is probable that the iron hydroxide present, which gives the weathered concretions their buff brown colour, is from the re-mobilisation of iron from the carbonates during weathering. This conclusion appears valid, as even if all possible sources of error were summed, the results would still show that no iron had been added to the system and that carbon is present in excess.

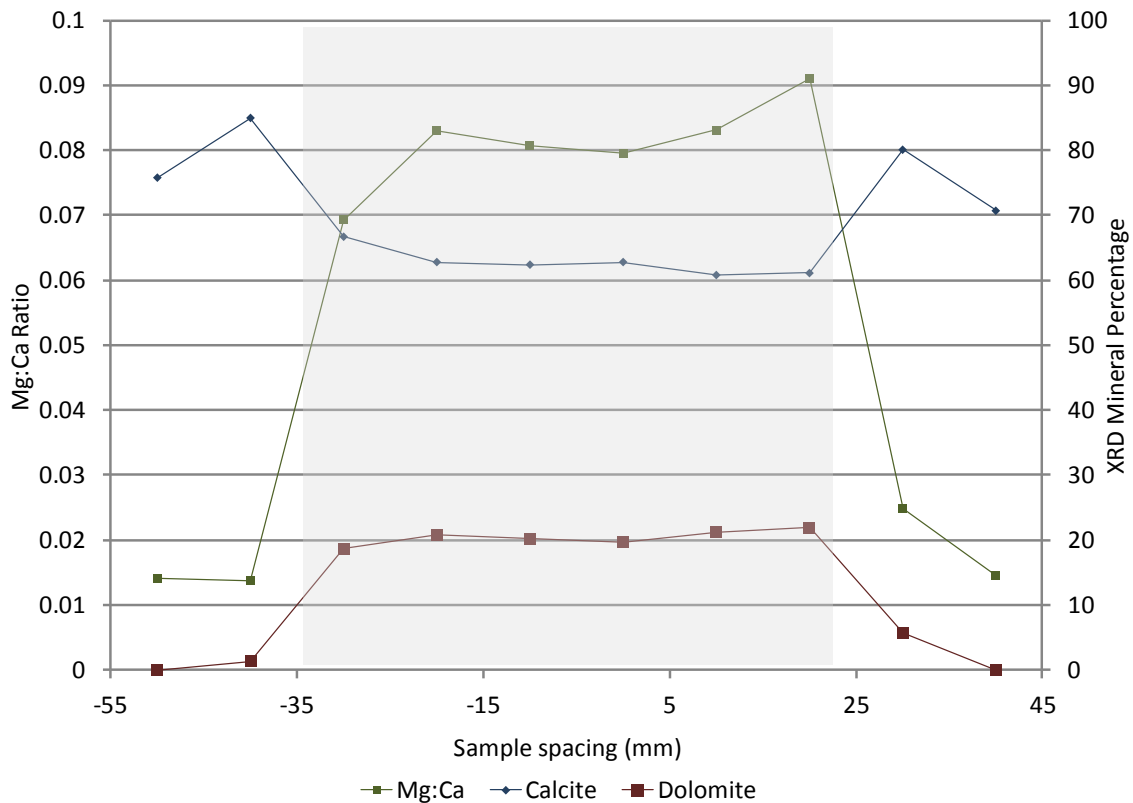


Figure 4.17: Mg:Ca ratio across the concretion and the percentage of dolomite and calcite. Point 0 represents the centre of the concretion, and the grey shading represents the unweathered centre of the concretion.

Interestingly, these analyses infer that the initial formation of dolomite was towards the centre of the concretion. The decrease in both the Mg:Ca ratio (Fig. 4.17) and the percentage of dolomite towards the edge of the concretions may indicate that the precipitation of dolomite was superseded by the precipitation of calcite. In fact, the depletion of magnesium may be responsible for the change from dolomite to calcite and may signify the point at which the available magnesium from the volcanic ash was exhausted. However, it may also reflect a weathering zone and the re-mobilisation of the magnesium.

The timing of the dolomitization needs consideration given the evidence presented above. The radial changes in the distribution of dolomite and the Mg:Ca, infers that the precipitation of the dolomite may have been an earlier event. Orr *et al.*

(2000a) suggested that the dolomite represented a later dolomitization event: brought about by the illitization of the smectite. However, the mechanism proposed by Orr *et al.* (2000a) does not account for the higher percentage of smectite recorded in the host bentonite (Chapter 2) in comparison with the concretions, as this smectite would have gone through the same alteration as well. In addition, the process of illitization typically occurs between 100 and 140°C, but has been suggested to initiate at about 70°C (Bjørkym *et al.*, 1993; Cuadros & Linares, 1996; Cuadros, 2006). But the examination of the conodont colour alteration index (CAI) of locally collected conodonts indicates that the temperature of the deposit was never above 80°C (Königshof, 2003). It is therefore unlikely that the process of illitization had reached any substantial advancement within the host bentonite. Also if the dolomitization does represent a later event then it would be expected that the percentage of dolomite and Mg:Ca ratio would decrease towards the centre, recording the advancing dolomitization from the edges inwards, assuming that diffusion is equal in all directions.

This study suggests that there are two possible phases of dolomite formation: an initial phase, which forms the euhedral ankerite/ferroan-dolomite crystals, and a secondary phase, which forms the anhedral dolomite, and which represents the later alteration of the initial phase after iron remobilisation. The prerequisite for the process of dolomite (and ankerite) formation is a pore fluid with an elevated Mg:Ca (and Fe:Ca) ratio, a pore fluid saturated with carbonate ions, and enhanced alkalinity (Hardie, 1986; Hendry, 2002). These conditions can be explained through the interaction of the andesitic volcanic ash. As previously mentioned, the volcanic ash goes through a series of cation exchanges with the pore fluid and is an ideal source of magnesium and iron. It has also been suggested in this study that the interaction of sodium ions from the ash could generate the enhanced alkalinity and supersaturate the pore fluid with carbonate

ions. However, as the pore fluid is derived from seawater there is likely to be also a concentration of sulphate ions, which have been documented to inhibit the formation of carbonates (Walter, 1986). The sulphate reduction of organic matter is typically inferred as the process which removes this inhibitor to allow dolomite to precipitate in a normal marine setting (Raiswell & Fisher, 2004; Wright & Wacey, 2005), but, this presents this hypothesis with a problem; as already stated, one in three concretions appears to contain fossils. For these fossils to have survived, it would have required a considerable additional amount of organic material to have been available for sulphate reducing bacteria to have removed all the sulphate ions from the pore fluid. However, this study suggests a different mechanism for removing the sulphate inhibitor without the need for vast amounts of organic matter decay by sulphate reduction. Experimental work by Shiraki *et al.* (1987) has demonstrated the absorption of sulphate ions during the early, rapid, cation exchanges which occur between the volcanic ash and the seawater shortly after deposition. This process could have been responsible for depleting the pore fluid of sulphate ions during the carbonate formation in the host bentonite.

Therefore, this study proposes that dolomite, and ankerite precipitated early rather than late and this would account for the radial distribution where the greatest proportion of dolomite is at the centre of the concretions.

Isotope discussion

Concretions which obtain their carbon from the recycling of organic matter have characteristic carbon isotopic ratios which are typically -20 ‰ PDB (Irwin *et al.*, 1977). However, the new carbon isotopic data presented in this study are too high, indicating that the concretions are not the result of organic matter decay, but instead are influenced by the environment of deposition. Transects across the concretion demonstrate that

carbon becomes isotopically lighter towards the edge of the concretion. The range of carbon isotopic ratios for the concretions varies from -3.10‰ to -6.34‰. These values do not characteristic of organic matter decay, which is typically -20‰ (Irwin *et al.*, 1977). The variation in the carbon isotopes across the transects may represent the varying proportions of carbon which originated from the seawater compared to the carbon from the organic carbon; the greater proportion could have only been sourced from the seawater as the volcanic ash is thought to have been considerably de-gassed at this stage. Woo and Khim (2006) suggest that concretions with this isotopic trend form within a few centimetres of the sediment-water interface and would utilise carbon from the pore fluid, which contains a residual seawater composition, and with burial an increased proportion of organically derived carbon would be incorporated.

The oxygen isotopes have not exhibited a similar trend; instead the isotopic ratio is, unusually, light in the centre and becomes heavier towards the edges. It is also important to note the small light excursions on the edges of the concretions correlate to the brown, buff, weathered regions. Wenlockian brachiopods have been shown to have $\delta^{18}\text{O}$ values of -2‰ to -6.5‰ (PDB), and Wenlockian seawater is estimated to have been about -3.5‰ (SMOW) (Azmy *et al.*, 1998). These values indicate that the carbonate within these concretions is enriched with isotopically light oxygen, and implies that seawater is not the source of the oxygen within the carbonate minerals. There are several possible causes for the occurrence for isotopically light oxygen at the centre of the concretions and they will be discussed below.

It is conceivable that these $\delta^{18}\text{O}$ values are either the result of meteoric water incorporation into the concretions during the initial precipitation, or the oxygen isotopic ratios have been reset through re-equilibration of the calcite with meteoric water during diagenesis. Through kinetic fractionation, meteoric water is typically enriched with

oxygen-16 and as a result negative values are usually associated with its occurrence (Hays & Grossman, 1991). However, meteoric water was not involved during the concretions' initial formation as the emplacement method of the host bentonite has been suggested to be a sub-aqueous turbidity current (Chapter 2), which would have entrained seawater, and the environment of deposition has already been identified as an outer shelf marine environment (Briggs *et al.*, 1996). However, it is possible that there has been later resetting by later interaction with meteoric water. Although, the conodont colour alteration index indicates that the deposit has never exceeded temperatures of 80°C this does not rule out low temperature diagenesis, to test this oxygen isotope values can be used to calculate a palaeotemperature, because minerals precipitated from low temperature fluids are preferentially enriched with ^{18}O , and in comparison minerals precipitated from warmer fluid are enriched in ^{16}O (Kasting *et al.*, 2006). Estimates of the temperature of formation made using the temperature equation of O'Neil *et al.* (1969) (Equation 3.2) produces estimates of 40 to 50°C which infers low temperature diagenesis, but also supports the argument that these oxygen isotopic signatures are not a primary feature.

Organic matter which is going through sulphate reduction has been demonstrated by Sass *et al.* (1991) to deplete the pore fluid of oxygen-18; it is another process that could account for the enrichment of oxygen-16 in the concretion. However, this process can be disregarded, because typically only one in three concretions examined were associated with a fossil, and also because, as the carbon for the carbonate has not been acquired from the decay of organic matter alone, it is unlikely that organic matter is responsible for the unusually light oxygen ratios.

Oxygen fractionation must also be considered. Equilibrium fractionation occurs as the crystal precipitates from the pore fluid; the precipitating crystals attempt to reach

equilibrium with the fluid, and the rate of growth may determine the extent of this equilibrium. Work by Dietzel *et al.* (2009) demonstrated that when a calcite crystal precipitates at a rapid rate it is not in oxygen isotopic equilibrium with the solution it is precipitating from. Further to this, the work of Coplen (2007), who examined slow inorganic calcite growth at the Devils Hole in Nevada, showed that slowly precipitating calcites were in oxygen isotopic equilibrium. However, Coplen (2007) suggested that a re-evaluation of the oxygen isotope fractionation factor was required; if Devils Hole represented isotopic equilibrium then marine calcites were enriching oxygen-16 preferentially.

As the pH of this system is hypothesised to be pushed towards alkaline conditions there is also a possible kinetic fractionation associated with the formation of CO_3^{2-} ions under alkaline environments. This fractionation was first noted by Spero *et al.* (1997) who observed that an increase in seawater alkalinity resulted in the formation of a foraminiferal test which was preferentially enriched in oxygen-16. Zeebe (1999) later suggested a mechanism for this fractionation which involved the distribution of carbonate species (i.e. H_2CO_3 , HCO_3^- , and CO_3^{2-}), which is a function of the pH of the solution. For example, under alkaline conditions the dominant carbonate species is CO_3^{2-} . This mechanism is supported by the experimental work of Kim *et al.* (2006) who demonstrated that the CO_3^{2-} ions are depleted in oxygen-18, relative to their parent HCO_3^- ions and concluded that this was because of the preferential dissociation of lighter isotopologues and incomplete re-equilibrium of the CO_3^{2-} with the water.

The precipitation of early minerals also needs to be taken into account as they may have resulted in a pore fluid that was enriched with oxygen-16. Mozley and Burns (1993) suggested this concept, which involves precipitating authigenic minerals that are enriched in oxygen-18. Mozley and Burns (1993) suggested that after the precipitation

of minerals rich in oxygen-18 the remaining pore fluid, from which the final carbonate cement phase precipitated, which would have been enriched in oxygen-16.

There is also a documented association of oxygen-16 enrichment within concretions that are associated with volcanic ash. Woo and Khim (2006) carried out isotopic analysis on concretions from Korea, and suggested that the enrichment in oxygen-16 was the result of the pore fluid interacting with volcanic sediment. In addition, Cuadros *et al.* (1999) conducted laboratory based experiments on the effect that alteration of volcanic glass had on the fractionation of oxygen isotopes; they identified an enrichment of oxygen-18 within the altered glass. This would result in a pore fluid that was enriched in oxygen-16, and as the carbonates precipitated from that fluid it would become, unusually, enriched in oxygen-16.

All of the processes described above can cause the enrichment of oxygen-16. Consequently, the data is inconclusive and is unable to distinguish between the processes described above.

Mechanism of concretion formation

Any mechanism of formation must answer the key observations: a lack of internal radial structures/fabric, a lack of association with fossils, radial variation of the chemistry, and accommodate rapid precipitation. The key control for the formation of the carbonate concretions is the rate of diffusion of reactants to the site of nucleation. Based on the work by Seilacher (2001) spherical concretions, recovered from the host bentonite, infer a rate of diffusion that was equal in all directions. Typically in homogeneous sediment it is assumed that concretions will grow spherically, as diffusion is equal in all directions. However, Seilacher (2001) concluded that as compaction occurred the permeability in the vertical directions would be reduced and therefore the

shape would be affected. It is likely, therefore, that the lens-shaped concretions recovered from the host bentonite are the result of increasing compaction. The occurrence of plano-convex shaped concretions within the bentonite does not concur with work by Seilacher (2001); his work suggests they occur within slowly depositing sediment, whereas the evidence presented in Chapter 2 suggests that the deposition of the bentonite was a single, rapid, event. Therefore, the plano-convex concretions may be the result of reduced permeability by rapid clay precipitation within the bentonite.

While a substantial amount of work has been carried out on the formation of carbonate concretions in mudrocks and limestones (e.g. Raiswell, 1971; Coleman & Raiswell, 1993; Mozley & Burns, 1996; Raiswell & Fisher, 2000) there has been little attention paid to the formation of carbonate concretions in volcanic sediment. However, concretions and nodules have been recorded within volcanoclastic deposits. For example, Fukue (2010) used the existence of nodules within bentonite formations as evidence of carbonate production and dissolution, and Püspöki *et al.* (2008) recorded the occurrence of non-fossiliferous carbonate concretions within bentonite deposits, but did not elucidate on their mechanism of formation. Some concretions recovered from volcanic sediment are associated with fossils, for example, the mammal-bearing carbonate concretions from the Miocene, Sucker Creek Formation in south-eastern Oregon (Downing & Park 1998), but there is little discussion surrounding their formation.

For the mechanisms of concretion formation within mudstones and limestones the reader is directed to Raiswell & Fisher (2000), but to summarise there are two methods of concretion formation: pervasive and concentric growth. Pervasive growth is typical of sideritic/dolomitic concretions and occurs when there is simultaneous nucleation and precipitation of isolated patches of carbonate crystals followed by a final

cementation phase. Alternatively, concentric growth is typical in concretions which are composed of microsparite. This mechanism occurs when there is continuous precipitation of crystals that are mineralogically and chemically uniform. In addition, concentric growth typically results in radial variations in mineral textures. Raiswell and Fisher (2000) also concluded that the only certain way to distinguish between the two end-members (pervasive or concentric growth) was to use fabrics and textures within the concretions' matrix. They also concluded that apparent radial variation in the chemistry may equally reflect an early to late cement phase and that those lines of evidence should only be used once the fabric has established a growth mechanism. Mozley and Burns (1996) had already acknowledged the difficulty with interpenetrating geochemical evidence due to the typical low resolution of the geochemical data (i.e. 10 mm³) and suggested that the data may represent mixed chemical zones.

The lack of the radial fabric variation could be put down to the nature of the sediment, a volcanic ash, which has deposited heterogeneously. The apparent radial chemistry could be the cementation phase that precipitated in the pore space, which radiated out from a central nucleation point. A nucleation point has yet to be identified, but is rarely the fossil, as typically only 1 in 3 concretions contain a fossil. Rapid precipitation would be aided by the chemical interactions of the volcanic sediment with the pore fluid, which has been described above.

Raiswell and Fisher (2000) also summarise three chemical models for the growth of concentric carbonate concretions, which achieve the carbonate supersaturation necessary for the formation and will be discussed below.

The equilibrium model elaborates on the work of Raiswell (1971). Its occurrence is typically associated with sediment in which the supersaturation of carbonate is widespread. Raiswell and Fisher (2000) concluded that the concretion

could nucleate around any suitable nucleus, which does not necessarily have to be organic. The concretionary carbonate is derived from the pore fluid and reflects the overall chemical and isotopic trends. However, Raiswell and Fisher (2000) noted a lack of carbonate precipitation in modern day sediment, which was supersaturated with carbonate, and consequently suggested that the equilibrium model only occurs over large burial depths, and with time.

The local-equilibrium suggested by Coleman and Raiswell (1993) requires microbial processes, such as sulphate reduction of organic matter, to create a microenvironment within the concretion-forming zone. The microenvironment has a prolonged carbonate supersaturation and alkalinity. The isotopic and chemical signature generated by this model reflects the microenvironment, with organic matter typically forming the nucleation point of the concretion.

The fluid-mixing model, which was generalised by Raiswell and Fisher (2000), requires the mixing of meteoric water, which is instrumental for concretion growth. The external fluid decreases the concentrations of magnesium and sulphates, which inhibit calcite growth.

Of these three models the equilibrium model is most likely although it was defined on mudrocks, the mechanism does appear to fit the criteria of the Herefordshire Lagerstätte. The supersaturation of the pore fluid with carbonate can be explained through the cation exchanges of the volcanic ash and the seawater. In addition, it does not require an organic nucleus, which suggests that any volcanically derived feature that could be overlooked may form the nucleation centre. Although, this process is absent from modern seawater, the reactive nature of the ash may have increased the rates of reaction allowing the process to occur on a shorter timescale. The other two

mechanisms, local-equilibrium and fluid-mixing, can be ruled out due to the lack of organic matter and the lack of meteoric water association, respectively.

There is evidence to favour both styles of concretionary growth, pervasive and concentric. However, although all the mechanisms are defined by mudrock and limestone concretions, the majority of the evidence suggests a concentric growth mechanism which was initiated by an equilibrium chemical model. This study suggests, therefore, that the growth of the Herefordshire Lagerstätte concretions begins with the deposition of the volcanically derived sediment, which would have been homogeneous and would have widespread carbonate supersaturation as a result of its rapidly altering chemistry. During the exchanges with the seawater the volcanic ash would become preferentially enriched with oxygen-18 (Fig. 4.18A), leaving a pore fluid unusually enriched in oxygen-16. The calcite within the fossils is precipitated and these calcite crystals are free of magnesium and iron. Afterwards conditions become reducing and iron(III) becomes iron(II), the initial carbonate precipitation would begin with the random precipitation of euhedral ankerite crystals (Fig. 4.18B). The final stage of carbonate precipitation begins around an unidentified nucleus, and precipitates outwards (Fig. 4.18C). As the carbonate precipitation continues through the pore space, its changing chemistry reflects the evolving chemistry of the pore fluid, producing the radial variation in the element and isotopic data.

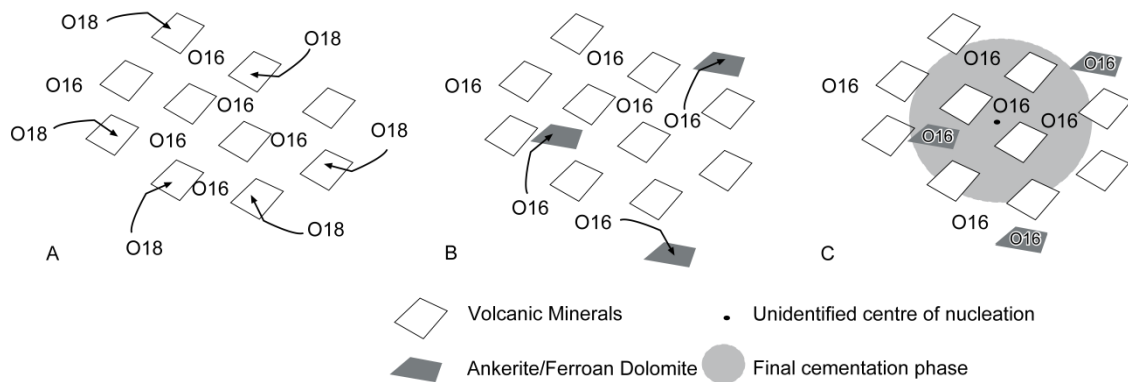


Figure 4.18: Schematic concretion formation. A. Oxygen isotope exchange between the seawater and the volcanic ash. B. Initial precipitation of the randomly placed ankerite crystals. C. Final cementation phase.

Relationship to the fossils

One hundred concretions were examined in order to evaluate the relationship between the fossils and the carbonate concretions. The following points can be concluded. The majority of the fossils are not typically found at the centre of the concretion. However, the larger the fossil, relative to the concretion, the more likely that the fossil is to be found at the centre of the concretion. For example, out of the brachiopods examined — which were the largest faunal elements relative to their concretion (length of the shell on average 35% of the concretion diameter) — 100% of them were at the centre of the concretion. The exception to this rule is *Offacolus kingi*; it is one of the smallest species and out of 19 specimens examined 73% were within 6 mm of the measured centre point of the concretion. There also appears to be no significant link between the mechanisms causing the formation of the concretions and those causing the inclusion of fossils within them; inclusion into the carbonate concretions is an apparently random event. However, to date no fossil has been recovered from the bentonite that does not have a concretion enclosing it.

CONCLUSIONS

The formation of carbonate concretions on its own is a concept that is yet to be fully understood. The evidence to identify the methods of growth is ambiguous and contradictory, as is evident in this example. Whilst a uniform matrix texture supports a pervasive growth mechanism, radial variations within the chemical and isotopic data support the concentric growth mechanism. As emphasised previously, the majority of the mechanisms for carbonate concretion formation (Raiswell & Fisher, 2000, 2004; Coleman & Raiswell, 1993, 1995) are all modelled on mudrocks from marine settings and the ability to apply these models to volcanic sediment has yet to be established.

However, this new data have demonstrated for the first time that the carbonate concretions within the bentonite host of the Herefordshire Lagerstätte are not the result of the decay of more organic matter, as previously suggested by Orr *et al.* (2000a), but that they initially formed just below the sediment water interface and continued to form during the process of compaction.

While it would seem a pervasive growth mechanism would explain the lack of correlation between the concretion and the fossils, the chemical and isotopic transects favour the formation of the concretions by concentric growth through the equilibrium model described by Raiswell and Fisher (2000). There is compelling evidence to suggest that the volcanic ash has facilitated the growth of these carbonate concretions; the cation exchanges between the ash and the seawater established the high pH, supersaturated the pore fluid with carbonate ions, removed the kinetic inhibitor of dolomite formation and elevated Mg:Ca (and Fe:Ca) ion ratio to promote the precipitation of dolomite (and ankerite).

CONCLUSIONS AND FURTHER WORK

Despite the palaeobiological importance of the Herefordshire Lagerstätte, only one investigation (Orr *et al.* 2000a) has addressed the mechanics of preservation of this extraordinary window into a Silurian marine ecosystem. The present study has used a holistic approach to expand on, test and refine the Orr *et al.* (2000a) model.

The holistic approach involved not only the analyses of the fossils, but also examined the concretions and the bentonite host, and defined the chemical pathways between them. The host bentonite has been geochemically characterised in order to determine its original source and tectonic setting (Chapter 2). A comparison of four of the commonly occurring taxa has been carried out to assess any possible species-specific variation (Chapter 3). Geochemical and isotopic data has been presented for the growth of the concretions, which encase the fossils and increase their preservation potential. The present study also examined and discussed the mechanism of formation of the concretions of the Herefordshire Lagerstätte (Chapter 4).

The style of preservation of the Herefordshire Lagerstätte is rare on a global scale. This study demonstrates that to truly understand such Lagerstätten it is necessary to employ a holistic approach that covers multiple fields of geology. The main conclusions of this study are summarised below.

GEOCHEMISTRY OF THE VOLCANIC ASH

The host metabentonite sediment sits within the Coalbrookdale Shale Formation, 10cm above the Dolyhir-Nash Scar Limestone-Coalbrookdale Formation boundary. The deposit originated from an andesitic eruption from a destructive plate margin (Chapter

2). Its unique signature has been confirmed through evaluation and comparison with other bentonites in the Welsh depositional basin. Evidence has also been presented that suggests the deposit was emplaced through a sedimentary mass movement flow event. In addition, geochemical analyses indicate that its source is not the same as that for the other Welsh Borderland bentonites and suggest two other possible sources: the Dingle Peninsula in southwest Ireland, or the Mendip Hills in Somerset, England. A mechanism has also been suggested through the analyses of the host sediment to account for the accumulation of the carbonates, within the fossils and the concretions: mobile sodium enhanced and prolonged the alkalinity of the pore fluid. Furthermore, it has been shown that the andesitic ash would act as another reservoir of the key cations, such as calcium, magnesium, iron and manganese, which are required for carbonate precipitation. In contrast, an evolved, acidic magma would only be rich in silica, sodium and aluminium and therefore would be unable to support the preservation mechanism proposed, which has been shown to require the availability of calcium. XRD analyses indicate that, due to the greater proportion of illite to smectite, the host deposit should be more correctly defined as a metabentonite.

PRESERVATION AND TAPHONOMIC PATHWAY

An assessment of four of the common Herefordshire taxa demonstrates they have a similar style of preservation, denoting a similar taphonomic pathway. The association of calcites and kaolinite suggests that the pH of the pore fluid altered during the preservation process. The authigenic precipitation of the clay minerals surrounding the organism is regarded as the initial phase; this is associated with the decay of the soft tissues and is confirmed through decay experiments. Subsequently a link was established with the decaying organic matter and the composition of the clay minerals

precipitated. The occurrence of the gut traces in the fossils, in life position, denotes that these fossils had not gone through a significant amount of decay before the precipitation of the sparry calcite. This would indicate that there was no void stage as proposed in the model by Orr *et al.* (2000a). Rather, this study proposes a model in which the nucleation and growth of calcite crystals occurred through the soft tissues, moulding and replacing the organic tissues. The stepwise breakdown of the volcanic ash accounts for the unusual occurrence of sparry calcite within a marine setting, and explains the difference between the fossil calcite composition and the matrix of the concretions.

CONCRETION FORMATION

The new isotopic data presented (Chapter 4) indicates that the formation of the concretions is not due to the decay of more labile organic matter as previously suggested (Orr *et al.* 2000a). This study provides evidence for the precipitation of the concretions as an inorganic event, and suggests that the chemical conditions favourable to the formation of dolomite occurred during the initial formation. The alteration of volcanic glass provides a suitable sink for the sulphate ions in the seawater, mitigating the need for sulphate reduction, but also maintains a pH favourable to the formation of carbonates and elevates the Fe:Ca and the Mg:Ca ratios. The mechanisms of concretion formation have been previously developed on concretions which have been formed in mudrocks and limestones. Therefore, it is not yet fully known if they can be applied to concretions from volcanic rocks. While concretions formation by the pervasive mechanism, as defined by Raiswell and Fisher (2000), best accounts for the uniform mineral texture, zoned ankerite/dolomite, and preserves the fossil, without the need for the fossil to be the nucleus of the concretion's formation, and also explains why concretions are found without fossils preserved within them. Alternatively, the

concentric growth mechanism, defined by Raiswell and Fisher (2000), is supported by the radial variation in the chemical and isotope data sets. Interestingly, the equilibrium model defined by Raiswell (1971), which involves pore fluid supersaturated with carbonate and a nucleus that does not have to be organic, may have been established during the volcanic ash – seawater interaction, which promoted the formation of the Herefordshire Lagerstätte concretions.

Given that both mechanisms do not require an organic nucleus to initiate the concretion precipitation and growth they are equally as likely to have occurred, but the majority of the evidence and the hypothesised supersaturation of the pore fluid (see Chapter 1) would favour the concentric growth mechanism. Interestingly, a concretion which grew by a concentric growth mechanism initiated through an equilibrium model would have no direct relationship to the fossil.

OUTCOMES

This study has completed the key objectives, as stated in Chapter 1. In addition, this study has identified the key factors leading to the formation of the Herefordshire Lagerstätte:

1. **emplacement of the deposit.** The rapid emplacement of the sediment by a sedimentary mass movement flow would acts as a suitable kill mechanism, because ash falls, typically, do not have a significant impact on nektobenthic fauna.
2. **composition of the volcanic ash and its rapid alteration.** As an andesite, the ash is a likely source of the Ca, Mn, Mg and Fe cations, which are essential for the formation of the carbonate.

3. **cation exchanges.** Removing inhibitors to the formation of sparry calcite, and the kinetic inhibitors to dolomite formation.
4. **clay precipitation.** The authigenic precipitation of clay minerals, templating the organic matter, provides a mould for the calcite and may extend the preservation window.
5. **rate of reaction.** Being a fine grained ash, it was able to react at a fast rate. Decay of the animal carcass and the alteration of the volcanic ash are the two key processes that would have occurred on the same timescale, implying the possibility for the two chemical processes to interact with one-another.

EVALUATION OF THE TAPHONOMIC MODEL

This taphonomic model requires some evaluation to determine if there are any other possible pathways the preservation could follow.

This model assumes a stepwise release of ions from the volcanic ash. However, what if there was a total release of the ions from the volcanic ash in one single cation exchange event? There are two reasons why this can be disregarded. Firstly a single cation exchange event is unlikely as all experimental work demonstrates stepwise cation exchanges occur (Shiraki *et al.*, 1987; Stefánsdóttir & Gíslason, 2006). Secondly, sparry calcite is not typically found precipitating within modern marine environments because Mg^{2+} ions can interact with the growing crystal surface and cause elongation in the c-axis forming fibrous calcite crystals (Folk, 1974; Davis *et al.*, 2000). The calcite crystals responsible for the preservation of this fauna are free of impurities of iron and magnesium and the clay minerals surrounding the fauna also show a lack of magnesium. Magnesium can exist as an Mg^{2+} ion across a range of pH and Eh (Fig. 3.8

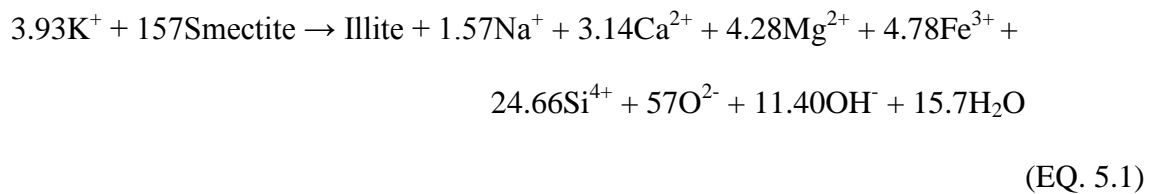
B) and occurs within significant concentrations within seawater (Krauskopf, 1989). As $2+$ ions can readily substitute into the calcite structure, this means that if magnesium ions had been in solution during the sparry calcite precipitation then the substitution of magnesium into the calcite crystal structure would have occurred. Therefore, the lack of magnesium in the sparry calcite of the fossils infers a removal of magnesium ions from the pore fluid prior to the formation of the calcite, but a release in time for the concretion formation to form the magnesium calcite and other carbonates.

Another possibility, given that sparry calcite does not usually form within normal marine settings (Folk, 1974), is that of a precursor precipitation event involving another mineral prior to the formation of the sparry calcite. The possibility of a precursor stage is supported by the work of Berner (1968). During his decay experiments of fish he recorded an increase in the carbonate activity, but was unable to identify the crystallisation of calcite. Berner (1968) did, however, record the presence of calcium soaps, which have an alkaline pH. This may suggest that there was a possible precursor stage to the precipitation of calcite, but there is no evidence of this within the fossils.

In Chapter 3 evidence was presented to suggest that the void stage suggested by Orr *et al.* (2000a) did not occur. Further to this, the evidence used by Orr *et al.* (2000) to support the conclusion of a void stage was the presence of fibrous calcite on the edge of the fossil. Fibrous calcite is typical of a void fill, but the crystals are usually elongate to the c-axis with a height-to-width ratio of $>6:1$ (Flügel, 2009). The sparry calcite crystals at the margins of these fossils have a height to width ratio of $1.3:1$, with some also demonstrating pyramid terminations and undulose extinction. This would indicate they are bladed or micro-granular rather than fibrous in nature (Flügel, 2009). Although the pyramid terminations of the crystals do indicate growth normal to the edge of the

fossil, their formation is the result of a low number of nucleation points, which typically causes an equant fabric (González *et al.*, 1990). A total void stage as proposed by Orr *et al.* (2000a) is inconsistent with the presence of gut traces of *K. clementsii* (see Chapter 3), as during a void stage they would collapse against the body. Although the gut traces show collapse within their own structures, the current specimens found show the gut preserved within their “life position”. The level of decay suggested (Chapter 3) is consistent with the decay sequence established by Briggs and Kear (1993). Therefore, these polychaete fossils represent early stage decay prior to the gut collapse stage, which occurs when the muscles within the body have completely decayed away.

The possibility that the preservation occurred during illitization also needs to be considered. The conversion of smectite to illite is a chemical reaction that releases a host of chemical ions into solution (Equation 5.1) (Elliott and Matisoff, 1996).



This reaction, however, requires a long time. It is usually associated with hydrocarbon maturation and is an important diagenetic reaction. There have been various attempts to model this reaction under controlled laboratory conditions. The experimental work of Bjørkym *et al.*, (1993), Cuadros and Linares (1996) and Cuadros (2006) suggests that the process of illitization typically occurs between 100 and 140°C, but is thought to initiate at about 70°C. However, other authors have stated even higher temperatures of 350°C and time spans of 4 to 5 months (Kim *et al.*, 2004). In addition, the reaction causes an increase in dissolved silica and a decrease in the pH of the pore

fluid (Cuadros & Linares, 1996), which would put any precipitated carbonates at risk of dissolution.

Experimental work by Kim *et al.* (2004) suggested that it was possible for microorganisms to promote the transformation of smectite to illite. Their experimental work showed the development of illitization at room temperature and one atmosphere within 14 days. The reduction of the structural iron(III) within the smectite to iron(II) promotes the smectite dissolution; it also explains the uptake of the potassium ions which balances the lost charge resulting in the illite (Kim *et al.*, 2004). This would certainly put the illitization process on a time scale similar to that required for preservation of decaying carcasses. However, it is unlikely that the preservation of the fauna occurred during the conversion of smectite to illite. Comparing the volume of the host sediment to the number of fossils recovered suggests there is not enough organic matter there to account for the percentage of illite to smectite recorded in the host metabentonite (see Chapter 2). This does not rule out any accelerated alteration that may or may not have occurred around the fossil.

FUTURE WORK

Two areas of research would provide further evidence with which to constrain the preservation of the Herefordshire Lagerstätte.

- 1) **Decay Experiments.** Briggs and Kear (1993) conducted several decay experiments to examine the chemical changes that occurred during the decay of organic matter. It seems logical that now the fundamentals of the preservational pathway of the Herefordshire Lagerstätte are understood, decay experiments could be used to fully test the model. Using the decay of organic matter and andesitic ash from a suitable, chemically identical source, the importance of the andesitic ash could be fully

tested. Removal of samples during the experiments for analysis by SEM could be used to assess the progress of the reaction. In addition, ICP analysis of the pore fluid and XRF analyses of the sediment would elucidate the cation exchanges occurring.

- 2) **Laser ablation ICP-MS.** The ankerite crystals (see Chapter 4) could be examined with laser ablation ICP-MS to determine any isotopic and chemical variation between ankerite crystals within the concretion core and those on the concretion edge. Should no variation be found then this would provide strong evidence that they nucleated at the same time, from the same pore fluid, and would further support the argument (Chapter 4) that these concretions developed through a pervasive mechanism.
- 3) **Comparison with the only other reported example.** The style of preservation of the Herefordshire Lagerstätte is rare within the fossil record. There has been one other recorded example of fossils preserved in calcite, entombed within a carbonate concretion (or nodule): the Miocene Barstow Formation, Southern California, USA, which has exceptionally preserved arthropods (Palmer, 1957). The majority of the fossils recovered are preserved in alpha quartz, apatite, celestite, or gypsum (Park 1995). However, Palmer (1957) also recorded the preservation of dragonfly larvae by calcite within the calcium carbonate concretions. A study of the Barstow material may be used to test the mechanisms described herein for the Herefordshire Lagerstätte.

APPENDIX A: POWDER PELLETT

Powder pellets are made using 7 grams of the powder weighted out in to a beaker. 10 drops of the binding agent Moviol 88 is used stick the powder together. Moviol 88 is a solution of polyvinyl alcohol in a 1:6 mix of methanol and distilled deionised H₂O and does not affect any analytical results. The mix is then placed in the die; the die is then placed in the hydraulic press, 10 tonnes of pressure are then applied to the die. The die is then removed from the press and the powder pellet removed, while avoiding touching the analytical faces the pellet is then placed on a drying rack for 12 hours. The die, press and worktop are cleaned with methylated spirit in-between preparation of each pellet.

APPENDIX B: FUSION BEAD

About 4 to 5 grams are weighed out into a 10 ml glass vial; this is then dried overnight at 110°C. The first test it the loss on ignition (LOI) some of the sample is transferred to a fused Al₂O₃ ceramic crucible. The initial weight of the empty crucible (W₁) is measured along with the weight of the crucible plus sample (W₂). The crucible is then transferred to a 950°C oven for 1 to 1.5 hours after, which the ignited weight (W₃) is taken; from this the loss on ignition is then calculated (Equation B.1).

$$\text{LOI} = 100 * (\text{W}_2 - \text{W}_3) / (\text{W}_2 - \text{W}_1) \quad (\text{Eq. B.1})$$

Initially on each day a flux weight loss determination should be made, carbonate samples the flux used is pure lithium tetraborate. 3 grams of dried flux is weighed in to a Pt/5% Au crucible and placed on the 'Spartan' gas burner for 5 minutes. When cooled

the crucible and flux are reweighed and the weight loss determined and compensated for. Then 0.6g of the ignited sample is weighed on top of the flux and placed back on the burner. The content is then poured in to the Pt/Au casting dish and allowed to cool.

APPENDIX C: XRD ANALYSES OF HOST BENTONITE

Percentage of minerals presented in Chapter 2.

Table C.2: Mineralogy of bentonite

Sample Numbe	DAR_as h_1	DAR_as h_2	DAR_as h_3	DAR_as h_4	DAR_as h_5	DAR_as h_6	DAR_as h_7	DAR_as h_8	DAR_as h_9	DAR_ash _10	DAR_ash _11	DAR_ash _12
Whole rock analysis	%	%	%	%	%	%	%	%	%	%	%	%
Kaolinite	16.75	12.17	27.65	17.52	18.52	14.44	15.10	13.10	12.28	16.72	15.83	13.60
Chlorite	1.30	0.80	2.00	1.00	1.27	1.02	1.00	1.40	0.66	0.83	1.00	1.20
Illite/Mica	27.40	27.00	26.00	23.00	26.30	28.00	28.00	34.00	33.00	28.00	29.00	32.00
Ca Smectite	5.00	5.00	2.00	3.40	3.85	5.24	4.30	4.35	8.00	5.00	4.40	5.40
Apatite	1.15	1.01	1.95	1.16	1.34	1.25	1.16	1.21	1.49	1.22	1.21	1.24
Anatase	1.27	1.17	1.91	1.25	1.40	1.36	1.27	1.32	1.52	1.36	1.33	1.37
Albite	0.51	0.59	0.51	0.51	0.50	0.97	0.85	0.85	0.85	0.51	0.85	1.95
K Feldspar	0.59	0.00	0.00	0.00	0.00	0.59	0.59	0.59	0.59	0.59	0.59	0.59
Fe Oxide	2.62	0.97	3.00	2.48	2.00	1.66	1.45	0.00	0.00	1.36	2.19	1.65
Calcite	2.00	3.37	0.00	6.12	3.83	3.35	4.11	3.21	7.59	0.62	3.41	1.16
Quartz	41.33	45.00	34.00	42.00	38.41	39.00	43.00	40.00	29.00	43.00	40.00	39.00
Fe(III)(OH)3	0.00	2.79	0.00	2.01	2.40	2.69	0.00	0.00	4.38	0.00	0.00	1.00
Total	99.92	99.88	99.02	100.46	99.82	99.58	100.82	100.03	99.36	99.22	99.80	100.16
<2 Clay fraction												
Kaolinite	2.35	9.61	0.95	11.91	10.21	6.79	14.11	6.79	11.76	10.19	13.62	11.57

Illite	53.56	51.84	61.28	66.55	62.36	61.28	62.36	31.34	41.54	55.60	66.57	52.07
Chlorite	6.74	1.16	18.75	6.11	6.78	6.73	1.66	0.75	1.89	0.73	2.44	1.14
Smectite	37.36	37.40	2.71	15.43	20.65	21.54	21.87	61.12	44.81	33.48	17.37	35.22
Illite/Smectite Interlayering	Yes	None	None	None	None	None	None	Yes	Yes	None	None	None
% Weight of <2um fraction:	28.00	24.00	30.00	22.00	26.00	30.00	26.00	30.00	26.00	31.00	30.00	32.00

APPENDIX D: EDX POINT-AND-ID DATA OF THE BENTONITE HOST.

Chemical compositions of minerals used in Chapter 2; all data acquired from an Oxford INCA 350 Energy-dispersive X-ray spectroscopy system attached to a Hitachi S-3600N Environmental Scanning Electron Microscope running at 15 kV. Chemical analysis were normalised to the cobalt standard (99.99% pure cobalt). Results are expressed as weight percent and oxygen was calculated by stoichiometry. bd = below detection limit.

Table D.1: EDX data of mineral chemical composition from bentonite thin sections

	Na	Mg	Al	Si	P	S	K	Ca	Mn	Fe	Sr	O	Total
1	0.14	0.12	0.16	46.47	bd	bd	0.12	0	bd	0.23	bd	52.64	97.81
2	0.12	0.02	0.55	46.58	bd	bd	0.11	0.08	0.11	0.13	bd	53.36	99.89
3	0.07	0	0.02	47.56	bd	0.1	0	0	bd	0.21	bd	54.03	100.55
4	bd	0.04	0.49	45.31	bd	bd	0.17	0.03	0.08	0.4	bd	51.84	96.92
5	0.12	0.42	0.01	0.88	bd	bd	0.05	37.87	0.02	0.14	bd	16.28	55.78
6	0	0.05	1.14	3.12	bd	0.09	0.25	0.38	bd	6.77	bd	6.8	18.66
7	0.14	0.19	1.98	42	bd	bd	0.71	0.03	0.05	0.39	bd	49.63	93.89

8	bd	bd	0.08	45.16	bd	0.07	0.1	0.07	bd	0.3	bd	51.42	95.99
9	3.08	0.21	7.12	27.54	bd	0.08	1.9	0.11	0.01	6.45	bd	41.09	86.81
10	0.21	0.51	6.14	36.3	bd	0.05	2.71	0.16	bd	1.06	bd	47.89	93.81
11	0.25	bd	20.36	21.33	bd	0.14	0.17	0.05	bd	0.04	bd	42.54	84.31
12	0.09	0.11	2.18	44.29	bd	0.01	0.94	0.07	0.16	0.44	bd	52.62	99.78
13	0.21	0.22	4.12	39.61	bd	0.06	1.43	0.29	bd	0.61	bd	49.42	95.04
14	0	0.47	0.5	0.9	bd	0.01	0.2	37.6	0.02	0.14	bd	16.81	56.55
15	0.09	0.12	1.18	44.73	bd	0.04	0.25	0.01	0.12	0.13	bd	52.03	97.63
16	0.1	0.05	0.28	46	bd	0.01	0.16	0.05	0.07	0.03	bd	52.52	97.93
17	0.06	1.18	11.25	23.91	bd	bd	7.51	0.08	0.03	5.91	bd	41.07	90.32
18	0.07	0.87	14.55	24.62	bd	0	5.47	0.68	0.02	1.36	bd	43.21	90.3
19	0.15	0.18	1.15	6.05	bd	bd	0.32	1.22	bd	40.91	0.21	20.28	70.35
20	bd	0.33	0.01	1.36	bd	0.02	0.03	37.29	0.26	0.51	0.04	16.84	56.62
21	0.04	0.21	1.99	44.68	bd	0.08	0.84	0.09	bd	1.03	bd	53.2	101.13
22	0.05	0.09	1.22	46.2	bd	0.03	0.36	0.01	bd	0.21	bd	53.67	100.47
23	0.13	0.38	6.4	33.64	bd	0.12	2.74	0.14	bd	5.91	bd	46.61	95.36
24	0.07	0.01	19.99	21.35	bd	0.09	bd	0.01	bd	0.19	bd	42.18	83.33
25	0.03	0.03	bd	46.39	bd	bd	bd	0.1	bd	0.24	bd	52.69	98.57
26	bd	0	0.08	45.61	bd	bd	0.1	0	bd	0.17	bd	51.78	96.43
27	0.11	0.01	0.76	45.86	bd	0.07	0.04	0.06	0.16	0.22	bd	53.02	99.43
28	0.13	0.41	4.5	6.79	bd	bd	0.25	0.46	0.06	33.93	bd	21.88	68.09
29	bd	1.23	14.15	23.96	bd	0.07	5.58	0.86	0.01	1.22	bd	42.52	89.08
30	0.18	0.62	14.02	21.51	bd	bd	8.93	0	bd	5.89	bd	40.67	91.19
31	0.06	0.03	-0.1	48.35	bd	bd	0.03	0.02	bd	0.08	bd	54.73	101.67
32	0.18	0.28	5.47	39.31	bd	0.05	2.79	0.12	bd	0.27	bd	50.48	97.99
33	0.2	0.38	11.94	28.71	bd	0.02	4.05	0.51	bd	0.83	bd	44.81	90.79
34	0.03	1.13	13.65	23.04	bd	0.1	5.72	0.69	bd	2.9	bd	41.47	88.28
35	0.11	0.29	1.54	23.7	bd	0.03	0.54	7.74	0.03	14.77	bd	35.85	83.39
36	0.04	0.01	0.2	47.9	0	0.07	0.11	0.01	bd	0.27	bd	54.68	101.72
37	bd	0.12	1.86	43.11	0	bd	0.97	0.09	0.21	0.32	bd	50.94	96.47

38	0.06	bd	19.64	21.15	0	0.12	0.08	0.23	bd	0.29	bd	41.79	82.55
39	0	0.63	9.21	28.48	0	0.06	3.55	0.44	0.03	0.76	bd	42.19	84.9
40	0.15	2.74	13.54	21.72	0	bd	6.8	0.52	0.04	2.64	bd	40.93	88.81
41	0.03	0.62	12.55	26.09	0	0.05	4.38	0.56	0.15	1.22	bd	42.87	88.4
42	0.08	0.07	0.17	46.12	0.01	0.03	0	0.04	bd	0.43	bd	52.73	98.48
43	0.07	0.17	2.41	43.62	0.01	bd	1.05	0.05	bd	0.57	bd	52.09	98.95
44	0.14	0.89	16.43	22.29	0.01	0.09	7.19	0.1	bd	2.61	bd	42.98	92.42
45	0.03	0.23	3.67	29.77	0.01	0.17	1.69	0.11	0	1.07	bd	38.23	74.6
46	0.15	0.15	3.2	40.62	0.01	0.05	1.21	0.12	bd	0.46	bd	49.62	94.7
47	0.25	0.23	4.86	39.26	0.01	0.02	1.93	0.15	0.1	0.55	bd	49.84	96.51
48	bd	0.2	1.18	7.79	0.01	bd	0.22	0.33	0.04	5.78	0.07	11.79	27.32
49	0.1	0.26	4.47	40.56	0.01	0.06	1.57	0.37	0.19	0.51	bd	50.94	97.82
50	0.15	0.38	8.87	33.55	0.01	0.1	3.23	0.39	0.29	1.37	bd	47.76	95.49
51	0.12	0.5	14.32	22.68	0.02	bd	8.54	0.06	0.19	5.07	bd	42.17	93.37
52	0.15	0.53	7.57	31.57	0.02	bd	3.2	0.14	bd	4.04	bd	44.74	90.94
53	0.13	0.47	9.13	33.16	0.02	0.08	4.08	0.14	bd	1.46	bd	47.57	95.56
54	8.62	0	10.14	31.47	0.02	bd	0	0.16	bd	0.16	bd	47.75	97.47
55	0.15	0.16	4.4	41.12	0.02	0.07	0.77	0.17	0.07	0.02	bd	51.13	97.15
56	0.1	0.12	0.21	46.6	0.02	bd	0.04	0.21	bd	0.13	bd	53.26	99.49
57	0.22	0.23	3.6	39.57	0.02	0.04	1.41	0.22	bd	0.86	bd	49.02	94.13
58	0.02	0.53	8.88	34.43	0.02	0.13	3.17	0.42	0.11	0.85	bd	48.71	96.84
59	0.1	0.18	4.16	35.19	0.02	0.1	1.87	1.09	0.19	0.88	bd	45.1	88.09
60	0.06	0.02	19.97	20.98	0.03	bd	0.07	0.04	bd	0.61	bd	41.77	83.01
61	0.12	0.48	7.12	34.11	0.03	0.09	3.51	0.05	0.02	4.58	bd	47.65	97.01
62	0.11	0.34	6.01	38.34	0.03	bd	2.24	0.1	0.05	1.2	bd	50.04	97.97
63	0.21	0.82	7.25	32.81	0.03	0.01	4.31	0.12	bd	2.28	bd	45.99	93.34
64	0.08	0.21	3.48	39.53	0.03	0.13	1.52	0.24	bd	2.15	bd	49.38	95.95
65	0.52	0.87	15.83	23.24	0.03	bd	6.84	0.26	0.15	1.79	bd	43.32	92.78
66	0.19	0.37	4.27	27	0.03	0.09	1.56	0.36	0.03	16.38	bd	40.14	89.99
67	bd	0.58	0.05	0.39	0.03	0.03	-0.01	38.21	bd	0.15	0.2	16.26	55.79

68	0.29	0.11	2.26	40.87	0.04	0.01	0.94	0.09	0.05	0.37	bd	49.01	93.2
69	0.1	0.06	1.23	43.2	0.04	bd	0.63	0.09	0.12	0.35	bd	50.67	96.2
70	0.11	0.17	2.86	41.08	0.04	0.07	1.18	0.1	0.08	0.48	bd	49.93	95.16
71	0.07	bd	0.67	36.27	0.04	0.01	0.16	0.11	0.13	1.75	bd	42.44	80.67
72	0.09	0.41	5.61	38.69	0.04	0.07	2.73	0.13	0.14	0.79	bd	50.2	97.81
73	0.24	0.63	12.82	28.21	0.04	0.03	6.32	0.2	0.01	1.67	bd	45.89	95.57
74	0.02	0	0.98	1.59	0.04	0.17	0.23	0.26	bd	7.11	bd	5.23	15.93
75	0.39	0.11	1.88	3.74	0.04	0.95	1.1	0.8	bd	0.09	bd	8.14	16.99
76	0.35	0.3	3.67	12.67	0.04	0.77	0.71	1.26	0.08	15.88	bd	24.4	59.81
77	0.13	0.19	3.99	41.35	0.05	0.04	1.03	0	-0.11	0.62	bd	51.12	97.39
78	0.2	0.64	11.14	27.6	0.05	0.04	5.75	0.05	bd	2.94	bd	43.95	91.98
79	0.18	0.23	4.39	37.9	0.05	bd	1.97	0.11	bd	0.9	bd	47.87	92.66
80	0.09	0.01	20.44	21.48	0.05	0.1	0.23	0.12	0.12	0.09	bd	43.01	85.48
81	0.04	1.58	12.93	25.55	0.05	0.08	8.65	0.13	bd	5.54	bd	45.18	99.36
82	0.01	0.96	13	22.06	0.05	bd	7.76	0.15	bd	5.91	bd	40.63	90.03
83	0.07	0.04	20.07	21.38	0.05	0.06	0.36	0.18	0.09	0.16	bd	42.48	84.09
84	0.05	0.24	3.08	41.12	0.05	bd	1.1	0.19	bd	0.41	bd	49.98	95.35
85	0.09	0.6	9	33.09	0.05	0.05	3.49	0.28	bd	2.03	bd	47.55	95.62
86	0.12	0.29	5.98	38.53	0.05	0.09	1.8	0.3	bd	0.37	bd	50.08	96.79
87	0.05	bd	0.72	36.39	0.06	bd	0.14	0.05	bd	2.07	bd	42.56	81.05
88	0.31	1.73	13.44	22.88	0.06	0.09	8.18	0.06	0.08	3.33	0.04	42.16	92.36
89	0.05	1.01	11.39	30.03	0.06	0.03	6.75	0.06	0.05	3.14	bd	47.38	99.58
90	0.11	0.03	20.26	21.26	0.06	0.03	0.19	0.11	bd	-0.04	bd	42.45	84.25
91	0.08	0.8	12.08	24.9	0.06	0.11	6.51	0.15	bd	2.54	bd	41.92	88.6
92	0.12	0.34	6.33	33.94	0.06	0.13	2.59	0.16	0.17	4.6	bd	46.62	94.07
93	0.03	0.15	19.11	22.19	0.06	0.02	1.07	0.2	0.15	0.2	bd	42.84	85.72
94	0.08	0.44	4.87	38.11	0.06	0.07	2.38	0.27	bd	1.27	bd	49.02	95.59
95	0.1	bd	0.15	46.53	0.07	0.09	-0.01	0	0.19	0	bd	53.28	99.54
96	0.24	0.14	2.49	41.82	0.07	0.1	0.77	0.01	0.19	0.21	bd	50.44	95.82
97	0.18	0.21	3.7	39.2	0.07	bd	1.38	0.12	0.02	0.78	bd	48.6	93.5

98	0.27	0.62	14.92	20.91	0.07	0.02	8.86	0.13	bd	5.49	bd	41.09	92.03
99	0.07	0.13	19.21	21.32	0.07	0.11	0.17	0.21	-0.1	0.41	bd	41.94	83.47
100	1.46	0.34	7.68	27.39	0.07	0.04	2.21	0.27	bd	5.17	bd	40.82	84.78
101	0.24	0.52	7.26	32.66	0.07	0.12	3.18	0.34	0.05	1.68	bd	45.57	91.27
102	0.14	0.1	1.46	44.03	0.07	0.03	0.37	0.4	bd	0.2	bd	51.85	97.82
103	bd	0.42	0.09	0.36	0.07	bd	0.04	38.14	bd	0.13	0.17	16.07	55.28
104	0.17	0.01	0.93	46.09	0.08	bd	0.4	0.02	bd	0.14	bd	53.28	99.34
105	0.03	0.26	3.91	37.6	0.08	0.03	1.81	0.08	0.03	3.05	bd	47.72	93.44
106	0.07	0.15	18.55	21.83	0.08	0.01	1.22	0.11	0	0.32	bd	41.93	83.86
107	0.23	0.2	3.76	40.98	0.08	bd	1.28	0.15	bd	0.59	bd	50.47	96.62
108	0.19	0.38	7.08	32.5	0.08	0.07	3.23	0.19	0.01	1.82	bd	44.92	89.45
109	0.11	1.05	15.25	24.04	0.08	0.05	5.6	0.66	bd	0.74	bd	43.47	90.96
110	0.13	0.12	1.25	45.23	0.09	0.04	0.5	0.1	0.05	0.07	bd	52.99	99.84
111	bd	0.16	5.87	38.5	0.09	0.04	1.8	0.19	0.03	0.71	bd	49.87	96.45
112	0.3	0.6	12.9	28.33	0.09	0.11	6.22	0.2	bd	1.19	bd	46.03	95.1
113	0	0.42	8.46	33.69	0.09	0.02	3.87	0.21	0.01	1.08	bd	47.4	94.7
114	0.05	0.31	2.42	12.34	0.09	0.15	0.63	0.48	0.06	31.52	bd	26.19	74.48
115	0.04	0.15	20.5	21.41	0.1	0.15	0.23	0.07	bd	0.29	bd	43.18	85.77
116	0.2	0.07	19.5	21.57	0.1	bd	1.1	0.11	0	0.22	bd	42.29	84.61
117	0.07	0.01	19.37	20.7	0.1	0.11	0.23	0.12	0.07	1.13	bd	41.55	83.39
118	0	0.14	19.32	21.72	0.1	0.12	1.23	0.18	bd	0.6	bd	42.68	85.38
119	0.1	0.63	8.68	31.58	0.1	0.14	2.72	0.26	0.03	2.09	bd	45.52	90.62
120	0.16	0.36	7.25	30.68	0.1	0	2.66	0.28	0	2.24	bd	43.02	86.29
121	0.01	0.54	4.43	26.54	0.1	0.05	1.85	0.28	0.1	17.55	bd	40.31	91.91
122	0.14	0.33	6.27	37	0.1	0.18	2.26	0.28	0.07	1.94	bd	49.4	97.14
123	0.24	0.3	5.34	36.98	0.1	bd	2	0.29	bd	0.64	bd	47.78	92.9
124	0.59	1.01	16.04	23.76	0.1	0.01	6.66	0.43	0.13	1.93	bd	44.44	94.93
125	0.06	1.19	13.38	23.73	0.1	0.05	5.46	0.63	bd	2.22	bd	41.91	88.49
126	0.02	0.12	0.94	46.29	0.11	0.02	0.44	0.03	bd	0.17	bd	53.78	100.82
127	0.08	0.13	18.04	22.72	0.11	bd	0.76	0.07	0	0.3	bd	42.31	83.94

128	0.01	0.09	18.24	20.45	0.11	0.04	0.83	0.09	bd	0.35	bd	40.06	80.12
129	0.15	0.1	17.17	22.95	0.11	0.09	1.3	0.14	0.12	0.57	bd	42.26	84.57
130	0.12	0.49	11.13	31.73	0.11	0.05	3.21	0.17	0.01	1.35	bd	47.62	95.36
131	0.38	0.69	14.28	19.39	0.11	0.1	6.23	0.25	bd	2.76	bd	37.81	81.92
132	0.05	0.33	14.53	27.76	0.11	0.05	2.78	0.27	0.05	1.01	bd	45.94	92.67
133	0.07	0.5	3.04	11.91	0.11	0.04	0.69	0.41	0.27	29.07	bd	25.53	71.51
134	0.06	0.45	5.44	5.94	0.11	0.08	0.15	0.5	0.02	25.32	bd	19.64	57.56
135	0.06	0.35	3.27	23.48	0.11	0.1	1.05	0.51	bd	22.01	0.09	36.91	87.83
136	0.15	bd	20.06	21.46	0.12	bd	0.37	0.03	bd	0.11	bd	42.4	83.97
137	0.17	0.33	5.25	38.55	0.12	0	2.31	0.18	0.09	0.51	bd	49.64	96.62
138	0.21	0.71	10.43	29.21	0.12	0.1	4.76	0.38	bd	2.68	bd	45.09	92.57
139	0.08	0.68	9.14	31.55	0.12	0.01	3.5	0.63	bd	0.98	bd	45.91	92.35
140	0.19	0.11	19.6	21.41	0.13	bd	1.43	0.03	bd	0.11	bd	42.3	84.58
141	0.03	bd	19.85	20.73	0.13	0.14	0.03	0.12	bd	0.84	bd	41.8	82.99
142	0.18	0.06	19.55	21.61	0.13	bd	1.74	0.12	bd	0.62	bd	42.8	86.68
143	0.18	0.83	12.81	25.55	0.13	bd	6.69	0.2	0.09	2.2	bd	43.31	91.8
144	0.02	0.07	20.04	21.92	0.14	bd	0.51	0.13	bd	0.52	bd	43.29	86.42
145	0.36	0.1	1.43	5.11	0.14	0.98	0.61	0.47	bd	0	bd	9.22	18.29
146	0.11	0.08	19.43	22.44	0.15	0.09	0.54	0.12	bd	0.43	bd	43.53	86.79
147	0.16	bd	20.12	20.9	0.15	0.18	0.03	0.15	0.07	0.41	bd	42.35	84.14
148	0.01	bd	17.5	24.22	0.15	bd	0.26	0.21	0.21	0.25	bd	43.49	85.82
149	0.13	0.47	4	13.93	0.15	0.04	1.38	0.39	0.22	28.12	bd	28.52	76.97
150	0.08	0.31	2.89	7.2	0.15	0.15	0.48	0.41	0.34	37.39	bd	22.47	71.74
151	0.06	0.07	20.16	21.27	0.15	0.08	0.08	0.64	0.12	0.37	bd	42.8	84.92
152	0.21	0.26	3.19	18.58	0.15	0.21	0.81	1.44	0.11	17.77	bd	30.55	72.92
153	0	0.02	19.72	20.63	0.16	bd	0.2	0.13	0.1	0.56	bd	41.48	82.89
154	0.16	0.01	20.03	21.86	0.17	0.02	1.54	0.05	0.02	0.62	bd	43.47	87.53
155	0.09	0.44	7.27	34.28	0.17	0.05	3.06	0.09	bd	1.14	bd	47	92.99
156	0.15	0.54	9.36	31.19	0.17	0.04	3.97	0.21	0.11	1.18	bd	45.74	92.31
157	0.24	0.06	19.51	21.58	0.17	0.09	0.58	0.22	bd	0.54	bd	42.6	84.77

158	0.16	0.17	12.11	29.95	0.18	0.03	2.1	0.26	0.08	0.97	bd	46.11	91.78
159	0.07	0.3	5.12	36.67	0.18	0.06	2.18	0.27	bd	0.74	bd	47.48	92.26
160	0.22	0.21	4.82	36.64	0.19	0.02	2.12	0.16	0.06	1.28	bd	47.24	92.09
161	0.16	0.24	4.15	40.49	0.19	0	1.56	0.21	0.09	0.41	bd	50.74	97.77
162	0.1	0.25	19.55	21.97	0.19	0.09	1.61	0.39	0.04	0.49	bd	43.55	87.73
163	0.1	bd	20.57	21.64	0.2	0.08	0.16	0.14	0.1	0.34	bd	43.45	86.26
164	0.06	bd	20.13	22.15	0.2	0.1	0.31	0.27	0.14	0.18	bd	43.75	86.96
165	0.26	0.38	2.53	22.75	0.2	0.03	0.41	0.75	0.22	25.6	bd	36.53	89.36
166	0.06	0.43	1.81	3.08	0.21	0.09	0.02	0.46	0.26	42.12	0.41	18.23	67.18
167	0.01	0.27	11.55	30.19	0.24	bd	2.24	0.31	bd	0.38	0.18	45.82	91.11
168	0.11	0.12	18.96	22.21	0.28	0.09	0.24	0.4	bd	0.83	0.05	43.21	86.44
169	0.08	0.09	15.55	27.09	0.33	bd	0.53	0.63	0.04	0.3	bd	45.51	89.53
170	0.08	0.36	17.86	21.97	0.34	0.12	2.15	0.97	bd	0.85	bd	42.77	86.99
171	-0.02	0.25	5.45	11.86	0.39	0.08	0.98	3.6	0.06	13.81	bd	24.7	60.85
172	0.13	0.4	7.54	21.73	0.41	0	2.09	0.69	bd	10.27	0.23	35.97	79.4
173	0.13	1.24	9.63	25.58	0.44	0.05	4.44	1.48	0.09	2.47	bd	41.39	86.65
174	0.11	0.32	14.94	25.06	0.67	0.19	2.55	0.6	bd	0.77	0.27	44.23	89.58
175	0.13	0.07	19.15	20.25	0.76	0.25	0.05	0.61	bd	0.52	0.01	41.91	83.55
176	0.06	0.03	19.56	21.36	0.78	0.07	0.19	0.96	bd	0.13	bd	43.3	86.2
177	0.29	0.1	7.18	8.05	13.13	0.07	0.24	23.82	bd	0.04	1.62	42.61	97.04
178	0.17	0.1	3.4	5.85	16.98	0.12	1.1	30.75	bd	0.17	1.24	44.69	104.55
179	bd	0.29	1.42	7.79	18.29	0.01	0.43	31.76	bd	0.76	1.76	47.21	109.56
180	0.17	0.07	1.73	2.22	19.55	0.03	0.18	36.61	bd	0.07	1.28	44.35	106.18
181	0.06	0.29	0	0.31	20.75	0.16	0.06	38.55	0.23	0.64	1.44	43.51	106.01
182	0.08	0.22	0.04	0.31	20.91	0.15	0.06	38.52	0.23	0.59	1.35	43.66	106.12

APPENDIX E: XRF DATA OF HOST BENTONITE

Table E.1: XRF analyses of host bentonite

Sam ple	DAR_a sh_1	DAR_a sh_2	DAR_a sh_3	DAR_a sh_4	DAR_a sh_5	DAR_a sh_6	DAR_a sh_7	DAR_a sh_8	DAR_a sh_9	DAR_a sh_10	DAR_a sh_11	DAR_a sh_12	DAR_a sh_13	DAR_Nodu le(w)_1	DAR_Nodul e(uw)_1
SiO ₂	62.87	63.11	59.87	57.27	56.86	56.34	62.16	60.15	50.41	63.66	60.79	72.88	61.09	17.71	12.71
TiO ₂	1.27	1.17	1.25	1.91	0.79	0.73	1.27	1.32	1.52	1.36	1.33	0.60	1.37	0.45	0.30
Al ₂ O ₃	18.31	16.42	16.59	22.65	19.80	18.47	18.03	18.88	20.40	19.21	18.99	11.85	19.65	7.28	5.10
Fe ₂ O ₃	3.34	3.71	4.56	3.91	8.29	7.37	2.16	3.09	4.56	2.37	2.95	3.03	3.24	4.05	2.81
MnO	0.04	0.04	0.07	0.08	0.03	0.04	0.03	0.04	0.09	0.03	0.06	0.04	0.03	0.52	0.63
MgO	0.83	0.84	0.73	0.88	3.15	2.94	0.83	0.98	1.12	0.85	0.84	0.66	1.03	0.42	2.33
CaO	2.52	3.60	4.86	1.43	0.10	0.09	3.94	3.47	6.92	2.19	3.59	2.49	2.59	35.95	39.27
Na ₂ O	0.06	0.07	0.06	0.06	0.06	0.04	0.10	0.10	0.10	0.09	0.10	0.49	0.23	0.01	0.01
K ₂ O	3.11	2.83	2.434	2.791	4.879	4.771	3.098	3.570	3.712	3.206	3.286	2.800	3.556	0.99	0.47
P ₂ O ₅	0.48	0.43	0.49	0.82	0.27	0.23	0.49	0.51	0.63	0.52	0.51	0.08	0.52	0.24	0.39
Total	99.2	99.15	99.34	98.95	99.82	99.27	99.23	99.03	99.55	99.57	99.58	99.66	99.58	99.29	99.82
Ba	87.8	94.0	117.8	112.0	109.4	116.6	129.2	205.5	266.5	105.3	136.5	289.2	201.6	77.48	35.07
Ce	93.7	84.2	83.9	118.5	86.9	101.5	89.9	110.8	112.7	104.0	94.6	42.0	95.8	73.87	45.66
Cr	1.3	1.3	1.3	1.3	2.6	2.2	bd	bd	bd	bd	bd	63.6	bd	5.34	2.55
Cu	1.4	bd	1.4	bd	2.4	0.9	bd	bd	bd	bd	bd	11.5	bd	5.51	3.43

La	37.6	33.6	38.3	46.4	36.8	46.5	36.5	46.0	48.3	44.0	39.6	25.9	40.9	38.19	20.40
Nb	14.5	9.5	12.7	17.4	13.7	17.0	14.3	15.0	15.9	15.6	15.2	11.1	15.6	5.84	3.87
Nd	52.5	44.8	44.5	65.6	48.5	54.5	48.5	58.3	61.5	60.4	54.4	18.2	54.4	32.79	24.98
Ni	3.0	1.7	0.9	6.7	2.2	9.3	3.8	4.9	7.2	4.7	7.5	11.5	6.8	1.42	0.82
Pb	11.2	11.0	12.1	24.6	12.9	29.7	25.0	12.1	20.1	21.6	15.4	28.8	19.8	12.88	9.55
Rb	98.3	85.8	74.2	91.4	91.9	128.1	96.3	112.7	120.6	105.0	103.3	110.1	117.0	23.71	10.70
Sr	215.7	170.7	203.1	206.7	194.8	141.7	166.1	169.6	149.5	162.6	192.0	92.7	150.1	169.85	322.17
Th	11.6	10.3	10.3	13.6	10.9	14.5	11.9	12.3	13.4	13.2	12.4	8.4	13.4	3.52	1.75
U	3.1	6.0	3.0	3.9	3.1	4.3	3.7	3.4	4.2	3.4	3.4	2.9	4.0	1.77	1.46
V	53.4	49.9	58.5	95.3	52.2	60.3	55.8	61.0	73.2	58.4	59.2	92.6	61.1	25.22	17.28
Y	56.2	42.9	49.4	71.1	52.3	73.4	54.3	60.2	63.2	60.1	59.2	14.0	60.7	48.16	27.77
Zn	53.8	56.2	75.2	137.4	50.2	184.8	23.7	101.2	135.4	87.7	105.3	64.7	105.7	60.33	67.20
Zr	297.1	218.3	268.0	372.7	282.0	345.7	294.2	308.9	329.3	317.3	310.6	143.3	318.7	114.94	76.55
Co	6.5	7.3	8.9	9.7	9.3	9.1	6.0	7.1	11.2	6.5	10.1	9.0	7.2	8.01	6.35
Sc	17.6	15.4	19.0	23.2	17.4	22.0	22.9	24.7	30.4	24.5	26.0	14.7	23.4	49.85	50.40
Ga	21.0	18.7	19.3	27.2	20.5	26.2	20.5	23.3	24.6	22.9	22.3	15.2	24.4	7.16	5.66
W	1.7	2.2	bd	2.6	3.1	2.9	2.5	2.1	2.7	1.9	2.9	bd	2.2	bd	bd
Mo	0.4	0.7	1.0	0.6	0.7	0.7	0.8	0.6	1.4	0.4	1.5	1.0	0.9	1.69	1.29
Sn	2.7	2.2	bd	2.5	bd	3.4	2.5	2.0	1.5	2.9	2.6	bd	2.4	bd	1.24
As	5.5	4.8	2.6	7.8	5.1	6.2	4.2	6.8	4.1	4.3	8.8	17.8	7.5	4.94	1.86
Sb	bd	bd													

APPENDIX F: AVERAGE ANDESITE

XRF data in Chapter 2 was normalised to a published average andesite.

Table F.1: Major element data used for the normalisation of the data from Fitton *et al.* 1982

Al ₂ O ₃	SiO ₂	TiO ₂	Fe ₂ O ₃	MnO	MgO	CaO	Na ₂ O	K ₂ O	P ₂ O ₅	Total
17.76	59.98	0.91	7.54	0.2	2.83	4.75	2.67	2.97	0.19	99.8

APPENDIX G: COMPOSITION OF LOCALLY COLLECTED COALBROOKDALE FORMATION

XRF in Chapter 2 was normalised to a locally collected sample of the Coalbrookdale Formation. Samples Leicester University Fusion Bead

Number is LF29679.

Table G.1: Major elemental data

SiO ₂	TiO ₂	Al ₂ O ₃	Fe ₂ O ₃	MnO	MgO	CaO	Na ₂ O	K ₂ O	P ₂ O ₅	Total
72.8750	0.5983	11.8472	3.0277	0.0378	0.6590	2.4907	0.4898	2.8002	0.0777	99.6568

Table G.2: Trace elemental data

Ba	Ce	Cr	Cu	La	Nb	Nd	Ni	Pb	Rb	Sr	Th	U	V
289.23	41.98	63.59	11.45	25.87	11.13	18.23	11.49	28.77	110.0	92.67	8.39	2.85	92.57
Y	Zn	Zr	Co	Sc	Ga	W	Mo	Sn	As	Sb			
13.99	64.68	143.28	9.00	14.71	15.22	0.75	0.95	0.60	17.79	1.20			

APPENDIX H: CLAY MINERAL EMPA ANALYSES

Clay mineralogy data used in Chapter 3; all data acquired from a JXA8600 Superprobe operating voltage of 15 kV, a beam current of 30 nA and a beam diameter of 30 μm .

Kenostrychus clementsi

Table H.1: EMPA data of clay accumulations immediately adjacent to *K. clementsi*

	SiO ₂	TiO ₂	Al ₂ O ₃	Cr ₂ O ₃	FeO	MnO	MgO	CaO	Na ₂ O	K ₂ O	NiO	Total
1	47.44	0.10	31.31	0.00	1.94	0.03	0.88	0.94	0.03	4.22	0.00	86.88
2	49.28	0.61	31.18	0.00	2.47	0.03	1.02	1.05	0.05	4.47	0.00	90.15
3	53.05	0.33	30.86	0.01	2.90	0.02	1.04	0.95	0.05	4.63	0.13	93.96
4	51.17	0.43	30.39	0.00	3.23	0.03	0.91	1.06	0.04	4.20	0.00	91.46

5	49.41	0.12	32.68	0.02	3.84	0.01	0.92	0.86	0.04	3.93	0.11	91.94
6	49.29	0.70	30.11	0.00	4.46	0.00	1.00	1.01	0.06	4.42	0.00	91.04
7	50.38	0.66	27.01	0.00	6.15	0.00	0.92	0.95	0.07	4.28	0.06	90.48
8	50.71	0.57	30.29	0.00	1.79	0.00	0.99	1.03	0.03	4.84	0.08	90.33
9	45.11	1.87	29.10	0.00	1.69	0.04	0.83	3.95	0.04	3.87	0.00	86.49
10	49.21	0.51	32.73	0.03	1.39	0.03	0.91	1.06	0.05	4.34	0.13	90.39
11	49.39	0.46	31.83	0.00	1.35	0.00	1.10	0.86	0.06	5.76	0.09	90.89
12	53.38	0.88	26.75	0.03	2.12	0.02	1.00	0.99	0.07	4.68	0.00	89.93
13	50.80	0.54	32.13	0.02	1.51	0.00	0.97	0.99	0.02	4.41	0.00	91.37
14	49.86	0.22	32.03	0.00	1.11	0.00	0.99	0.99	0.01	4.59	0.00	89.80
15	45.89	0.56	27.27	0.04	4.16	0.03	0.79	5.20	0.02	3.91	0.05	87.90
16	49.99	0.42	30.89	0.00	1.68	0.04	1.02	1.07	0.05	4.65	0.06	89.87
17	47.34	0.96	29.48	0.00	2.11	0.00	0.85	3.32	0.07	4.03	0.00	88.16
18	50.28	0.75	28.48	0.00	1.28	0.00	0.91	0.88	0.08	4.45	0.12	87.23
19	46.53	0.58	27.23	0.00	1.60	0.03	0.91	1.01	0.06	4.82	0.04	82.81
20	51.71	0.37	30.26	0.00	1.72	0.02	1.05	0.97	0.08	5.18	0.03	91.40
21	50.18	0.36	31.60	0.04	2.06	0.05	1.01	1.13	0.03	4.61	0.04	91.11
22	49.62	0.28	31.43	0.00	1.63	0.02	0.94	0.99	0.03	4.54	0.00	89.47
23	50.13	0.36	31.00	0.03	1.43	0.01	0.88	1.10	0.02	4.45	0.04	89.47
24	54.44	0.60	29.32	0.01	1.49	0.00	0.90	1.10	0.06	4.43	0.29	92.64
25	51.04	0.62	31.59	0.00	1.62	0.02	1.00	1.13	0.09	4.41	0.12	91.63
26	50.88	0.49	29.90	0.00	1.87	0.01	0.85	0.93	0.04	4.01	0.02	89.00
27	48.05	0.47	29.68	0.00	1.43	0.01	0.92	0.90	0.03	4.59	0.02	86.09
28	47.83	0.67	29.07	0.00	1.79	0.01	0.77	0.94	0.06	4.44	0.00	85.57
29	46.70	0.24	30.55	0.03	1.59	0.01	0.87	0.93	0.06	4.40	0.01	85.38

30	51.47	0.63	29.52	0.03	1.43	0.00	0.86	1.06	0.05	4.42	0.00	89.46
31	56.82	0.52	28.98	0.00	1.48	0.03	0.94	1.01	0.04	3.99	0.04	93.85
32	48.46	0.82	30.84	0.00	2.22	0.02	0.91	2.43	0.07	4.25	0.02	90.04
33	44.34	0.38	28.25	0.00	1.48	0.02	0.84	0.92	0.05	4.75	0.02	81.05
34	50.87	0.73	31.07	0.00	1.47	0.02	0.86	1.03	0.04	4.44	0.01	90.54
35	51.92	0.84	30.16	0.00	1.82	0.00	1.07	0.95	0.02	4.68	0.01	91.47
36	48.00	1.12	31.20	0.01	2.26	0.01	0.93	1.07	0.04	4.36	0.00	89.00

Table H.2: EMPA data of clay accumulations in the matrix of the concretion that contained *K. clementsi*

	SiO ₂	TiO ₂	Al ₂ O ₃	Cr ₂ O ₃	FeO	MnO	MgO	CaO	Na ₂ O	K ₂ O	NiO	Total
1	44.84	0.35	19.38	0.00	3.05	0.11	0.85	10.65	0.05	3.77	0.02	83.08
2	50.91	0.28	31.23	0.00	2.81	0.00	1.19	0.92	0.08	5.17	0.01	92.59
3	53.47	0.90	26.57	0.01	1.82	0.01	1.08	1.60	0.11	5.39	0.18	91.12
4	50.84	0.36	28.54	0.00	2.89	0.06	1.22	4.12	0.06	5.31	0.06	93.46
5	50.33	0.44	25.38	0.00	1.96	0.01	1.06	0.90	0.09	5.30	0.02	85.49
6	53.45	0.43	27.18	0.02	1.81	0.04	1.17	0.96	0.08	5.65	0.00	90.79
7	50.93	0.86	27.83	0.01	2.48	0.01	1.22	1.19	0.12	5.60	0.36	90.60
8	60.47	0.72	23.68	0.00	2.13	0.02	1.13	0.77	0.08	5.25	0.00	94.23
9	51.48	0.61	30.87	0.01	1.78	0.03	1.26	1.03	0.07	5.64	0.00	92.76
10	78.66	0.22	8.51	0.00	1.09	0.05	0.39	3.34	0.02	1.91	0.00	94.18

*Tanazios dokeron*Table H.3: EMPA data of clay accumulations immediately adjacent to *T. dokeron*

	SiO ₂	TiO ₂	Al ₂ O ₃	Cr ₂ O ₃	FeO	MnO	MgO	CaO	Na ₂ O	K ₂ O	NiO	Total
1	61.83	0.68	21.72	0.00	1.80	0.00	0.89	0.82	0.04	4.29	0.00	92.07
2	61.86	0.67	21.70	0.01	2.51	0.00	0.79	0.73	0.06	3.86	0.10	92.29
3	56.10	0.29	27.37	0.00	2.05	0.00	0.74	0.68	0.05	3.60	0.05	90.92
4	57.12	0.32	27.69	0.05	2.14	0.04	0.70	0.66	0.07	3.72	0.12	92.62
5	55.24	0.40	26.57	0.01	2.59	0.00	0.89	0.71	0.07	4.09	0.04	90.61
6	56.23	1.13	25.45	0.00	3.40	0.00	0.69	0.68	0.08	3.34	0.03	91.02
7	57.38	0.31	24.79	0.00	3.16	0.00	0.84	0.74	0.03	3.91	0.02	91.19
8	60.64	0.44	22.09	0.00	3.19	0.00	0.83	0.74	0.06	4.05	0.00	92.04
9	61.91	0.39	22.08	0.06	2.07	0.00	0.64	0.62	0.08	3.11	0.15	91.11
10	60.89	0.58	22.05	0.00	2.61	0.02	0.70	0.96	0.06	3.52	0.00	91.38
11	61.42	0.65	22.26	0.00	2.38	0.04	0.75	0.76	0.07	3.62	0.00	91.94
12	51.54	0.21	30.31	0.00	2.29	0.00	0.68	0.57	0.05	3.41	0.00	89.05
13	51.20	0.42	30.24	0.00	1.90	0.00	0.64	0.48	0.22	3.47	0.00	88.55
14	63.22	0.33	21.47	0.00	1.84	0.02	0.67	1.27	0.05	3.01	0.00	91.88
15	54.14	0.25	28.14	0.04	1.47	0.00	0.85	0.67	0.06	4.29	0.01	89.92
16	57.76	0.36	26.14	0.04	1.77	0.01	0.81	0.78	0.02	3.82	0.18	91.67
17	72.57	0.50	14.53	0.03	1.30	0.04	0.60	0.86	0.02	2.64	0.00	93.09
18	55.53	0.48	26.10	0.00	2.22	0.03	0.91	0.82	0.03	4.48	0.08	90.68
19	52.31	0.13	30.01	0.01	1.72	0.00	0.87	0.77	0.01	4.17	0.13	90.12
20	63.23	0.67	20.43	0.00	1.24	0.03	0.54	1.06	0.06	2.46	0.00	89.71
21	67.21	0.40	16.25	0.02	1.70	0.03	0.53	0.82	0.12	2.59	0.01	89.67

22	24.44	0.13	8.33	0.04	0.54	0.02	0.25	0.31	0.04	1.25	0.00	35.34
23	26.73	0.22	7.91	0.00	0.53	0.03	0.28	0.28	0.03	1.34	0.01	37.35
24	36.41	0.35	15.85	0.00	1.34	0.00	0.48	0.55	0.03	2.16	0.00	57.16
25	57.73	0.42	22.30	0.00	2.50	0.00	0.74	0.78	0.05	3.64	0.00	88.16
26	59.04	0.32	23.19	0.02	2.11	0.02	0.68	0.75	0.05	3.32	0.02	89.50
27	53.50	0.27	27.17	0.02	2.44	0.00	0.66	0.60	0.04	3.26	0.00	87.95
28	62.85	0.39	20.89	0.00	2.49	0.00	0.75	0.71	0.08	3.53	0.00	91.68
29	56.60	0.61	23.67	0.00	4.16	0.00	0.95	0.94	0.11	4.34	0.00	91.37
30	57.85	0.45	23.45	0.01	3.15	0.03	0.77	1.11	0.07	3.56	0.00	90.45
31	56.22	0.70	25.40	0.01	2.49	0.00	0.72	0.84	0.07	3.76	0.01	90.23
32	57.25	0.35	25.35	0.00	2.14	0.00	0.71	0.82	0.07	4.06	0.00	90.74
33	53.87	0.24	27.73	0.01	1.90	0.00	0.74	0.64	0.09	3.32	0.00	88.54
34	58.08	0.62	25.53	0.00	1.40	0.00	0.72	0.69	0.04	3.31	0.03	90.42
35	54.93	0.28	27.37	0.00	2.00	0.00	0.73	0.71	0.06	3.54	0.00	89.61
36	54.29	0.35	26.54	0.00	2.47	0.04	1.12	1.13	0.06	5.43	0.02	91.44
37	51.81	0.17	28.72	0.01	2.30	0.03	0.87	0.96	0.05	4.45	0.00	89.38
38	59.37	0.36	23.33	0.00	2.89	0.01	0.66	1.11	0.05	3.17	0.00	90.96
39	50.24	0.23	29.74	0.00	2.54	0.02	1.02	1.11	0.09	5.09	0.01	90.08
40	52.95	0.47	27.38	0.00	2.32	0.00	0.88	1.22	0.08	4.30	0.01	89.61
41	57.56	0.37	25.29	0.00	1.80	0.01	0.84	0.80	0.07	4.01	0.00	90.75
42	57.64	0.13	23.77	0.00	1.87	0.00	0.86	1.59	0.09	4.14	0.02	90.10
43	60.48	0.25	21.48	0.00	3.17	0.03	0.67	0.92	0.08	3.22	0.00	90.31
44	62.87	0.29	20.09	0.03	2.84	0.00	0.76	0.80	0.05	3.42	0.00	91.16
45	50.06	0.41	30.93	0.00	1.85	0.01	0.68	0.73	0.08	3.60	0.00	88.34
46	51.38	0.19	28.39	0.01	2.39	0.00	0.83	0.85	0.09	3.93	0.02	88.07

47	63.72	0.48	20.87	0.00	2.11	0.00	0.66	0.70	0.05	3.47	0.00	92.06
----	-------	------	-------	------	------	------	------	------	------	------	------	-------

Table H.4: EMPA data of clay accumulations in the matrix of the concretion that contained *T. dokeron*

	SiO ₂	TiO ₂	Al ₂ O ₃	Cr ₂ O ₃	FeO	MnO	MgO	CaO	Na ₂ O	K ₂ O	NiO	Total
1	64.19	0.59	18.92	0.00	2.03	0.00	0.88	0.79	0.03	4.03	0.27	91.74
2	47.34	2.31	25.26	0.03	6.48	0.04	1.61	0.95	0.04	5.44	0.14	89.62
3	61.23	0.54	18.41	0.00	3.21	0.00	0.97	0.88	0.08	4.33	0.00	89.65
4	59.71	0.61	20.65	0.02	2.78	0.00	0.94	0.89	0.10	4.41	0.20	90.30
5	52.53	0.84	26.49	0.00	2.38	0.00	1.19	0.98	0.07	5.75	0.00	90.23
6	62.49	0.43	17.27	0.00	2.26	0.01	0.94	0.77	0.01	4.02	0.00	88.20
7	65.59	0.66	16.70	0.02	1.84	0.02	0.81	1.28	0.04	3.93	0.00	90.89
8	54.39	0.25	26.96	0.03	1.94	0.00	1.16	0.97	0.06	5.52	0.22	91.49
9	54.23	0.57	25.13	0.00	1.84	0.00	1.21	1.56	0.07	5.17	0.00	89.77

*Acaenopax hayae***Table H.5: EMPA data of clay accumulations immediately adjacent to *A. hayae***

	SiO ₂	TiO ₂	Al ₂ O ₃	Cr ₂ O ₃	FeO	MnO	MgO	CaO	Na ₂ O	K ₂ O	NiO	Total
1	52.37	0.70	29.94	0.01	1.58	0.00	0.62	0.67	0.05	2.53	0.00	88.47
2	50.63	0.22	30.56	0.00	0.71	0.02	0.53	0.39	0.07	2.13	0.00	85.25
3	54.75	0.52	27.14	0.00	1.44	0.02	0.57	0.67	0.04	2.53	0.00	87.67
4	52.57	0.26	29.06	0.03	0.93	0.01	0.58	0.51	0.06	2.46	0.00	86.48

5	55.43	0.33	23.65	0.00	3.78	0.03	0.51	0.53	0.01	2.17	0.00	86.42
6	49.98	0.33	25.02	0.03	8.11	0.04	0.51	0.50	0.02	2.28	0.01	86.83
7	62.59	0.25	18.77	0.00	7.17	0.03	0.37	0.42	0.04	1.68	0.05	91.37
8	48.89	0.44	25.47	0.02	9.16	0.03	0.40	0.46	0.01	2.18	0.00	87.06
9	50.61	0.23	25.95	0.05	6.60	0.04	0.38	0.38	0.02	1.75	0.01	86.01
10	51.67	0.26	24.86	0.00	7.62	0.04	0.39	0.48	0.02	1.89	0.03	87.27
11	48.72	0.22	27.12	0.00	7.35	0.04	0.52	0.57	0.04	2.11	0.00	86.69
12	51.03	0.40	23.40	0.05	9.24	0.03	0.32	0.49	0.06	1.83	0.02	86.85
13	50.09	0.14	28.56	0.03	2.65	0.02	0.54	0.59	0.02	2.52	0.03	85.17
14	46.50	0.10	27.33	0.03	9.65	0.03	0.52	0.49	0.03	2.26	0.02	86.95
15	47.07	0.43	26.79	0.00	8.05	0.03	0.46	1.54	0.07	2.02	0.16	86.61
16	53.40	0.33	23.48	0.01	8.03	0.03	0.45	0.56	0.08	2.04	0.08	88.47
17	50.34	0.47	23.78	0.05	10.10	0.03	0.49	0.57	0.09	2.22	0.15	88.28
18	57.25	0.35	20.55	0.00	7.81	0.03	0.41	0.69	0.03	1.99	0.00	89.11
19	51.30	0.29	29.53	0.00	4.12	0.07	0.51	0.63	0.09	2.50	0.13	89.17
20	53.94	0.33	25.57	0.00	5.52	0.06	0.51	1.46	0.07	2.29	0.05	89.78
21	55.32	0.27	29.76	0.00	1.14	0.03	0.55	0.61	0.05	2.35	0.23	90.32
22	57.02	0.66	22.83	0.00	2.55	0.03	0.45	0.59	0.02	1.94	0.09	86.17
23	52.48	0.25	21.48	0.00	0.65	0.00	0.40	0.72	0.07	1.96	0.11	78.10
24	58.06	0.37	25.98	0.03	1.11	0.02	0.53	0.57	0.07	2.27	0.00	89.01
25	52.68	0.41	28.47	0.00	1.55	0.00	0.61	0.58	0.06	2.63	0.03	87.01
26	56.48	0.38	27.84	0.01	1.16	0.01	0.51	0.53	0.04	2.30	0.00	89.25
27	52.83	0.34	30.48	0.00	0.91	0.00	0.46	0.43	0.06	1.93	0.02	87.46
28	54.35	0.79	28.20	0.00	1.05	0.01	0.54	0.54	0.04	2.48	0.00	88.00
29	54.82	0.21	29.14	0.03	0.71	0.03	0.50	0.57	0.06	2.25	0.08	88.41

30	54.86	0.52	27.36	0.01	1.52	0.00	0.49	0.60	0.04	2.37	0.00	87.77
31	55.21	0.18	28.92	0.00	2.43	0.01	0.57	0.57	0.02	2.33	0.14	90.36
32	53.55	0.35	29.72	0.00	0.75	0.00	0.53	0.59	0.02	2.40	0.06	87.98
33	52.27	0.13	29.28	0.02	2.72	0.04	0.45	0.49	0.02	2.21	0.13	87.74
34	49.79	0.24	26.94	0.01	5.32	0.04	0.48	0.96	0.03	2.21	0.00	86.00
35	52.02	0.28	30.43	0.00	1.25	0.00	0.55	0.53	0.00	2.17	0.00	87.23
36	59.60	0.41	20.47	0.00	0.84	0.01	0.36	0.66	0.02	1.38	0.00	83.75
37	76.98	0.24	9.25	0.00	1.38	0.01	0.21	3.20	0.05	0.97	0.00	92.28
38	54.07	0.25	27.95	0.03	0.70	0.02	0.56	0.55	0.00	2.37	0.05	86.54
39	48.75	1.30	30.57	0.00	2.27	0.05	0.80	0.96	0.04	2.36	0.02	87.10
40	56.51	0.35	25.68	0.00	2.33	0.00	0.50	0.88	0.04	2.09	0.05	88.43
41	52.56	0.35	28.89	0.03	1.16	0.00	0.50	0.76	0.04	2.32	0.00	86.60
42	53.61	0.54	27.89	0.00	1.46	0.00	0.60	0.72	0.03	2.53	0.00	87.39
43	50.36	0.66	29.56	0.03	1.18	0.02	0.52	0.65	0.01	2.08	0.00	85.06
44	51.97	0.35	30.63	0.00	0.89	0.00	0.60	0.50	0.02	2.59	0.00	87.55
45	47.84	0.14	34.08	0.03	1.72	0.00	0.52	0.50	0.04	2.19	0.01	87.08
46	59.94	0.40	22.60	0.04	1.73	0.01	0.41	1.11	0.02	2.04	0.04	88.35
47	60.92	0.24	21.85	0.00	1.36	0.00	0.52	0.52	0.01	2.33	0.04	87.78
48	63.18	0.47	20.61	0.01	1.44	0.01	0.53	0.63	0.05	2.16	0.00	89.09
49	52.60	0.14	29.87	0.02	0.88	0.02	0.55	0.56	0.02	2.50	0.00	87.15
50	57.15	0.41	23.59	0.01	0.98	0.02	0.49	0.51	0.02	2.14	0.00	85.31
51	64.45	0.35	17.91	0.01	0.90	0.05	0.44	0.91	0.00	1.96	0.01	86.98
52	52.97	0.26	26.87	0.00	1.05	0.02	0.59	0.61	0.05	2.60	0.01	85.01
53	51.04	0.40	27.57	0.00	3.80	0.05	0.63	0.76	0.08	2.65	0.00	86.97

Table H.6: EMPA data of clay accumulations in the matrix of the concretion that contained *A. hayae*

	SiO ₂	TiO ₂	Al ₂ O ₃	Cr ₂ O ₃	FeO	MnO	MgO	CaO	Na ₂ O	K ₂ O	NiO	Total
1	63.60	0.12	15.97	0.00	1.11	0.04	0.42	0.59	0.04	1.89	0.00	83.76
2	49.93	0.00	32.46	0.01	1.13	0.04	0.92	0.70	0.04	4.26	0.02	89.50
3	51.87	0.36	25.30	0.02	1.68	0.08	1.47	3.96	0.07	4.91	0.00	89.75
4	53.54	0.41	26.58	0.01	2.32	0.04	0.65	1.41	0.10	2.78	0.00	87.83
5	52.49	0.62	32.30	0.00	1.16	0.03	0.95	0.97	0.06	3.91	0.11	92.59
6	67.98	0.28	18.54	0.00	1.37	0.01	0.48	0.52	0.04	1.99	0.00	91.22
7	52.98	0.00	32.30	0.00	2.32	0.01	0.59	0.67	0.03	3.91	0.00	92.82
8	61.52	0.70	23.13	0.00	1.33	0.05	0.60	0.53	0.03	2.82	0.11	90.82
9	64.70	0.38	14.90	0.00	1.06	0.05	0.58	0.51	0.08	2.72	0.00	84.98
10	63.94	0.52	15.43	0.02	1.38	0.00	0.58	0.55	0.02	2.69	0.00	85.12
11	73.77	0.52	10.94	0.01	1.15	0.00	0.36	0.55	0.00	1.91	0.00	89.21

*Offacolus kingi***Table H.7: EMPA data of clay accumulations immediately adjacent to *O. kingi***

	SiO ₂	TiO ₂	Al ₂ O ₃	Cr ₂ O ₃	FeO	MnO	MgO	CaO	Na ₂ O	K ₂ O	NiO	Total
1	33.35	0.13	3.55	0.00	1.24	0.66	0.73	32.03	0.10	0.28	0.04	72.11
2	54.06	0.41	27.43	0.00	1.66	0.07	0.84	1.29	0.28	3.10	0.00	89.12
3	57.43	0.49	25.41	0.00	1.30	0.06	0.73	1.37	0.29	2.68	0.00	89.74

4	52.78	0.62	29.71	0.02	1.13	0.02	0.89	1.25	0.23	3.24	0.03	89.93
5	53.33	0.93	22.55	0.01	2.66	0.07	1.00	3.33	0.22	2.21	0.02	86.33
6	57.02	0.36	24.92	0.00	1.40	0.03	0.78	1.65	0.25	2.72	0.03	89.13
7	57.23	0.35	25.17	0.03	1.46	0.04	0.77	1.59	0.28	2.93	0.01	89.87

Barren Concretion

Table H.8: EMPA data of clay accumulations within a barren concretion

	SiO ₂	TiO ₂	Al ₂ O ₃	Cr ₂ O ₃	FeO	MnO	MgO	CaO	Na ₂ O	K ₂ O	NiO	Total
1	49.16	0.25	33.69	0.02	1.10	0.00	0.99	0.84	0.06	3.26	0.04	89.42
2	49.43	0.42	33.32	0.00	1.19	0.01	0.91	0.90	0.05	3.19	0.00	89.42
3	72.68	0.27	14.36	0.01	0.87	0.01	0.51	2.02	0.06	1.87	0.00	92.65
4	47.26	0.02	35.11	0.05	1.06	0.00	0.70	1.15	0.06	2.20	0.03	87.64
5	47.27	0.00	35.65	0.01	0.91	0.00	0.73	0.67	0.04	1.82	0.01	87.11
6	54.85	0.73	27.44	0.00	2.04	0.02	0.83	0.72	0.14	3.23	0.03	90.03
7	53.46	0.27	30.64	0.00	1.02	0.01	0.68	0.78	0.16	2.58	0.02	89.63
8	14.21	0.15	5.18	0.02	1.44	0.81	0.92	39.78	0.09	0.36	0.00	62.96
9	51.58	0.39	29.70	0.04	2.06	0.00	0.83	1.24	0.05	3.06	0.00	88.95
10	68.71	0.17	11.72	0.00	0.72	0.15	0.46	6.87	0.05	1.38	0.00	90.24
11	47.46	0.00	34.40	0.00	0.99	0.01	0.78	0.92	0.05	2.72	0.00	87.32
12	51.10	0.38	32.28	0.00	0.98	0.00	0.66	1.03	0.05	2.42	0.06	88.96
13	59.71	0.15	24.55	0.03	1.42	0.00	0.63	0.65	0.18	2.28	0.00	89.60
14	49.05	0.21	32.50	0.01	1.27	0.00	0.78	0.73	0.05	2.95	0.00	87.55

15	58.42	0.20	25.21	0.00	2.12	0.02	0.98	0.79	0.05	3.58	0.01	91.38
16	50.54	0.18	31.66	0.00	2.14	0.00	1.04	1.01	0.07	3.98	0.00	90.64
17	52.00	1.27	28.88	0.00	2.40	0.01	0.95	0.82	0.05	3.54	0.00	89.92
18	56.91	0.33	21.16	0.03	2.78	0.00	1.22	3.26	0.07	3.70	0.00	89.45
19	49.91	0.40	29.45	0.00	2.88	0.00	0.99	1.21	0.02	3.83	0.01	88.70
20	49.47	0.13	32.67	0.00	1.34	0.00	0.79	0.56	0.18	3.35	0.01	88.49

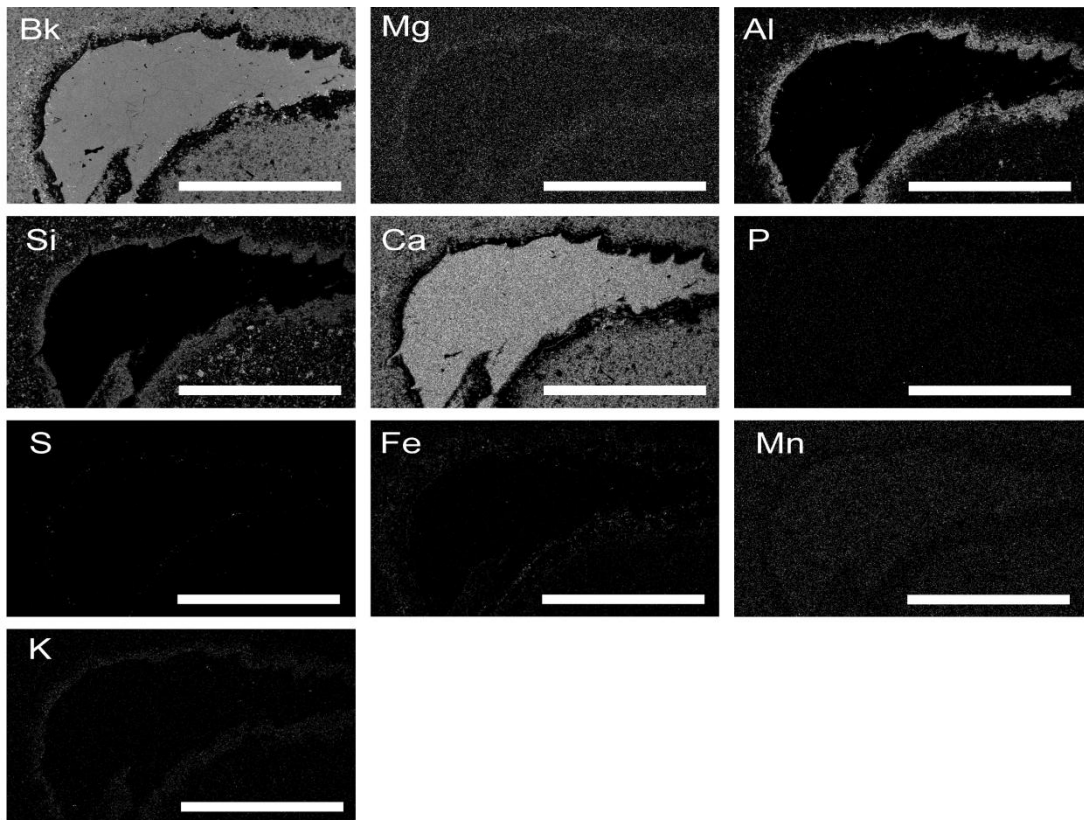
APPENDIX I: EDX MAPS OF *A. HAYAE*

Figure I.2: EDX maps of *A. hayae*; individual elements are labelled, Bk = backscatter detector image. All scale bars are 2 mm.

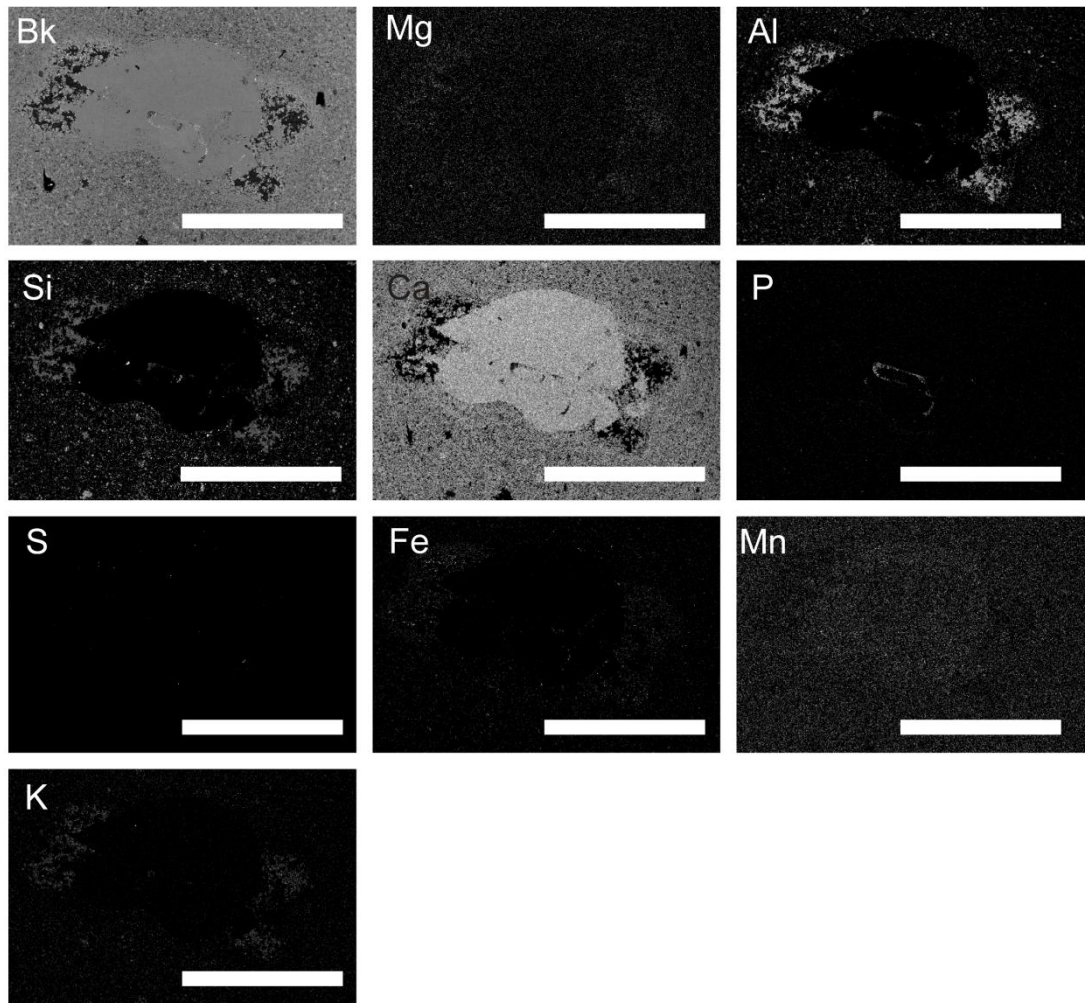
APPENDIX J: EDX MAPS OF *K. CLEMENTSI*

Figure J.1: EDX maps of *K. clementsi*; individual elements are labelled, Bk = backscatter detector image. All scale bars are 2 mm.

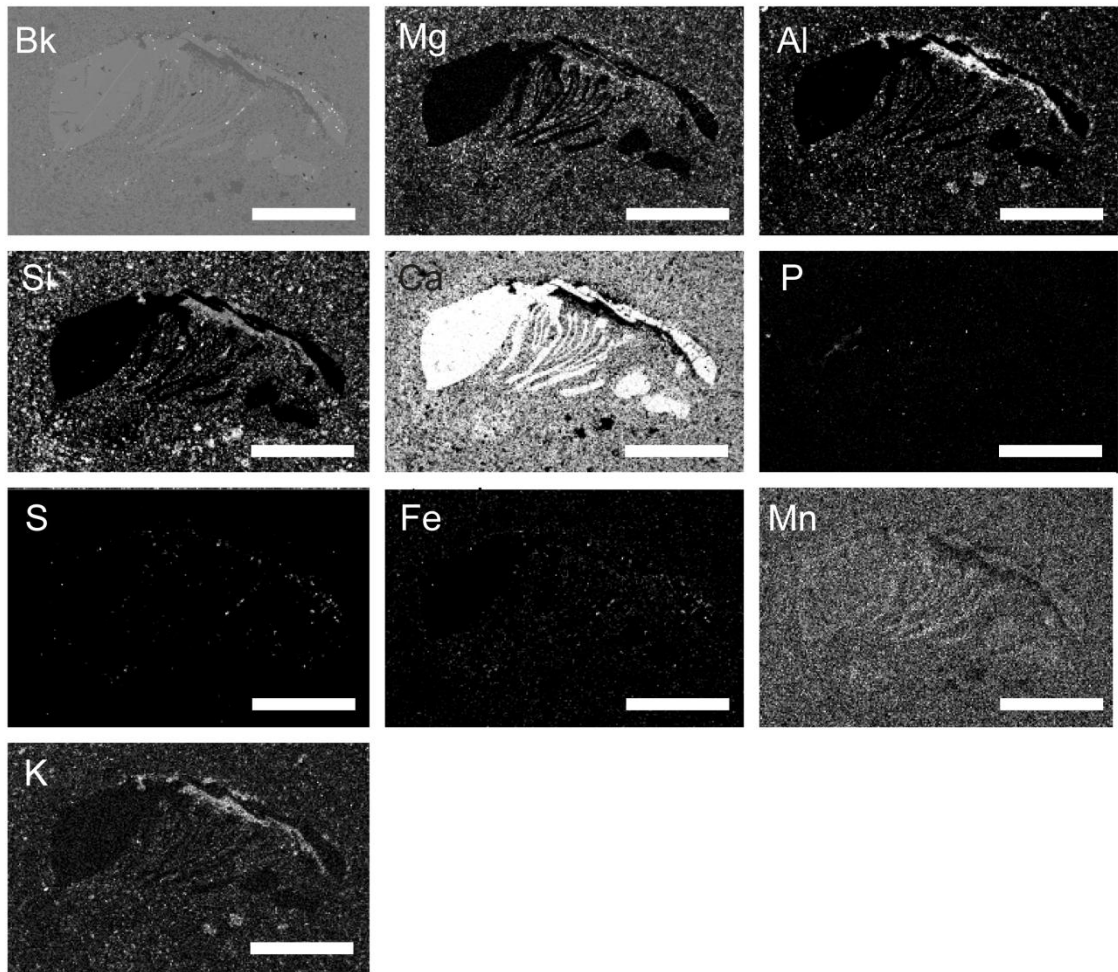
APPENDIX K: EDX MAPS OF *O. KINGI*

Figure K.1: EDX maps of *O. kingi*; individual elements are labelled, Bk = backscatter detector image. All scale bars are 1 mm.

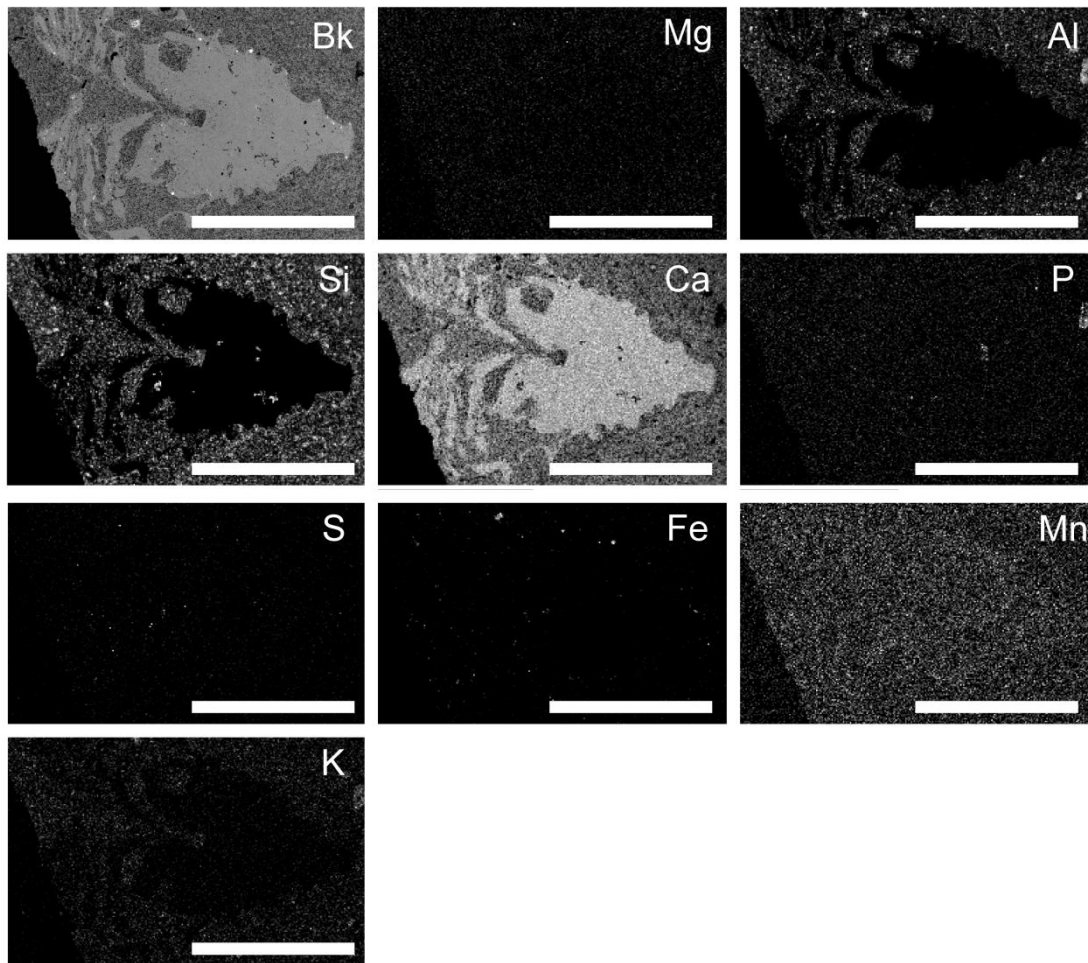
APPENDIX L: EDX MAPS OF *T. DOKERON*

Figure L.1: EDX maps of *T. dokeron*; individual elements are labelled, Bk = backscatter detector image. All scale bars are 2 mm.

APPENDIX M: EDX POINT-AND-ID DATA OF CONCRETION MATRIX

Chemical compositions of minerals used in Chapter 4; all data acquired from an Oxford INCA 350 Energy-dispersive X-ray spectroscopy system attached to a Hitachi S-3600N Environmental Scanning Electron Microscope running at 15 kV. Chemical analysis were normalised to the cobalt standard (99.99% pure cobalt). Results are expressed as weight percent. ID of the mineral is based on the chemical composition, appearance under backscatter detector.

Table M.1: EDX chemical analyses of minerals within the carbonate concretions.

	ID	Na	Mg	Al	Si	K	Ca	Mn	Fe	Total
1	Carbonate	0.24	0.02	-0.04	-0.22	-0.12	65.97	0.82	0.06	66.73
2	Carbonate	0.09	-0.08	0.04	-0.13	-0.06	65.3	1.22	-0.07	66.3
3	Carbonate	0.09	-0.11	0.03	-0.12	0.03	65.49	0.75	-0.15	66.01
4	Carbonate	0	0.09	-0.04	-0.1	0.08	48.03	1.59	0.63	50.27
5	Carbonate	0.15	0.06	0.11	-0.08	0.04	63.64	0.44	0.1	64.46
6	Carbonate	0.13	0.08	-0.07	-0.08	0.06	63.53	1.62	0.21	65.48
7	Carbonate	0.06	0.09	0.08	-0.06	-0.03	56.57	0.95	0.59	58.25
8	Carbonate	-0.01	0.03	0.16	-0.06	-0.09	64.63	0.89	0.24	65.79
9	Carbonate	-0.03	0.07	-0.1	-0.05	-0.02	63.77	1.13	0.11	64.87
10	Carbonate	0.24	0.03	0.15	-0.05	-0.08	64.48	1.49	0.15	66.4
11	Carbonate	-0.01	0.01	-0.1	-0.04	-0.09	63.79	1.38	0.22	65.15

12	Carbonate	0.15	0.08	0.1	-0.04	0.04	64.33	1.34	0.1	66.09
13	Carbonate	0.08	0.15	0.03	-0.04	-0.08	65.02	0.77	0.25	66.18
14	Carbonate	0.1	0.14	-0.01	-0.02	0.03	48.39	2.16	0.85	51.65
15	Carbonate	0.08	-0.06	0.13	-0.02	0	65.12	0.52	0.12	65.9
16	Carbonate	0.06	0.04	-0.02	0	-0.03	48.44	2.35	0.91	51.74
17	Carbonate	0.06	0.09	0.15	0	-0.08	63.89	1.18	-0.06	65.24
18	Carbonate	-0.08	0.02	0.19	0	-0.13	64.42	0.73	0.33	65.49
19	Carbonate	-0.06	0.08	-0.02	0	-0.12	64.9	0.96	0.26	66
20	Carbonate	-0.01	0.08	0.11	0.01	-0.02	63.73	1.55	0.16	65.61
21	Carbonate	0.01	-0.02	-0.04	0.01	-0.01	65.71	0.7	0.12	66.48
22	Carbonate	0.03	0.08	0.09	0.02	0.02	63.39	1.09	0.35	65.08
23	Carbonate	-0.04	0.1	0.12	0.02	-0.03	64.02	1.07	-0.11	65.14
24	Carbonate	0.1	-0.13	0.06	0.03	-0.15	64.76	0.63	0.25	65.54
25	Carbonate	0.07	-0.01	0.07	0.04	-0.09	46.21	2.04	0.76	49.09
26	Carbonate	0.05	0.13	0.14	0.04	0	54.9	1.56	0.77	57.59
27	Carbonate	0.07	0.21	0.06	0.04	-0.06	63.2	1.44	-0.09	64.87
28	Carbonate	0.2	-0.14	0.12	0.04	-0.02	63.31	1.26	0.16	64.93
29	Carbonate	0.05	0.04	0.01	0.04	-0.09	64.92	1.02	-0.01	65.99
30	Carbonate	-0.02	0.11	0.02	0.05	0.09	54.22	1.86	0.81	57.13
31	Carbonate	-0.09	0.15	-0.01	0.05	-0.04	55.52	1.31	0.53	57.43
32	Carbonate	0.21	-0.09	0.16	0.05	-0.08	64.83	0.74	0.25	66.07
33	Carbonate	0.05	0.18	0	0.06	0.02	47.51	1.66	0.52	49.99
34	Carbonate	0	0.11	-0.05	0.06	-0.03	54.72	0.67	0.38	55.87
35	Carbonate	-0.07	0.17	0.02	0.07	0.01	49.03	2.37	0.73	52.33

36	Carbonate	0.01	0.14	0.06	0.08	0.05	48.97	1.72	0.8	51.84
37	Carbonate	0.12	0.08	0.09	0.09	0.1	53.49	2.18	1.51	57.66
38	Carbonate	0.11	-0.08	0.02	0.1	0.1	52.56	1.81	0.42	55.05
39	Carbonate	0.09	0.21	0.11	0.1	0.02	52.19	2.66	1.85	57.23
40	Carbonate	0.21	0.11	0.1	0.1	-0.03	65.53	0.57	0.11	66.69
41	Carbonate	0.16	0.1	0.07	0.11	0.07	47.97	1.93	0.2	50.62
42	Carbonate	0.09	0.2	-0.03	0.11	-0.01	48.45	2.39	0.82	52.03
43	Carbonate	0.11	0.05	-0.04	0.12	-0.03	62.84	1.3	-0.02	64.33
44	Carbonate	0.06	-0.01	0.07	0.13	-0.07	63.79	1.29	-0.04	65.22
45	Carbonate	0.12	0.14	0.07	0.14	0.06	49.46	0.93	0.5	51.41
46	Carbonate	0.04	0.03	-0.1	0.14	-0.01	56.24	0.98	0.6	57.93
47	Carbonate	0.1	-0.1	-0.07	0.14	-0.05	65.65	0.54	-0.43	65.77
48	Carbonate	0.08	0.17	0.12	0.18	0.07	49.13	2.54	0.67	52.96
49	Carbonate	0.07	0.1	0.12	0.18	-0.02	54.69	1.1	0.26	56.5
50	Carbonate	0.21	0.07	0.1	0.19	-0.08	63.26	0.92	0.16	64.83
51	Carbonate	0.09	0.08	0.11	0.2	-0.04	63.44	1.15	0.04	65.07
52	Carbonate	-0.03	-0.05	0.06	0.22	0.01	64.41	1.08	0.22	65.93
53	Carbonate	0.27	-0.05	0.14	0.27	0.05	51.68	1.49	0.22	54.06
54	Carbonate	0.04	14.83	0.53	0.38	0	4.92	0.06	36.36	57.12
55	Carbonate	0.04	0.14	0.18	0.42	-0.01	52.05	1.49	0.42	54.73
56	Carbonate	0.02	1.28	0.28	0.45	0.01	51.55	1.17	1.38	56.12
57	Carbonate	-0.01	13.81	0.59	0.46	0.05	5.57	0.36	33.66	54.5
58	Carbonate	0.03	0.61	0.28	0.54	0.06	43.6	2.12	4.31	51.56
59	Carbonate	0.12	12.11	0.69	0.58	0.09	27.81	-0.12	9.99	51.27

60	Carbonate	0.02	0.34	0.32	0.58	0	48.71	1.42	0.75	52.15
61	Carbonate	0.08	12.06	0.29	0.58	0.03	33.77	0.38	10.64	57.83
62	Carbonate	-0.01	13.13	0.56	0.59	0.15	7.99	0.45	40.49	63.36
63	Carbonate	0	12.61	0.48	0.6	-0.05	32.31	0.05	11.37	57.37
64	Carbonate	0.07	13.11	0.37	0.6	0.07	4.96	0.22	38.23	57.63
65	Carbonate	-0.08	13.77	0.42	0.66	0.09	4.07	0.05	36.49	55.47
66	Carbonate	0	9.58	0.4	0.66	0.03	33.36	0.18	12.97	57.19
67	Carbonate	-0.05	11.68	0.66	0.67	-0.03	24.89	0.3	12.56	50.67
68	Carbonate	0.18	12.08	0.37	0.68	-0.01	4.15	0.31	36.75	54.5
69	Carbonate	0.15	14.79	0.5	0.7	0.02	4.85	0.16	40.64	61.8
70	Carbonate	0.08	13.34	0.51	0.71	0.15	4.01	0.2	37.52	56.51
71	Carbonate	0.13	13.44	0.65	0.77	0.03	4.42	0.42	38.36	58.22
72	Carbonate	-0.01	12.93	0.54	0.83	0.03	4	0.33	37.45	56.1
73	Carbonate	0.11	14.17	1.13	0.85	0.06	4.14	0.26	38.93	59.65
74	Carbonate	0.04	0.83	0.31	0.86	0	45.67	1.91	1.31	50.93
75	Carbonate	0.1	12.97	0.62	0.93	0.02	32.07	0.3	8.13	55.15
76	Carbonate	0.02	12.72	0.9	0.98	-0.03	3.84	0.37	35.56	54.35
77	Carbonate	0.09	14.11	1.09	1	0.04	30.3	0.16	9.57	56.36
78	Carbonate	0.17	13.11	0.69	1	0.13	9.93	0.27	37.83	63.14
79	Carbonate	0.15	10.42	0.87	1.01	0.1	28.94	0.61	11.04	53.14
80	Carbonate	-0.14	12.34	0.73	1.03	0.03	29.82	0.34	10.91	55.06
81	Carbonate	0.1	9.54	0.74	1.11	0.11	29.86	0.35	9.78	51.59
82	Carbonate	0.11	12.54	0.89	1.13	0.03	27.37	0.17	8.82	51.07
83	Carbonate	-0.14	11.49	0.76	1.13	-0.03	28.14	0.28	11.19	52.82

84	Carbonate	0.11	14.05	1.11	1.13	0.15	33.52	0.46	8.43	58.97
85	Carbonate	0.02	11.81	1.23	1.17	-0.01	26.94	0.14	10.86	52.17
86	Carbonate	0.1	9.15	0.88	1.17	0.06	35.55	0.38	8.8	56.09
87	Carbonate	0.1	13.77	0.67	1.18	-0.02	9.16	0.36	38.03	63.24
88	Carbonate	0.08	10.65	0.8	1.19	-0.01	27.16	0.15	11.15	51.15
89	Carbonate	-0.01	11.29	0.91	1.2	-0.03	14.89	0.51	31.06	59.81
90	Carbonate	0.28	11.69	1.64	1.22	0.03	5	0.19	36.81	56.86
91	Carbonate	0.02	14.55	0.5	1.28	0.05	3.71	0.29	41.02	61.42
92	Carbonate	0.07	14.44	0.64	1.29	0.02	7.72	0.3	39.11	63.59
93	Carbonate	-0.02	13.08	0.88	1.33	0.1	31.29	-0.1	8.95	55.49
94	Carbonate	0.01	14.91	1.1	1.42	0.13	30.72	0.22	8.49	56.99
95	Carbonate	0.07	10.47	0.86	1.44	0	39.05	0.33	6.47	58.68
96	Carbonate	0.04	11.21	1.17	1.47	-0.02	28.25	0.29	10.87	53.29
97	Carbonate	0.04	13.98	1.02	1.47	0.11	29.34	0.24	9.48	55.67
98	Carbonate	0.15	15.1	1.09	1.5	0.1	30.19	-0.04	8.94	57.03
99	Carbonate	0.16	0.41	0.41	1.52	0.11	54.3	0.9	0.88	58.69
100	Carbonate	0.09	14.45	0.77	1.55	-0.04	3.73	0.52	41.63	62.69
101	Carbonate	0.07	14.99	0.77	1.59	0.13	31.45	0.27	8.57	57.83
102	Carbonate	0.05	12.3	1.3	1.65	-0.04	10.29	0.12	32.67	58.35
103	Carbonate	0.2	13.26	1.17	1.65	0.03	6.89	0.12	35.97	59.3
104	Carbonate	0.13	14.58	1.04	1.7	0.01	3.19	0.24	41.07	61.96
105	Carbonate	0.03	13.92	1.1	1.8	-0.1	8.5	0.14	38.5	63.9
106	Carbonate	0.01	13.11	1.56	1.91	0	30.28	0.2	11.35	58.43
107	Carbonate	0.3	13.74	0.89	2.02	-0.02	7.41	0.23	37.42	62

108	Carbonate	0.31	12.97	1.46	2.09	0.09	4.14	0.38	37.13	58.58
109	Carbonate	0.14	11.83	0.97	2.26	-0.05	10.06	0.16	30.96	56.34
110	Carbonate	0.1	11.82	2.59	2.94	0.09	26.38	0.06	8.67	52.65
111	Carbonate	0.49	13.17	1.43	3.23	0.02	9.8	0.29	33.63	62.07
112	Carbonate	0.24	0.52	2.09	4.92	0.06	1.1	-0.02	46.75	55.65
113	Carbonate	0.19	0.82	3.21	5.82	0.41	50.51	0.13	0.85	61.93
114	Carbonate	-0.2	9.76	6.04	6.27	0.15	2.18	0.56	38.09	62.86
115	Carbonate	0.3	0.2	4.76	6.47	0.37	51.14	0.18	0.2	63.62
116	Carbonate	0.08	10.7	6.2	6.96	0.05	2.84	0.23	32.94	60.02
117	Quartz	0.08	0.05	0.61	95.21	0	-0.07	-0.12	0.23	96.01
118	Quartz	-0.01	0.1	0.61	95.37	0.14	-0.08	0.1	-0.02	96.2
119	Quartz	-0.07	0.08	0.55	95.5	0.08	0.07	0.24	0	96.47
120	Quartz	-0.1	0.09	0.58	96.65	0	0.01	-0.06	0.08	97.26
121	Quartz	0.08	0.13	4.75	96.72	1.36	0.11	-0.03	0.67	103.78
122	Quartz	0.13	-0.03	1	97.1	-0.05	0.03	-0.1	-0.01	98.07
123	Quartz	0.1	-0.02	0.25	97.16	0.01	-0.03	-0.07	0.2	97.61
124	Quartz	0.15	0.06	0.3	97.23	0.12	0.07	0.06	0.14	98.12
125	Quartz	-0.05	-0.07	0.25	97.36	0.05	0.04	-0.01	0.44	98.01
126	Quartz	0.1	-0.03	1.49	97.79	0.1	0.52	-0.03	0.29	100.24
127	Quartz	0.19	-0.03	0.65	97.92	-0.01	-0.16	0.02	0.36	98.95
128	Quartz	0.16	0.16	0.87	98.55	0.27	0.44	-0.02	0.47	100.9
129	Quartz	0.05	0	0.89	99.05	-0.02	0.01	0.03	0.24	100.24
130	Quartz	0.14	0.05	0.8	99.12	0.07	0.33	0.09	0.44	101.04
131	Quartz	0.17	0.11	1.15	99.16	0.15	-0.03	-0.05	0.16	100.83

132	Quartz	0.08	0.25	1.9	99.2	0.22	0.02	0.12	0.57	102.36
133	Quartz	0.25	0.14	0.46	99.21	0.12	0.1	-0.25	0.37	100.4
134	Quartz	0.18	0.1	1.55	99.61	0.35	0.11	0.15	0.53	102.58
135	Quartz	0.2	0.03	0.68	99.76	-0.1	0	0.3	0.14	101.02
136	Quartz	0.07	0.06	0.58	100.14	0.11	0.18	0	0.44	101.58
137	Quartz	0.02	-0.08	0.89	101.39	0.07	0.02	0.01	0.75	103.06
138	Quartz	-0.04	0.25	1.32	101.48	0.19	0.16	-0.09	0.25	103.51
139	Quartz	0.04	0.03	0.29	101.55	0.04	0.09	0.08	0.25	102.37
140	Quartz	0.14	0.08	0.81	101.65	0.14	0.02	-0.31	0.5	103.04
141	Quartz	0.23	-0.04	0.74	102.18	-0.05	0.18	0.12	0.13	103.49
142	Quartz	0.12	0.07	0.46	102.34	0.08	0.02	0.05	0.23	103.36
143	Quartz	0.03	0.14	0.95	102.62	0.31	0.16	0.04	0.18	104.43
144	Quartz	0.03	-0.07	0.58	102.71	-0.03	0.11	0.03	-0.03	103.33
145	Quartz	-0.02	0.01	0.41	103.28	0.12	0.02	-0.05	0.6	104.36
146	Quartz	-0.03	0.12	-0.01	103.86	0.08	-0.16	-0.04	-0.04	103.78
147	Quartz	0.01	-0.06	0.21	104.31	-0.07	0.14	-0.18	0.16	104.53
148	Quartz	0.02	-0.09	0.17	104.36	0.08	-0.02	0.14	-0.2	104.45
149	Quartz	-0.05	0.19	0.8	104.59	0.13	0	0.22	0.27	106.16
150	Quartz	-0.07	0.24	0.16	104.97	-0.02	0.13	-0.19	-0.05	105.17
151	Quartz	0.1	0.05	0.2	105.73	0.05	-0.01	0.03	0.46	106.61
152	Quartz	0.01	-0.11	-0.04	105.8	-0.05	0.1	-0.2	0.14	105.65
153	Quartz	0.18	0	0.02	106.09	-0.03	-0.06	0.08	0.04	106.31
154	Quartz	-0.05	0.04	-0.16	107.01	0.12	0.1	-0.02	0.19	107.21
155	Chalcedony	0.1	0.22	4.1	65.18	0.81	0.14	0.08	0.85	71.48

156	Chalcedony	0.14	0.36	9.92	68.91	0.85	0.13	0.19	0.51	81.01
157	Chalcedony	0.04	0.12	2.75	69.97	0.5	0.11	0.1	-0.02	73.57
158	Chalcedony	0.06	1.15	19.21	70.01	5.7	0.49	0.13	3.06	99.8
159	Chalcedony	0.05	0.04	1.45	70.79	0.06	0.13	-0.12	0.12	72.52
160	Chalcedony	0.1	0.1	0.92	71.76	-0.06	0.33	-0.06	0.01	73.1
161	Chalcedony	0.14	0	2.16	71.92	0.21	0.05	-0.09	0.03	74.43
162	Chalcedony	-0.13	0.1	1.15	72.51	0.14	0.05	-0.01	0.17	73.99
163	Chalcedony	0.15	0.06	0.52	73	-0.09	-0.01	-0.12	-0.11	73.39
164	Chalcedony	0.04	0	0.63	73.01	0.15	0.04	0.26	-0.01	74.1
165	Chalcedony	0.14	-0.04	0.36	73.1	0.06	-0.07	0.08	0.09	73.71
166	Chalcedony	0.12	0.09	0.67	73.13	0	0.18	-0.03	-0.13	74.04
167	Chalcedony	0.12	-0.03	2.03	73.26	0.12	0.11	-0.17	0.14	75.58
168	Chalcedony	0.07	-0.04	1.28	73.33	0.28	0.05	-0.04	0.16	75.09
169	Chalcedony	0.15	0.03	0.44	73.48	0.07	-0.05	0.05	-0.05	74.11
170	Chalcedony	0.02	-0.11	0.26	73.54	0.01	-0.04	-0.05	-0.06	73.56
171	Chalcedony	0	0.01	0.57	73.61	0.1	0.01	-0.08	0.03	74.24
172	Chalcedony	-0.05	0.12	1.34	73.61	0.32	0.08	0.08	0.29	75.78
173	Chalcedony	0.08	-0.01	0.72	73.7	0.08	0.02	0.07	0.16	74.81
174	Chalcedony	-0.03	0.08	2.02	73.71	-0.01	0.12	-0.02	-0.07	75.8
175	Chalcedony	0.11	-0.06	0.26	73.77	0	-0.04	-0.06	0.09	74.07
176	Chalcedony	0.15	-0.09	0.55	74.01	-0.08	0.1	-0.1	0.21	74.75
177	Chalcedony	0.11	0.07	0.87	74.04	-0.07	0.06	-0.09	-0.16	74.83
178	Chalcedony	0.14	-0.12	0.47	74.1	0.02	0.08	-0.17	-0.07	74.46
179	Chalcedony	0.13	0.08	0.47	74.16	-0.06	0.15	-0.16	0.07	74.84

180	Chalcedony	-0.02	-0.04	0.07	74.34	-0.07	0.12	-0.11	0.11	74.41
181	Chalcedony	-0.06	0.08	0.86	74.34	0.1	0.05	-0.04	0.07	75.41
182	Chalcedony	0.13	0.06	0.55	74.37	-0.03	0.2	0.11	0.04	75.43
183	Chalcedony	0.11	0.15	0.4	74.5	0.07	0.02	0.16	-0.08	75.35
184	Chalcedony	0.04	-0.08	0.62	74.65	0.11	0.06	0.21	0.02	75.63
185	Chalcedony	-0.01	0.16	0.54	74.73	-0.03	0.06	-0.12	0.68	76
186	Chalcedony	0.06	-0.07	0.72	74.87	0.04	0.01	-0.09	-0.01	75.53
187	Chalcedony	0.1	-0.03	0.55	75	0.02	0.11	-0.01	-0.12	75.62
188	Chalcedony	-0.04	0.01	0.16	75.03	-0.06	0.08	0.02	-0.21	75
189	Chalcedony	0.03	0.1	0.58	75.27	0.05	-0.03	0.26	0.27	76.53
190	Chalcedony	0.09	0.08	0.78	75.27	0	0.08	0.27	0.21	76.78
191	Chalcedony	0.07	0.17	0.39	75.57	0.12	-0.01	-0.24	0.21	76.27
192	Chalcedony	0.05	-0.03	0.21	75.61	0.06	0	0.07	0.11	76.07
193	Chalcedony	0.11	-0.15	0.76	75.61	0	0.07	0.12	0.01	76.53
194	Chalcedony	0.04	0.07	0.29	75.76	0.14	-0.02	-0.03	0.36	76.6
195	Chalcedony	0.02	0.07	0.27	75.89	0.08	0.08	-0.05	0.18	76.53
196	Chalcedony	0.01	0.18	0.26	75.89	0.07	-0.02	-0.28	0.59	76.69
197	Chalcedony	0.05	0	0.32	76.13	-0.04	-0.06	-0.07	0.17	76.5
198	Chalcedony	0.09	0.11	0.42	76.29	0.04	-0.01	0.1	0.28	77.33
199	Chalcedony	0.05	0.08	0.36	76.66	0.04	-0.05	0.13	0.15	77.42
200	Chalcedony	0.05	0.05	0.02	76.84	0.02	0	0.27	0.2	77.45
201	Chalcedony	0.06	0.04	0.14	77.26	0.1	-0.04	-0.07	0.14	77.62
202	Clay	-0.05	1.27	22.9	40.26	5.29	0.69	-0.06	0.93	71.23
203	Clay	0.24	0.35	33.34	40.73	0.61	0.71	0.12	1.35	77.44

204	Clay	0.23	1.09	31.25	43.9	3	1.16	-0.07	1.41	81.97
205	Clay	0.13	0.12	35.16	43.97	0.03	0.14	-0.01	1.04	80.59
206	Clay	0.12	0.51	21.44	44.36	2.59	10.34	0.07	1.58	81.02
207	Clay	-0.04	-0.04	37.24	45.55	0.2	0.23	-0.14	0.56	83.56
208	Clay	0.12	-0.07	37.83	45.66	0.11	0.03	-0.14	0.2	83.74
209	Clay	0.08	0.22	35.23	45.92	0.64	0.07	-0.08	0.64	82.74
210	Clay	-0.02	-0.08	39.16	46.45	0.02	0.13	0	0.43	86.1
211	Clay	0.18	-0.06	36.29	46.93	0.37	0	-0.08	0.41	84.03
212	Clay	0.13	-0.02	38.91	46.93	0.13	0.17	-0.05	0.9	87.09
213	Clay	0.1	0.03	39.57	47.05	0.1	0.2	-0.24	0.28	87.08
214	Clay	-0.03	0.14	38.5	47.39	0.26	0.1	-0.22	0.15	86.3
215	Clay	0.09	0.09	34.85	47.76	0.96	0.32	0.18	0.69	84.94
216	Clay	0.2	0.04	39.03	47.83	0.53	0.18	0.1	0.78	88.69
217	Clay	0.06	0.17	36.73	47.91	1.17	0.23	0.04	0.62	86.93
218	Clay	0.19	-0.01	39.57	48.08	0.52	0.17	0.01	0.5	89.04
219	Clay	0.05	0.27	32.81	48.49	0.71	0.15	-0.15	1.83	84.14
220	Clay	0	0.05	40.67	48.67	0.01	0.13	0.09	0.22	89.85
221	Clay	0.04	0.1	36.97	48.77	0.09	0.14	0.18	0.57	86.88
222	Clay	0.17	0.21	35.08	48.85	1.12	-0.02	0.13	0.15	85.69
223	Clay	0.01	0.44	37.12	48.94	1.77	0.22	0.15	0.91	89.57
224	Clay	0.08	-0.14	39.08	49.09	0.13	-0.06	-0.05	0.08	88.22
225	Clay	-0.01	0.57	36.17	49.31	2.68	0.58	0	0.65	89.94
226	Clay	0.09	0.03	36.21	49.58	0.22	0.24	-0.08	1.16	87.46
227	Clay	0.04	0.01	37.45	49.72	0.34	-0.09	-0.08	0.03	87.42

228	Clay	0.96	0.42	37.5	49.79	2.67	0.26	0	0.33	91.93
229	Clay	0.26	0.33	37.22	49.81	1.31	0.27	0.1	0.67	89.97
230	Clay	1.74	0.68	35.31	50.27	5.58	0.58	-0.09	1.16	95.22
231	Clay	1.47	0.69	34.49	50.86	4.93	0.53	0.31	1.34	94.61
232	Clay	0.06	0.34	37.35	51.51	1.06	0.13	0.22	0.4	91.07
233	Clay	0.03	1.78	29.75	52.52	6.3	1.09	0.05	2.72	94.23
234	Clay	0.32	1.57	30.78	52.52	9.23	0.26	-0.1	3.55	98.14
235	Clay	0.13	1.86	28.11	52.56	6.31	0.88	0.07	1.52	91.46
236	Clay	0.23	1.53	27	52.72	8	0.43	-0.08	2.78	92.6
237	Clay	0.25	0.56	12.64	54.07	3.15	0.44	-0.08	0.68	71.7
238	Clay	0.13	0.43	9.72	55.39	2.27	0.38	-0.11	0.81	69.03
239	Clay	0	1.54	27.07	56.63	6.22	1.26	-0.16	1.84	94.4

APPENDIX N: XRD OF CARBONATE CONCRETION

XRD analyses for concretion 1 (TABLE N.1) were carried out on a Phillips XRD (Phillips model PW1732 X-ray generator, with a PW1716 diffractometer and PW 1050/25 detector controlled by a PW1710). Sample spacing of 0 mm; transects across the height and depth were measured at 45 mm across the concretions length.

Table N.1: Whole rock XRD data of concretion 1 (HC1)

	Bead #	Sample Spacing	Kaolinite	Calcite	Dolomite	Ferric oxide	Quartz	Total
Across Length	LF31525	5	18	52	18	5	5	99
	LF31520	15	18	52	17	5	5	98
	LF31524	25	18	52	17	6	6	98
	LF31514	35	18	52	17	5	6	99
	LF31521	45	18	53	16	5	6	98
	LF31519	55	18	52	17	5	6	98
	LF31528	65	18	54	15	5	6	98
	LF31526	75	18	53	17	5	5	99
	LF31527	85	18	55	15	5	5	98
	LF31517	95	19	63	5	6	5	98
Across Height	LF31534	35	18	64	5	6	6	99
	LF31533	25	18	64	5	6	5	98
	LF31532	15	18	55	14	5	5	98
	LF31518	5	18	53	16	5	6	98
	LF31521	0	18	53	16	5	6	98
	LF31515	-5	17	53	17	5	6	99
	LF31531	-15	18	55	14	5	5	98
	LF31513	-25	18	64	5	6	5	98
	LF31530	-35	21	59	3	6	9	98
Across Depth	LF31521	5	18	53	16	5	6	98
	LF31529	15	18	53	16	5	6	98
	LF31522	25	18	52	17	5	5	98
	LF31512	35	18	58	12	6	5	99
	LF31516	45	19	65	4	6	4	98
	LF31523	55	21	56	5	7	9	98

XRD analyses for concretion 2 (TABLE N.2) were carried out on a Bruker D8 Advance with DaVinci. Sample spacing of 0 mm is the centre of the concretion.

Table N.2: Whole rock XRD data of concretion 2

	Bead	Sample spacing (mm)	Calcite	Dolomite	Quartz	Kaolinite	Siderite?
Across Length	LF32942	-50	75.8	0	16.3	7.9	0
	LF32949	-40	85	1.3	7	6.2	0.6
	LF32954	-30	66.7	18.6	7.4	5.7	1.6
	LF32951	-20	62.8	20.8	9.7	4.4	2.3
	LF32945	-10	62.4	20.2	11.1	4	2.3
	LF32952	0	62.8	19.7	10.9	4.3	2.3
	LF32950	10	60.8	21.2	11.8	3.8	2.5
	LF32953	20	61.1	21.9	9.4	5.5	2
	LF32955	30	80.1	5.7	7.5	6	0.7
	LF32943	40	70.7	0	20.1	9.2	0
Across Height	LF32948	30	79.1	0	13.4	7.5	0
	LF32956	20	85.1	0.9	7.5	6.6	0
	LF32947	10	64.4	20	8.5	5.2	1.9
	LF32945	0	62.4	20.2	11.1	4	2.3
	LF32946	-10	61.6	20	12.2	3.8	2.3
	LF32944	-20	74.1	8.2	10.2	6.7	0.7
	LF32938	-30	81.9	0	10.5	7.7	0
Across Depth	LF32958	40	83.3	0	8.2	8.6	0
	LF32940	30	67.2	14.4	12.7	4.4	1.3
	LF32960	20	60.2	18.6	16.5	2.5	2.3
	LF32957	10	58.2	19	17.9	2.6	2.4
	LF32945	0	62.4	20.2	11.1	4	2.3
	LF32941	-10	60.6	24	8.2	4.6	2.6
	LF32939	-20	84.9	0	8.7	6.4	0
	LF32959	-30	81.8	0	9.2	8.9	0

APPENDIX O: XRF OF CARBONATE CONCRETION

XRF data for concretion 1 (HC1); for the order of transects the reader is referred to Appendix N for the transect order.

Table O.1: XRF major elements of concretion 1. bd = below detection limit.

Bead #	SiO ₂	TiO ₂	Al ₂ O ₃	Fe ₂ O ₃	MnO	MgO	CaO	Na ₂ O	K ₂ O	P ₂ O ₅	SO ₃	LOI	Total
LF31512	13.23	0.53	6.31	5.78	0.99	1.76	35.36	bd	0.64	0.20	bd	34.54	99.35
LF31513	12.87	0.53	6.27	6.28	0.94	0.55	36.86	bd	0.63	0.20	bd	33.84	98.97
LF31514	14.48	0.53	6.10	5.47	0.98	2.78	33.36	0.01	0.78	0.18	0.01	34.55	99.26
LF31515	14.19	0.53	6.09	5.46	0.99	2.83	33.81	bd	0.76	0.19	bd	34.75	99.61
LF31516	12.96	0.54	6.57	6.19	0.94	0.52	36.78	bd	0.68	0.22	bd	33.83	99.23
LF31517	14.15	0.58	6.74	6.13	1.00	0.51	35.78	bd	0.70	0.22	bd	33.24	99.06
LF31518	14.23	0.54	6.05	5.34	0.99	2.79	33.59	0.02	0.77	0.19	bd	34.61	99.11
LF31519	14.14	0.53	5.96	5.43	0.98	2.78	33.48	0.01	0.80	0.18	0.03	34.61	98.94
LF31520	13.74	0.53	6.06	5.43	0.98	2.87	33.50	0.01	0.73	0.19	0.03	34.82	98.88
LF31521	14.40	0.54	6.08	5.50	0.97	2.72	33.30	0.02	0.80	0.19	0.01	34.41	98.95
LF31522	13.72	0.53	6.16	5.19	1.00	2.80	33.70	bd	0.76	0.19	0.05	34.80	98.90
LF31523	18.76	0.65	7.58	6.89	0.98	0.64	31.77	bd	1.26	0.20	bd	30.24	98.95
LF31524	14.27	0.53	6.12	5.53	0.99	2.91	33.32	bd	0.77	0.19	0.03	34.71	99.37
LF31525	13.39	0.54	6.16	5.49	1.00	3.05	33.75	bd	0.65	0.20	bd	35.14	99.39
LF31526	13.64	0.53	6.16	5.37	1.00	2.75	33.70	0.01	0.74	0.19	0.03	34.92	99.06
LF31527	13.01	0.53	6.13	5.40	1.00	2.45	34.49	bd	0.65	0.20	0.02	35.08	98.98

LF31528	13.96	0.53	6.03	5.48	1.00	2.79	33.78	0.01	0.76	0.19	bd	34.76	99.28
LF31529	14.25	0.53	6.03	5.45	0.99	2.83	33.58	bd	0.77	0.19	bd	34.71	99.34
LF31530	18.98	0.64	7.09	6.13	0.92	0.52	32.86	bd	0.85	0.19	bd	31.16	99.35
LF31531	13.46	0.53	6.10	5.43	0.98	2.20	34.52	bd	0.74	0.19	0.05	34.76	98.97
LF31532	13.79	0.53	6.13	5.30	0.98	2.50	34.21	bd	0.73	0.19	0.00	34.52	98.91
LF31533	13.50	0.55	6.34	6.37	0.97	0.51	36.30	bd	0.68	0.20	bd	33.51	98.93
LF31534	14.26	0.56	5.89	5.98	1.07	0.54	36.55	bd	0.67	0.17	bd	33.15	98.82

Table O.2: Trace element data for concretion 1; measured as ppm. Copper (Cu) was analysed, but has been removed as no samples contained copper above instruments detection limit (<2.3ppm).

	Rb	Sr	Y	Zr	Nb	Pb	Th	U	Ga	Zn	Ni	Co	Cr	V	Sc	Ba	La	Ce	Nd	Cs
LF31512	25.8	335.6	34.5	96.0	7.1	6.7	2.6	bd	10.4	92.7	14.9	6.0	15.4	18.6	13.2	528.8	14.7	50.1	17.8	bd
LF31513	25.1	162.4	38.6	95.9	5.8	7.7	1.6	bd	8.3	91.4	12.8	5.2	15.7	23.2	15.4	285.6	22.3	49.0	18.3	bd
LF31514	26.1	412.9	32.7	94.2	6.7	8.2	bd	bd	11.5	81.3	13.1	6.0	14.7	17.1	14.6	25.2	17.4	54.7	21.0	9.7
LF31515	30.2	416.8	32.5	93.8	7.3	8.0	1.8	bd	9.4	83.7	13.5	4.2	15.5	18.5	14.2	30.3	17.5	49.7	19.5	12.1
LF31516	24.3	176.9	44.3	98.1	7.1	8.4	bd	bd	8.9	101.0	16.1	6.3	12.2	17.8	16.8	363.6	23.9	53.4	21.4	6.5
LF31517	22.3	184.0	53.6	105.0	7.9	8.9	bd	bd	8.2	104.4	18.2	5.2	16.2	20.8	16.4	337.0	30.9	73.1	25.5	8.1
LF31518	27.4	409.8	33.2	93.8	6.7	7.3	bd	bd	8.0	78.9	14.1	3.3	16.3	18.2	13.7	29.5	18.6	53.2	23.3	11.3
LF31519	23.6	404.4	33.2	93.1	6.9	8.8	bd	2.0	8.1	87.9	12.8	6.6	15.7	15.0	14.3	23.9	23.0	49.5	16.7	10.0
LF31520	24.4	448.2	32.6	93.6	7.1	8.9	bd	bd	9.1	82.2	15.1	5.4	15.5	17.9	15.4	51.0	20.2	43.5	21.2	9.9
LF31521	25.6	400.4	33.8	94.4	7.0	7.0	bd	1.7	10.6	83.0	13.9	6.5	16.7	16.5	14.6	35.8	22.6	51.7	16.7	7.6
LF31522	21.2	429.3	33.2	93.8	6.8	8.4	bd	2.3	8.8	79.4	13.9	6.5	12.2	17.6	17.8	61.6	18.8	48.8	22.4	8.5
LF31523	41.7	195.4	56.6	124.7	9.1	18.4	bd	2.7	9.9	83.9	25.1	6.4	25.4	23.3	20.0	281.3	36.9	73.1	30.3	6.9
LF31524	26.1	429.4	31.9	92.7	6.4	6.8	bd	bd	9.2	81.2	14.1	7.9	15.0	19.3	14.6	38.7	17.6	54.0	17.9	bd

APPENDICES

LF31525	23.8	470.7	33.3	94.0	7.2	8.1	bd	bd	8.1	87.7	14.2	8.0	16.0	15.5	12.8	91.6	20.8	47.1	19.3	14.9
LF31526	23.0	422.2	32.7	94.6	7.9	9.1	bd	bd	9.0	85.3	13.7	5.4	15.1	17.9	14.3	38.8	23.4	49.4	16.0	7.3
LF31527	21.8	408.2	33.4	92.3	7.1	7.2	bd	bd	10.3	88.4	14.0	7.2	13.3	18.3	16.8	208.6	16.5	54.9	17.9	bd
LF31528	28.5	407.6	31.5	92.9	6.9	7.2	bd	bd	7.9	81.2	14.1	bd	12.6	16.4	13.4	32.0	22.6	51.5	16.9	9.8
LF31529	26.4	410.0	32.7	92.9	7.2	7.7	bd	bd	10.2	79.3	13.8	4.0	11.3	20.0	11.0	35.1	16.9	51.4	21.4	7.7
LF31530	33.3	202.2	53.3	116.5	8.7	6.6	2.9	1.9	9.0	66.7	18.0	7.0	9.8	21.4	15.5	184.9	35.7	79.9	30.6	9.4
LF31531	23.1	375.1	33.4	93.0	6.8	7.8	bd	1.6	7.4	78.3	12.8	6.0	14.7	19.2	13.6	259.6	18.2	48.6	20.1	bd
LF31532	25.9	400.6	33.2	92.5	7.7	6.8	bd	bd	10.0	83.9	14.5	7.5	12.9	19.4	14.8	169.1	17.1	52.5	24.5	7.5
LF31533	27.7	157.1	37.8	95.9	7.2	7.8	bd	bd	9.5	98.6	13.9	7.6	11.5	20.9	14.7	475.8	19.2	52.4	17.2	bd
LF31534	27.1	165.9	48.0	99.6	7.0	8.3	1.4	bd	6.0	76.8	16.4	6.0	9.3	18.7	12.5	448.7	28.9	63.1	24.0	5.6

XRF data for concretion 2 (HC2); for the order of transects the reader is referred to Appendix N for the transect order.

Table O.3: XRF major elements of concretion 2. bd = below detection limit.

Bead #	SiO ₂	TiO ₂	Al ₂ O ₃	Fe ₂ O ₃	MnO	MgO	CaO	Na ₂ O	K ₂ O	P ₂ O ₅	SO ₃	LOI	Total
LF32942	21.53	0.590	7.59	6.42	0.743	0.45	32.06	0.035	0.836	0.211	0.010	29.87	100.34
LF32949	14.06	0.523	6.56	6.27	0.890	0.51	37.02	0.039	0.576	0.232	0.038	33.24	99.97
LF32954	14.17	0.516	6.53	5.83	0.971	2.41	34.72	0.058	0.522	0.239	0.094	33.74	99.79
LF32951	15.29	0.482	6.06	5.48	0.965	2.85	34.37	0.069	0.472	0.300	0.045	34.47	100.85
LF32945	15.69	0.465	5.80	5.37	0.970	2.77	34.24	0.059	0.458	0.281	0.089	34.44	100.63
LF32952	15.85	0.467	5.76	5.41	0.985	2.72	34.23	0.055	0.447	0.284	0.081	39.89	106.18

LF32950	15.25	0.466	5.76	5.53	0.982	2.71	32.55	0.056	0.438	0.269	0.099	34.18	98.28
LF32953	15.61	0.510	6.57	6.07	1.031	3.03	33.23	0.064	0.473	0.257	0.064	34.15	101.06
LF32955	14.35	0.542	6.83	6.24	0.939	0.91	36.61	0.045	0.491	0.244	0.029	33.57	100.80
LF32943	24.53	0.608	8.34	6.51	0.644	0.43	29.78	0.031	0.889	0.214	0.007	28.47	100.45
LF32958	15.50	0.543	7.27	6.62	0.872	0.43	35.93	0.044	0.573	0.248	-0.003	32.14	100.17
LF32940	16.64	0.441	5.64	5.04	0.970	1.98	34.97	0.062	0.447	0.299	0.073	33.76	100.32
LF32960	17.63	0.417	4.95	4.76	0.967	2.57	34.59	0.053	0.378	0.339	0.051	33.52	100.22
LF32957	18.64	0.428	4.91	4.89	0.985	2.67	33.80	0.057	0.356	0.344	0.043	33.53	100.65
LF32959	16.77	0.590	7.49	7.81	0.816	0.46	34.03	0.039	0.837	0.253	0.005	31.22	100.32
LF32939	14.97	0.514	6.42	5.86	0.887	0.46	37.11	0.049	0.646	0.216	0.067	33.37	100.57
LF32941	14.38	0.513	6.21	5.98	0.968	3.16	33.94	0.066	0.560	0.230	0.131	34.90	101.04

Table O.4: Trace element data for concretion 2; measured as ppm. Copper (Cu) was analysed, but has been removed as no samples contained copper above instruments detection limit (<2.3ppm).

Bead #	Rb	Sr	Y	Zr	Nb	Pb	Th	U	Ga	Zn	Ni	Co	Cr	V	Sc	Ba	La	Ce	Nd	Cs
LF32942	24.3	176.9	44.3	98.1	7.1	8.4	bd	bd	8.9	101.0	16.1	6.3	12.2	17.8	16.7	363.6	23.9	53.4	21.4	6.5
LF32949	41.7	195.4	56.6	124.7	9.0	18.4	bd	2.7	9.9	83.9	25.1	6.4	25.4	23.3	20.0	281.3	36.9	73.1	30.3	6.9
LF32954	28.5	407.6	31.5	92.9	6.9	7.2	bd	bd	7.9	81.2	14.0	bd	12.6	16.4	13.4	32.0	22.6	51.5	16.9	9.8
LF32951	23.8	470.7	33.3	94.0	7.2	8.1	bd	bd	8.1	87.7	14.2	8.0	16.0	15.5	12.8	91.6	20.8	47.1	19.3	14.9
LF32945	23.6	404.4	33.2	93.1	6.9	8.8	bd	2.0	8.1	87.9	12.8	6.6	15.7	15.0	14.3	23.9	23.0	49.5	16.7	10.0
LF32952	23.0	422.2	32.7	94.6	7.9	9.1	bd	bd	9.0	85.3	13.7	5.3	15.1	17.9	14.3	38.7	23.4	49.4	16.0	bd
LF32950	26.1	429.4	31.9	92.7	6.4	6.7	bd	bd	9.2	81.2	14.1	7.9	15.0	19.3	14.6	38.7	17.6	54.0	17.9	bd

APPENDICES

LF32953	21.8	408.2	33.4	92.3	7.1	7.2	bd	bd	10.3	88.4	14.0	7.2	13.3	18.3	16.8	208.6	16.5	54.9	17.9	bd
LF32955	26.4	410.0	32.6	92.9	7.2	7.7	bd	bd	10.2	79.2	13.7	4.0	11.3	20.0	11.0	35.1	16.9	51.4	21.4	7.7
LF32943	22.3	184.0	53.6	105.0	7.9	8.9	bd	bd	8.2	104.4	18.2	5.2	16.2	20.8	16.4	337.0	30.9	73.1	25.5	8.1
LF32958	25.9	400.6	33.2	92.4	7.7	6.8	bd	bd	10.0	83.8	14.5	7.5	12.9	19.4	14.8	169.1	17.1	52.5	24.5	7.5
LF32940	26.1	412.9	32.7	94.1	6.7	8.2	bd	bd	11.5	81.3	13.0	6.0	14.7	17.1	14.6	25.2	17.4	54.7	21.0	9.7
LF32960	27.1	165.9	48.0	99.6	7.0	8.3	1.3	bd	6.0	76.8	16.4	6.0	9.3	18.7	12.5	448.7	28.9	63.1	24.0	5.6
LF32957	23.0	375.1	33.4	92.9	6.8	7.8	bd	1.6	7.4	78.3	12.8	6.0	14.7	19.2	13.6	259.6	18.2	48.6	20.1	bd
LF32959	27.7	157.1	37.8	95.9	7.2	7.8	bd	bd	9.5	98.6	13.9	7.6	11.5	20.9	14.7	475.8	19.2	52.4	17.2	bd
LF32939	25.1	162.4	38.6	95.9	5.8	7.7	1.6	bd	8.3	91.3	12.8	5.2	15.7	23.2	15.4	285.6	22.3	49.0	18.3	bd
LF32941	30.2	416.8	32.5	93.8	7.3	8.0	1.8	bd	9.3	83.7	13.5	4.2	15.5	18.5	14.2	30.3	17.5	49.7	19.5	12.1

APPENDIX P: ISOTOPIC DATA

Carbon and oxygen isotopic data measured at NIGL Laboratories, Keyworth.

Samples were processed for 72 hours at 25°C. Results are per mil (‰) deviations of the isotopic ratios ($^{13}\text{C}/^{12}\text{C}$, $^{18}\text{O}/^{16}\text{O}$) calculated to the VPDB scale using a within-run laboratory standard calibrated against NBS standards.

Table P.1: Carbon and Oxygen Isotope data (A) Concretion 1, (B) Concretion 2.

(A)	$\delta^{13}\text{C}$	$\delta^{18}\text{O}$	(B)	$\delta^{13}\text{C}$	$\delta^{18}\text{O}$
LF31512	-5.4	-8.6	LF32942	-5.2	-9.7
LF31513	-4.3	-8.3	LF32949	-4.0	-8.2
LF31514	-4.6	-10.3	LF32954	-3.8	-9.2
LF31515	-4.7	-10.3	LF32951	-3.3	-9.7
LF31516	-5.3	-8.0	LF32945	-3.5	-9.9
LF31517	-4.7	-8.4	LF32952	-3.2	-9.5
LF31518	-4.6	-10.4	LF32950	-3.1	-9.5
LF31519	-4.6	-10.3	LF32953	-3.2	-9.5
LF31520	-4.9	-10.1	LF32955	-4.4	-8.1
LF31521	-4.5	-10.5	LF32943	-5.4	-9.9
LF31522	-4.8	-10.1	LF32947	-3.6	-9.5
LF31523	-6.0	-8.5	LF32956	-3.8	-8.3
LF31524	-4.8	-10.1	LF32948	-4.6	-9.1
LF31525	-5.1	-10.0	LF32946	-3.0	-9.5
LF31526	-4.6	-10.1	LF32944	-3.4	-8.2
LF31527	-4.8	-9.7	LF32938	-4.9	-8.7
LF31528	-4.5	-10.3	LF32958	-3.8	-8.3
LF31529	-4.6	-10.3	LF32940	-3.0	-9.0
LF31530	-4.2	-9.6	LF32960	-3.3	-9.7
LF31531	-4.9	-9.6	LF32957	-3.3	-9.8
LF31532	-5.0	-9.7	LF32959	-5.2	-8.5
LF31533	-5.2	-7.6	LF32939	-5.1	-9.9
LF31534	-6.3	-8.3	LF32941	-5.1	-7.9

Table P.2: Carbon and Oxygen isotope data presented in Chapter 3 of 4 enigmatic fossils and, in addition, a sample of locally collected Dolyhir-Nash Scar Limestone Formation.

Sample	$\delta^{13}\text{C}$	$\delta^{18}\text{O}$
Fossil 1 (DAR1)	-11.83	-6.97
Fossil 2 (DAR2)	-2.25	-8.03
Fossil 3 (DAR3)	-13.1	-7.67
Fossil 4 (DAR4)	-17.31	-7.43
Dolyhir Limestone Formation	+2.24	-6.49

Table P.3: Sr isotope data measured from a selection of concretion samples.

Run	P Rpt	Batch N	Sample	SrTriple	\pm 1SE
Triton1-704 1	1	N668	LF31518	0.70968	0.000004
Triton1-704 2	1	N668	LF31521	0.709547	0.000005
Triton1-704 3	1	N668	LF31524	0.709803	0.000016
Triton1-704 4	1	N668	LF31532	0.709805	0.000020
Triton1-704 5	1	N668	LF31533	0.709352	0.000008
Triton1-704 6	1	N668	LF31534	0.709253	0.000008
Triton1-704 8	1	N668	LF32942	0.709007	0.000007
Triton1-704 9	1	N668	LF32945	0.709114	0.000034
Triton1-704 10	1	N668	LF32949	0.709885	0.000003
Triton1-704 11	1	N668	LF32951	0.709798	0.000005
Triton1-704 12	1	N668	LF32952	0.709538	0.000009
Triton1-704 13	1	N668	LF32954	0.709518	0.000005

APPENDIX Q: CALCULATIONS BASED ON STOICHIOMETRY

Calculations on based on stoichiometry referenced in Chapter 4 to determine if any extra iron has been added to the concretions at a later date from weathering.

Table Q.1: Stoichiometry.

Sample	LF31512	LF31513	LF31514	LF31515	LF31516	LF31517	LF31518	LF31519	LF31520	LF31521	LF31522	LF31523	LF31524	LF31525	LF31526	LF31527	LF31528	LF31529	LF31530	LF31531	LF31532	LF31533	LF31534
%C	9.42	9.19	9.71	9.78	9.11	8.95	9.78	9.69	9.81	9.75	9.76	8.02	9.75	9.78	9.82	9.75	9.81	9.75	8.27	9.65	9.72	9.15	9.08
% CaO	35.3	36.8	33.3	33.8	36.7	35.7	33.5	33.4	33.5	33.3	33.7	31.7	33.3	33.7	33.7	34.4	33.7	33.5	32.8	34.5	34.2	36.3	36.5
	6	6	6	1	8	8	9	8	0	0	0	7	2	5	0	9	8	8	6	2	1	0	5
% MgO	1.76	0.55	2.78	2.83	0.52	0.51	2.79	2.78	2.87	2.72	2.80	0.64	2.91	3.05	2.75	2.45	2.79	2.83	0.52	2.20	2.50	0.51	0.54
%MnO	0.99	0.94	0.98	0.99	0.93	1.00	0.98	0.98	0.98	0.96	1.00	0.98	0.99	0.99	1.00	1.00	0.99	0.98	0.92	0.97	0.98	0.97	1.06
	4	3	4	1	9	1	8	4	1	8	0	1	4	5	0	0	7	9	3	8	4	4	9
%Fe2O3	5.78	6.28	5.47	5.46	6.19	6.13	5.34	5.43	5.43	5.50	5.19	6.89	5.53	5.49	5.37	5.40	5.48	5.45	6.13	5.43	5.30	6.37	5.98
%CO2	34.5	33.7	35.6	35.8	33.3	32.8	35.8	35.5	35.9	35.7	35.8	29.3	35.7	35.8	36.0	35.7	35.9	35.7	30.3	35.3	35.6	33.5	33.3
	4	0	0	5	9	0	6	2	7	5	0	9	4	6	2	6	6	4	4	8	3	4	1
%FeO	5.20	5.64	4.92	4.91	5.57	5.51	4.80	4.89	4.88	4.95	4.67	6.20	4.97	4.94	4.83	4.86	4.92	4.90	5.52	4.88	4.77	5.73	5.38
CO2>CaC	78.5	76.5	80.9	81.4	75.8	74.5	81.5	80.7	81.7	81.2	81.3	66.8	81.2	81.5	81.8	81.2	81.7	81.2	68.9	80.4	80.9	76.2	75.6
O3	0	8	2	7	9	6	0	2	5	5	6	1	2	0	6	8	2	2	4	2	7	2	9
CaCO3>C	43.9	42.8	45.3	45.6	42.5	41.7	45.6	45.2	45.7	45.5	45.5	37.4	45.4	45.6	45.8	45.5	45.7	45.4	38.6	45.0	45.3	42.6	42.3
aO	6	9	1	2	0	5	4	0	8	0	6	1	8	4	4	2	6	8	1	3	4	8	9

DCaO	8.60	6.03	11.9 5	11.8 1	5.72	5.97	12.0 5	11.7 3	12.2 8	12.2 0	11.8 6	5.64	12.1 6	11.8 9	12.1 4	11.0 2	11.9 8	11.9 0	5.75	10.5 2	11.1 3	6.38	5.84
DCO2	6.76	4.74	9.39	9.28	4.49	4.69	9.47	9.22	9.65	9.59	9.32	4.43	9.55	9.35	9.54	8.66	9.42	9.35	4.52	8.26	8.75	5.01	4.59
MgCO3	3.68	1.15	5.83	5.92	1.09	1.08	5.83	5.81	6.01	5.69	5.85	1.33	6.08	6.39	5.76	5.12	5.84	5.91	1.09	4.61	5.23	1.06	1.13
dMg CO2	1.92	0.60	3.04	3.09	0.57	0.56	3.04	3.03	3.14	2.97	3.05	0.70	3.17	3.33	3.00	2.67	3.05	3.09	0.57	2.41	2.73	0.55	0.59
DCo2	4.84	4.13	6.35	6.19	3.93	4.13	6.43	6.19	6.51	6.61	6.27	3.74	6.38	6.01	6.53	5.99	6.37	6.26	3.95	5.86	6.02	4.46	4.00
MnCO3	1.61	1.53	1.59	1.61	1.52	1.62	1.60	1.59	1.59	1.57	1.62	1.59	1.61	1.61	1.62	1.62	1.62	1.60	1.50	1.58	1.59	1.58	1.73
dMn Co2	0.62	0.59	0.61	0.62	0.59	0.62	0.62	0.61	0.61	0.60	0.62	0.61	0.62	0.62	0.62	0.62	0.62	0.62	0.58	0.61	0.61	0.61	0.67
D CO2	4.22	3.54	5.73	5.57	3.34	3.50	5.81	5.57	5.90	6.01	5.64	3.13	5.76	5.39	5.91	5.36	5.75	5.65	3.37	5.25	5.41	3.85	3.33
FeCO3	8.38	9.10	7.94	7.92	8.98	8.89	7.74	7.88	7.87	7.98	7.52	10.0 0	8.02	7.97	7.79	7.84	7.94	7.91	8.89	7.87	7.69	9.23	8.68
dFe CO2	3.18	3.46	3.01	3.01	3.41	3.38	2.94	2.99	2.99	3.03	2.86	3.80	3.04	3.03	2.96	2.98	3.02	3.00	3.38	2.99	2.92	3.51	3.30
D CO2	1.03	0.09	2.72	2.56	0.07	0.13	2.87	2.58	2.91	2.98	2.79	0.67	2.72	2.36	2.95	2.39	2.73	2.64	0.01	2.26	2.49	0.34	0.04
% ex C	0.28	0.02	0.74	0.70	0.02	0.03	0.78	0.70	0.79	0.81	0.76	0.18	0.74	0.64	0.80	0.65	0.74	0.72	0.00	0.62	0.68	0.09	0.01

Initial stages of the stoichiometric calculations require % carbon to be converted to weight percent CO₂ and the Fe₂O₃ to be calculated as FeO. The carbon is then converted to calcium carbonate, and then to calcium oxide. A check of the calculation the dCO₂ indicates that there is more carbon than calcium within the rock. The remaining carbon is then subsequently assigned to individual ions then the % of excess carbon (% ex C) is calculated, which indicates that there is more carbon present within the rock than carbonate. This might be organic carbon on the surface of the clay mineral, or alternatively could be the errors accumulating.

Table Q.2: Stoichiometry Calculations

%FeO	1. %Fe = (Fe2O3 _{XRF} x 0.6994) 2. %FeO = (%Fe x 1.286)
Wt% CO ₂	= (%C / CA _M) x CO2M _M
CaCO ₃	= (Wt% CO ₂ / CO2M _M) x CaCO3M _M
CaO	= (Wt% CaCO ₃ / CaCO3M _M) x 56
DCaO	= CaO _{XRF} - Wt% CaO
DCO ₂ (1)	= (DCaO / CaOM _M) x CO2M _M x (-1) [†]
MgCO ₃	= (MgO _{XRF} / MgOM _M) x MgCO3M _M
dMg CO2	= (MgCO ₃ / MgCO3M _M) x CO2M _M
DCO ₂ (2)	= DCO ₂ (1) - dMg CO2
MnCO ₃	= (MnO _{XRF} / MnOM _M) x MnCO3M _M
dMn Co2	= (MnCO ₃ / MnCO3M _M) x CO2M _M
DCO ₂ (3)	= DCO ₂ (2) - dMn Co2
FeCO ₃	= (%FeO / FeOM _M) x FeCO3M _M
dFe CO2	= (FeCO ₃ / FeCO3M _M) x CO2M _M
DCO ₂ (4)	= DCO ₂ (3) - dFe CO2
% excess C	= (DCO ₂ (4) / CO2M _M) x CA _M

[†] multiplying by -1 converts the number back to a positive number

Table Q.3: Data and abbreviations used in Table Q.2

Element	A_M	Abbreviation	Compound	M_M	Abbreviation
Carbon	12	CA_M	CO_2	44	$CO2M_M$
			$CaCO_3$	100	$CaCO3M_M$
			CaO	56	$CaOM_M$
			MgO	40.3	$MgOM_M$
XRF Data		Abbreviation	$MgCO_3$	84.3	$MgCO3M_M$
Wt % CaO		CaO_{XRF}	MnO	70.9	$MnOM_M$
Wt % MgO		MgO_{XRF}	$MnCO_3$	114.9	$MnCO3M_M$
Wt % Fe_2O_3		Fe_2O_{3XRF}	FeO	71.85	$FeOM_M$
Wt % MnO		MnO_{XRF}	$FeCO_3$	115.85	$FeCO3M_M$

A_M = Atomic Mass, M_M = Molecular Mass

REFERENCES

- ALLISON, P.A. 1988. The role of anoxia in the decay and mineralization of proteinaceous macro-fossils. *Paleobiology*, **14**, 139-154.
- ALLISON, P.A. and BRIGGS, D.E.G. 1991. Taphonomy of Nonmineralized Tissues. 25-70. *In* ALLISON, P.A. and BRIGGS, D.E.G. (eds.) Topics in Geobiology: Taphonomy; Releasing the Data Locked in the Fossil Record. Plenum Press, New York and London, 560pp.
- AL-AGHA, M.R., BURLEY, S.D., CURTIS, C.D. and ESSON, J. 1995. Complex cementation textures and authigenic mineral assemblages in Recent concretions from the Lincolnshire Wash (east coast, UK) driven by Fe(0) to Fe(II) oxidation. *Journal of the Geological Society London*, **152**, 157-171.
- AMY, L.A., TALLING, P.J., PEAKALL, J., WYNN, R.B. and ARZOLA THYNNE, R.G. 2005. Bed geometry used to test recognition criteria of turbidites and (sandy) debrites. *Sedimentary Geology*, **179**, 163-174.
- ASTILLEROS, J.M., FERNÁNDEZ-DÍAZ, L. and PUTNIS, A. 2010. The role of magnesium in the growth of calcite: An AFM study. *Chemical Geology*, **271**, 52-58.

- AZMY, K., VEIZER, J., BASSETT, M.G. and COPPER, P. 1998. Oxygen and carbon isotopic composition of Silurian brachiopods: Implications for coeval seawater and glaciations. *GSA Bulletin*, **110**, 1499-1512.
- BAIRD, G.C., SHABICA, C.W., ANDERSON, J.L., and RICHARDSON Jr, E.S. 1985. Biota of a Pennsylvanian muddy coast; habitats within the Mazonian delta complex, Northeast Illinois. *Journal of Paleontology*, **59**, 253-281.
- BASSETT, M.G. 1974. Review of the stratigraphy of the Wenlock Series in the Welsh Borderland and South Wales. *Palaeontology*, **17**, 745-777.
- BATCHELOR, R.A. and JEPPSSON, L. 1999. Wenlock metabentonites from Gotland, Sweden: Geochemistry, sources and potential as chemostratigraphic markers. *Geological Magazine*, **136**, 661-669.
- BERNER, R.A. 1968. Calcium carbonate concretions formed by the decomposition of organic matter. *Science*, **159**, 195-197.
- BJØRKUM, P.A., WALDERHAUG, O. and AASE, N.E. 1993. A Model for the effect of illitization on porosity and quartz cementation of sandstones. *Journal of Sedimentary Petrology*, **63**, 1089-1091.
- BOGGS, S. JR and KRINSLEY, D. 2006. Application of cathodoluminescence imaging to the study of sedimentary rock, Cambridge University Press, Cambridge, 165 pp.

- BRAISSANT, O., DECHO, A.W., DUPRAZ, C., GLUNK, C., PRZEKOP, K.M. and VISSCHER, P.T. 2007. Exopolymeric substances of sulphate-reducing bacteria: Interactions with calcium at alkaline pH and implications for formation of carbonate minerals. *Geobiology*, **5**, 401-411.
- BRIGGS, D.E.G. and KEAR, A.J. 1993. Decay and preservation of polychaetes: taphonomic thresholds in soft-bodied organisms. *Paleobiology*, **19**, 107-135.
- BRIGGS, D.E.G. and KEAR, A.J. 1994. Decay and Mineralization of Shrimps. *Palaios*, **9**, 431-456.
- BRIGGS, D.E.G., SIVETER, D.J. and SIVETER, D.J. 1996. Soft-bodied fossils from a Silurian volcanoclastic deposit. *Nature*, **382**, 248-250.
- BRIGGS, D.E.G., SUTTON, M.D., SIVETER, D.J. and SIVETER, D.J. 2005. Metamorphosis in a Silurian barnacle. *Proceedings of the Royal Society B*, **272**, 2365-2369.
- BRIGGS, D.E.G., SIVETER, D.J., SIVETER, D.J. and SUTTON, M.D. 2008. Virtual Fossils from 425 Million-year-old Volcanic Ash. *American Scientist*, **96**, 474-481.
- BRYAN, S.E., CAS, R.A.F. and MARTÍ, J. 1998. Lithic breccias in intermediate volume phonolitic ignimbrites, Tenerife (Canary Islands): constraints on pyroclastic flow depositional processes. *Journal of Volcanology and*

Geothermal Research, **81**, 269-296.

- CLARK, J. D., BEYENE, Y., WOLDEGABRIEL, G., HART, W. K., RENNE, P. R., GILBERT, H., DEFLEUR, A., SUWA, G., KATOH, S., LUDWIG, K. R., BOISSERIE, J., ASFAW, B. and WHITE, T. D. 2003. Stratigraphic, chronological and behavioural contexts of Pleistocene *Homo sapiens* from Middle Awash, Ethiopia. *Nature*, **423**, 747-52.
- COLEMAN, M.L. and RAISWELL, R. 1981. Carbon, oxygen and sulphur isotope variations in concretions from the Upper Lias of N.E. England. *Geochimica et Cosmochimica Acta*, **45**, 329-340.
- COLEMAN, M.L. and RAISWELL, R. 1993. Microbial mineralization of organic matter: mechanism of self-organization and inferred rates of precipitation of diagenetic minerals. *Philosophical Transactions of the Royal Society London A*, **344**, 69-87.
- COLEMAN, M.L. and RAISWELL, R. 1995. Source of carbonate and origin of zonation in pyritiferous carbonate concretions: evaluation of a dynamic model. *American Journal of Science*, **295**, 282-308.
- COPLEN, T.B. 2007. Calibration of the calcite-water oxygen-isotope geothermometer at Devils Hole, Nevada, a natural laboratory. *Geochimica et Cosmochimica Acta*, **71**, 3948-3957.

- CUADROS, J. and LINARES, J. 1996. Experimental kinetic study of the smectite-to-illite transformation. *Geochimica et Cosmochimica Acta*, **60**, 439-453.
- CUADROS, J., CABALLERO, E., HUERTAS, J., DE CISNEROS, C.J., HUERTAS, F. and LINARES, J. 1999. Experimental alteration of volcanic tuff: smectite formation and effect on ^{18}O isotope composition. *Clays and Clay Minerals*, **47**, 769-776.
- CUADROS, J. 2006. Modeling of smectite illitization in burial diagenesis environments. *Geochimica et Cosmochimica Acta*, **70**, 4181-4195.
- DAVIS, K.J., DOVE, P.M. and DE YOREO, J. 2000. The role of Mg^{2+} as an impurity in calcite growth. *Science*, **290**, 1134-1137.
- DIETZEL, M., TANG, J., LEIS, A. and KÖHLER, S.J. 2009. Oxygen isotope fractionation during inorganic calcite precipitation – Effects of temperature, precipitation rate and pH. *Chemical Geology*, **268**, 107-115.
- DAI, S., REN, D., ZHOU, Y., CHOU, C.L., WANG, X., ZHAO, L. and ZHU, X. 2008. Mineralogy and geochemistry of a superhigh-organic-sulfur coal, Yanshan Coalfield, Yannan, China: Evidence for a volcanic ash component and influence by submarine exhalation. *Chemical Geology*, **255**, 182-194.

- DOWNING, K.F. and PARK, L.E. 1998. Geochemistry and Early Diagenesis of Mammal-Bearing concretions from the Sucker Creek Formation (Miocene) of Southeastern Oregon. *Palaios*, **13**, 14-27.
- DOYLE, E.E., HOGG, A.J., MADER, H.M. and SPARKS, R.S.J. 2008. Modeling dense pyroclastics basal flows from collapsing columns. *Geophysical Research Letters*, **35**, L04305.
- DYKE, G. J., WATERHOUSE, D. M. and KRISTOFFERSEN, A. V., 2004. Three new fossil landbirds from the early Paleogene of Denmark. *Bulletin of the Geological Society of Denmark*, **51**, 47–56.
- ELLIOTT, W.C. and MATISOFF, G. 1996. Evaluation of kinetic models for the smectite to Illite transformation. *Clays and Clay Minerals*, **44**, 77-87.
- EHRENBERG, S.N., PICKARD, N.A.H., SVÅNÅ, T.A. and OXTOBY, N.H. 2002. Cement geochemistry of photozoan carbonate strata (Upper Carboniferous-Lower Permian), Finnmark carbonate platform, Barents Sea. *Journal of Sedimentary Research*, **72**, 95-115.
- FISHER, Q.J., RAISWELL, R. and MARSHALL, J.D. 1998. Siderite concretions from nonmarine shales (Westphalian A) of the Pennines, England: controls on their growth and composition. *Journal of Sedimentary Research*, **68**, 1034-1045.

- FISHER, R.V. and SCHMINCKE, H-U. 1984 Pyroclastic Rocks. Springer-Verlag. Germany, pp 472.
- FITTON, J.G., THIRLWALL, M.F. and HUGHES, D.J. 1982. Volcanism in the Caledonian orogenic belt of Britain. *In* THORPE, R.S. (ed.). *Andesites Orogenic Andesites and Related rocks*: Wiley-Interscience. pp. 611-639.
- FLÜGEL, E. 2009. *Microfacies of Carbonate Rocks: Analysis, Interpretation and Application*, Springer, Germany, pp 976.
- FLYNN, J.J., WYSS, A.R. and CHARRIER, R. 2007. South America's missing mammals, *Scientific American*, **296**, 68-75.
- FOLK, R.L. 1974. The natural history of crystalline calcium carbonate: effect of magnesium content and salinity. *Journal of Sedimentary Petrology*, **44**, 40-53.
- FONTES, D.E., MILLS, A.L., HORNBERGER, G.M. and HERMAN, J.S. 1991. Physical and chemical factors influencing transport of microorganisms through porous media. *Applied and Environmental Microbiology*, **57**, 2473-2481.
- FOWLER, J., COHEN, L. and JARVIS, P. 1998 *Practical Statistics for Field Biology*. Wiley. Chichester, pp 259.

- FREUNDT, A. 2003. Entrance of hot pyroclastic flows into the sea: experimental observations. *Bulletin of Volcanology*, **65**, 144-164.
- FUKUE, M., FUJIMORI, Y., SATA, Y., NAKAGAWA, T. and MULLIGAN, C.N. 2010. Evidence of the production and dissolution of carbonate phases in bentonite formations. *Applied Clay Science*, **47**, 133-138.
- GABBOTT, S.E. 1998. Taphonomy of the Ordovician Soom Shale Lagerstätte: an example of soft tissue preservation in clay minerals. *Palaeontology*, **41**, 631-667.
- GABBOTT, S.E., NORRY, M.J., ALDRIDGE, R.J. and THERON, J.N. 2001. Preservation of fossils in clay minerals; a unique example from the Upper Ordovician Soom Shale, South Africa. *Proceedings of the Yorkshire Geological Society*, **53**, 237-244.
- GABBOTT, S.E., XAIN-GUANG, H., NORRY, M.J. and SIVETER, D.J. 2004. Preservation of Early Cambrian animals of the Chengjiang biota. *Geology*, **32**, 901-904.
- GAINES, R.R., KENNEDY, M.J., and DROSER, M.L., 2005. A new hypothesis for organic preservation of Burgess Shale taxa in middle Cambrian Wheeler Formation, House Range, Utah. *Palaeogeography, Palaeoclimatology, Palaeoecology*, **220**, 193-205.

- GEESLIN, J.H. and CHAFETZ, H.S. 1982 Ordovician Aleman cherts: an example of silicification prior to carbonate lithification. *Journal of Sedimentary Petrology*, **52**, 1283-1293.
- GONZÁLEZ, L.A., CAROENTER, S.J. and LOHMANN, K.C. 1990. Inorganic calcite morphology: roles of fluid chemistry and fluid flow. *Journal of Sedimentary Petrology*, **62**, 382-399.
- GUARINO, F. M., ANGELINI, F., VOLLONO, C. and OREFICE, C. 2006. Bone preservation in human remains from the Terme del Sarno at Pompeii using light microscopy and scanning electron microscopy, *Journal of Archaeological Science*, **33**, 513-520.
- HALL, C. and CULLEN, D.C. 1996. Scanning Force Microscopy of Gypsum Dissolution and Crystal Growth. Materials. *Interfaces and Electrochemical Phenomena*, **42**, 232-238.
- HARDIE, L.A. 1986. Perspectives Dolomitization: A critical view of some current views. *Journal of Sedimentology*, **57**, 166-183.
- HARRISON, T. 1981. New Finds of Small Fossil Apes from the Miocene Locality at Koru in Kenya. *Journal of human Evolution*, **10**, 129-137
- HAY, R.L. and LEAKEY, M.D. 1982 Fossil footprints of Laetoli. *Scientific American*, **246**, 50-57.

- HAYS, P.D. and GROSSMAN, E.L. 1991. Oxygen isotopes in meteoric calcite cements as indicators of continental paleoclimate. *Geology*, **19**, 441-444.
- HEANEY, P.J. 1993. A proposed mechanism for the growth of chalcedony. *Contributions to Mineralogy and Petrology*, **115**, 66-74.
- HEDGES, J.I. and KEIL, R.G. 1995. Sedimentary organic matter preservation: an assessment and speculative synthesis. *Marine Chemistry*, **49**, 81-115.
- HENDY, J.P. 2002. Geochemical trends and palaeohydrological significance of shallow burial calcite and ankerite cements in Middle Jurassic strata on the East Midlands Shelf (onshore UK). *Sedimentary Geology*, **151**, 149-176.
- de HEINZELIN, J., CLARK, J.D., WHITE, T., HART, W., RENNE, P., WOLDEGABRIEL, G., BEYENE, Y. and VRBA, E. 1999. Environment and behaviour of 2.5-million-year-old Bouri hominids. *Science*, **284**, 625-629.
- HENRICHS, S.M. 1995. Sedimentary organic matter preservation: an assessment and speculative synthesis – a comment. *Marine Chemistry*, **49**, 127-136.
- HOF, C.H.J. and BRIGGS, D.E.G. 1997. Decay and mineralization of mantis shrimps (Stomatopoda: Crustacea) - A key to their fossil record. *Palaios*, **12**, 420-438.

- HUFF, W.D. MORGAN, D.J. and RUNDLE, C.C. 1996. Silurian K-bentonites of the Welsh Borderlands: Geochemistry, mineralogy and K-Ar age of illitization. British Geological Survey Technical Report WG/96/45.
- IRWIN, H., CURTIS, C. and COLEMAN, M. 1977. Isotopic evidence for source of diagenetic carbonates formed during burial of organic-rich sediments. *Nature*, **269**, 209-213.
- JANOŮŠEK, V., FARROW, C.M. and ERBAN, V. 2006. Interpretation of whole-rock geochemical data in igneous geochemistry: introducing Geochemical Data Toolkit (GCDkit). *Journal of Petrology*, **47**, 1255-1259.
- KASTING, J.F., HOWARD, M.T., WALLMANN, K., VEIZER, J., SHIELDS, G. and JAFFRES, J. 2006. Palaeoclimates, ocean depth, and the oxygen isotopic composition of seawater. *Earth and Planetary Science Letters*, **252**, 82-93.
- KARAKOLTSIDIS, P.A., ZOTOS, A. and CONSTANTINIDES, S.M. 1995. Composition of the Commercially Important Mediterranean Finfish, Crustaceans, and Molluscs. *Journal of Food Composition and Analysis*, **8**, 258-273.
- KEIL, R.G., MONTIÇON, D.B., PRAHL, F.G. and HEDGES, J.I. 1994. Sorptive preservation of labile organic matter in marine sediment. *Nature*, **370**, 549-552.

- KIIPLI, T., SOESOO, A., KALLASTE, T. and KIIPLI, E. 2008. Geochemistry of Telichian (Silurian) K-bentonites in Estonia and Latvia. *Journal of Volcanology and Geothermal Research*, **171**, 45-58.
- KIM, J., DONG, H., SEABAUGH, J., NEWELL, S.W. and EBERL, D.D. 2004. Role of microbes in the Smectite-to-illite reaction. *Science*, **303**, 830-832.
- KIM, S.T., HILLAIRE-MARCEL, C. and MUCCI, A. 2006. Mechanism of equilibrium and kinetic oxygen isotope effects in synthetic aragonite at 25 °C. *Geochimica et Cosmochimica Acta*, **70**, 5790-5801.
- KÖNIGSHOF, P. 2003. Conodont deformation patterns and textural alteration in Paleozoic conodonts: examples from Germany and France. *Senckenbergiana lethaea*, **83**, 149-156.
- KORTE, C., HESSELBO, S.P., JENKYN, H.C., RICKABY, R.M. and SPÖTL, C. 2009. Palaeoenvironmental significance of carbon- and oxygen-isotope stratigraphy of marine Triassic-Jurassic boundary section in SW Britain. *Journal of the Geological Society*, **166**, 431-445.
- KRAUSKOPF, K.B. 1989. Introduction to Geochemistry. (second edition), McGraw-Hill, London, 617 pp.

- LIN, R. Y., ZHANG, J.Y and ZHANG, P.X. 2002. Nucleation and growth kinetic of synthesizing nanometer calcite. *Journal of Crystal Growth*, **245**, 309-320.
- MANCHESTER, S., R. 1994. Fruits and seeds of the Middle Eocene Nut Beds flora, Clarno Formation, Oregon. *Palaeontographica Americana*, **58**, 1-205.
- MANOLI, F., KOUTSOPOULOS, S. and DALAS, E. 1997. Crystallization of calcite on chitin. *Journal of Crystal Growth*, **182**, 116-124.
- MANVILLE, V. and WILSON, C.J.N. 2004. Vertical density currents: a review of their potential role in the deposition and interpretation of deep-sea ash layers. *Journal of the Geological Society*, **161**, 947-958.
- MARRIOTT, S.B., MORRISSEY, L.B. and HILLIER, R.D. 2009. Trace fossil assemblages in Upper Silurian tuff beds: Evidence of biodiversity in the Old Red Sandstone of southwest Wales, UK, *Palaeogeography, Palaeoclimatology, Palaeoecology*, **274**, 160-172.
- MARTILL, D.M. 1988. Preservation of Fish in the Cretaceous Santana Formation of Brazil. *Palaeontology*, **31**, 1-18.
- MARTIN, D., BRIGGS, E.G.D. and PARKES, J. 2004. Experimental attachment of sediment particles to invertebrate eggs and the preservation of soft-bodied fossils. *Journal of the Geological Society*, **161**, 735-738.

- MARTIN, E. and BINDEMAN, I. 2009. Mass-independent isotopic signatures of volcanic sulfate from three supereruption ash deposits in Lake Tecopa, California. *Earth and Planetary Science Letters*, **282**, 102-114.
- MAZZULLO, S.J. 2000. Organogenic dolomitization in peritidal to deep-sea sediment. *Journal of Sedimentary Research*, **70**, 10-23.
- MORAD, S., AL-RAMADAN, K., KETZER, J.M. and DE ROS, L.F. 2010. The impact of diagenesis on the heterogeneity of sandstone reservoirs: A review of the role of depositional facies and sequence stratigraphy. *American Association of Petroleum Geologists Bulletin*, **94**, 1267-1309.
- MORESE, J.W., ARVIDSON, R.S. and LUTTGE, A. 2007. Calcium carbonate formation and dissolution. *Chemical reviews*, **107**, 342-381.
- MOZLEY, P.S. 1989. Complex compositional zonation in concretionary siderite: Implications for geochemical studies. *Journal of Sedimentary Petrology*, **59**, 815-818.
- MOZLEY, P.S. and BURNS, S.J. 1993. Oxygen and carbon isotopic composition of marine carbonate concretions: an overview. *Journal of Sedimentary Petrology*, **63**, 73-83.

- MOZLEY, P.S. 1996. The internal structure of carbonate concretions in mudrocks: a critical evaluation of the convention concentric model of concentric growth. *Sedimentary Geology*, **103**, 85-91.
- MUSTOE, G., E., 2008. Mineralogy and geochemistry of late Eocene silicified wood from Florissant Fossil Beds National Monument, Colorado. *In*: MEYER, H. W. and SMITH, D. M. (eds.), *Paleontology of the Upper Eocene Florissant Formation, Colorado*. Special Paper of the Geological Society of America. 127-141.
- MURATA, K. J. 1940. Volcanic ash as a source of silica for the silification of wood. *American Journal of Science*, **238**, 586-596.
- NAKAGAWA, M. and OHBA, T. 2002. Minerals in volcanic ash. 1: primary minerals and volcanic glass. *Global Environmental Research*, **6**, 41-51.
- ODOM, I.E. 1984. Smectite clay minerals: properties and uses. *Philosophical Transactions of the Royal Society London A*, **311**, 391-409.
- OELKERS, E.H. and GISLASON, S.R. 2001. The mechanism, rate and consequences of basaltic glass dissolution: I. An experimental study of the dissolution rates of basaltic glass as a function of aqueous Al, Si, and oxalic acid concentrations at 25°C and pH = 3 and 11. *Geochimica et Cosmochimica Acta*, **65**, 3671-3681.

- OLIVERO, E.B. 2007. Taphonomy of ammonites from the Santonian–Lower Campanian Santa Marta Formation, Antarctica: sedimentological controls on vertically embedded ammonites. *Palaios*, **22**, 586-597.
- O'NEIL, R.J., CLAYTON, R.N., and MAYEDA, T.K. 1969. Oxygen isotope fractionation in divalent metal carbonates. *Journal of Chemical Physics*, **51**, 5547-5558.
- ORR, P.J., BRIGGS, D. E. G., and KEARNS, S.L. 1998. Cambrian Burgess Shale animals replicated in clay minerals. *Science*, **281**, 1173-1175.
- ORR, P.J., BRIGGS, D. E. G., SIVETER, D. J. and SIVETER, D. J. 2000a. Three-dimensional preservation of a non-biomineralized arthropod in concretions in Silurian volcanoclastic rocks from Herefordshire, England. *Journal of the Geological Society of London*, **157**, 173-186.
- ORR, P.J., SIVETER, D.J., BRIGGS, D.E.G., SIVETER, D.J. and SUTTON, M.D. 2000b. A new arthropod from the Silurian Konservat-Lagerstätte of the Herefordshire, England. *Proceedings of the Royal Society B*, **267**, 1497-1504.
- PARK, L. 1995. Geochemical and Paleoenvironmental Analysis of Lacustrine Arthropod-Bearing Concretions of the Barstow Formation, Southern California. *Palaios*, **10**, 44-57.

- PALMER, A.R. 1957. Miocene Arthropods from the Mojave Desert California. *Geological Survey Professional Paper*, **294-G**, 237-277.
- PATOCKA, F., VLASIMSKY, P. and BLEACHOVA, K. 1993. Geochemistry of Early Paleozoic volcanics of the Barrandian Basin (Bohemian Massif, Czech Republic): implications for paleotectonic reconstructions. *Jb Geol B-A Wien*, **136**, 871-894.
- PILLAI, C.K.S., PAUL, W. and SHARMA, C.P. 2009. Chitin and chitosan polymers: Chemistry, solubility and fiber formation. *Progress in Polymer Science*, **34**, 641-678.
- POKROVSKY, O.S. and SCOTT, J. 2001. Kinetics and mechanism of dolomite dissolution in neutral to alkaline solutions revisited. *American Journal of Science*, **301**, 597-626.
- POLE, M. 2001. Repeated flood events and fossil forests at Curio Bay (Middle Jurassic), New Zealand. *Sedimentary Geology*, **144**, 223-242.
- PÜSPÖKI, Z., KOZÁK, M. KOVÁCS-PÁLFFY, P., SZEPESI, J., MCINTOSH, R., KÓNYA, P., VINCZE, L. and GYULA, G. 2008. Geochemical Records of a bentonitic acid-tuff succession related to a transgressive system tract – indication of changes in the volcanic sedimentation rate. *Clays and Clay Minerals*, **56**, 23-38.

- PYLE, D.M. 1989. The Thickness, volume and grainsize of tephra fall deposits. *Bulletin of Volcanology*, **51**, 1-15.
- RICHARDS, A.G. 1951. The integuments of arthropods. University of Minnesota Press, Minneapolis, 411 pp.
- RAISWELL, R. 1971. Cementation in some Cambrian concretions. In: BRICKER, O.P. (ed.) Carbonate Cements. John Hopkins University Press, Baltimore, 196-197.
- RAISWELL, R. 1987. Non-steady state microbiological diagenesis and the origin of concretions and nodular limestones. In: MARSHALL, J.D (ed.) Diagenesis of Sedimentary sequences. *Geological Society London Special publications*, **36**, 41-54.
- RAISWELL, R. and FISHER, Q.J. 2000. Mudrock-hosted carbonate concretions: a review of growth mechanisms and their influence on chemical and isotopic composition. *Journal of the Geological Society London*, **157**, 239- 251.
- RAISWELL, R. and FISHER, Q.J. 2004. Rates of carbonate cementation associated with sulphate reduction in DSDP/ODP sediments: implications for the formation of concretions. *Chemical Geology*, **211**, 71-85.
- REEDER, R.J. and DOLLASE, W.A. 1989. Structural variation in the dolomite-ankerite solid-solution: An X-ray, Mössbauer, and TEM study. *American Mineralogist*, **74**, 1159-1167.

- RETALLACK, G. 2004. Ecological polarities of mid-Cenozoic fossil plants and animals from central Oregon. *Paleobiology*, **30**, 561-588.
- RIMSTIDT, J.D. and VAUGHAN, D.J. 2003. Pyrite oxidation: A state-of-the-art assessment of the reaction mechanism. *Geochimica et Cosmochimica Acta*, **67**, 873-880.
- RINAUDO, M. 2006. Chitin and Chitosan: Properties and applications. *Progress in Polymer Science*, **31**, 603-632.
- ROSE, W.I., RILEY, C.M. and DARTEVELLE, S. 2003. Sizes and shapes of 10- Ma distal fall pyroclasts in the Ogallala Group, Nebraska, *Journal of Geology*, **111**, 115-124.
- SASS, E., BEIN, A. and ALMOGI-LABIN, A. 1991. Oxygen-isotope composition of diagenetic calcite in organic-rich rocks: Evidence for ^{18}O depletion in marine anaerobic pore water. *Geology*, **19**, 839-842.
- SCARPATI, C., COLE, P. and PERROTTA, A. 1993. The Neapolitan Yellow Tuff — A large volume multiphase eruption from Campi Flegrei, Southern Italy. *Bulletin of Volcanology*, **55**, 343-356.
- SEILACHER, A. 2001. Concretion morphologies reflecting diagenetic and epigenetic pathways. *Sedimentary Geology*, **143**, 41-57.

- SHIRAKI, R., SAKAI, H., ENDOH, M. and KISHIMA, N. 1987. Experimental studies on rhyolite- and andesite-seawater interactions at 300°C and 1000 bars. *Geochemical Journal*, **21**, 139-148.
- SIVAN, O., SCHRAG, D.P., and MURRAY, R.W. 2007. Rates of methanogenesis and methanotrophy in deep-sea sediment: *Geobiology*, **5**, 141-151.
- SIVETER, D.J. OWENS, R.M. and THOMAS, A.T. 1989. Silurian Field Excursions: A geotraverse across Wales and the Welsh Borderlands, National Museum of Wales, Geological Series No. 10, Cardiff, pp 133.
- SIVETER, D.J., SUTTON, M.D., BRIGGS, D.E.G. and SIVETER, D.J. 2003. An ostracode crustacean with soft parts from the Lower Silurian. *Science*, **302**, 1749-1751.
- SIVETER, D.J., SUTTON, M.D., BRIGGS, D.E.G. and SIVETER, D.J. 2004. A Silurian sea spider. *Nature*, **431**, 978-980.
- SIVETER, D.J., SUTTON, M.D., BRIGGS, D.E.G. and SIVETER, D.J. 2007a. A new probable stem lineage crustacean with three-dimensionally preserved soft parts from the Herefordshire (Silurian) Lagerstätte, UK. *Proceedings of the Royal Society B*, **274**, 2099-2107.

- SIVETER, D.J., FORTEY, R.A., SUTTON, M.D., BRIGGS, D.E.G. and SIVETER, D.J. 2007b. A Silurian 'marellomorph' arthropod. *Proceedings of the Royal Society B*, **274**, 2223-2229.
- SIVETER, D.J., SIVETER, D.J., SUTTON, M.D. and BRIGGS, D.E.G. 2007c. Brood care in a Silurian orstacod. *Proceedings of the Royal Society B*, **274**, 465-469.
- SIVETER, D.J., AITCHISON, J.C., SIVETER, D.J. and SUTTON, M.D. 2007d. The radiolaria of the Herefordshire Konservat-Lagerstätte (Silurian), England. *Journal of Micropalaeontology*, **26**, 87-95.
- SIVETER, D.J., BRIGGS, D.E.G., SIVETER, D.J. and SUTTON, M.D. 2010. An exceptionally preserved myodocopid ostracod from the Silurian of Herefordshire, UK. *Proceedings of the Royal Society B: Biological Sciences*, **277**, 1539-1544.
- SLAUGHTER, M. and HAMAIL, M. 1970. Model for Deposition of Volcanic Ash and Resulting Bentonite. *Geological Society of America Bulletin*, **81**, 961- 968.
- SLOAN, R.J. and BENNETT, M.C. 1990. Geochemical character of Silurian volcanism in SW Ireland. *Journal of the Geological Society*, **147**, 1051-1060.

- SPERO, H.J., BIJMA, J., LEA, D.W. and BEMIS, B.E. 1997. Effects of seawater carbonate concretion on foraminiferal carbon and oxygen isotopes. *Nature*, **390**, 497-500.
- SPOKES, L.J. and JICKELLS, T.D. 1996. Factors controlling the solubility of aerosol trace metals in the atmosphere and on mixing into seawater. *Aquatic Geochemistry*, **1**, 355-374.
- STEFÁNSDÓTTIR, M.B. and GÍSLASON, S.R. 2006. Suspended basaltic glass-seawater interactions. *Journal of Geochemical Exploration*, **88**, 332-335.
- STOCKEY, R. A. 2001. The Princeton Chert. *In*: BRIGGS, D. E. G. and CROWTHER, P. R. (eds). *Palaeobiology II*. Blackwell Scientific Publications, Oxford; 359-362.
- SUTTON, M.D., BRIGGS, D.E.G., SIVETER, D.J. and SIVETER, D.J. 2001a. An exceptionally preserved vermiform mollusc from the Silurian of England. *Nature*, **410**, 461-463.
- SUTTON, M.D., BRIGGS, D.E.G., SIVETER, D.J. and SIVETER, D.J. 2001b. Methodologies for the visualization and reconstruction of three-dimensional fossils from the Silurian Herefordshire Lagerstätte. *Palaeontologia Electronica*, **4**.

- SUTTON, M.D., BRIGGS, D.E.G., SIVETER, D.J. and SIVETER, D.J. 2001c. A three-dimensionally preserved fossil polychaete worm from the Silurian of Herefordshire, England. *Proceedings of the Royal Society B*, **268**, 2355-2363.
- SUTTON, M.D., BRIGGS, D.E.G., SIVETER, D.J. and SIVETER, D.J. 2005. Silurian brachiopods with soft-tissue preservation. *Nature*, **436**, 1013-1015.
- SUTTON, M.D., BRIGGS, D.E.G., SIVETER, D.J. and SIVETER, D.J. 2006. Fossilized soft tissues in a Silurian platyceratid gastropod. *Proceedings of the Royal Society B*, **273**, 1039-1044.
- SUTTON, M.D., BRIGGS, D.E.G., SIVETER, D.J. and SIVETER, D.J. 2011. A soft-bodied lophophorate from the Silurian of England. *Biology Letters*, **7**, 146-149.
- TAKENO, N. 2005. Atlas of Eh-pH diagrams. Geological Survey of Japan Open File Report, 419.
- TEALE, C.T. and SPEARS, D.A. 1986. The Mineralogy and Origin of Some Silurian Bentonites, Welsh Borderland, UK. *Sedimentology*, **33**, 757-765.
- THINH, T.P. and LEROUX, J. 1979. *X-Ray Spectrom.* **8**, 85-91.
- VAN DE KAMP, P. C. 1969. The Silurian volcanic rocks of the Mendip Hills, Somerset; and the Tortworth area. *Geological Magazine*, **106**, 542-552.

- VELDE, B and MEUNIER, A. 1987. Petrologic phase equilibria in natural clay systems. 423-458. In NEWMAN, A.C.D. (ed.). Chemistry of clays and clay minerals. Mineralogical Society Monograph, Longman Scientific and Technical and the Mineralogical Society, Harlow, 480 pp.
- WALTER, L.M. 1986. Relative efficiency of carbonate dissolution and precipitation during diagenesis: a progress report on the role of solution chemistry. 1-11. In GAUTIER, D.L. (ed.) Roles of organic matter in sediment diagenesis. Society of economic paleontologists and mineralogists special publications 38, Oklahoma.
- WHITE, J.F. and CORWIN, J.F. 1961. Synthesis and Origin of Chalcedony. *The American Mineralogist*, **46**, 112-119.
- WILBY, P.R. and BRIGGS, D.E.G. 1997. Taxonomic trends in the resolution of detail preserved in fossil phosphatized soft tissues. *Geobios*, **30**, 493-502.
- WILLIAMS, M., SMELLIE, J.L., JOHNSON, J.S. and BLAKE, D.B. 2006. Late Miocene Asterozoans (Echinodermata) in the James Ross Island Volcanic Group, *Antarctic Science*, **18**, 117-122.
- WINCHESTER, J.A. and FLOYD, P.A. 1977. Geochemical discrimination of different magma series and their differentiation products using immobile elements. *Chemical Geology*, **20**, 325-343.

- WOOD, D.A., JORON, J.L., and TREUIL, M. 1979. A re-appraisal of the use of trace elements to classify and discriminate between magma series erupted in different tectonic settings. *Earth Planetary Science Letters*, **45**, 326-336.
- WOO, K.S. and KHIM, B.K. 2006. Stable oxygen and carbon isotopes of the carbonate concretions of the Miocene Yeonil Group in the Pohang Basin, Korea: Types of concretions and formation conditions. *Sedimentary Geology*, **183**, 15-30.
- WRIGHT, D.T. and WACEY, D. 2005. Precipitation of dolomite using sulphate-reducing bacteria from the Coorong Region, South Australia: significance and implications. *Sedimentology*, **52**, 987-1008.
- YAMADA, E. 1984. Subaqueous pyroclastic flows: their development and their deposits. In: KOKELAAR, B.P. and HOWELLS, M.F. (eds.) *Marginal Basin Geology: Volcanic and Associated Sedimentary and Tectonic Processes in Modern and Ancient arginal Basins. Geological Society London Special publications*, **16**, 29-35.
- ZEEBE, R.E. 1999. An explanation of the effects of seawater carbonate concentration on foraminiferal oxygen isotopes. *Geochimica et cosmochimica Acta*, **63**, 2001-2007.
- ZHONGHE, Z., BARRETT, P. M. and HILTON, J. 2003. An exceptionally preserved Lower Cretaceous ecosystem, *Nature*, **421**, 807-811.